

DITANET

Low Current, Low Energy Beam Diagnostics

- Proceedings -

Workshop in Hirschberg-Großsachsen, Germany
23rd – 25th November 2009



Organized by: Peter Forck, Rainer Haseitl, Andreas Peters (Editor)

For DITANET: Carsten Welsch



List of participants:

CERN-AD Experiments:

Masaki Hori (MPI for Quantum Optics)

masaki.hori@mpq.mpg.de

Anna Soter (MPI for Quantum Optics + CERN)

anna.soter@cern.ch

CERN ISOLDE + REX:

Gerrit Jan Focker

gerrit.focker@cern.ch

Manne Siegbahn Laboratories (MSL) Stockholm

Anders Kaellberg

kallberg@mssl.se

Susanta Das

das@mssl.se

GANIL

Christophe Jamet

jamet@ganil.fr

Jean-Luc Vignet

vignet@ganil.fr

University Liverpool

Carsten Welsch

C.P.Welsch@liverpool.ac.uk

Janusz Harasimowicz

Janusz.Harasimowicz@mpi-hd.mpg.de

Massimiliano Putignano

massimiliano.putignano@quasar-group.org

MPI f. Kernphysik, Heidelberg

Robert von Hahn

robert.von.hahn@mpi-hd.mpg.de

Manfred Grieser

manfred.grieser@mpi-hd.mpg.de

Felix Laux

felix.laux@mpi-hd.mpg.de

GSI, Darmstadt:

Peter Forck

p.forck@gsi.de

Marcus Schwickert

m.schwickert@gsi.de

Michael Witthaus

m.witthaus@gsi.de

Hansjörg Reeg

h.reeg@gsi.de

Rainer Haseitl

r.haseitl@gsi.de

Plamen Boutachkov

P.Boutachkov@gsi.de

University Frankfurt:

Jochen Pfister

j.pfister@gsi.de

HIT, Heidelberg:

Andreas Peters

andreas.peters@med.uni-heidelberg.de

Marion Ripert

marion.ripert@med.uni-heidelberg.de

Tim Winkelmann

tim.winkelmann@med.uni-heidelberg.de

INFN Catania:

Paolo Finocchiaro

finocchiaro@lns.infn.it

Luigi Cosentino

cosentino@lns.infn.it

University Aarhus:

Henrik Pedersen

hbp@phys.au.dk

Kristian Stöckel

krst@phys.au.dk

University Sevilla:

Marco Alvarez

malvarez@us.es

Alessio Bocci

alessio.bocci@lnf.infn.it

Ziad Abou Haïdar

ziadah@us.es

Begoña Fernandez

bfernand@us.es

MSU East Lansing:

Georgios Perdikakis

perdikak@nscl.msu.edu

University Jena:

Wolfgang Vodel

wolfgang.vodel@uni-jena.de

IFIN-HH, Bukarest

Hermann Schubert

totalvco@web.de

Dorin Dudu

ddudu@nipne.ro

Contents:

Monday, November 23rd: 19:00 Dinner and open discussion on Beam Diagnostics

Tuesday, November 24th

Session 1: Existing LINACs at high energy facilities

Chairman: P. Forck

08:30	P. Forck	Welcome	
08:50	G.J. Focker	CERN ISOLDE and REX instrumentation	1
09:30	P. Forck	The GSI facility and the layout for FAIR	8
09:40	M. Witthaus	Beam diagnostics for the HITRAP decelerator	10
10:10	J. Pfister	HITRAP low energy diagnostics and emittance measurement	13

10:30 Coffee break

Session 2: Existing storage ring facilities

Chairman: C. Welsch

11:00	A. Soter	Operational experience with profile monitors for MeV and keV antiproton beams at CERN's antiproton decelerator	17
11:40	A. Kaellberg	Diagnostics at CRYRING	19

12:10 Lunch

Session 3: Diagnostics for slowed down beams

Chairman: C. Welsch

14:00	P. Boutachkov	Development of detectors for slowed down beams at GSI (*)	22
14:30	M. Alvarez	Beam tracking detectors developments	26

Session 4: Existing Cyclotron based facilities and new LINAC based facilities

Chairman: P. Forck

15:00	P. Finocchiaro	Low-energy/low-intensity beam diagnostics detectors: experience at INFN-LNS	36
-------	----------------	---	----

15:40 Coffee break

16:10	C. Jamet	Secondary beam overview and low current measurements of SPIRAL1 and SPIRAL2 facility	43
16:40	J. Vignet	The beam profile monitors for SPIRAL2 RIB and experimental rooms	47
17:00	G. Perdikakis	Low-energy low-intensity diagnostics for ReA3 @ NSCL/MSU Diagnostics for the needs of FRIB (*)	50
17:40	Discussion		

18:00 End of session

Wednesday, November 25th

Session 5: Storage rings with low energy injection

Chairman: C. Welsch

08:30	C. Stöckel	Detectors and what we use them for at ELISA (*)	54
09:00	S. Das	Diagnostics at DESIREE	60
09:20	R. von Hahn	Overview of the CSR (*)	65
09:40	M. Grieser	Diagnostics at CSR (and TSR) (*)	69

10:10 Coffee break

Session 6: Special devices I

Chairman: P. Forck

10:50	C. Welsch	FLAIR: A facility for low-energy antiproton and ion research	74
11:10	J. Harasimowicz	Diagnostics for USR; Low current BPMs	77
11:40	M. Putignano	Design and performance of a ionization beam profile monitor based on a gasjet curtain for Applications on low energy accelerator systems	80

12:00 Lunch

Session 7: Special devices II

Chairman: P. Forck

14:00	F. Laux	Position pickups for the cryogenic storage ring CSR	85
14:20	M. Ripert	A pepper pot emittance device for 8 keV/u light ion beams – general layout and investigations on the screen material	89
14:40	H. Schubert	Various beams for RBS at IFIN-HH	92
15:00	W. Vodel	The SQUID based cryogenic current comparator – an useful tool for beam diagnostics	98
15:40	M. Schwickert	A cryogenic current comparator for FAIR	108
16:40	Final Discussion		

16:20 Coffee break and end of workshop at about 17:00

(*) The authors of the marked titles were not able to deliver a written contribution in time; therefore their slides were used instead in these proceedings.

CERN ISOLDE AND REX BEAM INSTRUMENTATION

G. J. Focker, CERN, Geneva, Switzerland

Abstract

An overview is given of the Instrumentation at Isolde, an on-line mass separator that gets its protons from the PS Booster at CERN. One of Isolde's beam-lines now feeds isotopes to a 3MeV post-accelerator, called Rex. For Isolde the Instrumentation consists mainly of wire scanners, Faraday-cups and wire grids, but Isolde couldn't operate without a tape-station. Rex is equipped with Instrumentation boxes containing a collimator, a Faraday-cup and an imaging system. Some additional equipment is proposed.

INTRODUCTION

The ISOLDE on-line mass separator facility at CERN is mainly used for the production of pure samples of short-lived radioactive isotopes. It consists of two electromagnetic isotope separators, the General Purpose Separator (GPS) and the High Resolution Separator (HRS). One of the beam lines connects to Rex, a post-accelerator of 3MeV.

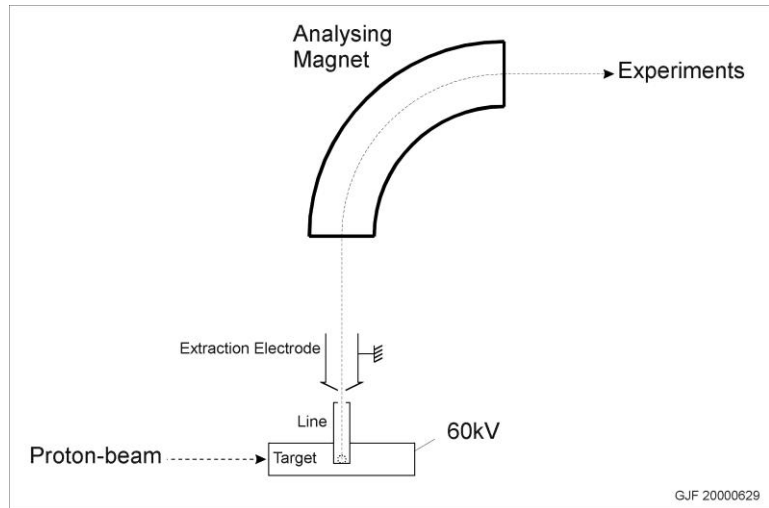
The radioactive nuclides are produced in a suitable target bombarded with the high intensity beam of 1GeV or 1,4GeV protons from the PS-Booster. The PS-Booster can deliver a beam-current up to 2 μ A. After ionisation and acceleration up to 60keV, the ions are mass analysed. The selected beam from either of the two separators is then fed into a beam transport system and steered to the experiments, or to Rex.

The aim of the beam instrumentation is to obtain information on intensity and profile of the low intensity (<10 μ A) d.c. ion beams all along the beam path. In the design of the ISOLDE mass separators attention was paid to provide access for beam observation at the most critical regions such as the entrance to the magnets and the different focal points. However, if one wants to introduce several probes and a slit in a given position the available space along the beam axis may be limited, in particular if the focusing is strong. Therefore they need to be compact in the direction of the beam. In addition, emphasis was put on the probes to be easily interchangeable and sufficiently radiation resistant because of the radioactive environment in which they have to operate.

For Isolde the beam detection is based on the deposition of electrical charge from the beam on a probe. Unless suppressed, the emission of secondary electrons enhances the measured current by a factor depending on the surface conditions and the species and charge of ions collected. Different are the Tape-stations with which radioactive particles can be detected by measuring their decay-products.

Rex uses an imaging device based on the secondary electron emission of the beam on a metal foil.

ISOLDE AND REX



The Isolde Separators

The General Purpose Separator (GPS) uses one analysing magnet; the High Resolution Separator (HRS) uses two. Until now more than 600 isotopes of more than 60 elements ($Z=2$ to 88) have been produced with half-lives down to milliseconds. Both machines use the same types of targets, which exist in several different configurations. The exchangeable targets have a heated container filled with the material to be radiated from which the resulting isotopes are extracted and ionised in the very hot "line". Normally the resulting charge per ion is +1, but Isolde can also be switched over to work with negative ions. This complete target-unit is held at a potential of 60kV, or lower if requested by experiments. The targets are exchanged with robots. With the high voltage between target-unit and the extraction electrode the ions are accelerated after which the wished mass is selected with the high precision analysing magnet.

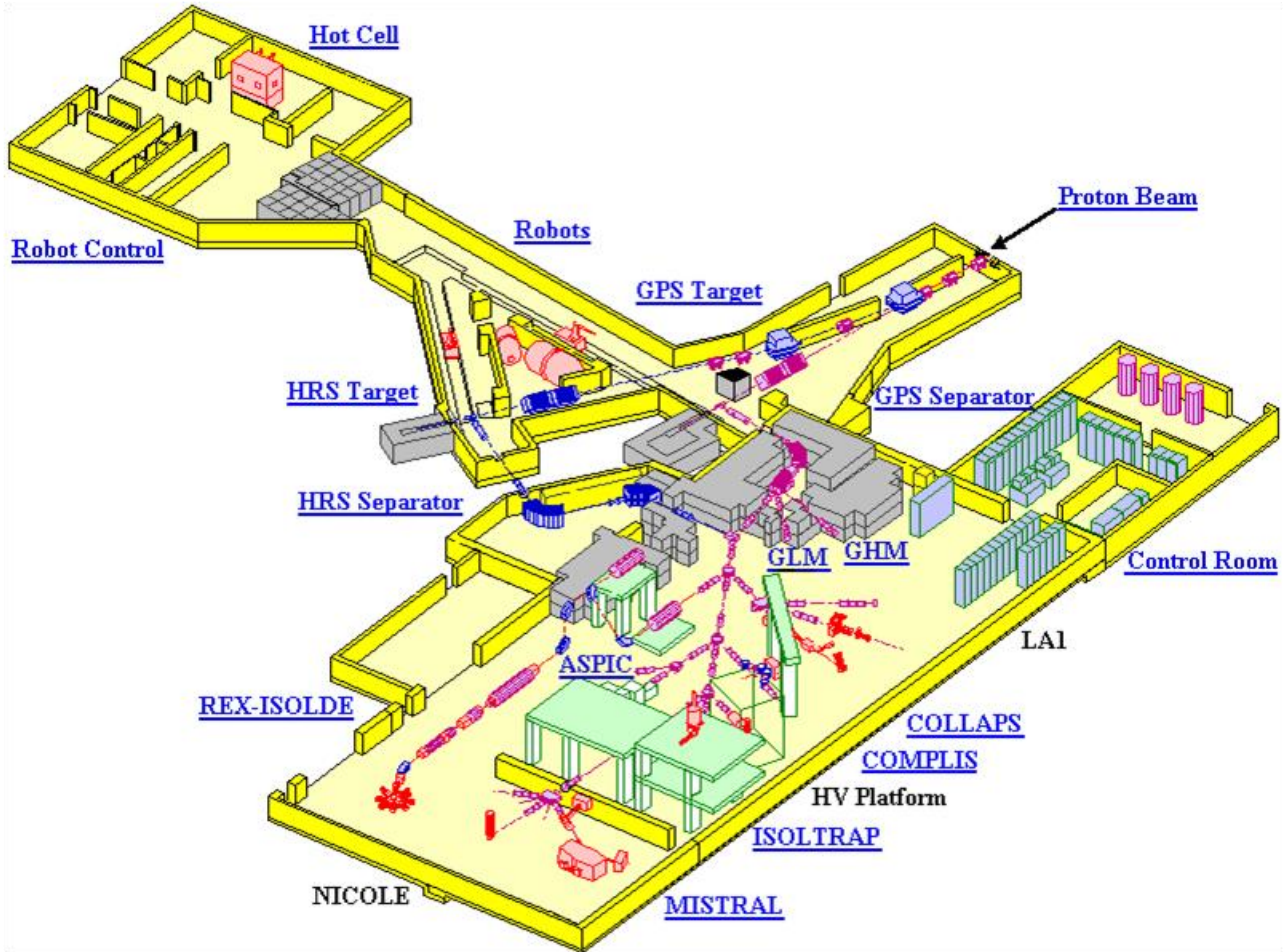
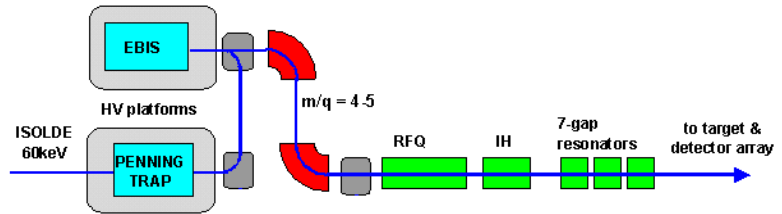
The HRS now has an RFQ to cool the beam, designed at Jyvaskyla.

The ion-beam intensities after the analysing magnets will typically be up to 10^{11} particles per second, but may be as low as a few particles per second and may exceptionally be higher, especially before the analysing magnets.

The GPS has three beamlines. Two beamlines can directly be used for experiments; the third beamline joins the HRS in a merging switchyard. From here the whole network of beamlines in the Isolde hall is fed, including Rex.

The Rex Post-accelerator.

Rex can only function with a pure beam such as provided by the HRS. First ions are trapped in a Penning-trap, then transported to “EBIS”, which is a charge-breeder. From there they are again mass-analysed and then accelerated up to 3MeV.



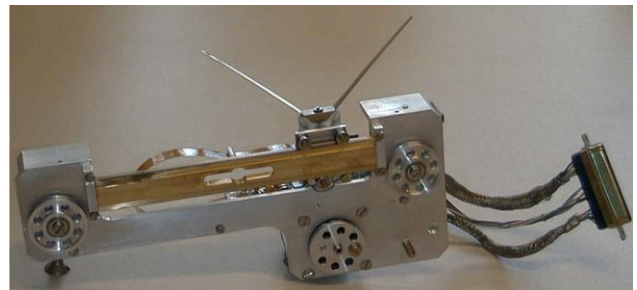
THE ISOLDE INSTRUMENTATION

Overview.

The Isolde instrumentation consists of Wire-scanners, Wire-grids, a “Fixed Needle Beam Scanner”, Faraday-cups and Tape-stations.

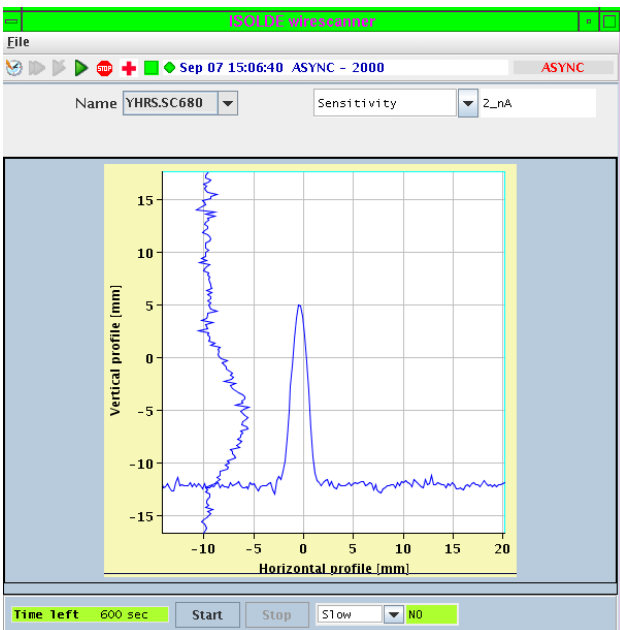
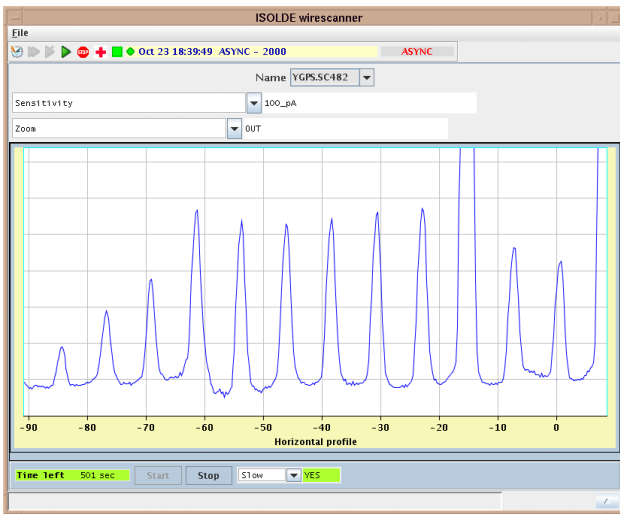
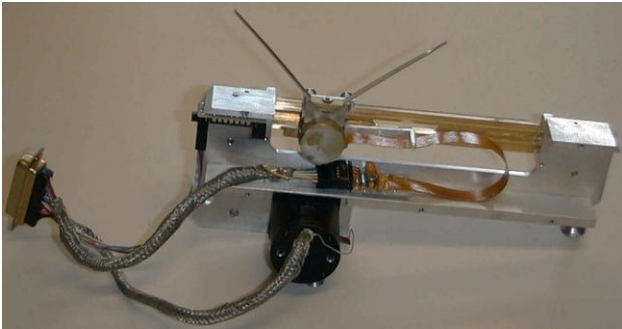
The Moving Wire-scanners.

The development of the Wire-scanners was started in the early 1980's by G. Sidenius and A. Lindahl at the Niels Bohr Institute in Copenhagen and since then it has been further improved at CERN. The pick-up needle is mounted on a small chariot which also carries the pre-amplifier. It is guided on a rail and driven back and forth by a stepping motor via a 0.1mm thick piano wire. There is only one position-reference and only one direction is used for data-taking to avoid the effect of mechanical hysteresis.



Most scanners at Isolde are x/y scanners. Equipped with a V-shaped pick-up (angle of 90°) the scanner chariot moves at 45° with respect to the horizontal plane thus producing both an x- and a y-scan of the beam profile. Originally equipped with pick-ups from Danfysik the pick-ups are now progressively being replaced by needles of material like that being used for medical syringes. The

stroke-length of these scanners is 97mm, which due to the 45° angle results in an effective length of 69mm.



There is one horizontal scanner with a stroke-length of 97mm and there are four horizontal scanners with a stroke-length of 182mm. All these horizontal scanners are mounted in areas with higher radiation, therefore the 182mm scanners are mounted in pairs for redundancy and

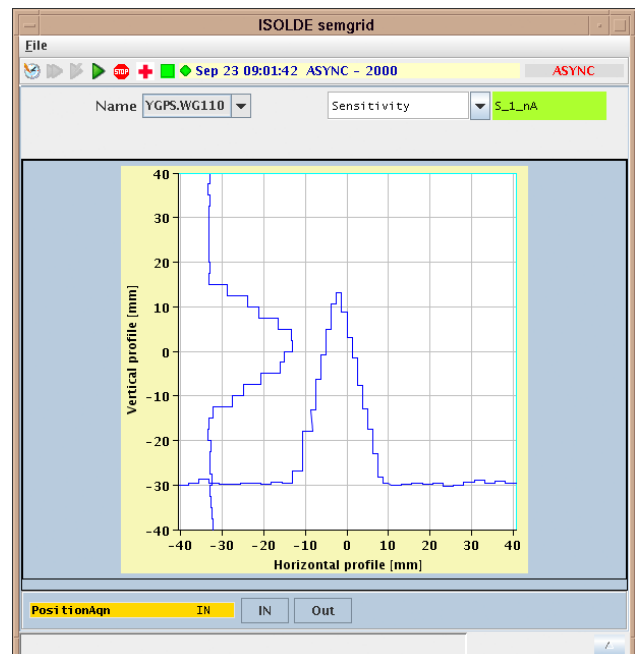
the 97mm is mounted close to a wire-grid, where must be remarked that the resolution of the scanner is so much higher than the grid's that the operators felt quite lost when the scanner was temporarily out of service.

The maximum electrical input current of the scanners is 20µA full scale, the lowest current range is 25pA. The scanners can move at speeds of 1m/s. they are normally used with 200mm/s while taking data and up to 800mm/s to return to its origin position. For high sensitivity (200pA or less) both the bandwidth of the amplifier and the scanning speed are reduced.

Wire-grids.

Wire-grids are used in those areas close to the targets where the radiation levels are too high for the scanners with their incorporated electronics. Five grids have wire-spacing's ranging from 1,25mm to 2,5mm and cover area's of 75 by 75mm. Then there are two grids of 20 horizontal wires with a wire-spacing of 1mm, combined with a fixed slit and a hole. The grids are moved in and out pneumatically.

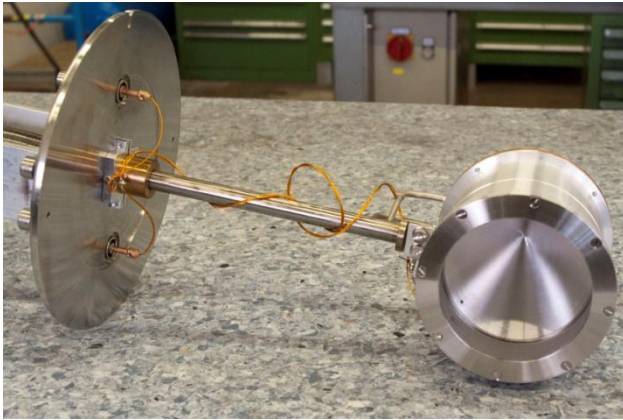
The electrical sensitivity ranges from 20pA full scale to 2mA. The latter was defined in a time that high output targets were expected. Until yet the study about how much energy the wires would be able to stand has not yet been started, but it seems unlikely that they would survive and luckily such targets were never constructed at Isolde (yet). For the highest sensitivities the system uses an integration time of 1 second.



Faraday-cups.

Faraday-cups are used everywhere at the separators, the beamlines and Rex. Both GPS and HRS Frontends each have one large Faraday-cup. The latest design for the new Isolde Frontend has an opening of 75mm. This Faraday-cup is prepared for water-cooling so that it would stand a

beam of 2mA. As for now such beams don't exist at Isolde the water-cooling will not yet be used.

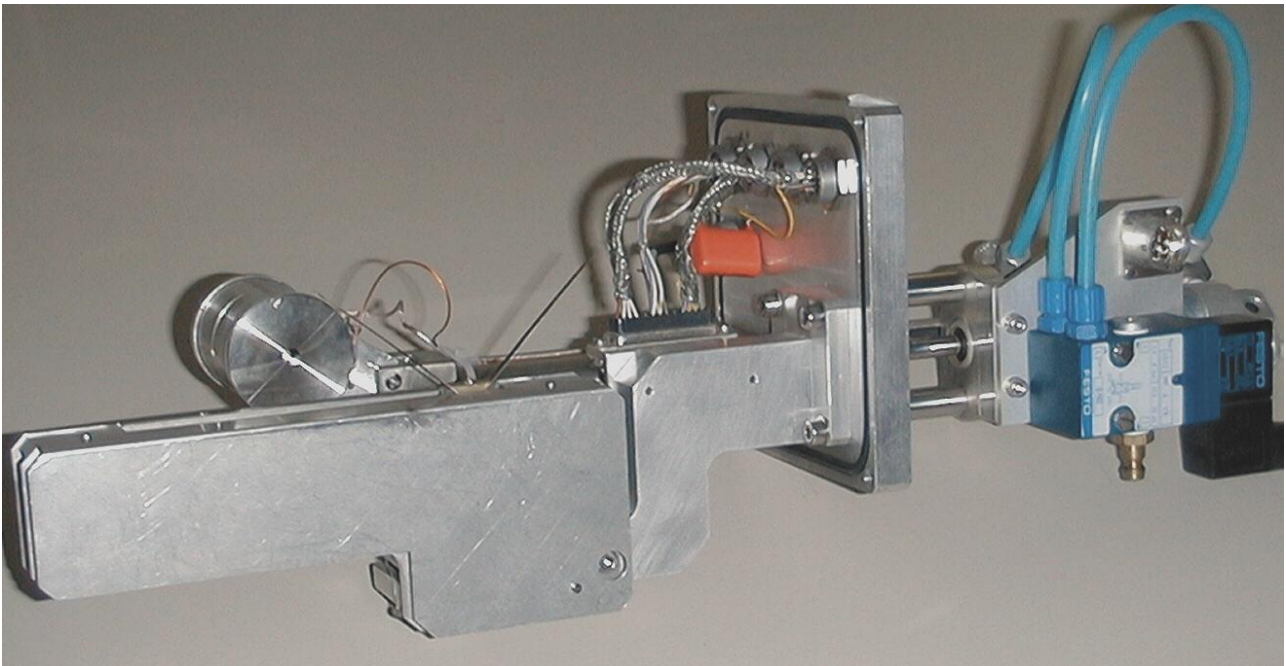


All other Faraday-cups have an opening of 25mm. Isolde counts 32 Faraday-cups and at the moment 9 are installed at Rex. Many of the 25mm Faraday-cups are

mounted on a flange together with an x/y scanner and form the standard instrumentation device used at Isolde.



The repeller voltages used for the Faraday-cups vary from 130V for the small ones to 250V for the large ones.



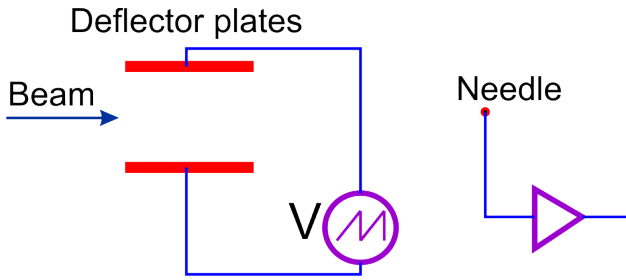
The readout of the Faraday-cups is done with Keithley electrometers and multiplexers. Though the Keithley devices themselves are very good, they can function properly only in electrically very clean environments. At Isolde the cables are too long, not of the best materials and pulled along all other cables, thus causing a background level of sometimes up to 2pA. At Rex the situation is better and noise-levels allow to measure down to 0,5pA. But at Rex the beam is pulsed, which the Keithleys can handle at very low input-currents, but not at more than 1nA. A special device has now been developed and is actually being tested at Rex-Trap. This device, called "PicoAmpèreMeter" or "PAM", solves the different problems by integrating over longer periods. The sensitivity of the "PAM" is not very special, in practice it allows to

measure down to 0,2pA. The integration time is programmable from 200ms to 1s. The device is small, mounted close to the Faraday-cup and also contains a miniature power supply for the repeller voltage and can control the pneumatic movement of the Faraday-cup. It is controlled via Profibus.

The "Fixed Needle Beam Scanner".

Problems with the Isolde wire-scanner are the vibrations of the mechanical movement causing electrical noise, the "inaccuracy" of the mechanics (even if that is smaller than 0,2mm) and the relative thickness of the pickup or needle. The "Fixed Needle Beam Scanner" (FNBS) is meant to provide more accurate measurements. The needle is replaced by a wire of 0,05mm and the mechanical movement is replaced by an electrostatic devia-

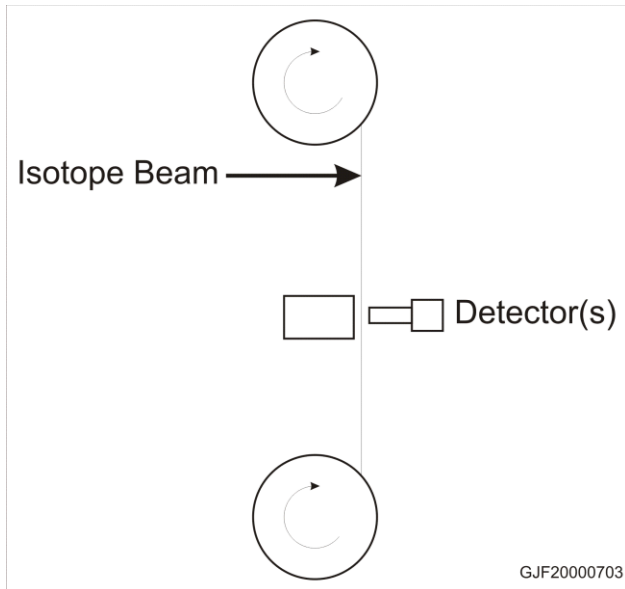
tion of the beam. The only mechanical movement remaining is the possibility to move the wire in and out the beam with a pneumatic movement. The maximum deviation of the beam is $\pm 9,8\text{mm}$, usually a deviation of maximum $\pm 5\text{mm}$ is chosen. Though the FNBS deviates the beam it doesn't quite stop the beam, but while it is active the beam will be distorted after the next focussing element. The FNBS is situated after the second analysing magnet of the HRS.



The Isolde Tape-stations.

A Tape-station allows to measure radioactive particles even if they cannot be seen by other beam instrumentation. The Tape-stations are used to:

- Optimise target and ion-source,
- Optimise the position of the proton-beam
- Measure half-lives of isotopes by using a Multi-Channel-Analyser. The latter now is part of the latest application program.



A Tape-station is very important at Isolde. Without it target and ion-source cannot be optimised which is equivalent to closing down the machine.

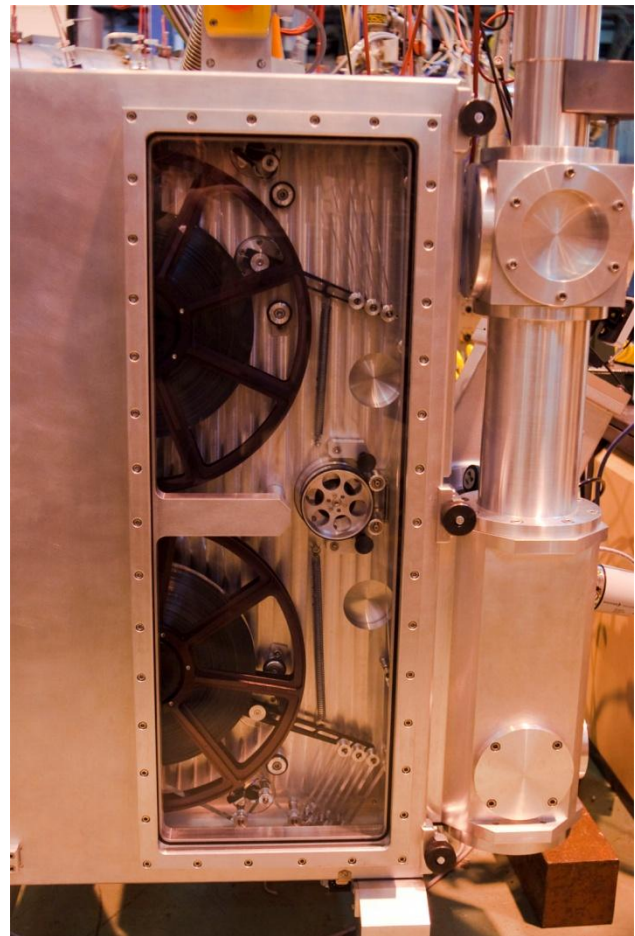
Important parts of the Tape-station are the timing and a good working beamgate. The beamgate will usually be closer to the target or at a spot that is suitable to dump the beam. The first step is to collect particles onto the tape. This collection may take place during a few milliseconds

up to seconds, it may be triggered by the arrival of a proton-beam pulse, or delayed, or be triggered by an experiment. After the collection the tape is moved as rapidly as possible to the detector(s), usually a scintillator and photomultiplier. While the detector(s) are counting a new collection may be made to gain time, allowing a series of measurements to be made to measure e.g. the release curve of the target.

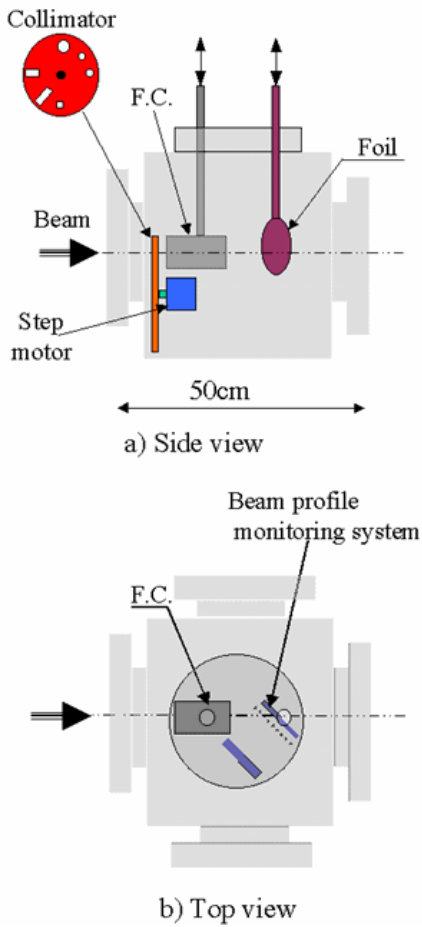
Isolde temporarily has two Tape-stations. The old one shall be removed when the new one is ready to take its place.

The original designs of the old Tape-station date from 1974. Though the mechanics are somewhat more recent, the electronics date from 1978 and were often modified. Though it runs better than ever this system isn't very reliable.

A new Tape-station has been developed by Philippe Dessagne and his collaborators at the IPHC (previously IRES) at Strasbourg. Modern, much more powerful and faster, this system will replace the old Tape-station once it has passed testing



REX INSTRUMENTATION



The Rex Instrumentation Box has been designed and manufactured by the Leuven University. At the moment 9

boxes are installed. Each box contains:

- A collimator,
- A 25mm Faraday-cup,
- An imaging system.

The collimator is a metal disc that can be rotated with a stepping motor. The disc has ten positions with different slits and holes and occasionally is used to insert filters in the beam.

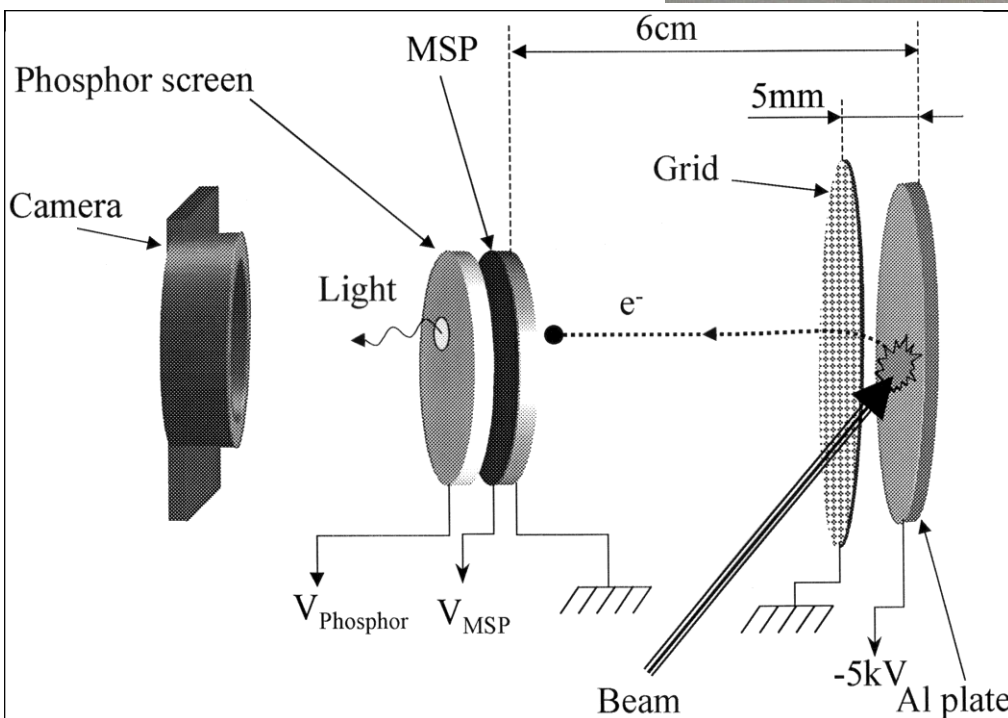
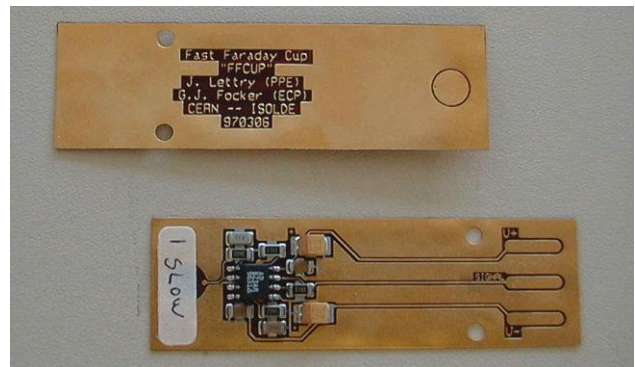
The imaging system is made with a metal foil placed in the beam at an angle of 45°. The secondary electrons are attracted by a close by mounted grid and travel to a MultiChannelPlate that is placed away from the beam. The amplified signals end at a phosphor screen that is filmed at again an angle of 45° by a CCD-camera.

A special case is where the foil is also used to measure currents directly. This setup is used at Rex-Trap for Time-of-Flight measurements.

SPECIAL INSTRUMENTATION

Special instrumentation that is used occasionally and is not connected to the control system.

The "Fast Faraday-cup".



What is called the "Fast Faraday-cup" isn't a Faraday-cup really, but merely a collector-plate as the repeller electrode is missing. It is made on a thin Kapton PCB, on one side the pickup electrode is situated and on the other side the electronics. The PCB is placed in a small brass housing that is moved in and out manually. The output connects to an oscilloscope. The bandwidth depends on the chosen amplification and can be up to 10MHz. The device was made in 1997; by

simply replacing the operational amplifier by a more modern type it should be possible to increase the bandwidth and/or the input sensitivity.

The NTG Emittance meter.

The NTG Emittance meter uses moveable slits, one vertical and one horizontal, and wire-grids. Though it is an enormous device, it is moved around everywhere to check any new or modified installation. Hence it is not permanently installed but yet quite regularly used.



CONCLUSION

Designing the Isolde Beam Instrumentation (mainly by E. Kugler, now retired) had as goal to make a user-friendly system, and relatively easy to repair. Though the standard scanner/Faraday-cup unit is easy to replace, the horizontal scanners are not, though rather due to the radiation levels. The scanners are very sensitive equipment and many make many more scans than what they were designed for. But the ones that are well-made seem to keep forever and the past years a lot of effort has been put in improving those that kept breaking down. Since last year's experience one may now carefully say that the effort carries its fruits, no mechanical problem has occurred.

The system could always be improved by increasing the sensitivity of the detectors. But then this is rather an environmental problem than a limitation of the electronics.

A device that is missing in the Isolde instrumentation is a small Allison scanner (a compact emittance-meter) like used at Triumf in Vancouver. Such a device could stay permanently in the machine and in places where the NTG cannot be installed, like for instance between the two analysing magnets of the HRS. A project was started, but does not advance at this moment.

I'd like to thank Thierry Stora and Erwin Siesling (both CERN) for their information helping me to write this document.

REFERENCES

[1] G. J. Focker, F. Hoekemeijer, O.C. Jonsson, E. Kugler, H. L. Ravn, CERN, Geneva, Switzerland, "The Beam Observation System of the ISOLDE Fa-

cility", BIW94, Vancouver, 2-6 October 1994. AIP-proceedings Vol. 333, p. 196

[2] G. J. Focker, E. Bravin, S. Bart Pedersen, CERN, Geneva, Switzerland, "The Renovation Of The Isolde Instrumentation", DIPAC'95, Lyon, June 2005, http://accelconf.web.cern.ch/AccelConf/d05/PAPER_S/POW003.PDF.

[3] E. Kugler, D. Fiander, B. Jonson, A. Przewloka, H. L. Ravn, D. J. Simon, K. Zimmer and the ISOLDE Collaboration, "The new CERN-ISOLDE on-line mass-separator facility at the PS-Booster," Nucl. Instr. and Meth. **B70**, 41-49 (1992).

THE GSI FACILITY AND THE LAYOUT FOR FAIR

Peter Forck for the GSI Beam Diagnostics Group, GSI, Darmstadt, Germany, p.forck@gsi.de

Abstract

The facility for achieving low energy radioactive ion beams or highly charged stable ion beams at GSI is briefly described. Using the HITRAP LINAC, deceleration down to 6 keV/u is foreseen for the collection of ions within an electro-static trap. Based on the present experiences, the layout of the projected FAIR facility is described.

THE PRESENT GSI FACILITY

This paper gives a short overview of the existing GSI facility to prepare the subject for the contribution of this workshop covering installations at GSI. The main purpose of the GSI facility is the acceleration of all ions from proton to Uranium with a very wide spectrum of beam parameters, see Fig. 1. Three ion source locations are operated, fulfilling different requirements concerning pulse length for fixed target beam delivery from the LINAC and the high current operation for the synchrotron SIS. The beams from the ion sources are bunched and accelerated by an RFQ and further accelerated by the efficient drift-tube LINAC of IH type. An increase of the charge state is achieved at a kinetic energy of 1.4 MeV/u e.g. in the case of Uranium from U^{4+} to U^{28+} . After a further acceleration to 11.4 MeV/u within an Alvarez DTL, a second stripping can be used to increase the charge state by a foil stripper, e.g. for Uranium to U^{73+} .

generation of a broad spectrum of in-flight Radioactive Ion Beams RIB, which are then investigated with different spectroscopic methods. The detection of beams slowed down by material interaction is discussed within the frame of this workshop [1]. The other extraction method from the SIS is a bunch-to-bucket transfer to the Experimental Storage Ring ESR. The charge state of the ions can be increased by a foil-stripper installed within the transfer line between SIS and ESR, the ion's kinetic energy of 300 to 500 MeV/u is large enough for complete ionization, in the case of Uranium to U^{92+} . Various nuclear and atomic physics experiments are performed with stored highly charged ions at the ESR. Electron and stochastic cooling is applied to decrease the beam emittance significantly.

The deceleration of heavy ions from the injection energy of about 300 MeV/u down to 4 MeV/u in the ESR is of interest for this workshop. Emittance enlargement is associated with the deceleration and beam cooling is required to keep the beam within the acceptance of the ESR. At injection level stochastic cooling is applied, while at an intermediate step of 30 MeV/u electron cooling is most efficient. In total about 60 s are required for the preparation of a beam of about 10^6 to 10^7 highly charged ions at a low energy of 4 MeV/u.

THE HITRAP FACILITY

The deceleration from 4 MeV/u to 6 keV/u is performed by the HITRAP facility [2, 3], for which the stepwise commissioning started in 2007 using different ion beams. This LINAC comprises of two bunchers, an IH-DTL and an RFQ as well as the ion trap are depicted in Fig. 2. The pulse length of the beam extracted within on turn inside the ESR is about 3 μ s. Bunches are formed by two bunchers operate at the base frequency of 108 MHz and the 2nd harmonics of 216 MHz. The functionality and a proper efficiency had been demonstrated [4]. The bunched beam is transported to an IH cavity, which is known as an efficient accelerator type for heavy ions. The nominal output is 0.5 MeV/u and deceleration was demonstrated [4]. However, the efficiency is only about 10 % which is lower than expected and a contamination of particles decelerated only to about 2.4 MeV/u was detected. The appearance of different beam energies is caused by the sensitive beam dynamics of the IH-DTL. To isolate the particles with the right energy of 0.5 MeV/u for further deceleration a horizontal dipole magnet will be installed in spring 2010 between the IH and RFQ. After this step the beam-based tests of the RFQ are foreseen with injection of a pure 0.5 MeV/u beam.

The beam diagnostics used at this decelerator is described in further articles at this workshop [5, 6] and in conference proceedings [7]. One has to state that a

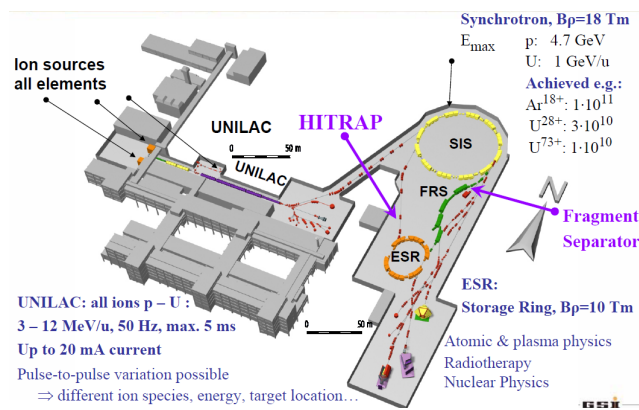


Figure 1: The existing GSI facility comprising of the LINAC UNILAC, the synchrotron SIS, the Storage Ring ESR and the target locations.

For further acceleration the ions are injected into the synchrotron SIS having a maximum magnetic rigidity of 18 Tm. This rigidity corresponds for heavy ions to about 1 GeV/u, where extraction is performed in two different manners: Either the beam is slowly extracted within typically some seconds to fixed target experiments. Namely, the Fragments Separator is used for the

commissioning of a LINAC with a repetition time of only 60 s is quite unusual and calls for reliable beam diagnostics.

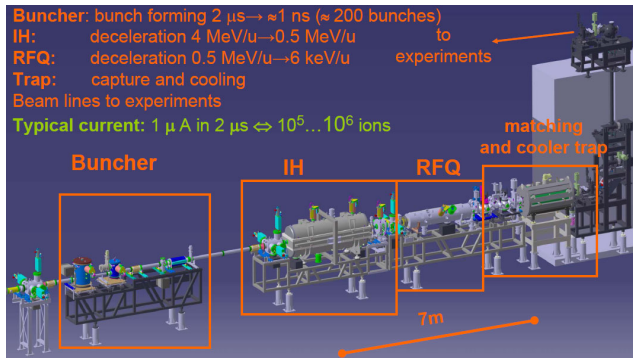


Figure 2: Sketch of the HITRAP LINAC and the Cooler Trap.

THE FAIR FACILITY

The Facility for Antiproton and Ion Research FAIR is the approved future project to be installed at the GSI site [8]. It will be the mayor facility for different communities using stable heavy ions, RIBs or anti-protons. The general layout is shown in Fig. 3. The existing GSI facility with UNILAC and SIS18 will serve as the injector chain delivering high current beams. Due to the scaling of the space charge limit in synchrotrons with the square of the ionic charge q^2 , higher currents will be accelerated with low charge states; for the design ion Uranium it will be U^{28+} . To reach the optimal energy for in-flight RIB production of about 1 GeV/u the synchrotron SIS100 with 100 Tm rigidity will be built, equipped with superconducting dipole and quadrupole magnets. The RIB production will take place at an optimized Super Fragment Separator S-FRS with a larger acceptance and therefore a factor of 100 higher transmission compared to the existing Fragment Separator. The radioactive ions can be investigated at fixed target locations including a low energy branch for slowed down RIBs [1] or the ions can be transferred to the Collector Ring CR or the New Experimental Storage Rings NESR for experimental investigations of stored high energy beams. Moreover, stable isotope beams can be stored in the NESR for various atomic physics investigations with highly charged ions.

REFERENCES

[1] P. Boutachkov, these proceedings (2009).
 [2] H.-J. Kluge et al., 'HITRAP: A Facility at GSI for Highly Charged Ions', Advances in Quantum Chemistry, Volume 53, p. 83 (2008).
 [3] O. Kester et al., Proc. LINAC 2006, Knoxville, p. 189 (2006).

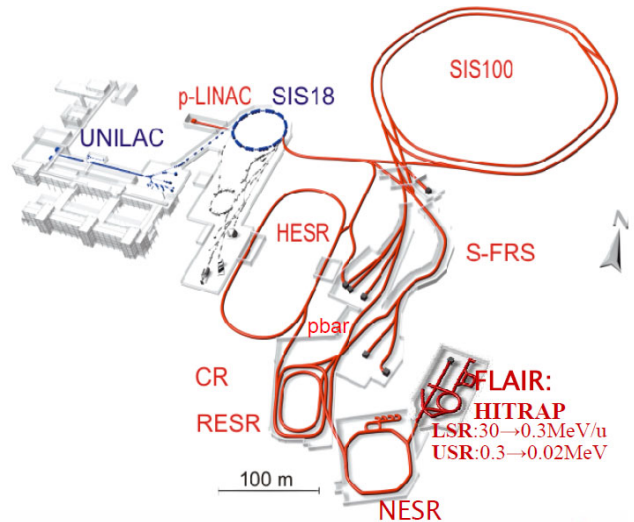


Figure 3: Sketch of the FAIR facility (red) and the existing GSI injector (blue).

Beside the program based on positive charged ions, versatile experiments with anti-protons are foreseen. A new p-LINAC is required because the UNILAC is optimized for large charge-to-mass ratio and will not deliver high currents of protons. After passing SIS18 these protons will be accelerated to 30 GeV in SIS100 and target generated anti-protons of 3 GeV kinetic energy will be stochastically cooled in the Collector Ring CR, the design intensity is 10^7 anti-protons per pulse. They will be either transferred to the High Energy Storage Ring HESR for high energy investigations or to the NESR for further deceleration. The latter branch is of interest here: Inside the NESR the anti-protons should be cooled and decelerated to 30 MeV. They can be transferred to the Low Energy Storage Ring LSR, which might be a re-installation of the existing CRYRING from Stockholm [9]. The task of this ring is further deceleration down to 0.3 MeV and a transfer to the modified HITRAP facility or to the Ultra Low Storage Ring USR, which is basically and electro-static ring, see [10] for more details.

The FAIR complex will be realized within several steps and a modular concept was recently accepted by the contributing international partners.

[4] L. Dahl et al., Proc. LINAC 2008, Victoria, p.100 (2008).
 [5] M. Witthaus et al., these proceedings (2009).
 [6] J. Pfister et al., these proceedings (2009).
 [7] J. Pfister et al., Proc. LINAC 2008, Victoria, p.564 (2008) and J. Pfister et al., Proc. EPAC 2008, Genoa, p. 3449 (2008).
 [8] see: www.gsi.de/fair/index_e.html
 [9] A. Källberg et al., these proceedings (2009).
 [10] C. Welsch et al., these proceedings (2009).

Beam Diagnostics for the HITRAP Decelerator

DITANET-Workshop "Low Current, Low Energy Beam Diagnostic" / 23.- 25. Nov. 2009

M. Witthaus, H. Reeg, C. Andre, P. Forck, R. Haseitl, W. Kaufmann, GSI, Darmstadt, Germany

Overview

In the six HITRAP beamtimes between May 2007 and April 2009 several diagnostic devices were used for the detection of low energy and intensity beams. The aim of the experiments was to extract the ions from the ESR into the HITRAP beam-line, and to guide it from the IH-structure to the third diagnostics chamber in front of the RFQ. The beam line from the RFQ to the Cooler TRAP and experimental area is currently still under construction [1].

The HITRAP poses three challenges:

- a single beam pulse with length of 3 μs
- a low beam intensity (in the μA region / $1\text{E}6$ particles per pulse)
- a low repetition rate (1 pulse every 60 to 70 seconds),

due to which it is necessary to work with different beam diagnostic devices like Faraday-Cups (FC), scintillation screens, harp systems (SEM-profile grids) and capacitive pick-ups in different locations at the HITRAP beamline [2]. Beam current transformers are not used, because their resolution (in the μA range) is not high enough.

Hardware Setup for Faraday-Cups

The HITRAP beamline from ESR to the RFQ is currently equipped with 3 FCs in each diagnostic chamber. Current-amplifiers DHPCA-100 (FEMTO Messtechnik GmbH, Berlin) are used, offering sufficient bandwidth for the given time structure of the extracted pulse. The gain range setting is controlled by a LabVIEW application (National Instruments Co.) and a Remote-Desktop-PC at the GSI control room (CR). The analogue signals are monitored by a LeCroy 6030A oscilloscope. This oscilloscope is controlled also by the Remote-Desktop PC at the CR. The pressure drives of FCs are controlled by the standard console-program via the GSI control system.

Measurement-Results with FCs

In spite of the low HITRAP beam current, all FC-systems could detect and display adequate beam signals with a time resolution down to 100 ns depending of the gain setting of the current-amplifier. The blue trace in Fig. 1 shows the FC signal of a $1.5 \mu\text{A}$ Ne^{10+} beam pulse.

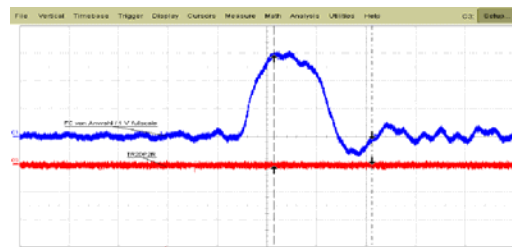


Fig. 1: FC signal (blue) recorded with 1 $\mu\text{s}/\text{Div}$ and 0.5 $\mu\text{A}/\text{Div}$.; Ne^{10+} , $\sim 1.8 \cdot 10^6$ particles

Hardware Setup for Scintillation Screens

To monitor beam positions and profiles, YAG scintillation screens with a diameter of 70mm are installed in the same locations as the FCs. The YAG material offers a good light yield at low energy. The screens are observed by CCD digital cameras (Marlin F033B, Allied Vision Technology) equipped with an IEEE1394 (Fire Wire) interface. The data acquisition was programmed in LabVIEW, while the Graphical User Interface is done in C++ using Qt libraries [3]. The software provides a raw image of the screen with an overlaid grid, as well as projections of the beam in horizontal and vertical direction for each camera. Fig. 2 shows an image of the scintillation screen with a beam spot, and the calculated profiles in x-/y direction. The image of the screen can be changed to B/W and false-colour display, where the latter shows more details from the YAG screen.

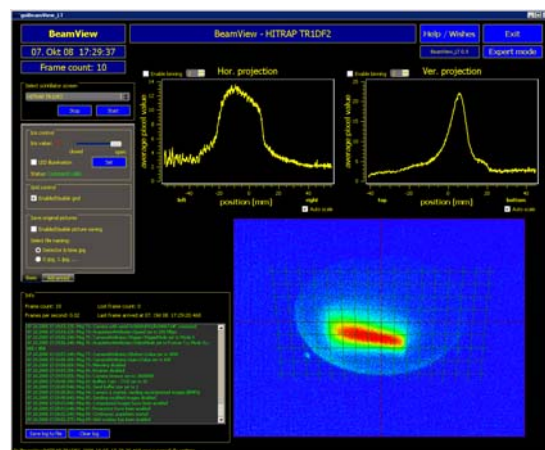


Fig. 2: Scintillation screen software – "BeamView"

A precise triggering of the digital camera allows using fast scintillation materials and the detection of short beam pulses with low repetition rate. The pressure drives of scintillation screens are operated by standard software at the HITRAP-PC-console (CR).

Measurement-Results with Scintillation Screens

The optical system and the YAG-screens are sensitive enough to acquire reasonable images for each individual shot. The beam profile data in dependence of the quadrupole lens settings have been used to estimate the beam emittance in the HITRAP DDB section, resulting in $3 \cdot 10^{-6}$ mm mrad at 4 MeV/u, approximately. After the decelerating IH-structure and the following dipole magnet (steerer), different energies produced in the IH-structure were detected. Fig. 3 shows two separated spots on the YAG-screen as caused by the varying energetic composition of the beam and the separation by a dipole magnet. These spots are not detectable with harp systems, or capacitive pick ups. The harps are limited in resolution because of the wire spacing. Pick-ups will not work correctly if the beam has different energies. So the scintillation screens are very important for HITRAP operating, and they were used extensively during the last beamtimes.

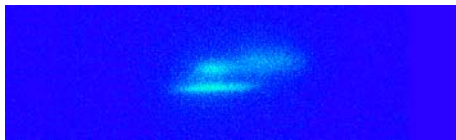


Fig. 3: Image for a scintillation screen behind the IH-structure and dipole magnet. The image shows two beam spots with 2.3 MeV/u (top) and 4 MeV/u (below); Ion species was Ne^{28+} .

Hardware Setup for Harp Systems

In addition, three secondary electron emission harp systems (SEM-grids) are installed in the same three diagnostic chambers as the FCs and the scintillation screens.

The harp systems are operated via the GSI control system and standard software. One big advantage of the harps is that they offers a transmission of about 93% as given by the wire spacing of 1.5 mm and the wire thickness of 0.1 mm, Therefore, it is possible to do measurements at different locations at the same time.

Measurement-Results with Harp Systems

Fig. 4 shows a measurement with all harps at HITRAP at the same time. Harp 1 is on the top of this Figure and in the first diagnostic chamber of the HITRAP beamline.

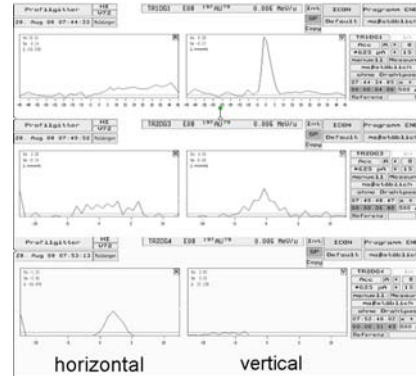


Fig. 4: Beam profiles, measured in August 2008 (Au^{79+}), taken in the lowest range (625pA, "Soft"-zoom)

Harp 2 is in the middle. Harp 3 is after the IH-structure and here in the bottom part of this Figure. The beam passes the first harp (number 1, top) and then through the second harp (middle) and the third harp (number 3, below). The result shows that the measurement with harps is not very practical in the HITRAP lattice. The intensities were too low, and the operating was heavily affected and therefore the screens, which shows sufficient signal strength are used in most cases.

Hardware Setup for Tubular Pick-up

A capacitive "tubular" pick-up is used in front of the first buncher, for monitoring the time structure of the extracted beam from the ESR.

The signal cable is routed directly to a high impedance amplifier (1M Ω , 150 MHz bandwidth, HVA-S, FEMTO). The amplifier's output is displayed on a single oscilloscope channel. This oscilloscope is as well controlled via remote desktop connection from the CR.

Measurement-Results with Tubular Pick Up

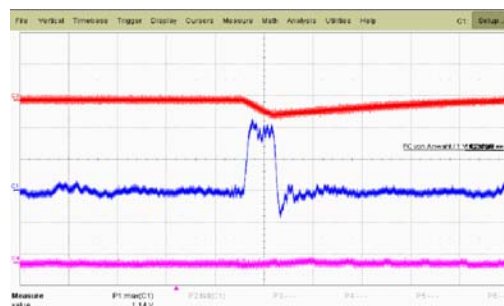


Fig. 5: Tubular pick up signal (red trace), with FC-signal (blue trace); the beam grazed the pickup's electrode.

Usually, the tubular pick up shows an output signal similar to a FC, but Figure 5 shows that this did not happen. The reason is, that the ring plate was hit directly by secondary electrons.

Hardware Setup for Ring Pick Ups

After bunching the macro-pulse passes a first "time of flight" (TOF) measurement section, consisting of two successive capacitive pick-ups with 50Ω termination, suited for the 108 MHz bunch frequency. The second TOF measurement section is located behind the decelerating IH-structure. Signals from bunchers and pick-ups are displayed simultaneously and time-correlated by a LeCroy 6100A oscilloscope.

Measurement-Results with Ring Pick Ups

The operating was affected by the insufficient characteristics of the pick up system. In the beamtime of Oct. 2008 the TOF measurements were possible, but it was necessary to activate the averaging mode of the oscilloscope. Figure 6 shows an image of the oscilloscope screen with typical output signals from two pick-ups.

The signal could only be detected by averaging of 6 measurements, resulting in a waiting time of about 7 minutes. For an effective operating this is not useful.

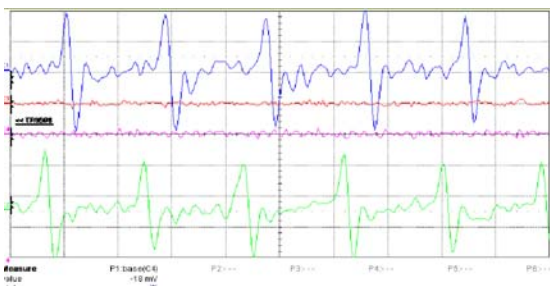


Fig. 6: Pick-up signals after averaging of 6 measurements at a time; the time scale was 5 ns/div and 20 mV/div, the beam current was $\sim 1.5 \mu\text{A}$.

Unfortunately, in most of the cases measurements were not possible with the ring pick-ups. Two typical and noisy signals of the pick-ups are shown in Figure 7. Several different attempts to achieve a signal like in Figure 6 were not successful. It is assumed that the signal/noise ratio was too low due to cable losses and mixture of different energies and non-uniform beam delivery.

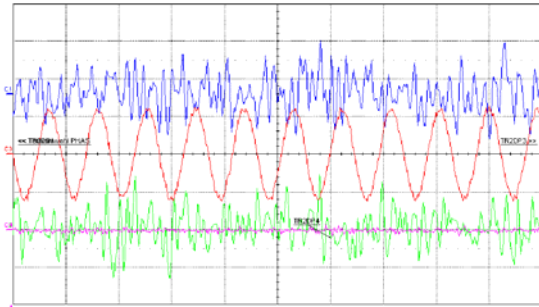


Fig. 7: Pick-up signals (blue and green trace). The red trace is the RF-reference. The time scale was 10 ns/div and 20 mV/div,

Summary and Outlook

Low energy and intensities were measured successfully with the FCs. A calculation of the particle transmission and time-resolved measurements were possible.

In addition, the scintillation screens were very helpful, and essential for operating. The detection of beam position was possible down to 300nA beam current and short ($< 2\mu\text{s}$) beam pulses.

The TOF-measurements are very important for operating, but the sensitivity of these devices is presently not high enough.

In March 2010 the next beamtime will be launched.

At the moment the beam diagnostic department works on some upgrades of the different pick-up devices. One suggestion is to reduce the length of the tubular pick-up.

For the 50Ω impedance pick-ups low noise pre-amplifiers between devices and transmission lines are foreseen, which will improve the signal/noise-ratio by 6dB.

References

- [1] O. Kester et al., GSI-Scientific Report 2007.
- [2] Beam Diagnostic for HITRAP, GSI-Scientific Report 2007; C Andre, et al.; Page 106
- [3] R. Haseitl et al., Proc. DIPAC 2009, Basel p. 134 (2009).

HITRAP Low Energy Diagnostics and Emittance Measurement*

J. Pfister[†], U. Ratzinger, IAP, Goethe-University Frankfurt, Frankfurt am Main, Germany
O. Kester, MSU/NSCL, East Lansing, MI 48824, USA
G. Vorobjev, GSI, Darmstadt, Germany

Abstract

The Heavy Ion TRAP (HITRAP) facility at GSI Helmholtzzentrum für Schwerionenforschung in Darmstadt is in the commissioning phase. Highly charged ions up to U^{92+} provided by the GSI accelerator complex will be decelerated and subsequently injected into a large Penning trap for cooling to the meV/u energy level. A combination of an inversely operated IH- and RFQ-structure decelerates the ions from 4 MeV/u to an intermediate energy of 500 keV/u and then down to 6 keV/u [1]. This contribution concentrates on construction of two new low energy diagnostics, use of a diamond detector as well as some emittance measurements.

THE HITRAP LINAC

After deceleration and cooling of the mainly bare or H-like ions down to 4 MeV/u in the experimental storage ring (ESR), they are ejected every 30-50 seconds via the transport line towards the HITRAP linac (see fig. 1). The Double-drift buncher is the first cavity of the HITRAP linac and is used for phase focussing. It was commissioned during two beam times in 2007. The following structure is the interdigital H-Mode structure (IH) - a special kind of drift-tube linac - that decelerates the ions down to 500 keV/u. Its initial commissioning took place in August 2008 with a partially cooled heavy $^{197}\text{Au}^{79+}$ beam [2] and was continued with various Nickel and Xenon beams. The RFQ and Cooler trap are still waiting for commissioning. Regarding beam diagnostics new devices had to be developed for being able to measure these low energy and low intensity beams during the deceleration process. A single-shot pepper pot emittance meter and a diamond detector were installed for transversal emittance and longitudinal bunch structure measurements.

NEW LOW ENERGY DIAGNOSTIC DEVICES

Due to the mixture of energies behind the IH-structure, new low energy and low intensity diagnostics had to be developed.

MCP-based Single-shot Emittance Meter

A new pepperpot emittance meter for low energy and low intensity beams has been designed and built. As the

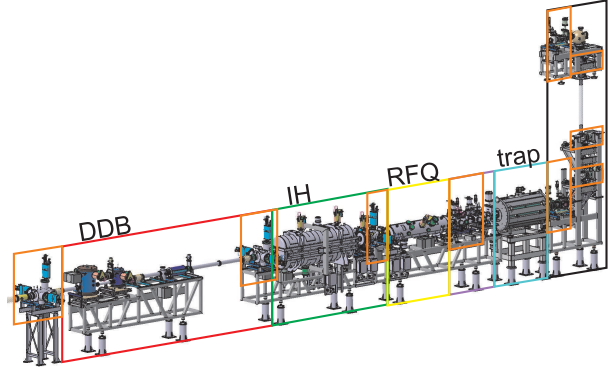


Figure 1: HITRAP linac. All sections are titled: Double-drift buncher (red), IH-structure (green), RFQ (yellow), Cooler Penning trap (cyan), beamline to experiments (black) and diagnostics (orange).

amplifying element a micro channel plate (MCP) has been chosen. It is only single plate for reaching the best spatial resolution possible. The gain of about 10^4 is enough to detect the predicted intensities. The pepperpot aperture is a $100\ \mu\text{m}$ thick Tungsten foil. The 29×29 holes with a diameter of $100\ \mu\text{m}$ were drilled with a laser. The spacing between the holes is 1 mm in both directions x and y . The transmitted ions are drifting 31.8 mm before hitting the MCP and then being detected on the backside on a phosphor screen which is captured with a CCD camera from outside the vacuum vessel. A picture of the measurement head is shown in fig. 2

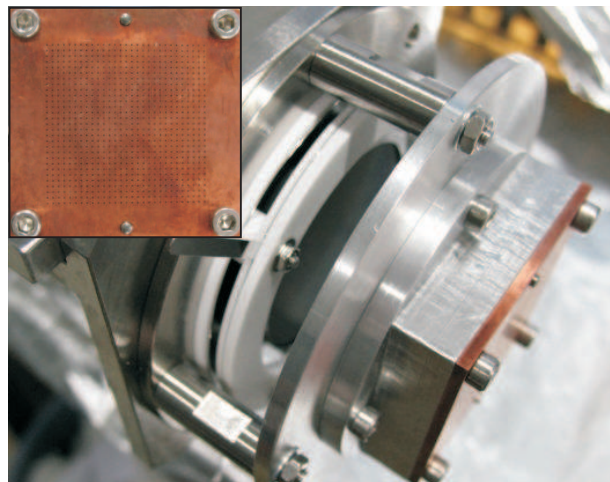


Figure 2: MCP pepperpot device. Copper: holder of the pepperpot, white rings: isolators of the MCP

* Work supported by BMBF under contract 06FY160I

[†] j.pfister@gsi.de

An evaluation software was previously developed. Some smaller adjustments have been done, though. The user has several possibilities for subtraction of noise during the evaluation process. Nevertheless the software can be operated in free-run mode with predefined settings.

The pepperpot measurement head is also equipped with a Faraday cup, which can also be used for current measurements in order not to destroy the MCP with too high current.

Diamond Detector

The complete diamond detector setup is built on a electronic printing circuit board. Four different diamonds are integrated. They are used according to their physical properties. Figure 3 shows the setup used at HITRAP.

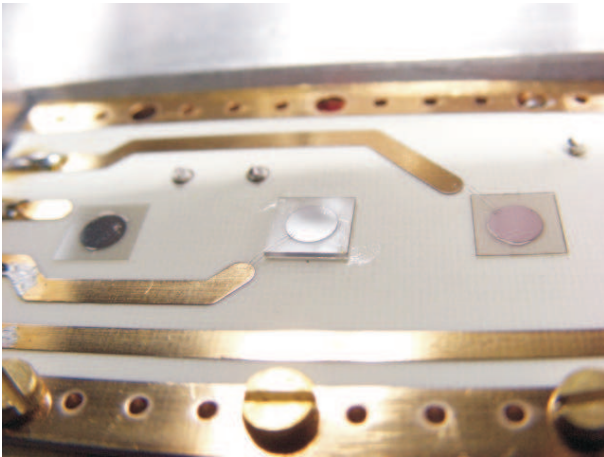


Figure 3: Diamond detector with three active areas. CVD-PC $10\mu\text{m}$, CVD-SC $480\mu\text{m}$ and CVD-PC $15\mu\text{m}$ (left to right). Diameter of metalization area: 3 mm. Diamonds are $5 \times 5 \text{ mm}^2$ each.

Single-crystal diamonds are thicker than the polycrystallines. They incorporate a better charge collection efficiency and therefore they are used for particle energy determination through analysis of the peakheight of the detected signal. In contrast polycrystalline structures are often thinner, which makes the charge collection efficiency worse than with single-crystals, because these structures act like small traps. Only charges created near the electrodes are collected effectively, that means that the signal is very fast but not proportional to the particles energy. Therefore polycrystals are used for time-structure measurements [3]. At HITRAP the following types and thicknesses of the diamonds are used:

- polycrystalline chemical vapour deposition (CVD) $10\mu\text{m}$,
- single-crystal CVD $480\mu\text{m}$,
- polycrystalline CVD $15\mu\text{m}$ and

- polycrystalline CVD $600\mu\text{m}$.

Each detector has an effective area of 3 mm in diameter. Results of these measurements are presented below.

Single-shot Energy Analyzer

The construction of the single-shot energy analyzer was triggered by the fact that not only decelerated ions exiting the IH-structure but also a big portion of non-decelerated particles reaching the intertank section. This makes analysis of beam properties difficult since the high energy signal is always overlaying the desired low energy signal. Since there is not enough space for installation of a big dipole magnet for scanning the energy spectrum, a single-shot energy analyzer was constructed and built. It consists of an horizontal slit (width 0.3 mm) and a permanent magnet of 0.5 T that is able to separate the 500 keV/u beam from all particles with energy higher than 1.3 MeV/u. This is not critical since the main energies that are transmitted are at 2.3 and 4 MeV/u. The particles then hit a Chevron-type micro channel plate, they are amplified and the resulting single-shot distribution is captured by a CCD camera. The setup is shown in figs. 4 and 5.

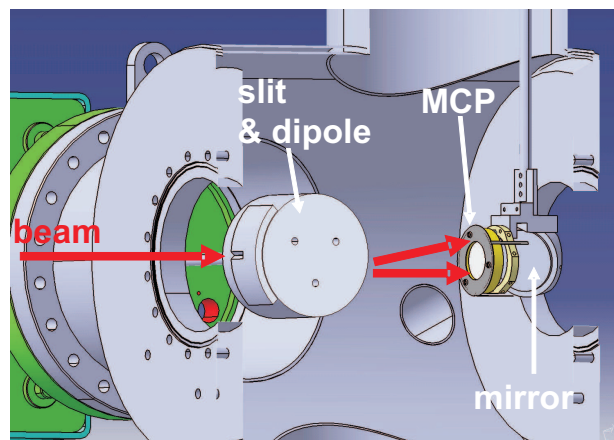


Figure 4: Schematic drawing: cut through the vacuum vessel housing the single-shot energy analyzer.

The dipole field was measured with a hall probe and was determined to be very homogenous (see fig. 6).

The influence of the permanent magnet on the beam, if moved out, is smaller than 0.1 mT on axis, which is a reasonable value.

MEASUREMENTS

During the last beam times three different kind of measurements had been performed. The emittance of the 500 keV/u beam behind the IH-structure was measured with the gradient method and the diamond detector, a test measurement with the new MCP-based pepperpot device

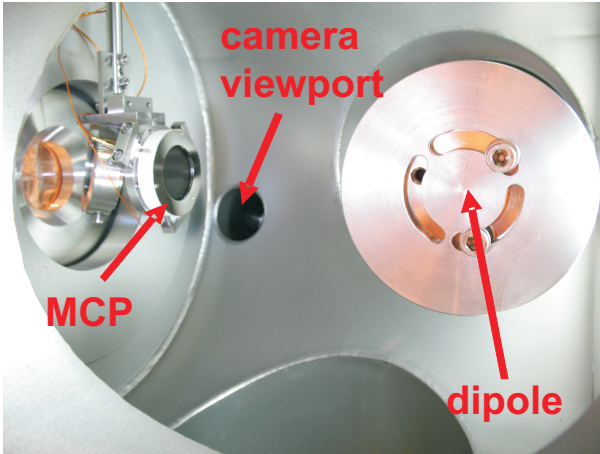


Figure 5: View of the single-shot energy analyzer.

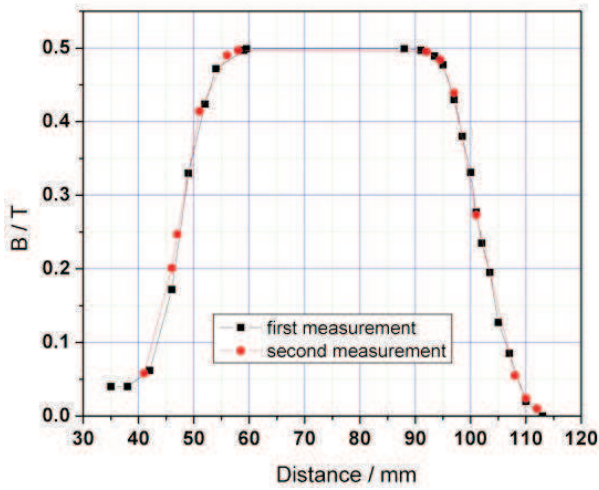


Figure 6: Homogeneity of the dipole field for the energy analyzer.

behind the RFQ and a bunch structure measurement in front of the IH.

3-Gradient Method

During commissioning of the IH-structure we were able to measure the emittance of the decelerated 500 keV/u ions behind the cavity. This was difficult because the structure also transports part of the beam non-decelerated which then causes troubles by detecting the underlying decelerated beam with no spatial separation. A steerer was used to separate the two beams by some mm and a 3-gradient emittance analysis was performed. The count rate on the sensitive diamond detector was always averaged over three consecutive shots. The determined beam radii together with the quadrupole gradients of the doublet are shown in table 1. With this data together with the beam transport matrices the vertical emittance of the decelerated beam is calculated to be $9.3 mm \cdot mrad$. The twiss parameters are calculated to be $\alpha = 1.15$, $\beta = 7.80 mm/mrad$ and

Table 1: Quadrupole gradients B' for emittance evaluation behind the IH in $[T/m]$ for $A/q = 3$. Radii are given in $[mm]$ and contain 90% of the particles.

gradients of quadrupole doublet	beam radius
33.6807 / 34.2925	6.22
30.3126 / 30.8633	3.89
26.9445 / 27.4340	2.11

$\gamma = 0.30 mrad/mm$. The phase space ellipse as well as restricting straight lines are plotted in fig. 7.

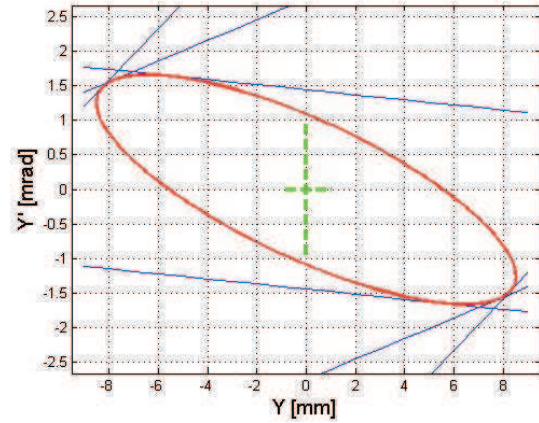


Figure 7: Phase space ellipse of 500 keV/u beam behind the IH-structure.

The three parallel line pairs in fig. 7 represent one gradient measurement each. The distance between the lines is equal to the beam diameter of each individual measurement and the rotation of the line pair is calculated from the transport distance from the lens to the target and the focussing strength of the lens.

Pepperpot Measurement

The MCP-Pepperpot emittance meter was placed behind the RFQ in a vessel of the low energy beam transport line. Some measurements were done with RFQ switched on and off and differences in emittance were measured. A sample of the captured images is shown in fig. 8.

Evaluation of this data resulted in the numbers given in table 2.

Table 2: Emittances measured behind the RFQ with RF on and off.

RF_{RFQ}	$\varepsilon_{x,90\%}$	$\varepsilon_{y,90\%}$
off	21.3	18.3
on	27.8	24.6

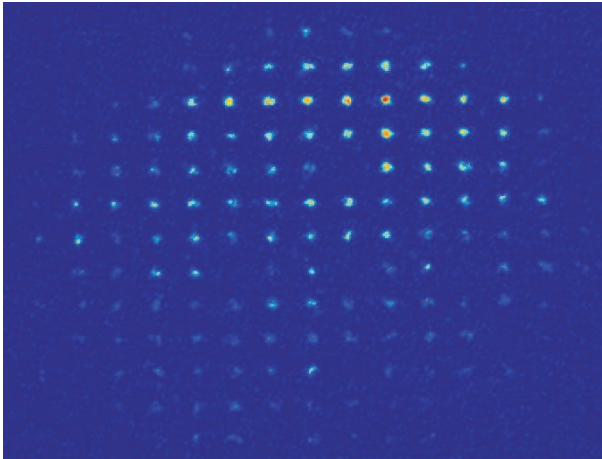


Figure 8: First picture from the MCP-Pepperpot behind the HITRAP-RFQ.

Since emittance grows with deceleration it seems that at least a part of the ions was decelerated by switching on the RF of the RFQ. A sample picture of the phase spaces is given in fig. 9

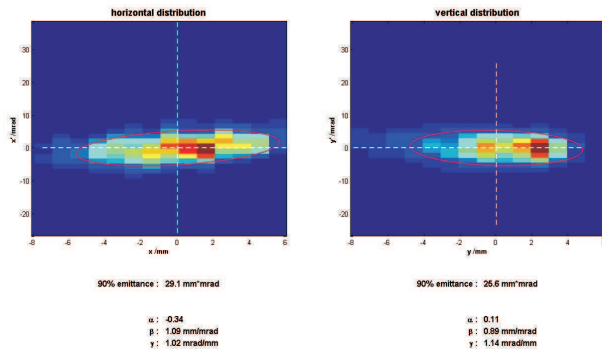


Figure 9: Phase space distributions from the first pepperpot measurement behind the RFQ.

Longitudinal Bunch Structure

The longitudinal bunch structure was measured only qualitatively. The diamond detector was used to show the arriving ions at the entrance of the IH-structure. The pictures of the macro bunch from ESR as well as the bunched ions are shown in figures 10 and 11.

OUTLOOK

Tests of the single-shot energy analyzer are ongoing and first online operation should occur during the next beamtime in spring 2010. This tool should make a fine tuning of the IH-structure possible in a fast and efficient way. During and after commissioning of the RFQ the MCP-based pepperpot emittance meter will measure again the emittance of the entirely decelerated beam.

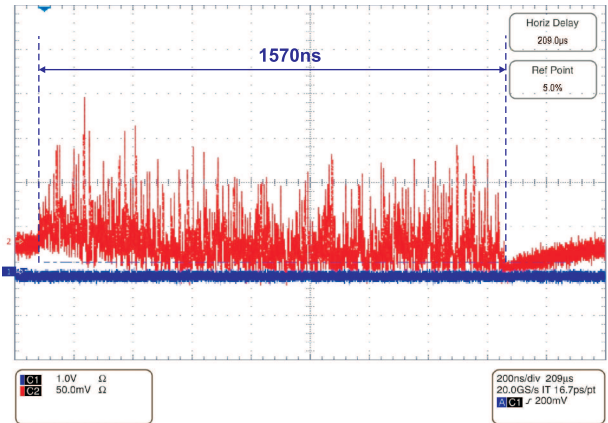


Figure 10: Macro bunch from ESR.

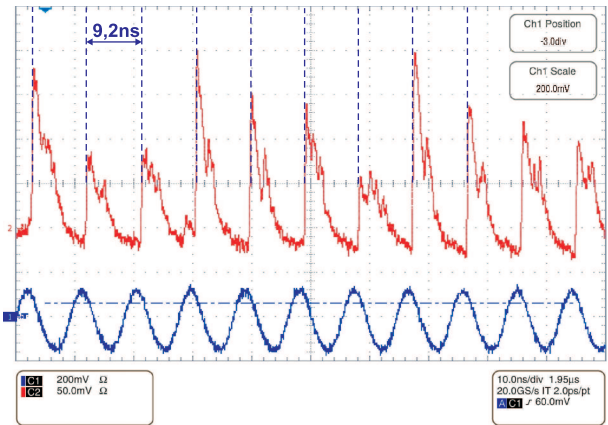


Figure 11: Bunched signal from diamond detector. Diamond signal of incoming ions on the diamond's surface (red) and 108 MHz RF-phase (blue).

REFERENCES

- [1] H.-J. Kluge et al., "HITRAP: A Facility at GSI for Highly Charged Ions", Advances in Quantum Chemistry, Academic Press, Volume 53 (2008) 83-98.
- [2] L. Dahl et al., "The HITRAP Decelerator Project at GSI - Status and Commissioning Report", Proc. of LINAC08 (2008) 100-102.
- [3] E. Berdermann et al., "CVD Diamond for Electronic Devices and Sensors", R.S. Sussmann (ed.), John Wiley & sons, England (2009) 227.

Operational experience with profile monitors for MeV and keV antiproton beams at CERN's Antiproton Decelerator

M. Hori and A. Soter

*Max-Planck-Institut für Quantenoptik, Hans-Kopfermann-Strasse 1, D-85748 Garching, Germany
Department of Physics, University of Tokyo, 7-3-1 Hongo, Bunkyo-ku, Tokyo 113-0033, Japan*

Abstract

In this talk we briefly overview some beam profile monitors used in CERN's Antiproton Decelerator to measure the profile of antiproton beams with keV and MeV-scale energies.

The ASACUSA (Atomic Spectroscopy and Collisions Using Slow Antiprotons) collaboration is currently carrying out various atomic physics experiments involving antimatter at the Antiproton Decelerator (AD) [1] facility of CERN. The AD delivers a 100-ns-long pulsed beam containing $N_{\bar{p}} = (3 - 4) \times 10^7$ antiprotons of kinetic energy $K = 5.3$ MeV, at a repetition rate $f \sim 0.01$ Hz. A radiofrequency quadrupole decelerator (RFQD) [2,3] is then used to further reduce the beam energy to $K \sim 10$ – 100 keV. This beam is used to synthesize antiprotonic helium atoms ($\bar{p}\text{He}^+ \equiv \bar{p} + \text{He}^{2+} + e^-$) [2,4–6] and ions ($\bar{p}\text{He}^{2+} \equiv \bar{p} + \text{He}^{2+}$) [7], and carry out precision laser spectroscopy [4,5,8] on them. In this paper, we describe several kinds of detectors [9–11] with position-sensitive electrodes which were used for this purpose.

A parallel plate ionization chamber (PPIC) [9] was constructed to monitor an antiproton beam of $K = 21$ MeV. It contained three parallel polyester foils of $1.5\text{-}\mu\text{m}$ thickness – an anode foil and two position-sensitive cathodes mounted at a distance 2 mm on either side of it. The foils were placed in a vacuum chamber filled with a mixture of 90% argon and 10% methane (P10 gas), at a low gas pressure $P = 6.5$ kPa which helped to minimize space-charge and recombination effects [12,13]. The antiproton beam was allowed to travel through the foils in a direction perpendicular to their surfaces.

The electron-ion pairs produced in the gas were accelerated between the foil electrodes. The position-sensitive cathodes consisted of 20 segmented strips of width 0.92 mm in each plane. The X- and Y- projections of the antiproton beam were obtained by using 40 charge sensitive preamplifiers to measure the charge induced in each strip. The electrodes were manufactured by sputtering gold

layers of thickness $t_d = 20$ nm onto the polyester foils. The strip patterns were cut by focusing the output of a Q-switched neodymium-doped yttrium-aluminium garnet laser of wavelength $\lambda = 1064$ nm on the foil. By slowly scanning this spot along the foil surface, $80\text{-}\mu\text{m}$ -wide lines were drawn where the gold was vaporized and the underlying polyester exposed. The polyester, being highly transparent at 1064 nm, was undamaged by the laser.

The PPIC was irradiated with 300-ns-long beam pulses containing $N_{\bar{p}} = 5 \times 10^7 - 1.4 \times 10^9$ antiprotons at the Low Energy Antiproton Ring (LEAR) facility of CERN. The number of antiprotons $N_{\bar{p}}$ in each pulse was roughly deduced from the anode signal, under the assumptions that, i): a 21-MeV antiproton produced ~ 30 ion pairs [14,9] in the PPIC, ii): the electrons were collected with unit efficiency by the anode. At fields of $E = 75\text{V/mm}$ applied between the anode and cathode, the collected charge became roughly equal to the value estimated above for an ideal ionization chamber. The horizontal and vertical centroid positions of antiproton pulses were thus measured, and systematic drifts in the beam position were studied [9].

We next constructed a parallel plate secondary electron emission detector [9], which measured the profiles of 5.3-MeV antiproton beams without the use of detector gas. As before, the detector consisted of an anode foil and two position-sensitive cathode foils. The foils were coated with a 50-nm thick layer of oxidized aluminium, which had a relatively large yield γ_e for secondary electron emission. These foils were placed in the vacuum pipe of the AD beam line, and evacuated to a pressure $P \sim 10^{-8}$ Pa.

When an antiproton struck a strip electrode on a cathode foil, an estimated $\gamma_e \sim 0.5$ – 1 [15,16] secondary electron were emitted. These were accelerated toward the anode foil

biased at 50–100 V. Charge sensitive preamplifiers measured the charge ejected from each strip. The spatial profile of the AD beam measured with the device was characterized by a dense core of cooled antiprotons of diameter $d = 5$ mm, surrounded by a large ($d > 20$ mm) halo. This result was in good agreement with emittance measurements of the antiproton beam circulating in the AD, which were carried out using a scraper detector [1].

The pulsed beam emerging from the RFQD [2,3] had an energy $K = 10$ –100 keV, a large diameter $d \sim 30$ mm, and contained $(5 - 8) \times 10^6$ antiprotons. At such low energies, parallel plate monitors could no longer be used since the antiprotons would stop in it. We therefore developed a secondary electron emission detector [10] based on grid electrodes of wires with diameter $d \sim 5$ –10 μm . This allowed most of the antiprotons to pass through without degradation, while a small portion (typically 1–2%) intercepted by the wires produced the signal. The monitor consisted of X and Y position-sensitive cathode grids, sandwiched between three anode grids with a distance $l = 2$ mm between them. Each grid consisted of 32 gold-coated tungsten wires stretched over a ceramic frame, with a pitch $\Delta x = 0.25$ –1 mm between neighboring wires. They were manufactured by first printing a pattern of gold readout microstrips with thickness $t_r = 30$ μm along the edges of the frame. An electrode tip made of tungsten pressed the microwire ends onto the corresponding microstrips. The wires were then embedded and fused into the microstrips by applying a pulsed current on the tip.

Due to the very small number of antiprotons intercepted by each wire, only ~ 1000 signal electrons were emitted from it per antiproton pulse. Of particular importance to achieving a high sensitivity in the charge-sensitive preamplifier [10] was the use of junction field-effect transistors with a low $1/f$ noise coefficient $K_f \sim 10^{-27}$ J, and a high transconductance gain $g_m \sim 50$ mS. The output voltage signal V_0 of the preamplifier was converted into a differential current one I_d using a transconductance amplifier. This signal was then transmitted from the preamplifiers to an active filter amplifier housed in a nearby electronic rack, over several meters of shielded twisted-pair cable [10,17]. The differential nature and low impedance of the signal ensured that any external interference picked up on the cable would not degrade the signal-to-noise ratio. This was essential because the monitor was used next to the RFQD, which was excited with MW-scale RF powers at frequency $f \sim 202.5$ MHz. The detector achieved an equivalent noise charge of $\varepsilon \sim 200$ electrons. This is within a factor 2 of the best values reported for any room-temperature detector of comparable capacitance $C_{\text{det}} \sim 10$ pF.

The monitor could also be used to measure the profiles of UV laser pulses, by employing the wires as photocathodes. Four such monitors were constructed, and operated in ultrahigh vacuum ($p \sim 10^8$ Pa), low temperatures ($T < 100$ K), and strong magnetic fields ($B > 0.1$ T) near an antiproton Penning trap [18]. A similar detector based on photon imaging of secondary electrons will be used in the Linac4

testbench facility now under construction at CERN [19].

This work was supported by the European Young Investigator Awards (EURYI) of the European Science Foundation and the Deutsche Forschungsgemeinschaft, and the Grant-in-Aid for Creative Basic Research of Monbukagakusho.

References

- [1] P. Belochitskii, Status of the Antiproton Decelerator and of the ELENA project at CERN, Proceedings of COOL 2007, Bad Kreuznach, Germany, 2007.
- [2] M. Hori *et al.*, Phys. Rev. Lett. 91 (2003) 123401.
- [3] A.M. Lombardi, W. Pirkel, Y. Bylinsky, First operating experience with the CERN decelerating RFQ for antiprotons, Proceedings of the 2001 particle accelerator conference, Chicago, 2001 (IEEE, Piscataway, NJ, 2001).
- [4] M. Hori *et al.*, Phys. Rev. Lett. 96 (2006) 243401.
- [5] M. Hori *et al.*, Phys. Rev. Lett. 87 (2001) 093401.
- [6] R.S. Hayano *et al.*, Rep. Prog. Phys. 70 (2007) 1995.
- [7] M. Hori *et al.*, Phys. Rev. Lett. 94 (2005) 063401.
- [8] M. Hori, R.S. Hayano, E. Widmann, H.A. Torii, Opt. Lett. 28 (2003) 2479.
- [9] M. Hori, Nucl. Instr. and Meth. A 522 (2004) 420.
- [10] M. Hori, Rev. Sci. Instrum. 76 (2005) 113303.
- [11] M. Hori, K. Yamashita, R.S. Hayano, T. Yamazaki, Nucl. Instr. and Meth. A 496 (2003) 102.
- [12] B. Jean-Marie, V. Lepeltier, D. L'Hote, Nucl. Instr. and Meth. 159 (1979) 213.
- [13] T.Z Kowalski, Nucl. Instr. and Meth. A 234 (1985) 521.
- [14] M. Agnello *et al.*, Phys. Rev. Lett. 74 (1995) 371.
- [15] D. Hasselkamp, H. Rothard, K.-O. Groeneveld, J. Kemmler, P. Varga, H. Winter, Particle Induced Electron Emission II, Springer-Verlag, Heidelberg, 1992.
- [16] S.P. Møller, *et al.*, Phys. Rev. A 56 (1997) 2930.
- [17] V. Radeka, Annu. Rev. Nucl. Part. Sci. 38 (1988) 217.
- [18] N. Kuroda, *et al.*, Phys. Rev. Lett. 100 (2008) 203402.
- [19] M. Hori, K. Hanke, Nucl. Instr. and Meth. A 588 (2008) 359.

DIAGNOSTICS AT CRYRING

A. Källberg for the CRYRING team at the Manne Siegbahn Laboratory, Stockholm, Sweden

Abstract

CRYRING, the storage ring for ions at the Manne Siegbahn Laboratory has been used for experiments with atomic and molecular ions since 1993. The beam diagnostics that is in use now, in 2009, towards the end of the lifetime of this ring, at least in Stockholm, is the result of developments during its around 20 years of use. These will be presented in this article, together with some experiences regarding the use of the diagnostic equipment that has been gained during this time.

OVERVIEW

CRYRING is a 52 meter accelerator/storage ring at the Manne Siegbahn Laboratory at the Stockholm University. Since 1993 it has been used to study a vast selection of atomic and molecular ions. Several different types of ion sources have been used to supply the desired ions to the experiments, such as an EBIS, an ECR and different discharge sources, mainly for the production of singly charged ions. Also a caesium-sputter ion source has been used to produce negative ions. The long list of ions that have been stored in the ring includes singly and multiply charged ions of masses from 1-208 amu, from protons to $^{208}\text{Pb}^{55+}$, at energies from 38 eV/u – 92 MeV/u. The full list of ions can be found at [1]. For many of these ions the intensities available from the ion sources have been very small, in some cases even below 1 nA. These low intensities have been a challenge for the diagnostics and have prompted necessary improvements of the sensitivity of the equipment which will be described in more detail in connection with the discussion of the different parts of the diagnostics below. A more comprehensive description of CRYRING can be found in [2,3].

The diagnostic equipment available in CRYRING consists mainly of the following parts:

Beamlines:

- Fluorescent screens
- Faraday cups
- Strip detectors

Storage ring:

- Faraday cups (one combined with a fluorescent screen)
- Electrostatic pickups
- Schottky detector
- DCCT (Bergoz)
- ACCT (ICT, Bergoz)
- Residual gas ionization beam profile monitor
- Neutral particle detectors

Most of the instruments in this list can be found also in most other storage rings, but I hope that a description of the different parts, together with some comments regarding our experiences and developments during the years, could be valuable for other users of similar equipment.

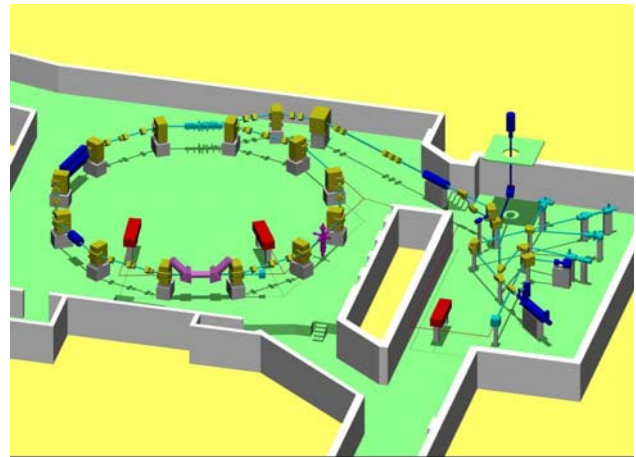


Figure 1: The CRYRING facility

BEAMLINE DIAGNOSTICS

The fluorescent screens used in the beamlines are of two kinds. Closest to the ion source a CsI(Tl) is used due to its high sensitivity, also for low energy ions. The other screens used are of the type called Chromox, from Morgan Technical Ceramics, made of aluminium oxide doped with chromium oxide. The main reasons for the use of Chromox screens in the beamline are their robustness and UHV compatibility. The outgassing properties of CsI(Tl) is not well known, but we suspect that it could be too high for a UHV environment, furthermore, they might not withstand the required baking temperature to 300°C. We do not exclude, however, that this material could also be used in a UHV environment, but in such a case, their properties would need to be tested. All the screens are covered with a thin metal mesh (95% transparency) to avoid charging up of the surface. The beam pulses after the RFQ is of the order of 1 ms long and intensities down to a few tens of nA can normally be seen on the Chromox screens when using standard video cameras. For ions with $Q/A < 1/4$, which are not accelerated in the RFQ and for which the RF amplitude used is much lower, we have used the possibility to increase the pulse length to be able to see weaker beams without exceeding the maximum average power that can be cooled away from the RFQ structure. since the light emitted from these screens is dark red, it is a good idea to increase the sensitivity of the camera by removing the IR filter that normally is

mounted in front of the detector of standard video cameras. Some darkening of the screens with exposure and a consequent loss of sensitivity has been observed, but not to an extent that frequent replacement of the screens has been necessary. The most important use of the screens has been to centre the beams in the quadrupoles by varying the magnetic fields and adjusting correction elements so the centre of the beam spot stays in the same place.

As an alternative to fluorescent screens, strip detectors are also used. They have the evident drawback that one only gets two one-dimensional profiles instead of a true two-dimensional picture. An advantage is that there is no need for an extra port with a window for a camera. Partly for historical reasons, there is only one strip detector in the beamline from the main ion source. However, in the beamlines from the EBIS as well as the one from the ECR source, they have been extensively used.

Faraday cups are used to measure the exact ion currents along the beamlines, and also in two positions in the ring, first inside the injection tank and then after almost one complete turn in the ring. After optimization of the current in the second cup, normally the beam is circulating when the cup is retracted.

RING DIAGNOSTICS

Electrostatic Pickups

As mentioned above, there are two Faraday cups in the ring. The rest of the diagnostics are non-destructive. There are nine pairs of electrostatic pickups. Initially, during the commissioning of the ring, these were essential for measuring and finding the corrections of the closed orbit of the beam, but once the basic settings of all the elements were found, we have mostly relied on scaling these parameters to find initial values that are good enough to store the beams. To improve the possibility to work with weak beams, four of the original preamplifiers have been replaced by state of the art low-noise amplifiers. These are home built and have input circuits with two FETs, type 2SK300, connected in parallel. The equivalent input noise is $5 \mu\text{V}_{\text{rms}} @ 10 \text{ MHz BW}$. The gain is 52 dB.

One of these pickups is used for optimization of the machine settings by maximizing the signal as measured by a spectrum analyzer set on zero span on the revolution frequency in the ring or a harmonic thereof. Since the optimization procedure often consists of making small changes of the settings of the elements while looking for improvements, a monotonous and tiring procedure for the operator, a LabVIEW program that performs these actions is instead used for the fine-tuning of the parameters. It systematically goes through a set of parameters which can be chosen by the operator and automatically stores any settings that give improved intensities. A screen shot of this program in action is shown in Fig. 2. Different input signals can be used, such as the pickup signal from the spectrum analyzer and the signals from the different

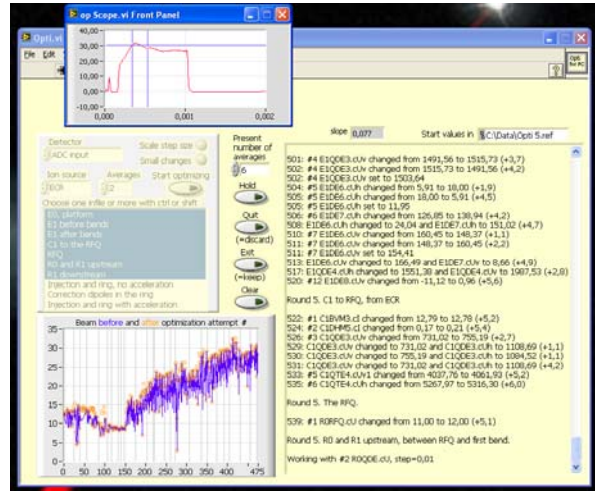


Figure 2: Screenshot from the automatic optimization program showing the result of several cycles of optimization.

Faraday cups. The history of the improvements can be found in the graph in the lower left corner of the screen.

Schottky Detector

The Schottky detector has mainly been useful for multiply charged heavy ions, since the signal is proportional to the ion charge squared. It is equipped with commercial low-noise amplifiers from Trontech. The most common uses of the detector are to monitor the intensity of the stored beam and to adjust the electron cooling. A particular use was the observation of ordering in the stored beam, which can be seen in Fig. 3, where the transition to a very narrow Schottky peak can be seen after 1000 seconds. [5]

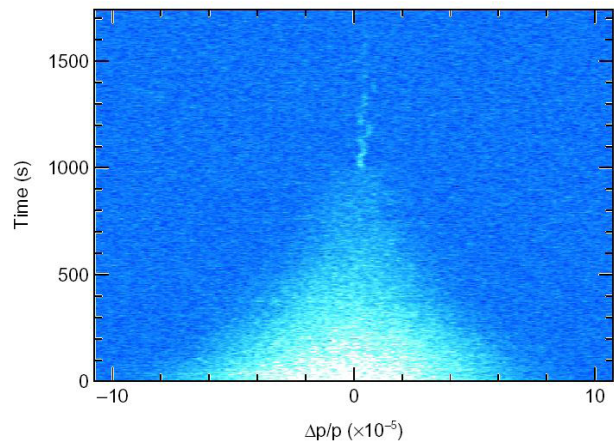


Figure 3: A sequence of Schottky spectra from a beam of Xe^{36+} ions showing the transition of the beam to an ordered state at around 1000 seconds.

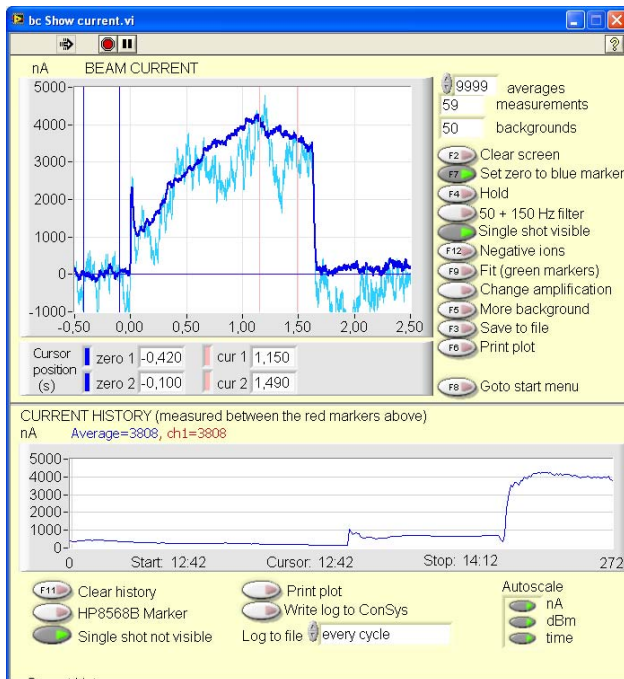


Figure 4: Screenshot from the LabVIEW program that is used for beam current measurements. This example shows injection, acceleration (1 s) and a short storage (0.5 s) of a beam of $^{19}\text{F}^{5+}$.

Current Measurements

Absolute measurements of the stored ion current in the ring are essential for many experiments. Two current transformers are used for this purpose, a DC Current transformer (DCCT) with which coating beams can be measured and an Integrating Current Transformer (ICT) which is used to measure pulsed beams. Both are manufactured by Bergoz Instrumentation. The DCCT has a noise level which is approximately 1 μA peak-peak while the noise of the ICT is more like a few nA. To improve the signal to noise levels, the signals from the transformers are in general averaged over several injections into the ring. Also, the background signal from the ramping of the magnets during acceleration normally needs to be subtracted. Another LabVIEW program is making this process easy. A screenshot from this program is shown in Fig 4. The original preamplifier of the ICT has been replaced by a home-built one with lower noise (1 nVrms/ $\sqrt{\text{Hz}}$) and higher gain (80 dB). Also the integrator electronics has been replaced by a new version with gate widths with a ratio of 2:1, instead of the original 1:1 to make it easier to fit the signal from the bunch inside the measuring gate. Further details of the improvements made on the ICT can be found in [4], where also the use of the signal from an electrostatic

pickup to extend the measurement range down to even lower beam currents is described.

Beam Profile Monitors

Two residual gas ionization beam profile monitors are installed, one for the vertical profile and one for the horizontal. These monitors detect ionized residual gas molecules that are created in collisions between the stored ions and the residual gas molecules. An electric field transports these ions towards a set of Micro Channel Plates (MCPs) from which a spatially resolved image of the area where collisions are taking place, i.e. of the beam trajectory, is obtained. The resolution is clearly less than 1 mm. This instrument is a very useful tool, in particular for optimizing the electron cooling. As can be seen in Fig. 5, it has also been used to measure the transverse cooling time [6].

Another MCP based detector, placed in the zero-degree exit of the straight section after the gas target, is used to register neutral particles. Since neutrals are created from collisions between stored singly charged ions and the residual gas molecules, this detector has been very useful to monitor the number of stored ions.

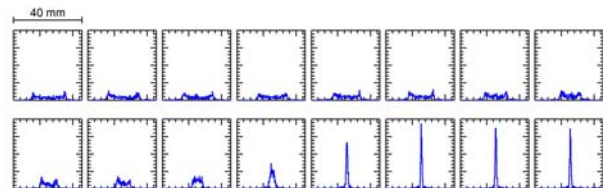


Figure 5: Vertical profiles of an F^{6+} beam during successive 61-ms intervals, starting 61 ms before the electron beam is realigned with the ion beam and cooling begins.

REFERENCES

- [1] http://www.msl.se/msl_files/ionlist.html
- [2] K. Abrahamsson, et al., Nucl. Instrum. Methods, B 79 (1993) 269.
- [3] http://www.msl.se/MSL_files/cryring.html
- [4] A. Paal, et al. "Bunched Beam Current Measurements with 100 pA rms Resolution at CRYRING", EPAC'06, Edinburgh, June 2006, TUOPCH08, p. 1196 (2006); <http://www.JACoW.org>.
- [5] H. Danared, et al. "One-dimensional Ordering in a Cold Heavy Ion Beam", EPAC'02, Paris, June 2002, THPLE120, p. 566 (2002); <http://www.JACoW.org>.
- [6] H. Danared, et al. "Studies of Transverse Electron Cooling", EPAC'00, Vienna, June 2000, WEOAF101, p. 301 (2000); <http://www.JACoW.org>.

Development of detectors for slowed down beams at GSI

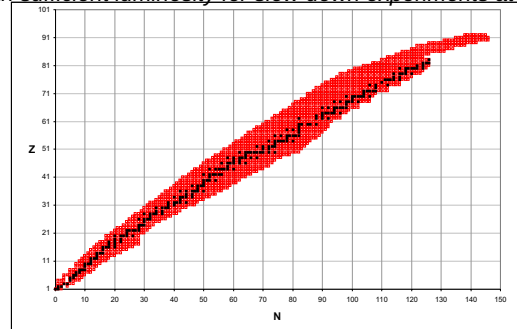
P. Boutachkov
 GSI Helmholtzzentrum,
 Helmholtz International Center for FAIR

- Physics objectives
- Proposed solution
- Test experiments. Detector development
- Future development

Project objective

Obtain **5 MeV/u to 10 MeV/u** RIB to be used for secondary reaction studies at FRS / Super FRS

RIB with sufficient luminosity for slow down experiments at S-FRS

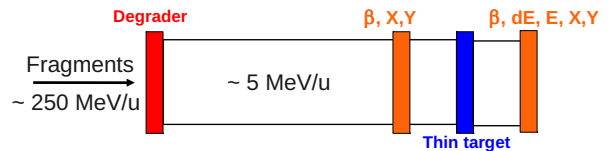


Development of slowed down beams around the world

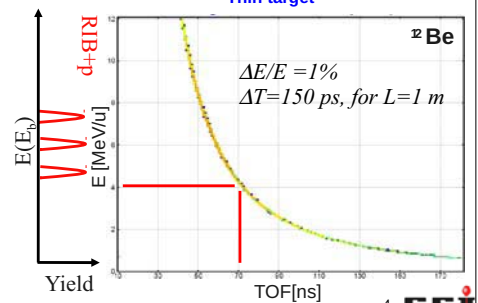
Fusion enhancement with neutron-rich RIB, $^{32,38}\text{S} + ^{181}\text{Ta}$,
 slowed from **9 MeV/u to ~ 4 MeV/u**
 K.E. Zyranski, et al. PRC **55**, R562 (1997)

High-spin states in ^{48}Ca , using 5 MeV/u ^{46}Ar beam
 slowed from **30 MeV/u to 5 MeV/u**
 E. Ideguchi, et al. EPJA **25**, 429 (2005)

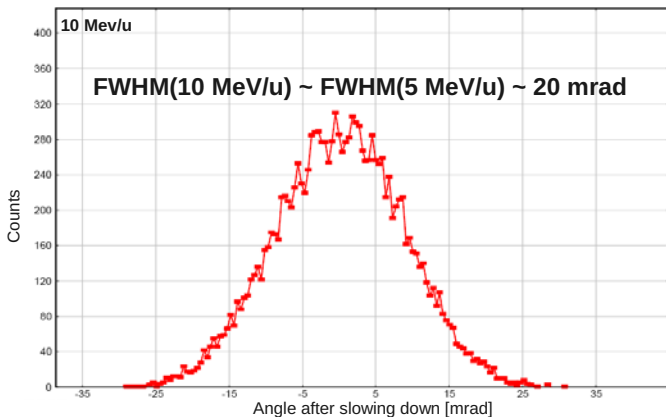
Simple binary reactions performed with white beam



- Energy straggling
 - Angular straggling
- Event-by-event tracking

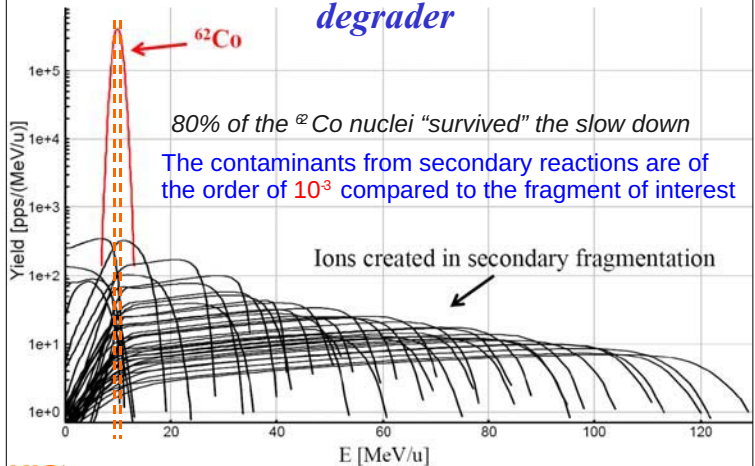


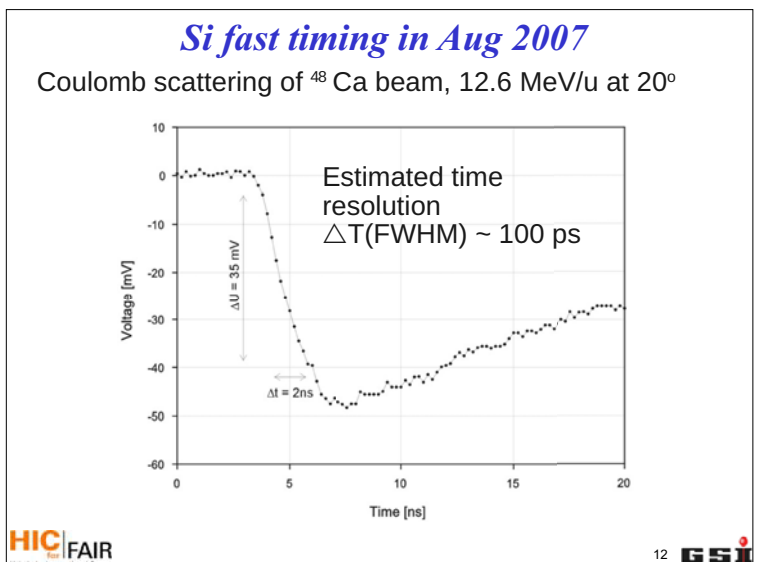
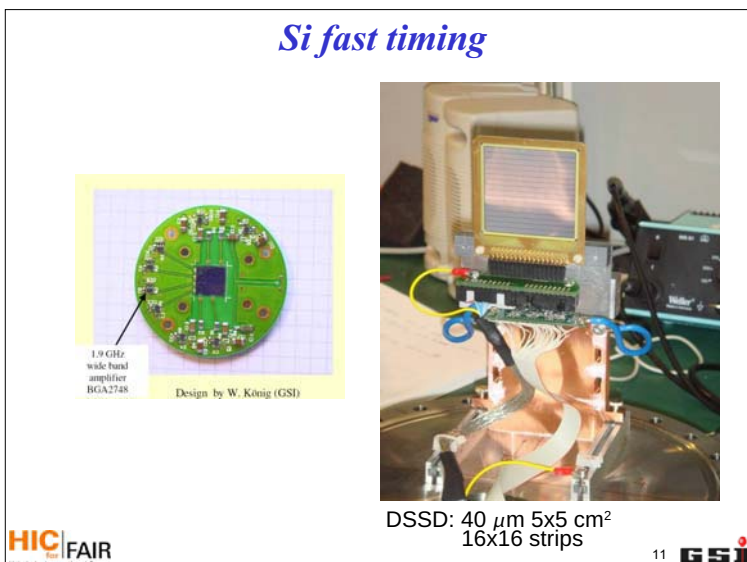
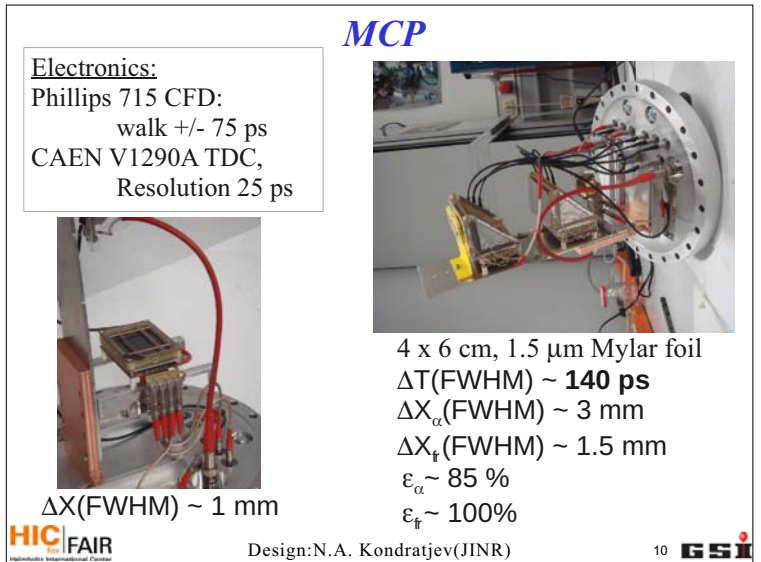
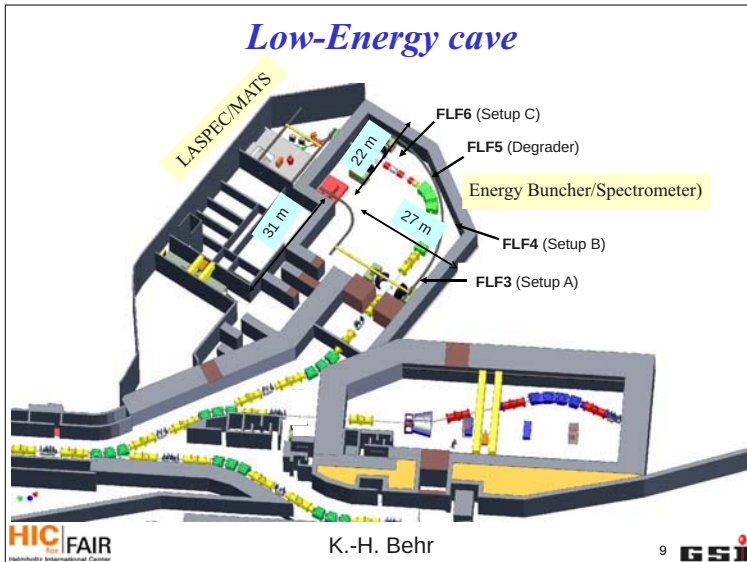
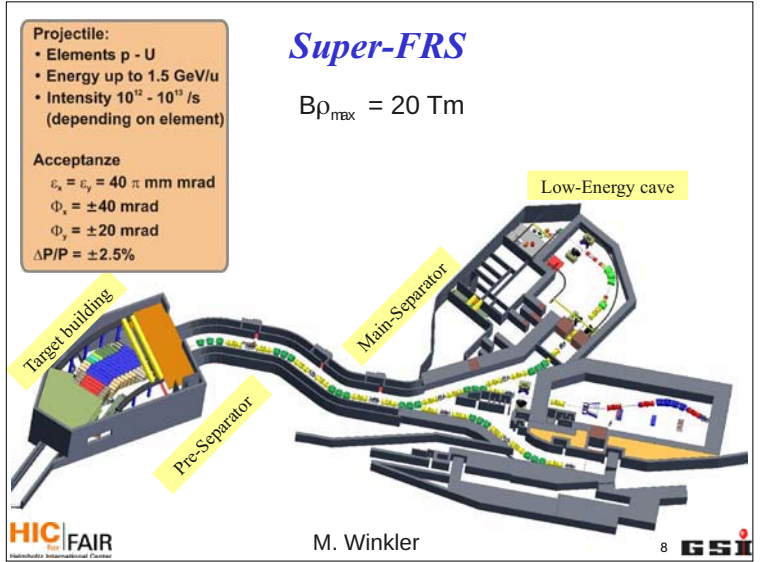
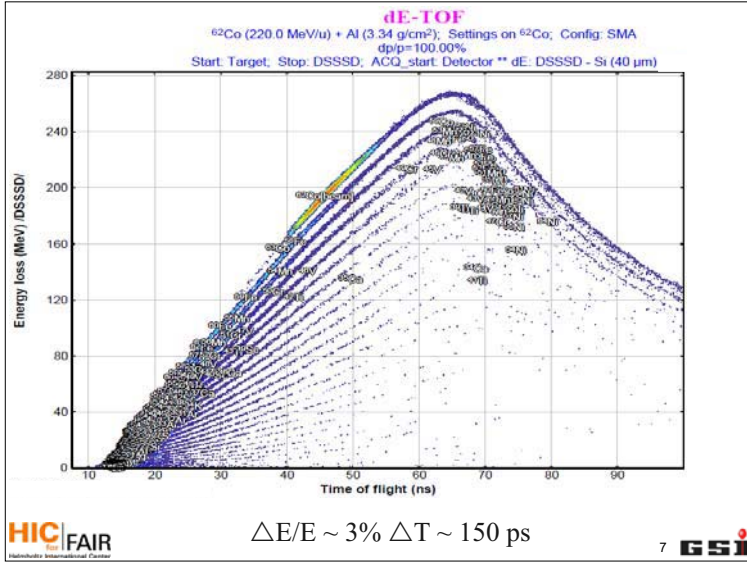
Angular straggling



20 mrad at a distance of 1.5 m → 3 cm

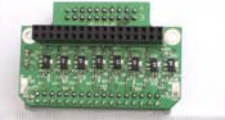
Contaminants from reactions into the degrader





Development

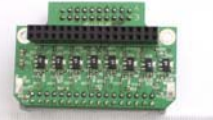
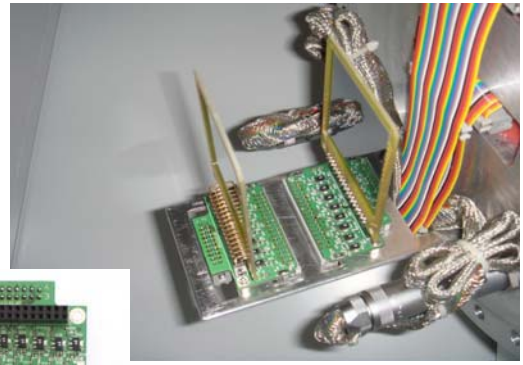
16 ch Fast pre-amp + 16 ch Level discriminators + 16ch ECL converters



Design: W. Koenig(GSI)

Development

16 ch Fast pre-amp + 16 ch Level discriminators + 16ch ECL converters

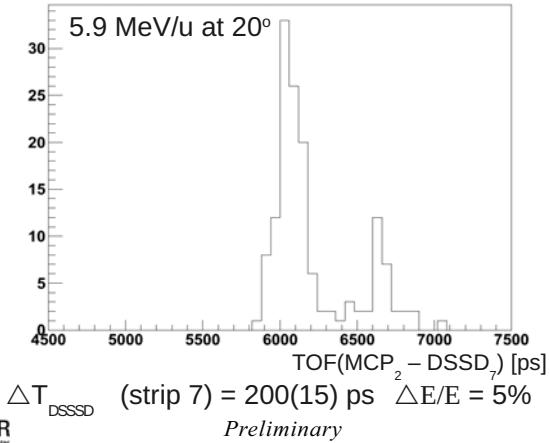


Additional electronics: CAEN V1290A TDC

Si fast timing Aug 2009

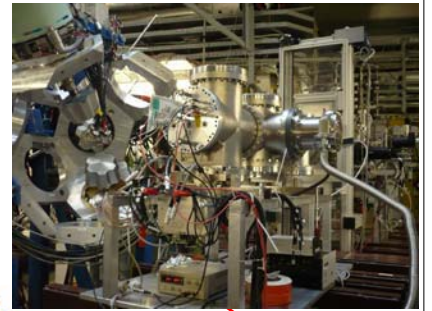
Coulomb scattering of ^{48}Ca beam,

5.9 MeV/u at 20°



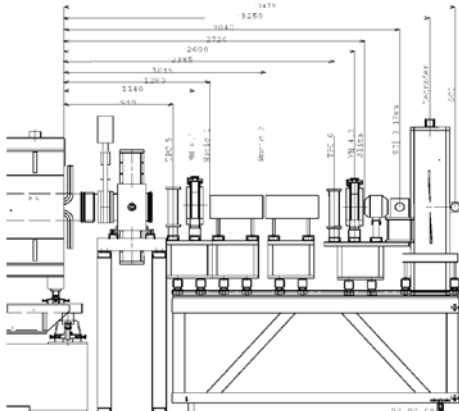
Slowed down beams test at FRS

^{64}Ni



S4: TPC, MUSIC, two SC41: 5mm(BC410),10mm(BC422) 2xMCP, 2xDSSD

S4-detectors



S4: TPC, MUSIC, two SC41: 5mm(BC410),10mm(BC422) 2xMCP, 2xDSSD

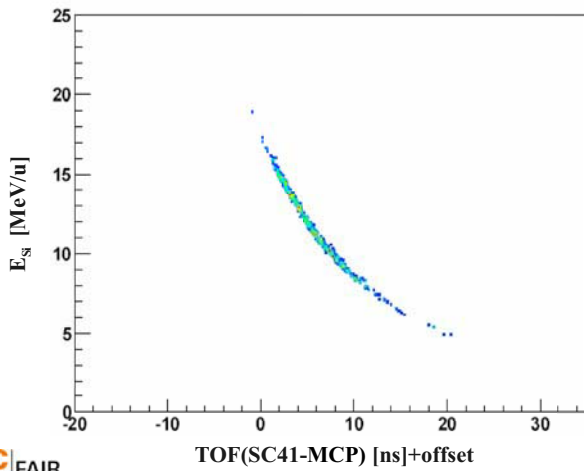
Slowed down beams test at FRS

2xMCP, 2xDSSD



- MUSIC resolution up to 50 kHz
- TOF: at 10^6 p/spill (4s spill)
- Phase space after slowing down
- Beam purity after slowing down
- Coulomb scattering on Au

^{64}Ni



Summary

- MCP detector and fast pre-amplifiers for Si DSSD were built to prove the concept of slowed down beam setup at FRS

Future

- Further development of fast timing with DSSD
- Further analysis

Collaboration

P. Boutachkov¹, F. Naqvi¹, M.Górska¹, J. Gerl¹,
W.Koenig¹, N.A. Kondratjev²,
W. Prokopowicz¹, E.Gregor¹, H.J.Wollersheim¹,
I. Kojouharov¹, H. Schaffner¹, H. Weick¹, M.A.G. Alvarez³,
I. Mukha³, Z.Abou-Haidar³, S. Pietri¹, A. Prochazka¹, F. Farinon¹,
C. Nociforo¹, R. Janik⁴, P. Strmen⁴, J.J. Valiente⁵, A. Gadea⁵

1. GSI, Darmstadt, Germany
2. FLNR, JINR, Dubna, Russia
3. Seville University, Seville, Spain
4. Komenského University, Bratislava, Slovakia
5. LNL, Legnaro, Italy

Beam Tracking Detectors Developments

B. Fernández^{a,b}, Z. Abou-Haidar^{a,b}, A. Bocci^{a,b}, M. A. Cortés-Giraldo^a, A. Garzón^b,
M. A. G. Alvarez^{a,b}, J. Pancin^c, A. Drouart^d, M. Kebbiri^d, M. Riallot^d

^a*Departamento de Física Atómica, Molecular y Nuclear (FAMN), Universidad de Sevilla, 41012 Sevilla, Spain.*

^b*Centro Nacional de Aceleradores (CNA), Universidad de Sevilla, 41092 Sevilla, Spain.*

^c*Grand Accelérateur National d'Ions Lourds (GANIL) 14076 Caen - France.*

^d*Commissariat à l'Énergie Atomique (CEA) 91191 Saclay - France.*

Abstract: New generation of Radioactive Ion Beam (RIB) facilities are being constructed in Europe under the projects SPIRALII (GANIL, France) and FAIR (GSI, Germany). The new particle accelerators foreseen by these projects will be able to produce beams of radioactive isotopes with high intensities ($\geq 10^6$ pps). These beams, at low energy, lower than 20 MeV/u, usually have large acceptance, which imposes the use of tracking detectors before the target in order to reconstruct the trajectory of the ions before a nuclear reaction. The group of Basic Nuclear Physics at the National Accelerator Center (CNA) in Seville, represents one of the institutions in charge of developing solutions of tracking systems for the low energy branch of FAIR (the HISPEC/DESPEC project). From this point of view, a collaboration with the Commissariat à l'Énergie Atomique (CEA-SACLAY) was established, with the following objectives: to simulate, develop, build and test a low pressure Secondary electron Detectors (SeD) and its related fast electronics. The construction and experimental results of the first prototype as well as a first set of simulations are presented below. We also present a new Nuclear Physics Line, as a valuable tool, projected and mounted at the CNA with the aim of being able to perform tests on any kind of detector and on its related nuclear instrumentation.

Keywords: beam tracking detectors, fast electronics, low energy accelerators.

Corresponding author: malvarez@us.es

INTRODUCTION

Nuclear reactions are an important tool to investigate the nuclear structure and reaction mechanisms. These reactions have been extensively used in the past with stable nuclei. During the last decades, the nuclear reactions experiments grew to reach the biggest radioactive beam facilities such as the European laboratories GANIL (France), GSI (Germany), CRC (Belgium) or CERN (European Organization for Nuclear Research).

Two of these RIB laboratories, GANIL and GSI, have recently started expanding their facilities with the SPIRAL II (GANIL) and FAIR (GSI) projects. These projects foresee the construction of new accelerators that will allow studying the nuclear structure of new isotopes such as super-heavy nuclei, neutron-rich and neutron-deficient or highly deformed nuclei. Despite the fact that the current generation of tools allows successful measurements, it is clear that significant improvements can be reached regarding the efficiency, time and spatial resolutions and simultaneous detection of gamma rays and particles for a complete study of the reactions. Moreover, due to the characteristics of exotic nuclei beams (high acceptance and low resolution in energy) and in order to identify the initial conditions of the particles, it is important to detect and reconstruct the trajectory of the particles that produced the reaction.

This implies on developing a new generation of instruments that allows us to work under the parameters of the future radioactive beams, such as the high counting rate ($\geq 10^6$ pps).

According to this framework, we present, in the following, the new Nuclear Physics Line of CNA, as a local facility, projected and mounted in order to test any kind of detector and its related nuclear instrumentation. Furthermore, we introduce the first mini-SeD (70x70mm) prototype constructed by a collaboration between the CEA-Saclay and the CNA. This detector has been built based on the concepts and parameters of the SeD (250x400mm) installed in the focal plane of the VAMOS spectrometer in GANIL [1,2]. The first idea was to guarantee the possibility of having a low pressure tracking detector system capable of working with position and time resolutions of around 1-2mm and 100-200ps, respectively, independent of its size. Afterwards the goal is to improve these resolutions by simulating and developing fast preamplifiers.

THE NEW NUCLEAR PHYSICS LINE OF CNA

A new line dedicated for developing Nuclear Physics instruments, is now available in the 3MV tandem of the CNA-Seville. This accelerator is able to accelerate protons and several heavy ions with a current range between 1pA and 1 μ A approximately, at energies between some keV and tens of MeV, depending on the charge state of the selected heavy ion.

With this tool we open the possibility of determining the particles trajectory, in an event by event basis, of low or high intensity of stable nuclear beams, at low energy, produced by the 3MV tandem accelerator. Therefore, the stable beams can be used to simulate the characteristics of radioactive beams (different counting rates with large acceptance).

The new installation includes two reaction chambers with high current and voltage connections, a gas control station, a cooling system as well as a high vacuum system, which allows working at pressures of around 10⁻⁶ mbar. Within the line, we are able to test different types of detectors that are used in the biggest RIB facilities around the world, nuclear instruments like fast electronics, as well as performing low energy nuclear reactions or training students under different academical or research proposals.



Figure 1: View of the new nuclear physics line in the CNA-Seville (Spain).

THE MINI-SED DETECTOR PROTOTYPE

Detector structure and operation principles

The mini-SeD is a low pressure gaseous detector. It is a mini-prototype (70x70mm) of the Secondary electron Detector (SeD) (250mm x 400mm) developed at CEA-Saclay and installed in the focal plane of VAMOS spectrometer in GANIL [1,2]. The ion beam passes through an emissive foil of aluminized mylar of 0.9 μ m. The impact of ions on this emissive foil produces secondary electrons that are drained and focused towards the detector by a parallel electric (10KV) and a magnetic (100 G) field [3].

The mini-SeD is filled with pure isobutane at 4 torr. Once the secondary electrons pass through the 0.9 μm thick aluminized mylar window of the detector, the amplification occurs over two different zones: the "parallel-plate" zone where the field is constant and a zone of amplification around the anode wires where the gradient of the electric field is high [1,2].

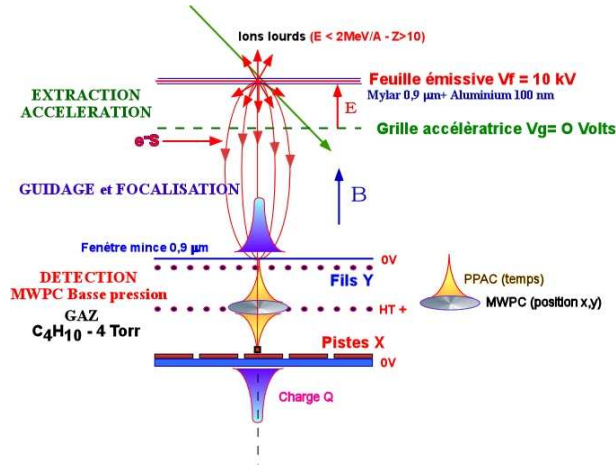


Figure 2: Operation principles of the SeD

The anode is a plane of golden tungsten wires of 20 μm diameter with 1mm pitch. The entire anode plane is at the same potential (600V). At 1.6mm of the anode, we have two cathodes, one on each side. The one located at the entrance of the detector is also a plane of golden tungsten wires, with a diameter of 50 μm , and a pitch of 1mm. They are linked by three and referenced to the ground through their electronics. The other cathode is an FR4, printed circuit board (PCB) with Copper strips. The strips are 2.34mm wide, and they are separated by 0.8mm. The active area of the mini-SeD is 70x70 mm^2 .

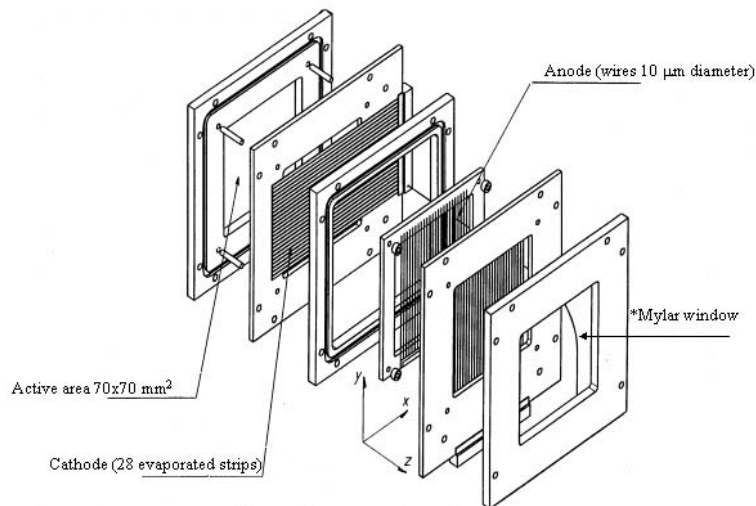


Figure 3: Different mechanical parts of the mini-SeD prototype.

CONSTRUCTION

In Figure 4, we present some steps of the (70x70mm) mini-SeD prototype construction. The mini-SeD was built to study the possibility of having a small and big active area tracking detector, based on the same technology, with comparable and reliable resolutions.

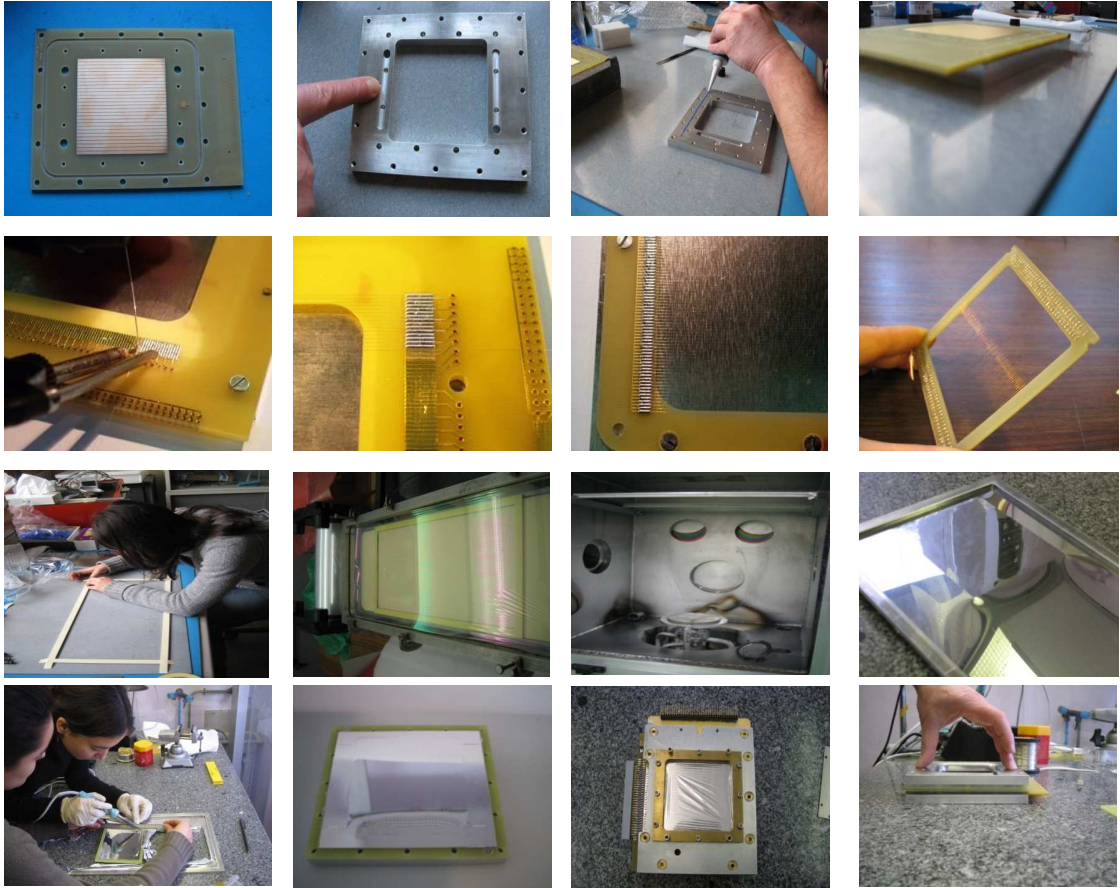


Figure 4: Details of the construction and assembly of the mini-SeD prototype.

TESTS AND RESULTS

The tests of the mini-SeD have been performed using a home made fast voltage amplifier (AR8) developed at CEA-Saclay to read out anode time signals and a MATAcq card [4] as the ADC. The cathodes are read out using the CPLEAR preamplifiers developed for SeD and a commercial QDC V792 model from CAEN.

Time Resolution

In order to measure the time resolution we use three detectors: a prototype of SeD, a surface barrier Si detector and the mini-SeD of which we want to measure the time resolution. The measurements are performed using a ^{252}Cf radioactive source. Figure 5 presents a scheme of the setup and Figure 6 presents typical anode signals. The time resolution (FWHM) obtained for the mini-SeD is 200ps, and it is the same value as the one obtained for the SeD.

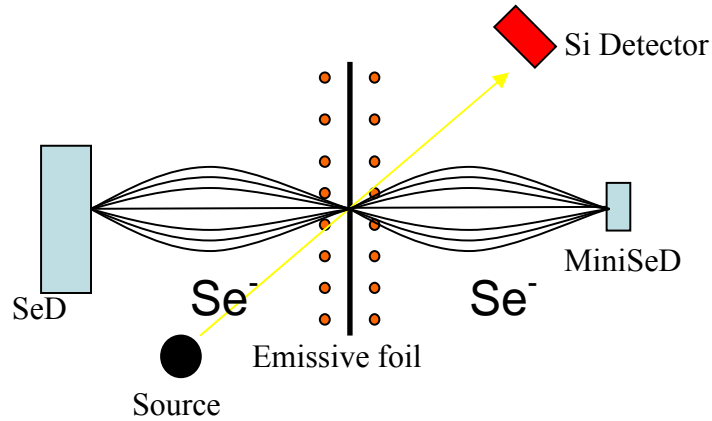


Figure 5: Scheme of the setup used to obtain the mini-SeD time resolution.

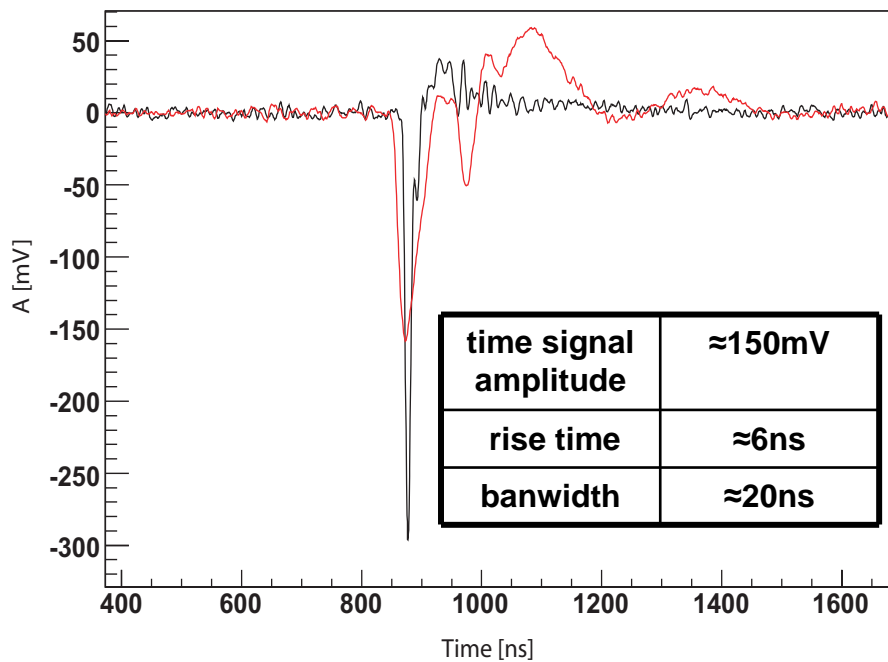


Figure 6: Typical time signals obtained from the anode of the mini-SeD prototype.

Spatial Resolution

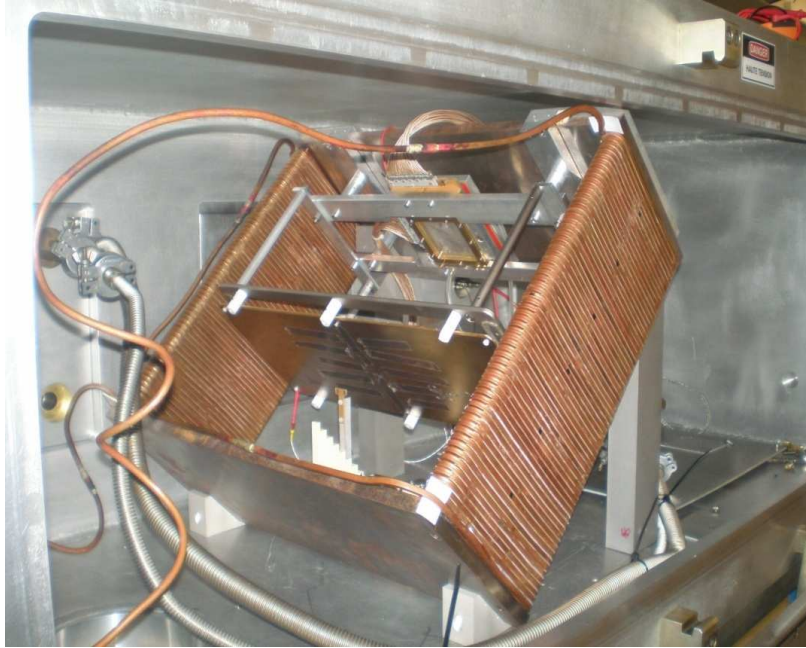


Figure 7: Setup used to obtain the spatial resolution of the mini-SeD.

In order to measure the spatial resolution, two methods of analysis, using different algorithms, were used. The first one consisted on calculating the geometric center of gravity of the measured charge on a given number of strips, as for the other, it consisted on approximating the distribution of charge with an analytic function (sechs) [5]. The best result obtained for the mini-SeD position resolution is 1.2mm (Figure 8), which is of the same order as the one obtained for the SeD, using the same preamplifiers.

Final Experimental Results

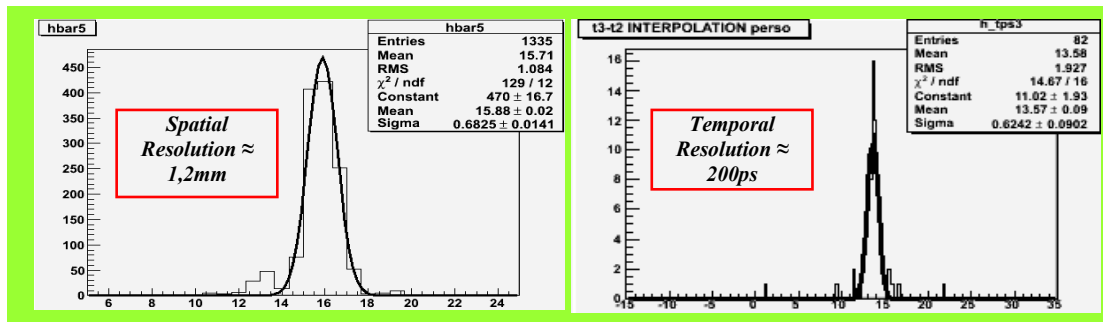


Figure 8: Final experimental results of the mini-SeD prototype: position resolution of 1.2mm and time resolution of 200ps. The results are comparable with the SeD installed in GANIL.

SIMULATIONS

Following the promising experimental results of the mini-SeD, and in order to improve them, we started a series of simulations using the Monte Carlo code GEANT4 (version 9.2). This code simulates the transport of the particles through matter. The geometry of the detector (mini-SeD) has been accurately reproduced in the simulations, especially the different parts and materials of the prototype (including the gas at low pressure) as well as the presence of the electric and magnetic fields. The so called “Physics List” used in the simulations is based on the QGSP-BIC-HP package provided in the GEANT4 official release. Some important data of the GEANT4 simulation are listed below:

- Energy of the incident beam = 1 MeV/u
- Aluminized mylar thickness = 0.9 μm
- Extraction voltage = 10KV
- Magnetic Field = 100G
- C₄H₁₀ gas at ~4 Torr
- 20 μm goldened tungsten (anode)
- 50 μm goldened tungsten (cathode)
- 1.6 mm gaps
- FR4 PCB
- Cu strips (2.34 cm \times 7.0 cm) (cathode)
- Electric field = 600 V/m

Thus, GEANT4 simulates the secondary electrons produced after the collision of the beam particle with the emissive foil, which is placed in the beam trajectory. These secondary electrons are extracted from the emissive foil by a 10-kilovolt high voltage and guided to the detector placed outside of the beam trajectory. Moreover, GEANT4 simulates the transportation of the electrons in the volume of the detector, as a result of the gas ionization. In addition, the fluence of the secondary electrons through the different electrodes is calculated in order to allow us to obtain the current produced in each strip or wire of each electrode (cathode or anode). The energy deposited in the Cu strips is calculated as well. We were mainly interested in the current produced in the cathodes, which will generate the position measurement and for which we develop new fast amplifiers.

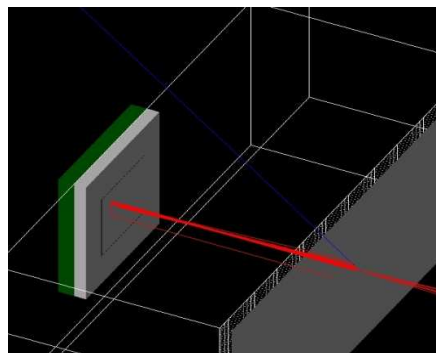


Figure 9: Illustration of charge produced in the emissive foil simulated by GEANT4.

So far, the simulations calculate a current of the order of $0.64\mu\text{A}$ in the cathodes. These current values, in the cathode, are our input source in the MULTISIM National Instruments code (Figure 10), which is used to simulate Trans-Impedance Amplifiers (TIA), RC filters and shaper-amplifiers elements and circuits.

The objective is to obtain the maximum performance of the system in terms of gain and bandwidth. The current of $0.64\mu\text{A}$, given by the simulations, obtained from the electrons fluence in the detector cathodes implies on very fast signals. The signal rise time is of the order of 300ps (obtained by GEANT4 simulations), which gives, using the commercial tested TIA, a signal of 2.25mV . The bandwidth of the TIA is 240MHz , which means that up to this frequency the value of the gain is 10000 . However, when the signal is faster, the gain decreases, in our case, the gain is of 3515 ($\text{Gain}=2.25\text{mV}/0.64\mu\text{A}=3515$).

On one hand, the simulations give the expected order of magnitude, with extremely good and fast signals; on the other hand the 300ps signals are very fast, and out of the range of the nominal gain and performance of the commercial TIA; this results in having an output signal amplitude, after the TIA, of the same order of the measured noise. Our research now is concentrated on improving the GEANT4 simulations, increasing the rise time and getting maximum gain performance, besides keeping the ideal compromise between gain and bandwidth (amplitude and velocity).

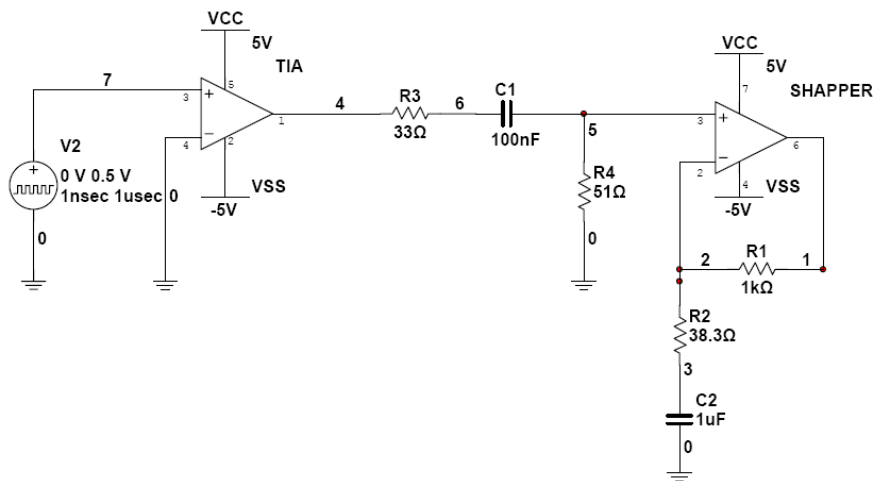


Figure 10: Circuit of the pre-amplifier: from left to right we can identify the current/voltage source, the trans-impedance amplifier (TIA), the RC filter and the shaper.

Cathode signal amplitude	$\approx 50\text{mV}$
Rise time	$\approx 8\text{ns}$
bandwidth	$\approx 30\text{ns}$

Cathode signal amplitude	(Simulations) $\approx 2.25\text{mV}$
Rise time	$\approx 300\text{ps}$
bandwidth	BW x GAIN

Table 1: Parameters of the experimental spatial signals (cathodes) compared to the parameters extracted from Geant-4 and the National Instrument Multisim simulations codes.

CONCLUSION

In a collaboration between CEA-Saclay, GANIL and CNA laboratories, we have built and tested, with a ^{252}Cf source, a first low pressure gaseous detector prototype as a candidate of tracking detector for FAIR, the mini-SeD. This ($70 \times 70 \text{ mm}^2$) detector, based on the characteristics of the SeD ($250 \times 400 \text{ mm}^2$) installed in the focal plane of VAMOS in GANIL, gives a temporal resolution of 200ps and a spatial resolution of 1.2mm. These results are consistent with the SeD. Therefore, we can say that this type of detector gives compatible and reliable results independently of the size of its active area. Never the less, these results can still be improved by coupling the mini-SeD to its fast adapted electronics. Within this framework, first simulations have been performed that gave better and faster signals. In addition, this detector is very cheap compared to Silicon or Diamond detectors and easy to repair. Now, the compromise between bandwidth and gain is under investigation in order to get maximum performance from preamplifiers circuits and from their coupling to the mini-SeD.

In the near future, the mini-SeD detector will be put under test at the ion beam facility of GANIL with the corresponding specific electronics and, later on, at the CNA. For this proposal a new structure is already working in the CNA. A new nuclear physics line has been prepared for the possibility of receiving several instrumental nuclear physics tests, including beam tracking and profile detectors or fast electronics.

REFERENCES

1. A. Drouart, et al., Nucl. Instr. And Meth. A 477 (2002) 401.
2. E. Bougamont, et al., Nucl. Instr. And Meth. A 518 (2004) 129.
3. O. H. Odland, et al., Nucl. Instr. And Meth. A 378 (1996) 149.
4. E. Delagnes, et al., Nucl. Instr. and Meth. A 567 (2006).
5. S. Ottini-Hustache, et al., Nucl. Instr. And Meth. A 431 (1999) 476.

Low-energy/low-intensity beam diagnostics detectors: experience at INFN-LNS

Paolo Finocchiaro*, Luigi Cosentino, Alfio Pappalardo

INFN Laboratori Nazionali del Sud, via S.Sofia 62, 95125 Catania, Italy

Abstract

In the framework of the interest in radioactive ion beam facilities, as well as in low energy ion traps, special diagnostic tools are needed in order to cope with low and very low intensity beams, sometimes also at very low energy. Particle detection techniques seem attractive under several aspects. In this paper we describe the main features of devices that we have tested throughout several years, as well as of those we are currently employing, at the EXCYT and FRIBS facilities at INFN-LNS.

INTRODUCTION

Recently an increasing interest has come out around many applications of particle beams sharing a common feature, namely the low intensity of the produced ion beams. Examples of such applications are the production of radioactive ion beams (RIB), facilities for low energy ion storage/trapping, low energy antiproton facilities, the cancer therapy by means of protons and ions.

Sometimes one might also wish to handle very low energy beams, thus complicating the already difficult task of a reliable beam diagnostics. Moreover, sometimes the need arises for single particle counting, hence the ideal device should be able to operate in two, partially overlapped, intensity regimes.

In the following a few possible ways are highlighted to borrow some hints from the nuclear detection techniques, in order to develop powerful beam diagnostic tools. Citation of work already done in this field will be helpful in this task, and for this reason we also list several interesting papers in the references section .

PHYSICAL BACKGROUND

One of the main requests for low intensity beam diagnostic tools comes from the RIB facilities. Unfortunately the produced beams may have a weak intensity, due to the small cross section for the production of several interesting nuclear species and to the obvious limitations in the primary beam intensity. A general recipe cannot be formulated since each particular species has a different cross section and lifetime: the final beam current can span several orders of magnitude, becoming critical when reaching below $\approx 10^8$ particles per second (pps), and still worsening when below 10^5 pps.

In such an intensity range the ordinary diagnostic techniques approach their intrinsic electromagnetic limitations, that are mainly due to electronic noise, that limits the attainable signal-to-noise ratio, and to the

contamination of the useful signal by secondary emission of electrons from parts of the sensor exposed to the beam.

The required features, whenever possible, are: improved sensitivity, non-interceptivity, reliability, ease-to-use, robustness, this last especially regarding sudden variations of the beam intensity, operator mistakes, failures.

AVAILABLE TECHNIQUES

In order to increase the sensitivity of a beam sensor device there are two possible strategies: either reducing the noise or increasing the signal. The former should be attained by improving the electronic design and the shielding of usual devices, while the latter can be pursued by borrowing some hints from the experimental nuclear physics. In fact a nice method to increase the useful signal is to use a particle detector, that is usually sensitive to the energy released by the particle rather than to the carried charge.

Conversely, the main drawback of devices based on particle detectors is that their response is strongly dependent on the beam type and energy: we do not measure anymore the electric current carried by the beam. Moreover, the thickness of possible dead layers can introduce an energy threshold on the detectable beams, while the radiation hardness, as compared to the cost, is one of the most important parameters that have to drive the choice of a type of detector.

The available techniques are based on semiconductors, gas detectors, secondary emission (with physical amplification), scintillators; some further technique, like Cherenkov detectors and others, that can be used in particular cases, will not be described here.

SEMICONDUCTOR DETECTORS

The most widely used semiconductor detector is silicon. The signal in a silicon detector is due to the energy lost in it by an impinging particle, that can cross it or be stopped inside. The silicon is quite efficient in this process, since the average energy needed to produce an electron/hole pair in the depleted region is 3.62 eV. Unfortunately its radiation hardness is not high, while its cost, including the needed electronics, is a little bit expensive. Nevertheless the ease-of-use and reliability are enough to allow its use for specific applications.

Several groups have already developed and used silicon microstrip and/or pixel detectors for high energy physics experiments. They consist of a structure with typical pitch of $\approx 100 \mu\text{m}$ and thickness of $\approx 100\text{-}300 \mu\text{m}$; the overall size can be up to 10-15 cm. Such a device is best suited for single particle counting and tracking, even though it

* e-mail: FINOCCHIARO@LNS.INFN.IT

can also measure the energy deposition. Its use in current mode is obviously possible, but radiation hardness and cost impose severe limitations to it.

In particular cases a silicon detector can however represent a nice tool, as for instance the beam isotopic identification [1]. Such a device consists of a thin Au target and a silicon telescope that can be positioned around it. This method, that can be applied for not too energetic beams, allows the unambiguous isotopic identification of particles by building a typical ΔE -E scatter plot. An example of such a telescope, built at INFN-LNS, is shown in Fig. 1

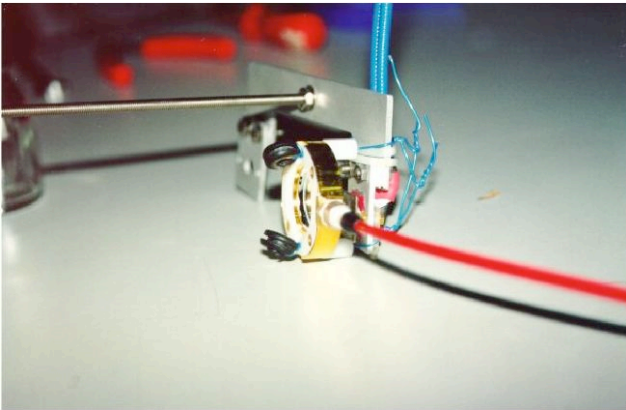


Fig. 1: example of a silicon telescope used at INFN-LNS for beam identification.

Quite recently we started to employ a $5 \times 5 \text{ cm}^2$ position sensitive silicon detector, readout at the four corners and from the back electrode. By using a well suited algorithm we are able to remove the position non-linearity and reconstruct the transverse profile of the beam. In Fig. 2 we show the reconstruction of the transverse beam profile after crossing a pepper-pot mask.

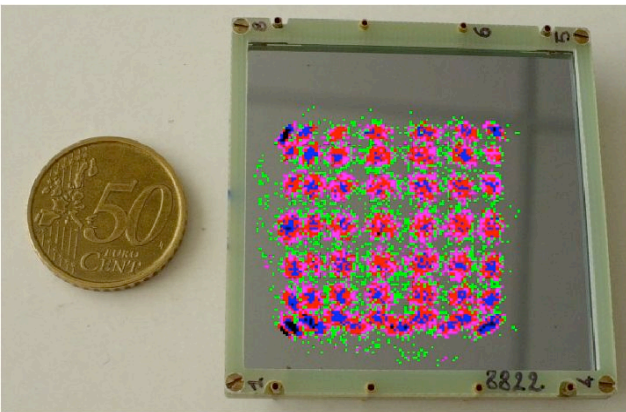


Fig. 2: a $5 \times 5 \text{ cm}^2$ position sensitive silicon detector. Superimposed to the picture one can see the linearized plot obtained after sending the beam on the sensor across a pepper-pot mask.

Another well known semiconductor detector is germanium, generally used as very high resolution gamma ray detector. Due to the very poor radiation hardness and to

the high cost these detectors are completely unsuitable for particle detection. Nevertheless, in spite of their complex usage and low reliability as beam sensors, they can be successfully employed to identify very weak RIBs by means of their gamma decay “fingerprints” [2], [3].

DIAMOND DETECTORS

Unlike semiconductors diamond is rather a good insulator, even though its operating mode resembles the semiconductors. The detection principle is still the creation of pairs by energy loss, but in this case the noise is strongly reduced because of the high energy gap. The average energy to create a pair is $\approx 18 \text{ eV}$, the radiation hardness is very good since it is not a diode that is damaged because of the displacement of its dopants. Moreover, the thermal conductivity of diamond is better than copper, hence it can tolerate a high power deposition. So far the chemical vapour deposition (CVD) technique allows to produce good diamond films, that however are not monocrystalline: this implies that the charge collection length is limited by crystal defects that trap charges.

Nowadays detectors with $50\text{-}100 \mu\text{m}$ collection length are available, that can be usefully exploited both in pulse counting mode and in current mode. In addition the high electron mobility and dielectric constant, together with the short collection length, make the signal development very fast, thus allowing to build also segmented devices with $< 50 \text{ ps}$ time resolution [4] and capable to sustain up to 10^8 pps count rate in pulse counting mode [5].

An example of the performance of CVD diamond films in current mode readout can be found in [6], where the authors report on tests made with a strip electrode structure of $100 \mu\text{m}$ pitch. The overall cost of this technique is still high, even though it is expected to decrease in the next future; concerning reliability and ease-of-use the technique looks promising.

Recently thin monocrystal diamond detectors have become available on the market, even though their cost is still quite high.

GAS DETECTORS

Gas Chambers

Gas detectors are very well known since many years, and they have been developed in a wide variety of shapes and sizes. The signal in a gas detector is due to the energy lost by a particle in a chamber filled with a suitable gas. The average energy to produce an e^-/ion pair is generally of the order of 30 eV .

The radiation hardness is good since the gas is continuously flowed through the chamber, and the cost is usually cheap. Several operating modes are possible for gas detectors, depending on the pressure and on the electric field applied to the electrodes.

The main techniques mentioned here as suitable for beam diagnostics purposes are the ionization chamber and the wire chamber. Both of these detectors have been employed in a large number of nuclear physics experiments so far, and they are used as beam counters and/or trackers in

several laboratories. They can be used in pulse counting and in continuous mode, starting to lose linearity around an incoming rate of $\approx 10^9$ pps due to space-charge effects.

A remarkable improvement in gas detectors has come years ago with the introduction of the microstrip gas chamber (MSGC) [7]. Such a detector is based on the same principle of the wire chamber, with the difference that the wires (cathodes and anodes) are lithographically drawn and lay on the same plane. The main advantages are:

- high precision, with a pitch of $\approx 100\text{-}200\ \mu\text{m}$;
- simplification of the overall mechanical structure.

A prototype beam profile monitor employing an MSGC has been tested at LNS with remarkable results. It is based on a $5 \times 5\ \text{cm}^2$ glass microstrip plate used as collecting electrode of a small ionization chamber. The collecting field is perpendicular to the beam direction, while the strips are parallel to it. It can be inserted/removed on the beam path and the signals, collected strip by strip, give rise to the beam profile (Fig. 3).

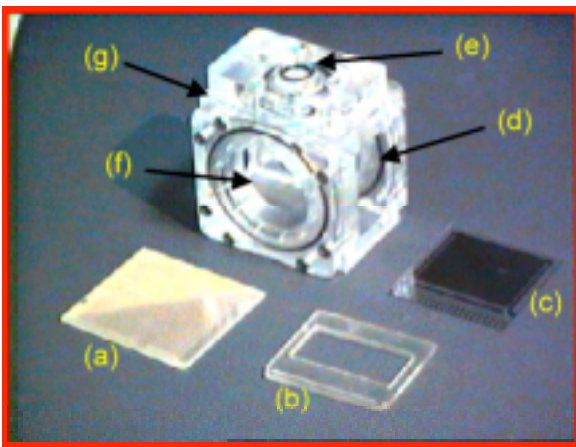


Fig. 3: a prototype gas detector, developed at INFN-LNS, based on MSGC. (a) electrical connection board ; (b) holding frame; (c) the MSGC plate; (d) the three parts (a+b+c) are sandwiched and installed here; (e) gas in/out; (f) mylar window; (g) chamber body.

A variation of this technique, still with transverse collecting field but with strips perpendicular to the impinging particle direction, becomes a multilayer ionization chamber. Such a device used in single particle counting can replace a silicon telescope in applications where low energy beams are involved: Z values up to 10 have been recently identified with an energy threshold around $200\ \text{keV}/\text{amu}$ ($< 1\ \mu\text{m}$ silicon equivalent) [8].

Residual Gas Detectors

These detectors are based on the ionization produced by beam particles on the residual gas along the beam pipe. The very few ionizing collision events need some sort of physical amplification. What is generally used is a microchannel plate (MCP) onto which the electrons (or ions) produced are driven by a transverse electric field. Care has to be taken to prevent the MCP from being accidentally hit by the beam, that would destroy it.

MCP: Readout by Electrodes

This kind of device is rather sensitive and is mainly used in pulse counting mode. It can be employed for transverse beam profiling, with the collecting electrodes shaped in separate strips parallel to the beam [9], [10]. It is also used successfully for longitudinal beam profiling, due to its good timing resolution ($\approx 100\ \text{ps}$) [10]. An application of such a device was proposed, where both ion and electron drift times are recorded, also allowing to identify the ion species drifting toward the electrodes [11].

An example of this application is shown in Fig. 4, where we report a Time Of Flight spectrum used at INFN-LNS to identify a ^8Li beam.

MCP: Readout by Scintillating Screen

An interesting device is made of an MCP coupled with a phosphor scintillating screen. By means of a suitable choice of the voltages applied to the MCP electrodes, the output electron cloud can be further accelerated toward the screen, thus producing a visible image that can be observed by means of a usual CCD camera. The device can easily reconstruct the beam trace across the active field of the sensor and the image is best acquired with a frame grabber that also allows a digital analysis [12].

A more complicated configuration can also reconstruct the 2D transverse profile of the beam, by exploiting two different field cages, as shown in [13].

SECONDARY EMISSION DETECTORS

These detectors exploit the emission of secondary electrons from several materials when hit by energetic particles [14], [15]. To this aim wires and/or thin foils are generally used, choosing a material with a sufficient mechanical strength and capable of withstanding or dissipating the foreseen power deposition. The generally used foils are made from carbon or aluminium, the wires from tungsten.

In case of low intensity beams the number of electrons produced is very low - usually from few units to two hundred per incident ion [15] - thus a physical amplification process is needed to get a useful signal.

This technique, exploiting an MCP to amplify the number of electrons, is well known since many years in heavy ion physics for time of flight measurements [16], and has also been used for longitudinal ion beam profiling [17], see an example in Fig. 4. Other devices have been proposed using a channeltron for integral beam current measurements [11] or an MCP plus scintillating screen combination to get an immediate 2D transverse profile image by means of a CCD camera and a frame grabber [12].

SCINTILLATORS

Scintillators are well known to the physicists since a long time. Their basic property is to emit as light part of the energy deposited by an impinging particle. A large family of polymeric plastic scintillators is today available on the market, and they are usually rather cheap and easy to be produced in any shape. Plastics can be practically chosen

within a wide spectrum of characteristics like decay time, emission wavelength, attenuation length, etc.

Their main drawbacks are the poor radiation hardness and power dissipation; so special care should be taken when using a plastic scintillator in a high counting rate environment. The usage of a plastic on the beam is practically limited to a low intensity regime and for short time intervals: after irradiation with $\approx 10^{10}$ - 10^{12} particles/cm² all hydrogen atoms are completely ejected, and only carbon atoms are left (graphite) [18].

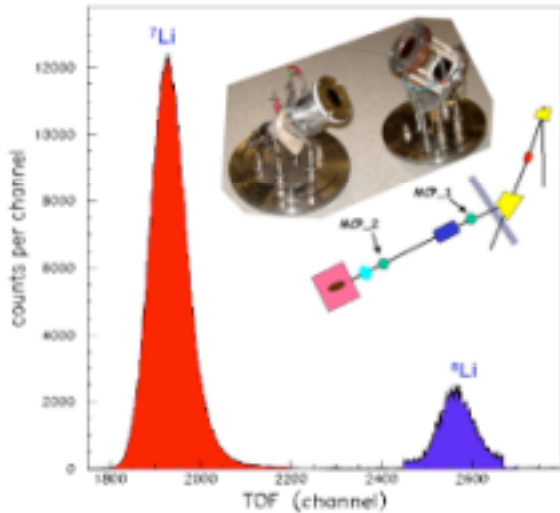


Fig. 4: example of Time Of Flight technique for online identification and tagging of the ⁸Li radioactive beam by means of two MCPs detecting secondary electrons emitted by a thin carbon foil.

During the last years new families of inorganic scintillator crystals have come up to the attention of physicists, with rather good mechanical properties, radiation hardness, scintillation efficiency, and some of them have a surprisingly short decay time, even shorter than plastics.

Most of the currently used scintillators have an average energy to produce a scintillation photon of the order of ≈ 10 - 100 eV. The cost has large variations due to type, shape, quantity, doping, purity, but we can still say that it is cheap.

Among the inorganic scintillators we can also put some amorphous materials, like glasses, usually doped with rare earths elements like terbium, gadolinium, cerium, etc.

Concerning the light readout devices, many types of photosensors exist on the market, some of them suitable for current readout (photodiodes), some others for pulse counting (photomultipliers, avalanche photodiodes). Special devices also exist that are suitable for single photon counting (photomultipliers, hybrid photodiodes, silicon photomultipliers or SiPM).

So far the application of scintillators for beam diagnostics has been basically limited to plastics, mainly used for timing (e.g. [19]) or for integral current measurement (e.g. [20]) in pulse counting mode; the count rate limit is $I < 10^6$ pps. The timing resolution of such a device can easily reach < 100 ps [21] [22], and if used in

shape of a scintillating optical fibre bundle it can also be used as tracker, allowing a transverse profile reconstruction [23].

A R&D activity has been conducted at INFN LNS concerning the application of scintillators to low intensity beam diagnostics, moving along different lines. The main results so far obtained are outlined below.

Scintillating Fibres

Our interest has been attracted by scintillating fibres since they allow to rebuild a scanning wire beam profiler by replacing the wire with a fibre. The sensitivity is improved since the signal is due to energy loss, the electronic noise is strongly reduced. Such a device, named FIBBS (Fibre Based Beam Sensor) is capable of sensing even the single beam particle [24]. The usage of only one fibre per direction avoids calibrations, while the fibre diameter and the step size can be varied more or less at will (Fig. 5). An example of X and Y profiles is shown in Fig. 6.

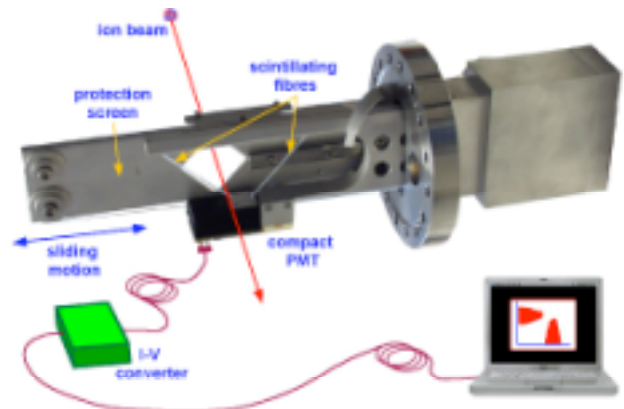


Fig. 5: the FIBBS XY beam profiler, exploiting two perpendicular scintillating fibres readout by means of a compact photomultiplier.

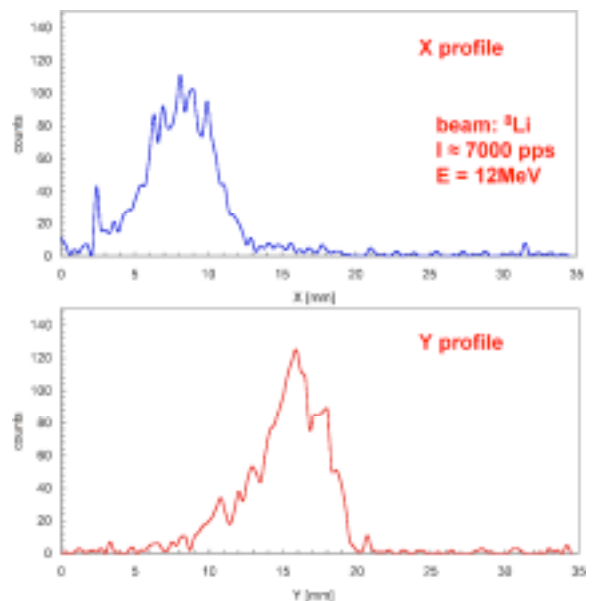


Fig. 6: example of X and Y beam profiles taken with plastic fibres, by counting particles at ultra-low beam intensity (≈ 7000 pps ^8Li).

The employed photosensor is a compact photomultiplier. A special I-V converter has been developed for the photosensor readout: it allows both the pulse counting and the continuous readout modes to be simultaneously performed on two different outputs [25].

Two fibres are installed on the same moving structure, rotated by 90° with respect to each other but still connected to the same photosensor, thus allowing to reconstruct both the X and Y profiles in a single scan.

Two types of fibres have been tested so far: plastic and Tb-doped glass. The plastic fibres allow the pulse counting mode, since their decay time is short (3 ns); unfortunately they are not enough radiation hard, so they need to be used with care. Tb glass fibres are pretty harder but their decay time of 3 ms only allows the continuous readout mode. Nevertheless their light yield is good, and makes the device capable of sensing beam profiles even down to 10^5 pps integral current.

Bulk Inorganic Crystals

We have also built a scanning slit beam profiler, based on a moving slit and a small CsI(Tl) brick ($1 \times 1 \times 0.5 \text{ cm}^3$). The operating principle of such a device is quite similar to the FIBBS, with a few differences. On the one hand it is completely interceptive while scanning the beam; on the other hand its overall light yield is about 50 times higher than a fibre.

The output signal is sent to the already mentioned I-V converter, in order to have both pulse and current measurements. This device has allowed us to reconstruct profiles even down to 10^4 pps integral beam current in continuous mode, and at the same time it is able to count pulses in order to have an absolute intensity calibration. A very strong point in favour of this device is that we have recently proved it is useful also for very low energy beam profiling. In fact it showed it can easily reconstruct a beam profile of 10^6 pps of $^{12}\text{C}^+$ ions at 50 keV [26].

Scintillating Plates

We have also developed a beam diagnostic set-up based on the direct optical inspection of the transverse profile [27]. To this aim we use some scintillating screen, directly hit by the beam, and a CCD camera that looks at it sending the images to a TV monitor and to a frame grabber system for digital analysis.

Several different plates have been tested so far, each one with interesting features and minor drawbacks. Among them it is worth mentioning CHROMOX6 (a doped alumina), NE102A, YAG, CsI(Tl).

An interesting screen type is the scintillating fiberoptic plate (SFOP): we tested thin plates made from a slice of a bundle of Tb doped glass fibres, whose light can thus be readout from the back. The light diffusion is constrained within the fibre diameter ($\approx 10 \mu\text{m}$), and the light yield allows to sense beam images even at 10^5 pps; the 3 ms decay time gives no evident afterglow. The SFOPs are

radiation hard, but they break at high temperature; therefore they need some care when exposed to intense beams.

CsI(Tl) and SFOP proved to be the tools of choice when we want to perform precision diagnostics on very low energy/intensity beams. In particular we exploited them, for instance, when performing Deep Lithography with Ions [28]. On the one hand the SFOP allows a precision imaging of low intensity microbeams (we tested it down to a $20 \mu\text{m}$ diameter collimated beam), on the other hand a CsI(Tl) plate was successfully used as scintillating imaging Faraday cup in the same application.

In Fig. 7 we show an example of transverse profile of a low intensity proton microbeam after collimating it to $150 \mu\text{m}$ diameter, with a primary current of 30pA. The honeycomb structure of the SFOP is clearly visible, whereas the black dots are black fibres periodically interspersed in the plate to operate as Extra Mural Absorbers, in order to suppress the stray light. The halo around the beam spot is due to gamma rays produced in the collimator.

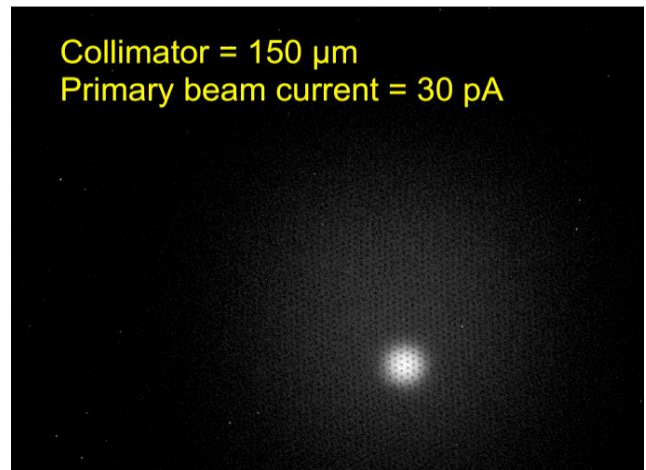


Fig. 7: transverse profile of a low intensity proton beam after collimating it to $150 \mu\text{m}$ diameter. The primary current was 30pA.

THE LEBI SYSTEM FOR RIBs

The main achievement of our R&D was the design and construction of the multipurpose Low Energy Beam Imager/Identifier system, basically employed in the EXCYT unstable beams facility at INFN-LNS. It consists of a box, operated under high vacuum, capable of diagnostics on stable and radioactive beams down to $\approx 10^3$ pps and to 10keV [29]. A LEBI features a $50 \times 50 \times 1 \text{ mm}^3$ CsI(Tl) scintillator plate, part of which is covered by a thin aluminized Mylar tape. In order to image a stable beam, we expose the plate directly to the beam itself, looking at it via a cheap and compact CCD camera installed outside of a quartz porthole. When imaging a radioactive beam, we use the Mylar tape to implant the beam (in order not to contaminate the scintillator). The scintillation light, in such a case, is produced by the decay products (typically beta rays) hitting the plate (Fig. 8). LEBI also features a $5 \times 5 \times 5 \text{ cm}^3$ plastic scintillator, wrapped

in aluminum foil and readout by means of a PMT, in order to count beta particles and identify the unstable beam by means of its half-life (Fig. 9).

Moreover, in case one wishes to perform RIB identification by means of gamma decay fingerprints, LEBI features two cylindrical hollow cups, made from thin Ergal, to allow for the insertion of two Germanium detector heads to be placed very close to the beam implantation position.

In spite of the two initially foreseen systems, so far we have built and installed thirteen LEBIs.

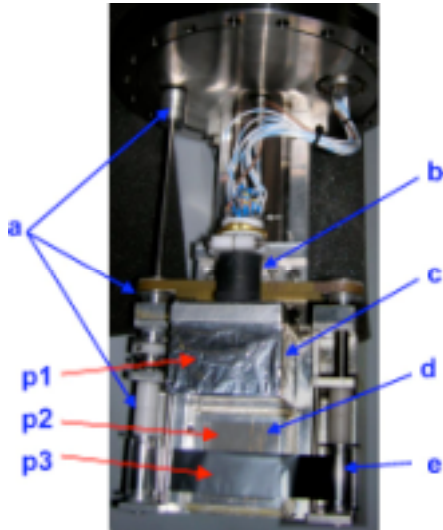


Fig. 8: the LEBI system for low energy and low intensity stable and radioactive beam imaging and identification. Shown are: (a) the tape transport system; (b) photomultiplier; (c) the plastic scintillator; (d) the CsI(Tl) plate; (e) the Mylar tape. The system can be positioned in beam into three measuring positions: (p1) beam rate measurement; (p2) imaging of stable beams; (p3) imaging of radioactive beams.

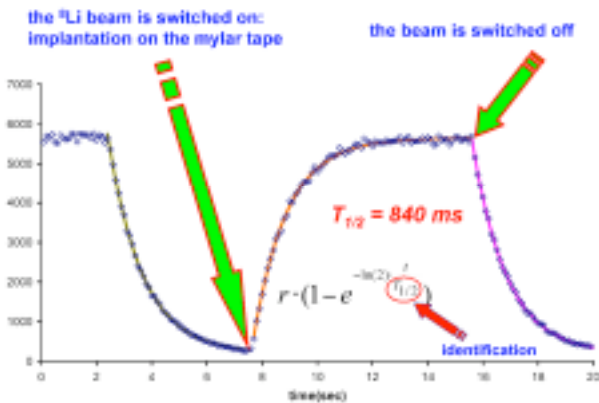


Fig. 9: identification of the ^8Li beam by means of its beta-decay curve.

TOWARD THE SENSITIVITY LIMITS

Recently we have started to investigate the lowest detection limits of the scintillation/imaging techniques, and found out that the CsI(Tl) screens actually have powerful

performance. In particular we proved that such a screen can sense down to the fA regime, with beam energies below 100keV (Fig. 10 and Fig. 11) [30].

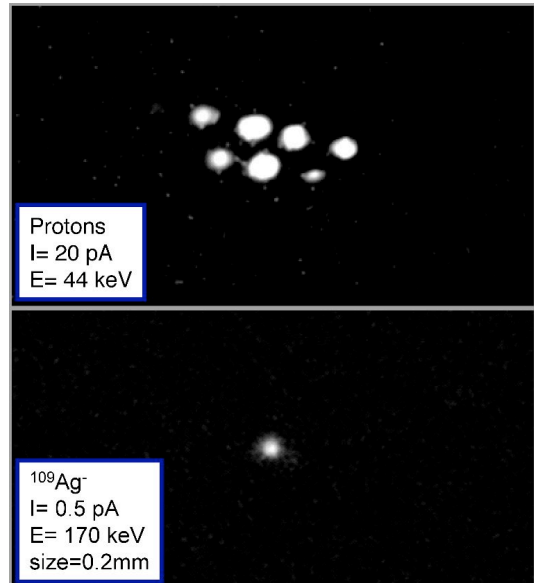


Fig. 10: sample images of very low energy and intensity proton and Silver beams detected by means of a CsI(Tl) screen and a CCD video camera. The spots are due to a pepper-pot grid placed in front of the beam, the hole size is $200\mu\text{m}$.

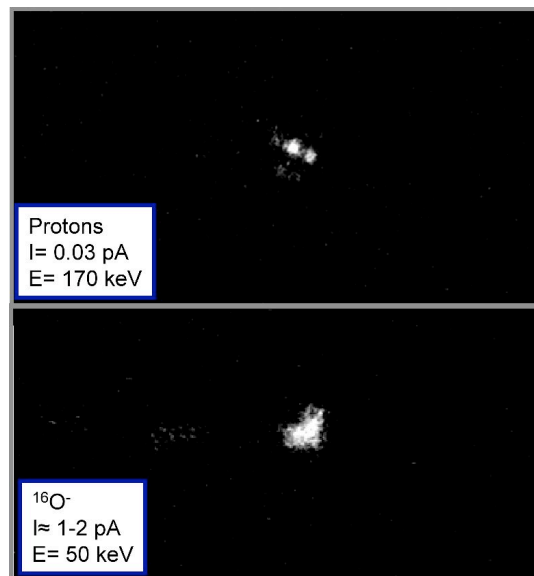


Fig. 11: sample images of very low energy and intensity proton and Oxygen beams detected by means of a CsI(Tl) screen and a CCD video camera. The spots are due to a pepper-pot grid placed in front of the beam, the hole size is $200\mu\text{m}$.

We have also been able, by means of this technique, to detect and identify the impurities and/or previous species accelerated by our ion source months before, both in elemental and molecular form [30].

We have also become involved in the test of a possible diagnostic technique for low energy antiproton beams,

based on scintillators. For this reason we have set up a test configuration employing a plate holder with three different scintillators (Tb-glass SFOP, CsI(Tl), YAG), looked at by means of a high performance 14-bit CCD camera. The CCD can be cooled down, in order to reduce its noise.

The preliminary results, obtained with low energy and very low intensity proton beams, are quite promising for CsI(Tl) and also for the SFOP. As to the YAG, in spite of its much better radiation hardness, the light yield was disappointingly low [31].

In Fig. 12 we show a few preliminary sample images, taken with this setup, with a CsI(Tl) screen (upper plots) and a SFOP (lower plots).

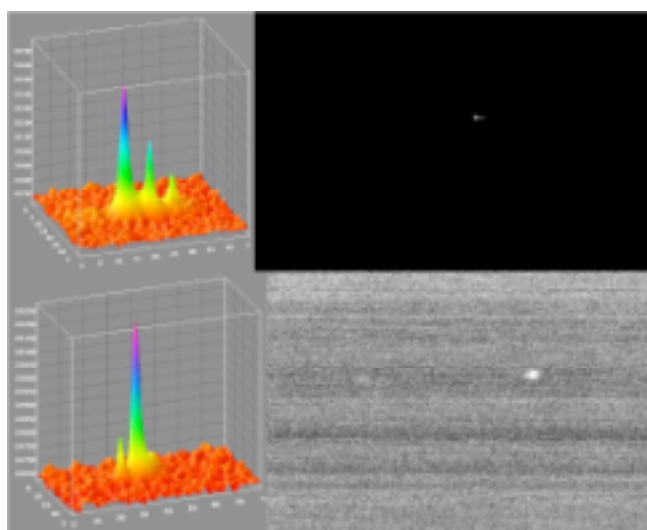


Fig. 12: attenuated (by means of a pepper-pot grid) proton beam images taken at $E = 200\text{keV}$, $I \approx 2.5\text{fA}$ [$5\text{pA}/2000$], $t_{\text{exposure}} = 20\text{s}$. Upper plots: CsI(Tl) screen. Lower plots: Tb-glass SFOP. The still camera features a 14-bit cooled CCD.

SUMMARY AND CONCLUSIONS

Several techniques have been explored in order to help in ion beam diagnostics at low intensity, and the know-how already available with particle detectors has been quite useful in this respect. The envisaged devices, mainly based on semiconductors, gas detectors, secondary emission and scintillators, seem capable of satisfying most of the requirements so far needed. However the most promising techniques seem to be inorganic scintillators and doped glasses, even though many ad-hoc devices based on other types of detectors are (and will be) helpful. It is worth to be mentioned that beam imaging by means of Tb-doped glass or CsI(Tl) plates appears as a very promising technique for beam diagnostics a very low energy and intensity.

REFERENCES

[1] Pardo, R. et al, presented at the RIB workshop, May 1997, Vancouver (Canada);
Finocchiaro, P. et al., presented at the RIB workshop, May 1997, Vancouver (Canada).
[2] Launé, B. et al, Nouvelles du Ganil 60(1997)25.

[3] Tomizawa, M. et al, presented at the RIB workshop, May 1997, Vancouver (Canada).
[4] Berdermann, E. et al., proceedings of the XXXVI Int. Winter Meeting on Nucl. Phys., Bormio 1998.
[5] Jungmann, K. et al., presented at the HADES coll. meeting, July 1997, Darmstadt (Germany).
[6] Fenker, H. et al., proceedings of the IEEE Nuclear Science Symposium, November 1995, S.Franisco (CA, USA) .
[7] Oed, A., NIM A263(1988)351;
Angelini, F. et al., NIM A323(1992)229;
Beckers, T. et al., NIM A346(1994)95 and refs therein;
Alunni, L. et al., NIM A348(1994)344 and refs therein;
Bouclier, R. et al., IEEE Trans. Nucl. Sci. 43(1996)1220;
Bouclier, R. et al., NIM A369(1996)328;
[8] Aiello, S. et al., NIM A400(1997)469.
[9] Anne, R. et al, presented at the 7th Beam Instrumentation Workshop, May 1996, Argonne (IL, USA).
[10] Meyer U., Thesis, Institut fur Kernphysik der Johann Wolfgang Goethe Universitat, Frankfurt am Main, November 1995, unpublished.
[11] Shapira, D. et al, NIM A400(1997)185.
[12] Cuttone, G. et al, presented at the Particle Accelerator Conference, May 1997, Vancouver (Canada).
[13] Mikhailov, V. G. et al, proc. of EPAC-94, June 1994, London (UK), World Scientific Singapore 1994.
[14] Sternglass, E. J., Phys. Rev. 108(1957)1-12.
[15] Clerc, H. G., NIM A113(1973)325.
[16] Coffin, J. P., and Engelstein, P., TOF systems for heavy ions, A.Bromley vol.7 p.292;
Girard, J., and Bolore, M., NIM 140(1977)279;
Busch, F. et al., NIM 171(1980)71;
Starzecki, W. et al., NIM 193(1982)499;
D'Erasmus, G. et al., NIM A234(1985)91;
Zebelman, A. M. et al., NIM 141(1977)439;
Odenweller, T. et al., NIM 198(1982)263.
[17] Calabretta, L. et al., INFN LNS, unpublished.
[18] Torrisi, L., INFN LNS, private communication.
[19] Launé, B. et al, presented at the RIB workshop, May 1997, Vancouver (Canada).
[20] Rezzonico, L. et al., presented at the RIB workshop, May 1997, Vancouver (Canada).
[21] Kleinevoss, U. for the ALADIN collaboration, GSI Annual Report (1995)179.
[22] Agodi, C. et al, IEEE Trans. Nucl. Sci. 45(1998)665.
[23] Cub, J. for the LAND collaboration, GSI Annual Report (1995)180.
[24] Finocchiaro, P. et al., NIM A385(1997)31;
Ciavola, G. et al., NIM B126(1997)258;
Finocchiaro, P. et al., NIM A419(1998)83;
[25] Amato, A. et al., LNS Report 14-10-97.
[26] P.Finocchiaro et al., NIMA437(1999)552;
P.Finocchiaro et al., IEEE Trans. Nucl. Sci. vol.45, n.3, (1998)508
[27] Finocchiaro, P. et al., IEEE Trans. Nucl. Sci. vol.48, n.4, (2001)1132.
[28] Cosentino, L. et al, NIM B209 (2003)340;
Amorini, F. et al., NIM B266 (2008)3325;
Cosentino, L. et al, IEEE Trans. Nucl. Sci. vol.50, n.4, (2003)774
[29] Cappello, S., Cosentino, L., Finocchiaro, P., NIM A479 (2002)243
[30] Cosentino, L., Finocchiaro, P., NIM B211 (2003)443
[31] Pappalardo, A., Cosentino, L., Harasimowicz, J., Welsch, C., Finocchiaro, P., in preparation

SECONDARY BEAM OVERVIEW AND LOW CURRENT MEASUREMENTS OF SPIRAL1 AND SPIRAL2 FACILITY

Christophe Jamet on the behalf of the Electronic Group,

The Operation Group and the SPIRAL2 Project (GANIL, Caen).

Abstract

Since 2001, radioactive beams have been accelerated in the CIME cyclotron of the SPIRAL facility at GANIL. In order to tune low intensity and low energy beams in the transport line, low current measurements and an identification stations have been used.

For the new project SPIRAL2, the production of high intensity radioactive beams will be based on fission of uranium target induced by neutrons.

These exotic particles will be produced, ionized, selected in a dedicated production building and transported to the existing CIME cyclotron for post-acceleration.

The beam diagnostics, required for the production facility allow a pre-tuning with a stable beam followed by an extrapolation of the tuning to the radioactive beam. Some diagnostic devices may also be used for equipment protections and for the safety systems.

This proceeding describes the present secondary beam diagnostics in the SPIRAL1 facility and the future secondary beams diagnostics foreseen by the SPIRAL2 project. These low current, low energy beams are/will be produced by the ISOL Method.

GANIL ACCELERATOR

GANIL which means “Great National Accelerator of Heavy Ions” is located in the town of CAEN, France.

The complete accelerator installation is composed by five cyclotrons. Two ion sources and two compact cyclotrons produce and accelerate two ion beams at an energy around 1MeV/A for the lightest beam. One of the two beams is accelerated by two separated sector cyclotrons up to 95 MeV/A. The facility delivers a wide spectrum of high intensity ion beams ranging from ^{12}C to ^{238}U .

The primary beam at the exit of SSC2 can be sent directly through an alpha spectrometer toward experimental rooms. This beam can also be driven, since 2001, in the SPIRAL1 facility to produce secondary radioactive beams.

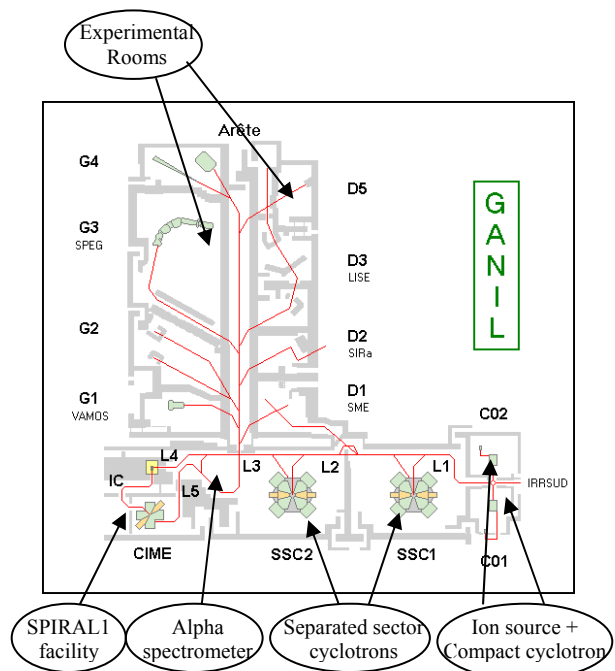


Figure 1: GANIL Accelerator Layout

SPIRAL1 FACILITY

The primary beam from SSC2 with a current up to $15\mu\text{A}$, is driven through the HEBT line on a thick carbon target.

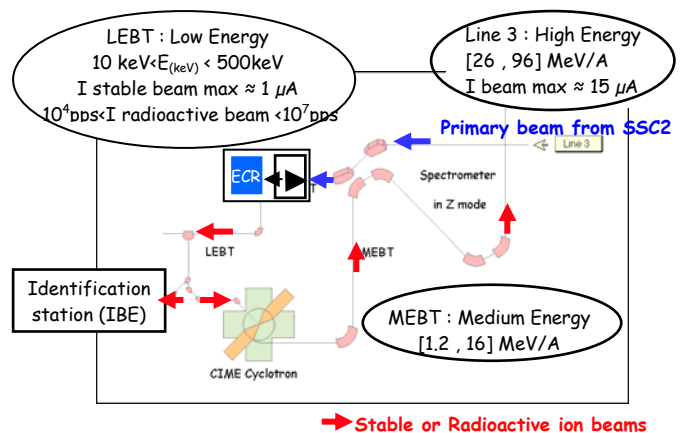


Figure 2: SPIRAL1 Layout

The production of atoms is done by projectile collisions on a thick carbon target. Then atoms are ionized by an ECR ion source.

The stable beams at the source exit have an intensity value up to $1\mu\text{A}$. The radioactive beam intensity is included between 10^4 pps and 10^7 pps.

Radioactive beams can be driven either in an Identification station either in the CIME cyclotron. The energy range available, at the exit of CIME, goes from 1.2 MeV/A to 25 MeV/A.

SPIRAL1 TUNING

Tunings are done by three stages.

1 Tuning with a stable beam

The initial tuning of LEBT, CIME and MEBT is realised with a stable beam delivered by the ion source. (Allow the use of classic diagnostics)

2 Shift of electrical and magnetic fields

Electrical and magnetic values are changed by a factor depending of the ratio Q/M of stable ions and Q/M of radioactive ions. The frequency or the magnetic field is shifted in the CIME cyclotron.

3 Controls of the radioactive beam

The radioactive beams are controlled by:

- Germanium detector in the LEBT (Identification Station)
- Silicon detectors in the CIME cyclotron
- Gas profilers in the MEBT

LEBT DIAGNOSTICS

1 Beam current measurements

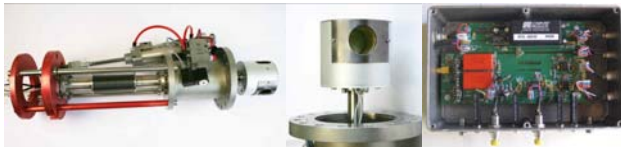


Figure 3: Faraday Cup & Logarithmic Converter

Faraday cups and logarithmic converters are designed for low beam current measurement. The intensity range is included between 10^7 to 10^{14} pps in correspondence to around 1pAe to 1mAe .

The principle of a logarithmic converter is to give a proportional voltage to the logarithm of the current. In the SPIRAL case, the voltage is equal to zero for a current of 10 nAe and two volts correspond to a factor of ten on the input current.

$$V = 2 \log \frac{I}{I_0} \quad \text{With } I_0 = 10\text{nAe}$$

Faraday cups with log. electronics are easy to use without gain switch but the sensitivity is limited by the reverse current in diodes and Ibias influence of amplifier.

2 Beam Profile measurements

(See the DITANET proceeding of J.L. Vignet)

3 Radioactive beam diagnostics

An identification station characterises the radioactive ions. In the vacuum chamber, a faraday cup, a plastic detector and a silicon detector are installed or can be installed and behind the chamber a germanium detector is available to measure gamma rays.

Ions can also be implanted onto a tape and be transported to the front of a remote germanium detector. This system gives the possibility to count gamma ray for long life radioactive ions with a germanium detector.

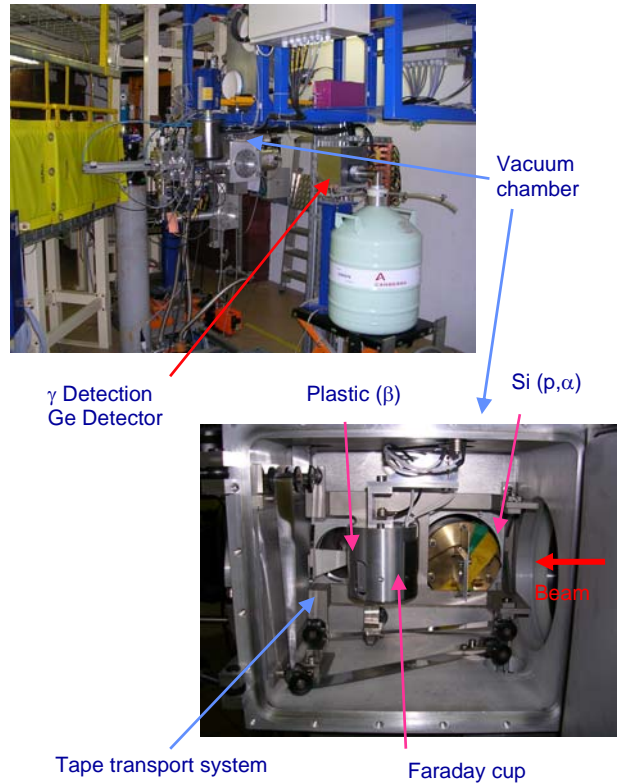


Figure 4: IBE setup

These detectors are used by physicists during dedicated studies. In general, the germanium detector is only used for the beam counting. In this case, the beam is stopped and gamma rays produce by the radioactive ions are detected by a Germanium detector.

$$I_{\text{beam}} = \frac{\text{Disintegration_number}}{\text{Efficiency}}$$

The beam current is proportional to the disintegration number and the efficiency. An estimation of the beam current can be done.

This station enables to identify radioactive species and estimate the number of ions but with a complicated use.

SPIRAL2 PROJECT

The SPIRAL2 project consists in building a new facility near the GANIL accelerator in order to produce new exotic beams in the GANIL experimental rooms.

The accelerator is divided in 3 main parts, an injector, a superconducting linac and a high energy line. The injector part is composed of a deuteron/proton line, an ion line (LEBT), a RFQ and a MEBT line. Two kinds of superconductivity cavity are used for the Linac ($\beta=0.07$,

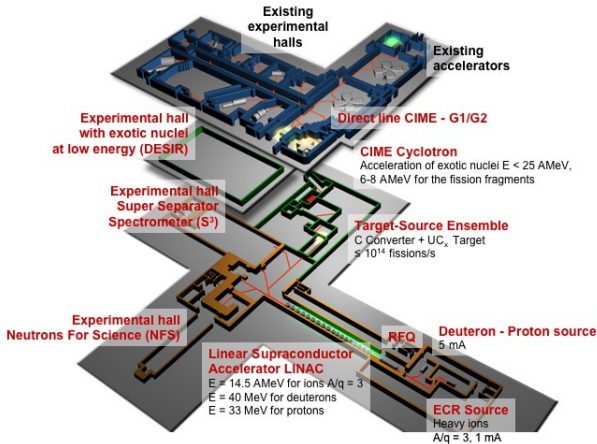


Figure 5: SPIRAL2 layout

The beam energy will be up to 14.5MeV/A for ions, 40MeV for deuterons and 33 MeV for protons. The beam intensity is foreseen to be up to 1mA for ion beams and 5 mA for deuteron beams. At the Linac exit, the beam could be sent in experimental halls NFS and S3. The third possibility will be to drive the deuteron beam in a target source system to produce radioactive beams.

RADIOACTIVE BEAM SECTION

The primary beam arrives on a carbon wheel in which the deuterons are broken. The neutrons, without electric charge, go through the converter and produce radioactive atoms by fission of an uranium carbide target.

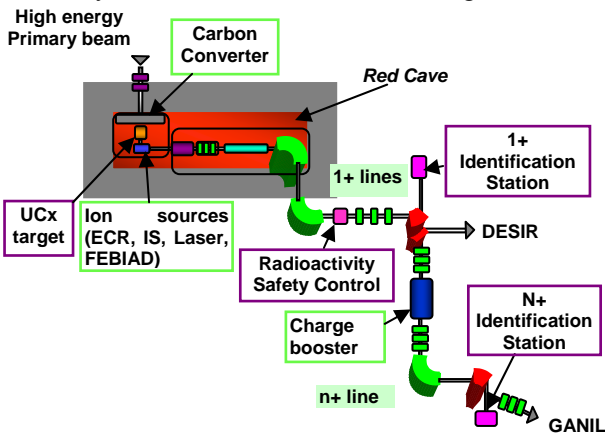


Figure 6: RNB general scheme

Mono-charged secondary beams are selected in the 1+ beam line, used for low energy experiment or multi ionized to be post accelerated in the existing Ganil.

The red cave is an unauthorized area where all interventions will be done by remote controls with robots. A safety system has to control the beam radioactivity at the exit of the red cave.

TUNING AND CONTROL METHODS

The tuning principle of the SPIRAL2 beams consists in a pre-tuning with a stable beam, followed by an extrapolation to the radioactive beam (SPIRAL1 method).

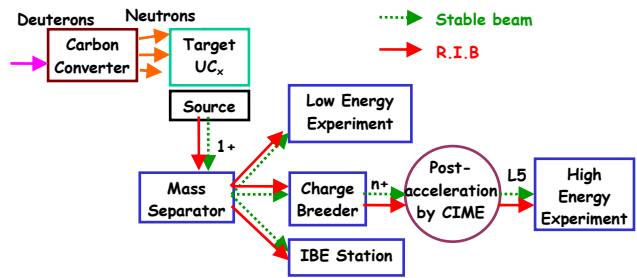


Figure 7: Stable beam tuning and R.I.B. tuning

The radioactive beams will be controlled at special points and identified in identification stations.

BEAM CURRENT MEASUREMENTS

A new electronic device will be needed to measure low beam currents. The choice is to use linear I/V converters with different gains for measuring current under 0.1 pA.

- Two I/V converters will be tested in 2010:
A new commercial I/V: FEMTO DDP-300
Very High Dynamic Range: Sub-fA to 1 mA
Transimpedance Gain Switchable from 10^4 to 10^{13} V/A
- A GANIL I/V prototype with the amplifier LMP7721. The typical input bias current is 3fA

R.I.B. CONTROL

The R.I.B (Radioactive Ion Beams) control is foreseen with the use of devices containing implantation foil and semiconductors to measure the beam radioactivity (gamma radiation) and control the transmission in the beam lines.



The XR-100T-CdTe represents a breakthrough in x-ray detector technology by providing "off-the-shelf" performance previously available only from expensive cryogenically cooled systems.

Figure 8: CdTe detector

This CdTe detector is under development at Ganil (resolution: 0.8 % FWHM at 662 keV).

IDENTIFICATION STATIONS

The goal of the Identification Stations will be:

- to identify the radioactive ions by their characteristic radioactive decay
- to measure the intensity of the nucleus of interest and the contaminants
- to enable an optimization/tuning of the target-ion source and the charge-breeder system

The developments and realisations will be done by the LPC Laboratory from CAEN.

RADIOACTIVITY SAFETY CONTROL

An intensity control of the continuous radioactive beam is necessary in a range of 10^9 to 10^{13} pps (100pAe to $1\mu\text{Ae}$) at the exit of the red production cave.

This control must ensure that the radioactivity and the associated contamination never reach a maximum rate in the production building and Ganil.

Beam intensity measurement is a possibility, three solutions are studied, and each one requires a beam modulation.

Beam Current Transformer

The best measurement resolutions at GANIL with these sensors are of the order of nAe ($\approx 10^{10}$ pps). The minimum threshold value is fixed ten times bigger than the resolution ($\approx 10^{11}$ pps). This resolution can't respond for the safety control needs.

Pick-Up

The modulated beam produces pick-up signal amplitudes proportional to the beam intensity.

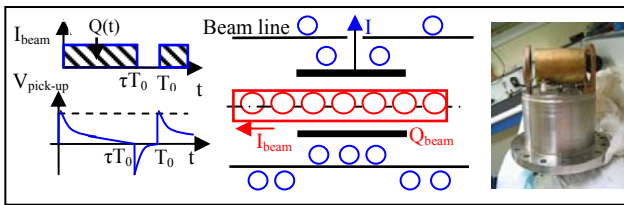


Figure 9: Views of the GANIL pick-up.

$$|Q_{\text{pick-up}}| = |Q_{\text{beam inside the pick-up}}| \\ = I_{\text{beam}} * \text{time inside the pick-up}$$

The beam charge inside the pick-up is equal to the product of the beam intensity by the time done to go through the pick-up.

$$V_{\text{pick-up}} = \frac{Q_{\text{pick-up}}}{C} = \frac{1}{C} \cdot I_{\text{beam}} \cdot \frac{L}{v}$$

L: Pick-up length
v: beam velocity

Measurements were done with a preamplifier and a lock-in amplifier Stanford Research SR830 at a frequency around 10kHz.

The best measurement resolutions for these sensors at low energy (20keV) are of the order of 10nAe ($\approx 10^{11}$ pps). A threshold value under $\approx 10^{12}$ pps can't be guaranteed.

Faraday Cup Associated With a Fast Electrostatic Deflector

A device equipped with an electrostatic deflector and a low intensity Faraday cup enables to measure a part of the beam current. This electrostatic deflector could deflect, for example, at a frequency of 1kHz, with a useful ratio for measurement of 5 %, leaving 95 % of the continuous beam for the users (Fig. 10).

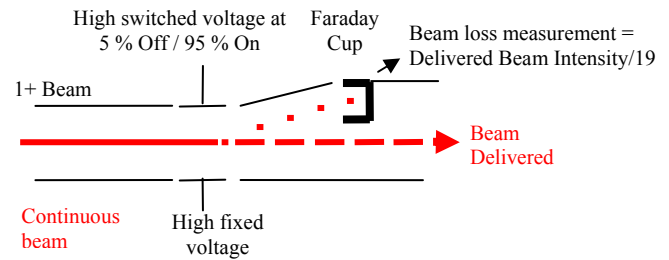


Figure 10: Faraday cup associated with a fast electrostatic deflector.

In this case, a Faraday cup resolution of 1 pAe, by guaranteeing the "deflector" function, provides an indirect resolution of 20 pAe on the beam users. This device could control and guaranty in all circumstances a user beam threshold of about 200 pAe ($2 \cdot 10^9$ pps). This solution gives a sufficient sensitivity.

CONCLUSION

The feedback of the GANIL and SPIRAL1 operation contributes to define the beam tuning methods and to design diagnostics.

However, all diagnostics in the RIB facility will have to operate in a new and strong nuclear environment. Diagnostics will have to be simple, robust, and reliable.

REFERENCES

- [1] JL. Vignet & al, The beam profile monitors for Spiral 2 RIB and Experimental rooms, DITANET 09 Workshop on "Low current, low energy beam diagnostics"
- [2] P. Anger & al, Beam Diagnostics for SPIRAL2 RNB facility, DIPAC09, Basel, MOPD30
- [3] P. Ausset & al, SPIRAL2 Injector Diagnostics, DIPAC09, Basel, MOPD27
- [4] C. Jamet & al, Injector Diagnostic Overview of SPIRAL2 Accelerator, DIPAC07, Venice
- [5] M. H. Moscatello et al., Technical report of the radioactive beam section of SPIRAL2. Ganil report (2007, DECEMBER).

THE BEAM PROFILE MONITORS FOR SPIRAL 2 RIB AND EXPERIMENTAL ROOMS

Jean Luc Vignet, Eloïse Guérout, Patrice Gangnant, Alexandre Delannoy
GANIL, BP 55027, 14076 Caen Cedex 5, France

In order to visualize the SPIRAL 2 radioactive ion beams, several beam profile monitors are under development.

Multiwires beam profile monitors (SEM), low pressure gas monitor (LPGM) and low intensity beam profile monitor (EFM) will be used on the RIB lines.

For the signals acquisition of all this kind of monitors, a new associated electronics will be used. This electronic digitizes 94 channels in a parallel system. Each channel integrates the current of the associated wire or strip and performs a current-voltage conversion.

The dedicated GANIL data display software has been adapted for these different new monitors.

SPIRAL2 DESCRIPTION

The SPIRAL2 facility is based on a high-power superconducting driver LINAC which delivers a high-intensity, 40-MeV deuteron beam, as well as a variety of heavy-ion beams with mass-to-charge ratio equal to 3 and energy up to 14.5 MeV/u. The driver accelerator will send stable beams to a new experimental area and to a cave for the production of Radioactive Ion Beams (RIB). The Accelerator building construction (phase 1) will started in 2010 and the RIB production building (phase 2) in 2012. (Figure 1)

The commissioning of the driver should start in 2011 at GANIL.

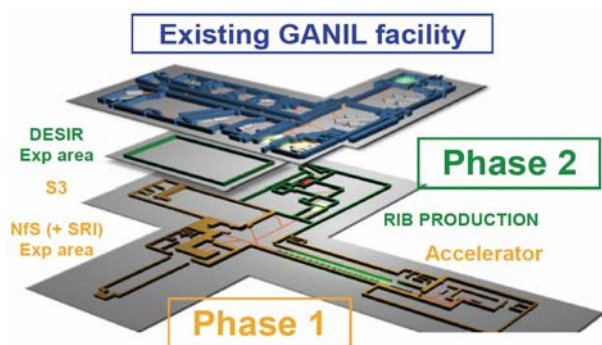


Figure 1 : Spiral 2 and GANIL facilities

RIB PRODUCTION

The 40 MeV, 5 mA deuteron beam impinging on the converter, produces an intense neutron flux with an energy centered at 14 MeV. Neutrons induce fission in the UC target located downstream of the target converter. The converter has to withstand up to 200kW beam power. The converter is a high speed rotating target which limits the peak surface temperature of converter materials far below 2000°C. The thermal power deposit in the converter material is dissipated only by thermal radiation (Figure 2).

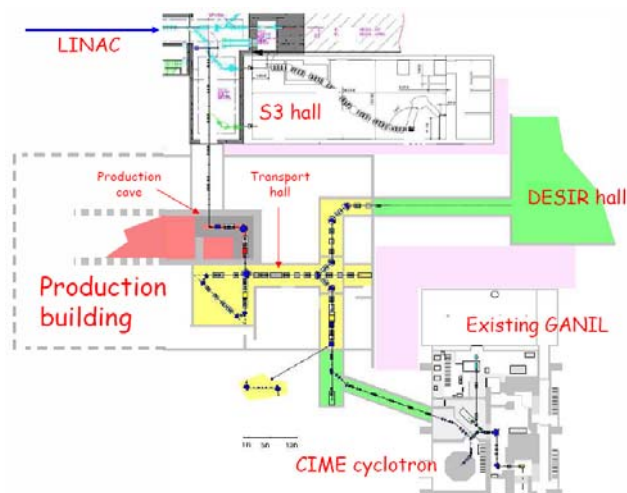


Figure 2 : radioactive beam facilities

RADIOACTIVE BEAM CHARACTERISTICS

	Line 1+	Line n+	Existing ganil
Ion mass range	6 to 240	6 to 160	6 to 160
Intensity range	10^3 to 10^{11} pps	10^3 to 10^{10} pps	10^3 to 10^9 pps
Beam energy	10 to 60 keV	10 to 45 keV	1.2 to 25 MeV/u
Example of RIB	$^{132}\text{Sn}^{1+}$	$^{132}\text{Sn}^{20+}$	$^{132}\text{Sn}^{20+}$
	20 keV	400 keV	792 MeV

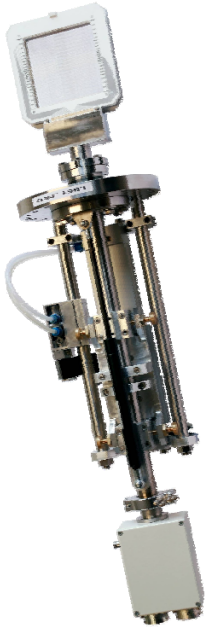
BEAM DIAGNOSTICS

In order to drive the SPIRAL2 radioactive beam along the beam transport three kinds of beam profile monitor are under development at GANIL.

Profiler type	Energy range	Intensity range	Quantity needed
EMS	$20 \text{ keV} < E$	$10^8 \text{ pps} < I < 10^{11} \text{ pps}$	40
LPGM	$500 \text{ keV/A} < E$	$10 \text{ pps} < I < 10^7 \text{ pps}$	10
EFM	$20 \text{ keV} < E$	$10 \text{ pps} < I < 10^9 \text{ pps}$	10

EMS profilers are the same as those used for the Spiral2 accelerator lines. Gas profilers are soon in used at Ganil and have been adapted for the low energy and the low intensity Spiral2 beam (LPGM). Emissive foil profilers (EFM) are new kind of profile monitors and should be operational in 2013.

SECONDARY EMISSION MONITOR (SEM)



These monitors are composed of an horizontal and a vertical grid of golden tungsten wires of 150 μm diameter. Three kinds of grid can be installed, depending on the maximum size needed to be measured (Figure 3). These wires are welded on an alumina board to obtain a maximum out-gassing rate of $1.10^{-8} \text{ Pa}\cdot\text{m}^3\cdot\text{s}^{-1}$. The total mechanical precision of this diagnostic is 0.2 mm.

Figure 3 : SEM profiler

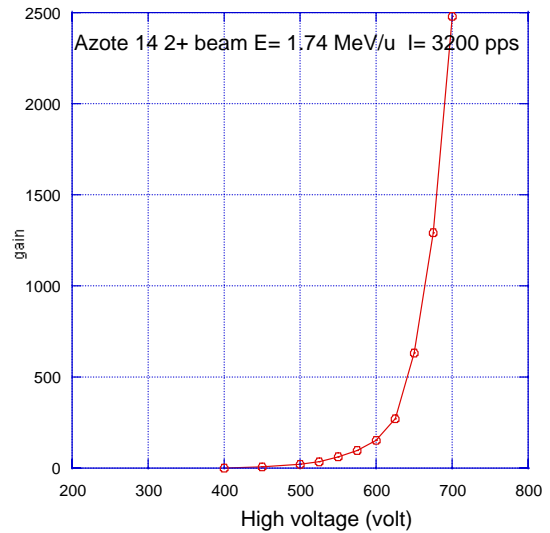


Figure 6: amplification signal versus high voltage variation

The acquisition datas are read by the standard electronics Ganic device and displayed on PC with Ganic acquisition software (Figure 7).

LOW PRESSURE GAZ MONITOR (LPGM)

In order to visualize radioactive beam energy in the range of 0.5 MeV/u - 25 MeV/u with intensity of a few pps to 10^7 pps a new kind of beam profile have been studied (Figure 4). A low pressure gas monitor working like a ionization chamber and is constituted by a secondary electron emission profiler that is in a octafluoropropane (C3F8) pressure of 10 mBar. The gas volume is contained in the profiler head with a 6 microns Mylar entrance window.

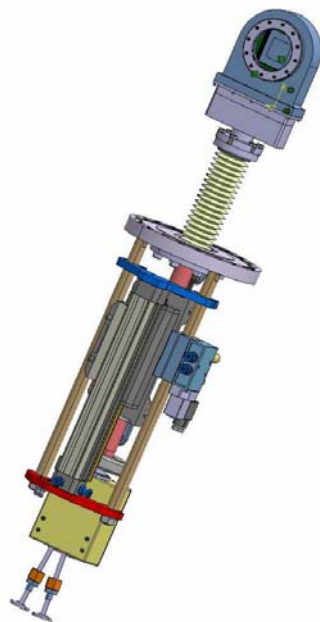


Figure 4 : LPGM profiler

A gas regulation central is connected to the Profiler in order to regulate the gas pressure. The signal amplification depending of the beam characteristics is adjusted by the high voltage applied on grid that are disposed on each side of the wires plane (Figure 5 and 6).

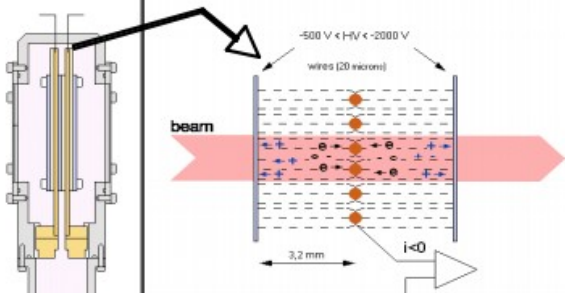


Figure 5 : operating principle

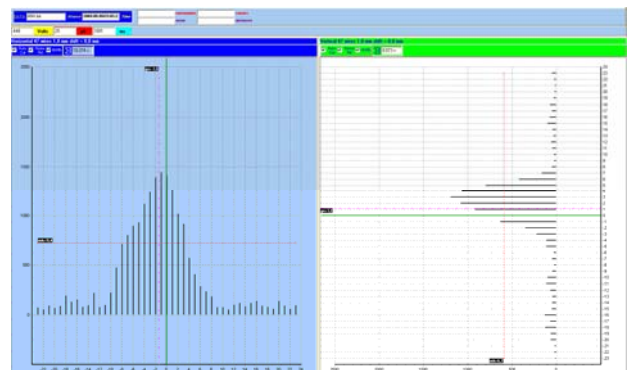


Figure 7 : Azote14 2+ beam profile
E= 1.74 MeV/u, I= 3200 pps

LOW INTENSITY BEAM PROFILE MONITOR (EFM)

A secondary emission foil profiler is under development (Figure 8) and will be used on the SPIRAL 2 radioactive beam lines and the experimental rooms. It will monitor low intensity in the range of 10^1 to 10^9 pps and low energy beams from 20 keV. The impact between the beam and the foil will create secondary electrons. These electrons are guided by electric and magnetic field through a drift space. Micro-channel plates will amplify the number of electrons in order to be collected on an X-Y grid.

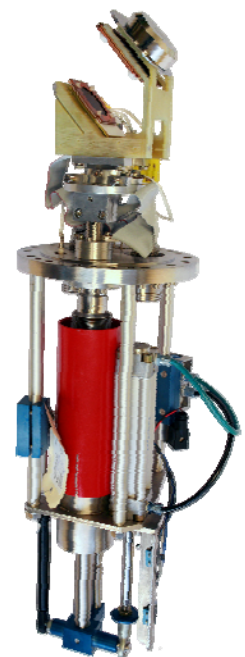


Figure 8 : EFM profiler

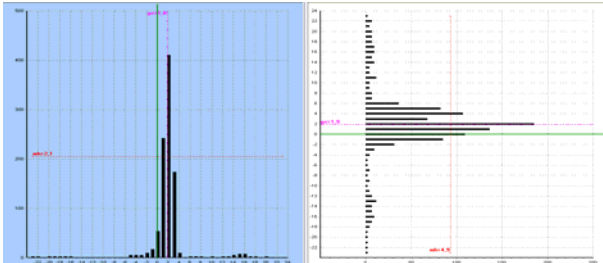
The desired resolution is 1mm in each dimension.

During a test with a $^{12}\text{C}^{2+}$ Beam at 5 Mev/u with 10^5 particles per second, the EFM Beam Profile has been compared with a standard gas monitor profile. Acquisition results are shown below (Figure 9).

Standard gas beam profile

Horizontal plane

Vertical plane



EFM beam profile

Horizontal plane

Vertical plane

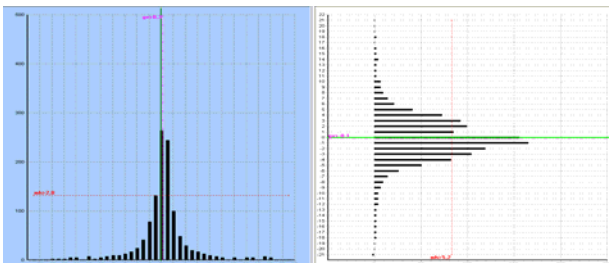


Figure 9 : beam profile acquisition

This detector is under redesigning in order to have an homogeneous magnetic field.

ASSOCIATED ELECTRONICS FOR ALL BEAM PROFILE MONITORS

These electronics digitize 94 channels in a parallel system. Each channel integrates the current of the associated wire or strip and performs a current-voltage conversion with two possibilities: passive system for high intensity beams and active system for low intensity beams.

The front end (active or passive signal integration) is implanted on 12 daughter boards of 8 channels to streamline the maintenance and to keep the electronic modularity. For the digitalization, we have chosen a heavily parallel organization for a good A/D conversion speed (about 4 μs) and best signal shape conservation. Acquisition of this digital data and their treatments is done by a FPGA (ALTERA Cyclone 3). All the automatism related to the sensor (high voltages, insertion, Micro-channels plates protection, front end protection) are managed by a microcontroller (FREESCALE 68HCS12). Communication with the command/control (Modbus protocol over TCP/IP) and global equipment setup (integrated WEB server) are managed by a microprocessor (FREESCALE coldfire 5282) executing RTOS.

A first prototype of this electronic system (without control of automatism) was successfully tested in 2008. A pilot series with all facilities will be developed in 2009.

The series of 20 electronics for LBE and LME will have to be ready for the end of 2010.

CONCLUSIONS

The development of these different kinds of beam profile will permit to cover all the dynamic of the Spiral 2 energy and intensity radioactive beam. Last test are now in progress to perform LPGM and EFM profile solution before fabrication.

REFERENCES

- [1] R. Anne et al., A non interceptive heavy ion beam profile monitor on residual gas ionisation, NIM, A329 (1993) 21-28
- [2] R. Anne et al., Beam profile and beam time structure monitors for the extracted beams from the Ganil cyclotrons, 15th International Conference and their application. Caen France 14th – 19 th June 1998
- [3] JL Vignet et al., The beam profile monitors for SPIRAL2. DIPAC 2009 (TUPB07)
- [4] P. Anger et al. Beam diagnostics for SPIRAL2 RNB facility. DIPAC 2009 (MOPD30)

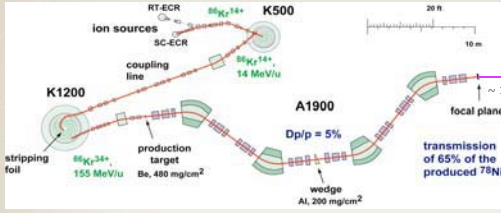
LOW-ENERGY LOW-INTENSITY DIAGNOSTICS FOR REA3 @ NSCL/MSU

DIAGNOSTICS FOR THE NEEDS OF FRIB

G. Perdikakis for the ReA3 team



National Superconducting Cyclotron Laboratory

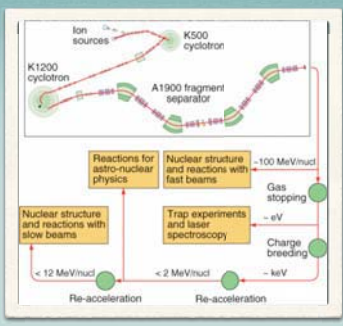


Experiments with fast RIBs

- Cyclotron-based facility
- Fast Radioactive Beams by projectile fragmentation
- Fragments Energy ~ 100 MeV/u

2

Science opportunities @ ReA3



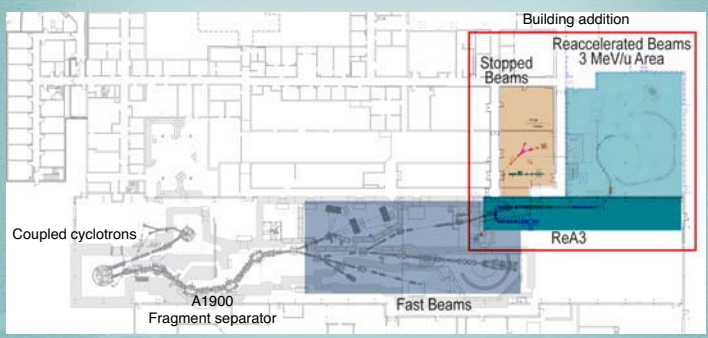
- ReA3 part of FRIB - to be extended to 12 MeV/u (ReA12)
- Allows to develop techniques and programs before FRIB operation

to be completed in 2010

3

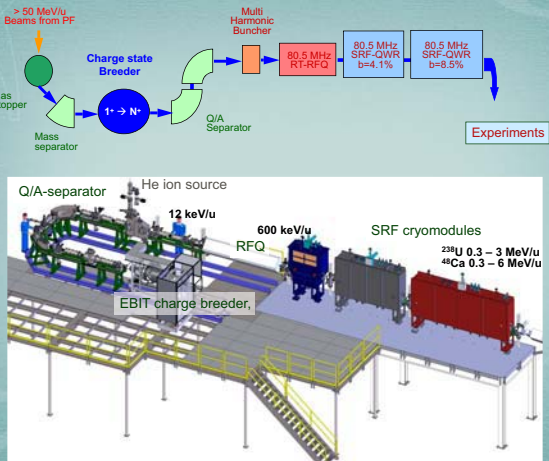
ReA3 at the Coupled Cyclotron Facility

- Coupled cyclotrons beams : ~ 100 MeV/u
- ReA3 beams : 0.3 - 3 MeV/u for Q/A=1/4 rare isotope beams

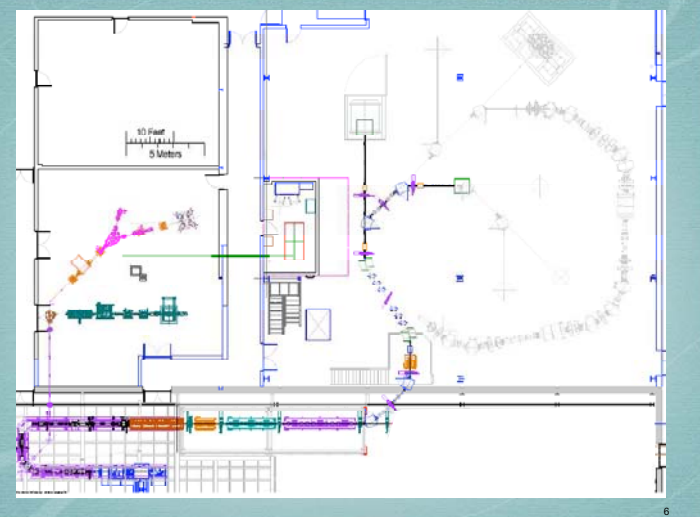


4

THE REA3 CONCEPT



5



6

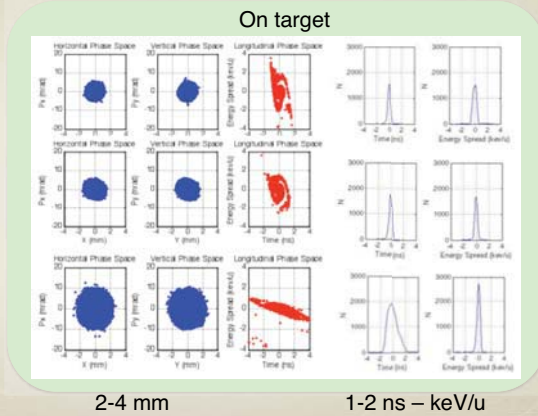
Beam Phase Space

• Q/A=0.25

4.6 MeV/u

3.0 MeV/u

0.3 MeV/u



Challenges for ReA3 diagnostics

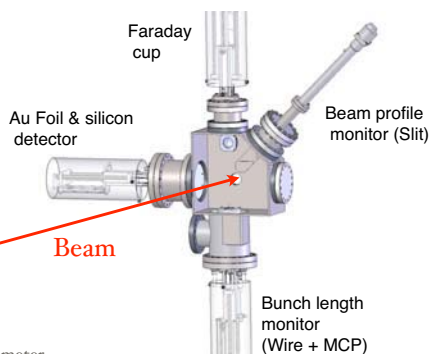
- * Intensity of radioactive beam <math>< 10^6</math> pps
- * Broad range of projectile mass and energy
- * Energy loss limiting
- * High Resolution required
- * Tuning with higher intensity stable beam

Diagnostics wish-list for ReA3

- * **Detect presence of radioactive beam**
- * **Measure beam properties**
 - * Beam rate
 - * Time structure (pulse width) – longitudinal emittance
 - * Transverse profiles— transverse emittance
 - * Energy
- * **Facilitate optimizing cavity voltage and phase**
- * **Facilitate transport to experiment**

Analog beam for setting accelerator

- * Beam provided from the stable ion source
- * Same Q/A as the radioactive ion
- * Charge breeding done in EBIT
- * ReA3 is tuned up using the stable ion beam with intensity - nA



also:
Emittance meter
YAG viewer plate
MCP+phosphor screen
Decay counter

Elastic Scattering Detector

- 40 nm Gold foil @ 15° to the beam
- PIPS Si detector @ 30° to beam
- Phasing of Cavities
- Energy measurement
- Fair timing resolution (down to 200ps)

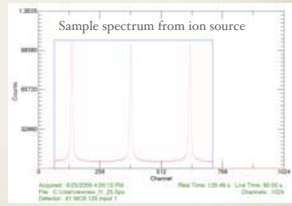


Design based on TRIUMF diagnostics

Timing Wire Detector

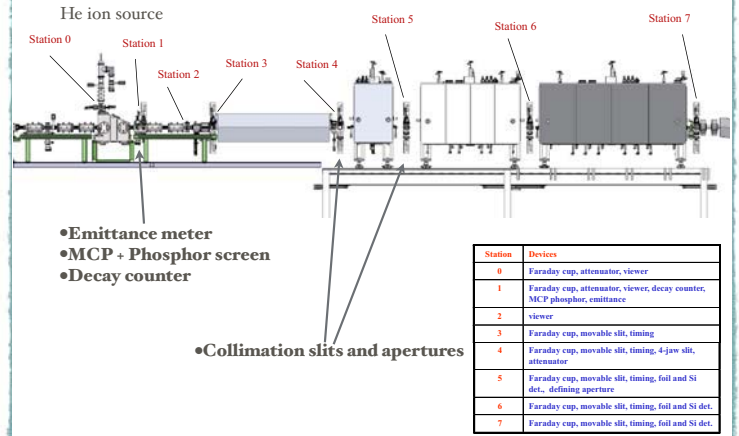


- Thin Nb Wire + MCP detector
- Time resolution < 100ps possible
- Longitudinal Phase-Space
- Energy by Time-of-Flight



Design based on TRIUMF diagnostics

Low Energy Beam Transport



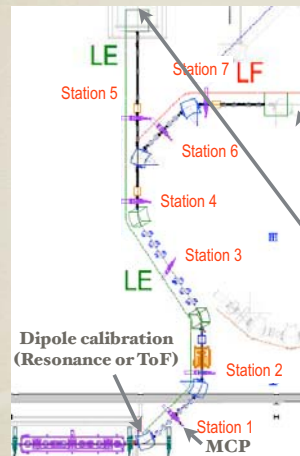
High Energy Beam Transport

Wish-list

- * Measure radioactive beam properties
- * Beam rate
- * Time structure (pulse width) – longitudinal emittance
- * Transverse profiles— transverse emittance
- * Energy distribution of beam
- * Purity and Particle identification of beam species



High Energy Beam Transport



Name	Diagnostics device
DP1	VP, FC, Collimation Aperture
DP2	FC, SL, WC, FS
DP3	VP, FC
DP4	VP, FC, WC
DP5	VP, FC
DP6	VP, FC, Collimation Aperture
DP7	VP, FC
VP:	Viewer/Camera
WC:	Wire and cylinder
SL:	Movable slit
FS:	Foil + Si detector
FC:	Faraday Cup

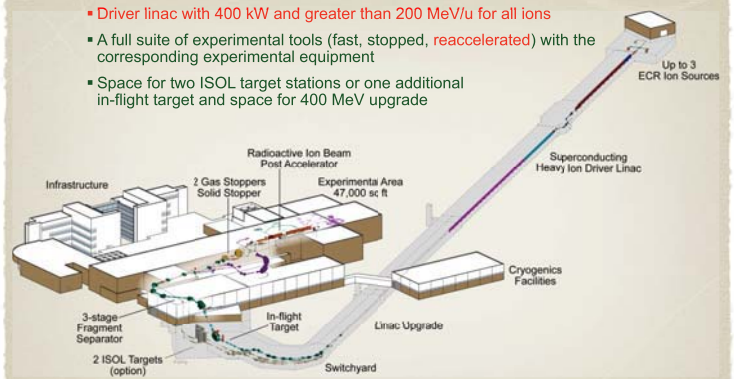
- + General Purpose Diagnostic Station
- Segmented Anode Ionization Chamber
- PID by differential energy loss
- Event by event diagnostic

Linac commissioning in mid-2010

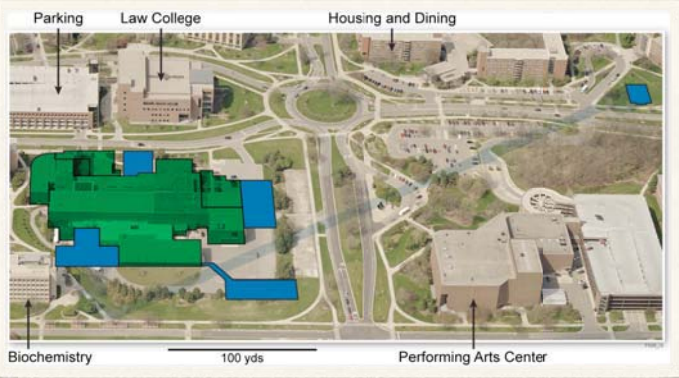


FRIB General Features

- Driver linac with 400 kW and greater than 200 MeV/u for all ions
- A full suite of experimental tools (fast, stopped, reaccelerated) with the corresponding experimental equipment
- Space for two ISOL target stations or one additional in-flight target and space for 400 MeV upgrade



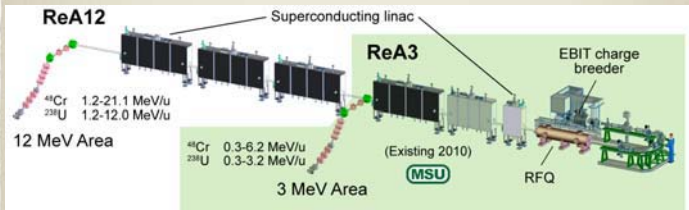
FRIB @ MSU Campus



• Green – existing
• Blue - new

19

Upgrade ReA3 to ReA12



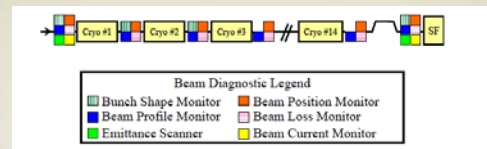
20

Special needs of FRIB

- High Power accelerator (400Kw at exit of Linac)
- Beam loss tolerance of $\leq 1W/m$ (i.e $\leq 2.5 \times 10^{-6}/m$ fractional loss at exit)
- Fast detection of Beam loss accidents
- Long linac with many SRFcavities
- Suboptimal performance critical. Has to be detectable by diagnostics

21

Conceptual design of Diagnostics for Segment 1



Diagnostics system currently being designed

Important elements:

- Beam Dynamics simulations for critical operation scenarios
- Radiation transport simulations
- Final linac design
- Upgrade possibilities?

22

Conclusions

- * Diagnostics important for ReA3 linac tuning
- * Special diagnostics needed for RIB experiments
- * ReA3 Linac + Diagnostics under construction
- * Commissioning in 2010 with stable beam
- * First RIB experiments in 2011
- * FRIB diagnostics a challenge - design kicked off
- * Stay tuned ...

23

THE END

24

Detectors and what we use them for at ELISA

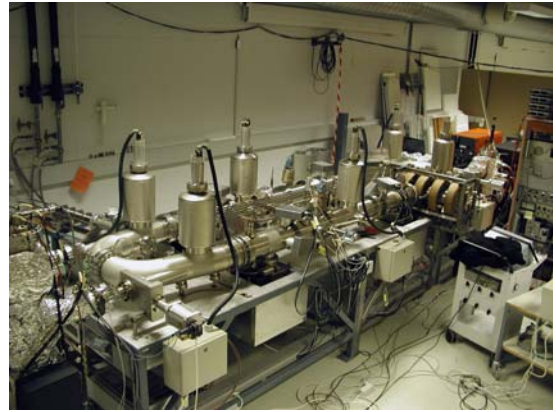
Kristian Støchkel

Department of Physics and Astronomy
Aarhus University

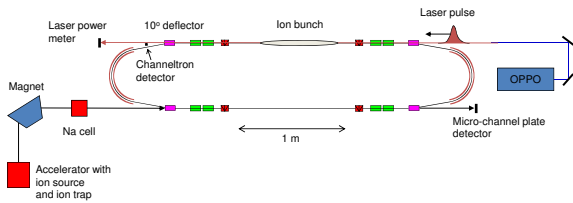


Low Current, Low Energy Beam Diagnostics, November 25, 2009

Electrostatic Ion Storage ring in Aarhus (ELISA)



Elisa data



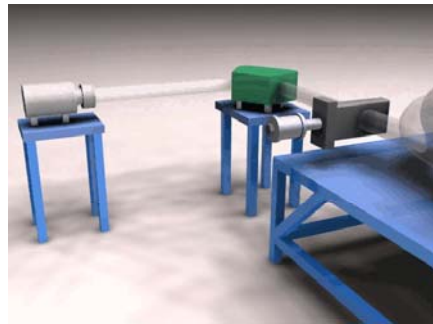
Ring design:

- 8.3 m in circumference
- 160° deflectors
- 10° deflectors
- Stores ions with energies up to 22 keV per charge

Beam diagnostics:

- 4 horizontal pickups
- 4 vertical pickups
- Scrapers
- MCP detectors

Electrostatic Ion Storage Ring Aarhus (ELISA)



S.P. Møller, *NIM A* 394, 281 (1997).

J.U. Andersen, J.S. Forster, P. Hvelplund, T.J.D. Jørgensen, S.P. Møller, S. Brøndsted Nielsen, U.V. Pedersen, S. Tomita, H. Wahlgreen, *Rev. Sci. Instrum.* 73, 1284 (2002).

ELISA = Electrostatic Ion Storage ring Aarhus

Commisioned in 1999

ENTIRELY ELECTROSTATIC

Advantages:

- Store ions of fixed charge and energy with arbitrary mass
- Useful for study of heavy ions: fullerenes, biomolecules and other macromolecules

Combined with an electrospray ion source and a multipole ion trap to accumulate the ions for injection into ELISA.

Two others are operating in Japan, rings in Stockholm, Frankfurt and Heidelberg are under construction.

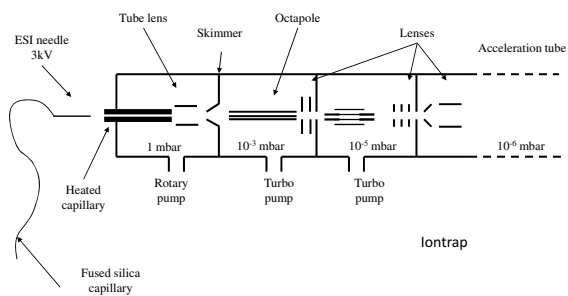
Three pieces of information

Lifetimes with respect to dissociation

At what wavelengths ions absorb light

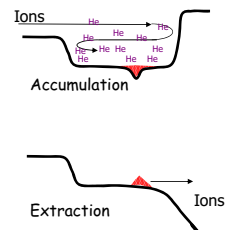
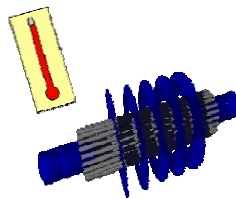
Daughter ion masses

Electrospray ion source



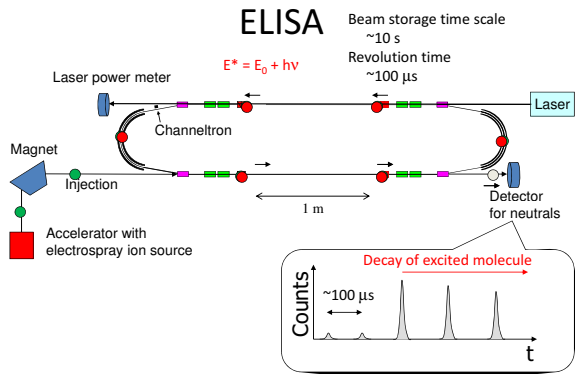
7

22-pole ion trap



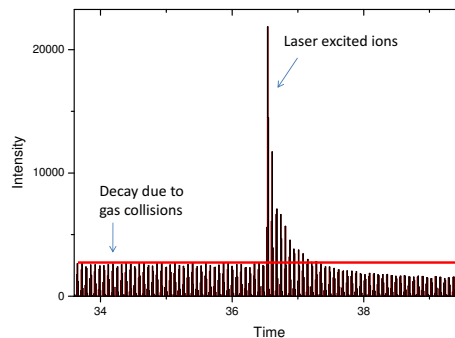
8

ELISA



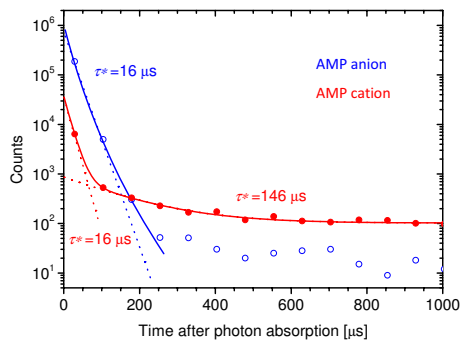
9

LASER EXCITED IONS



10

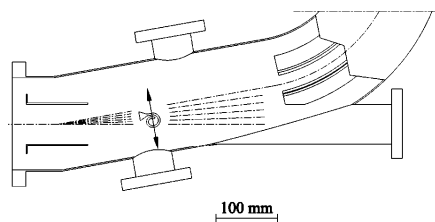
Lifetimes for statistical dissociation of photoexcited ions



S. Brøndsted Nielsen, J.U. Andersen, J.S. Forster, P. Hvelplund, B. Liu, U.V. Pedersen, and S. Tomita, *Phys. Rev. Lett.* **91**, 048302 (2003)

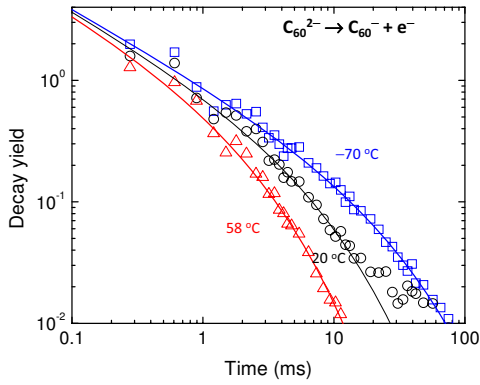
11

Channeltron detector



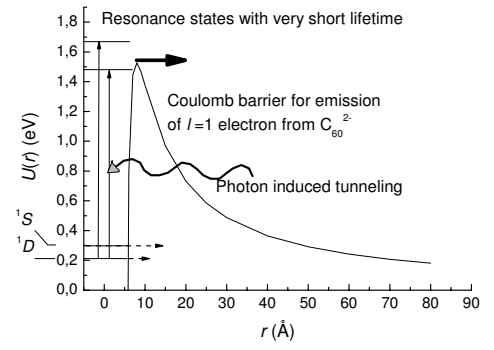
12

LIFETIME SPECTRA OF C_{60}^{2-} WITH RESPECT TO ELECTRON LOSS



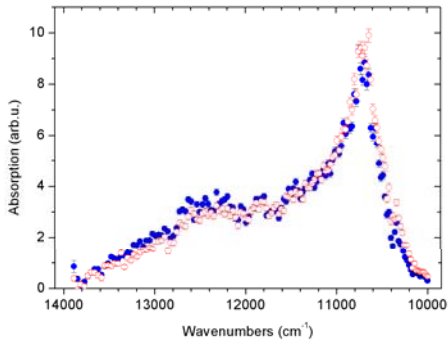
13

SPECTROSCOPY OF C_{60}^{2-} STATES



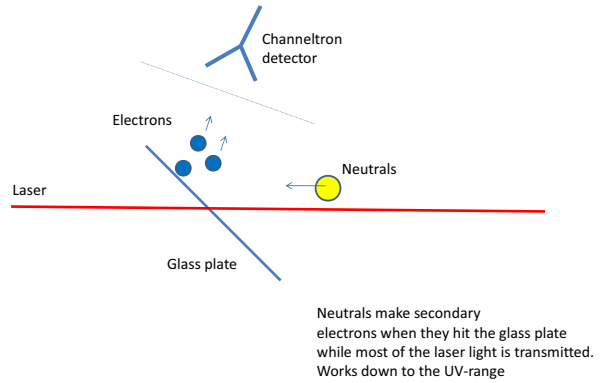
14

ABSORPTION SPECTRA OF C_{60}^{2-} AFTER DIFFERENT STORAGE TIMES



15

Glass plate detector / secondary electron detector.

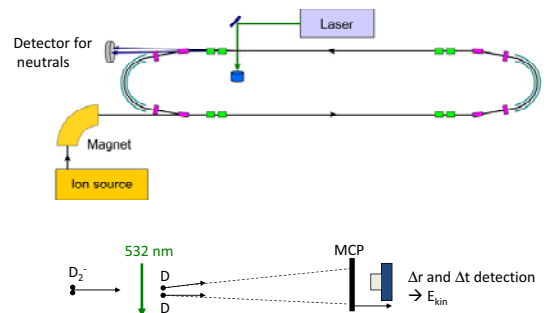


16

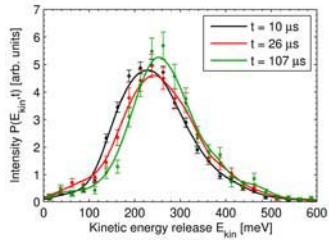
Momentum imaging of ions stored in ELISA

17

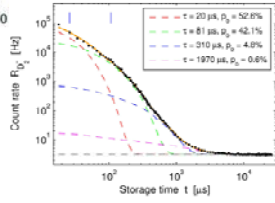
Momentum imaging of ions stored in ELISA



18

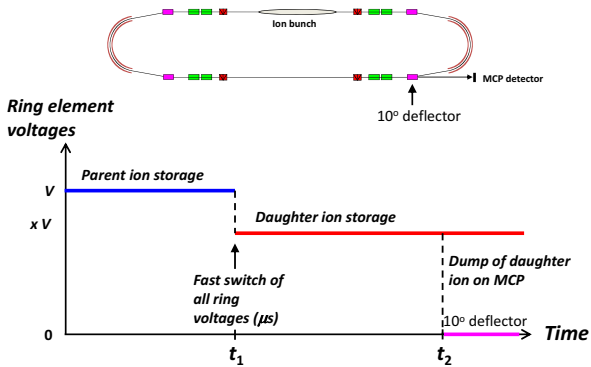


$$E_{kin} = \frac{1}{2} \mu [(\Delta r)^2 + (\Delta t v_b)^2] \left(\frac{v_b}{L} \right)^2$$

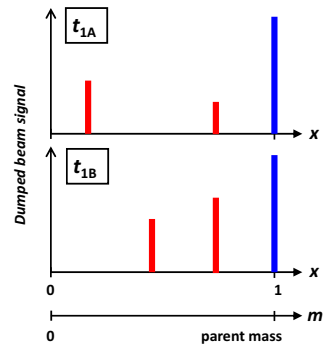
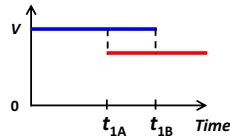


ELISA: A new scheme for daughter ion mass spectrometry

ELISA: A new scheme for daughter ion mass spectrometry

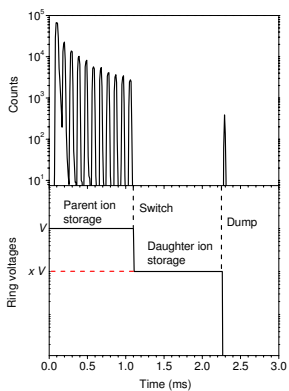


Signal in MCP detector as a function of scaling parameter x and storage time t1



Time-resolved fragmentation mass spectrometry on the μs to ms time scale

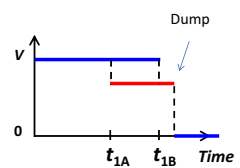
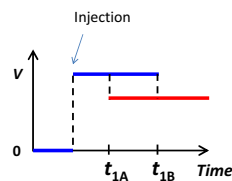
Dissociation of a molecule in the ring



- 1) Molecule was stored in the ring
- 2) After 1.1 ms, ring voltages were switched to store daughter ion
- 3) After 1.15 ms of storage, the daughter ion was dumped in the MCP detector

Consideration for switching times, type of switches ..

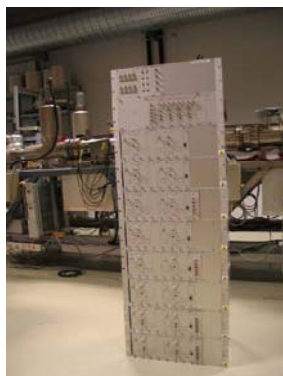
- Switch times faster than 1 μs
- Voltages up to 3 kV
- Vertical needs to be bipolar
- Injection and dump switch – 3 levels.



Horizontal deflectors:
16 new solid state switches with power supplies

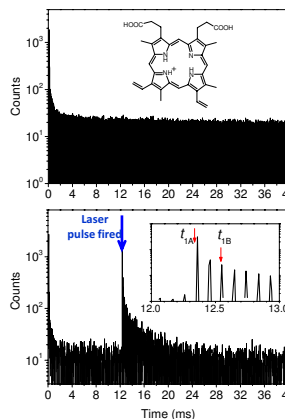
Vertical deflectors:
Replaced by fast amplifiers (bipolar).

All is integrated into the control system.



25

Photodissociation of protoporphyrin ions in ELISA with 390-nm light

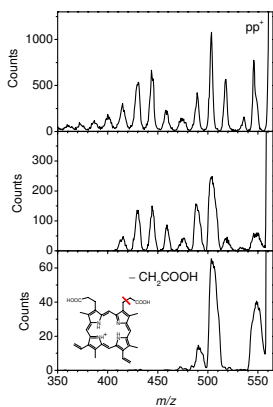


Neutrals from collisions with residual gas

Laser pulse fired after 12.4 ms.
Daughter ion mass spectra were recorded right after (t_{1A}) and after 190 μ s (t_{1B}) of storage.

26

Daughter ion mass spectra



High-energy CID spectrum (50-keV collisions) recorded at another instrument

ELISA switch at t_{1A} :
Fragmentation due to both one-photon and two-photon absorption

ELISA switch at t_{1B} :
Fragmentation due to one-photon absorption since all ions that have absorbed two photons have decayed.

27

K. Støchkel, U. Kadhane, J.U. Andersen, A.I.S. Holm, P. Hvelplund, M.-B. S. Kirketerp, M.K. Larsen, M.K. Lykkegaard, S. Brøndsted Nielsen, S. Panja, and H. Zettergren,

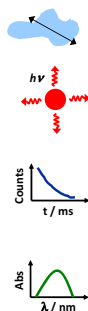
“A new technique for time-resolved daughter ion mass spectrometry on the microsecond to millisecond time scale using an electrostatic ion storage ring,”

Rev. Sci. Instrum. **79**, 023107 (2008).

28

ELISA experiments

- Collisional cross sections (geometrical size of molecule)
- Radiative cooling (emission from infrared active vibrations)
- Lifetimes after photon absorption:
statistical decay processes
excited state lifetimes, e.g., triplet states
- Electron autodetachment lifetimes
- Absorption spectroscopy



29

THE GROUP

Principal investigators:

Preben Hvelplund Jens Ulrik Andersen Steen Brøndsted Nielsen

Post docs:

Jean Wyer Kristian Støchkel

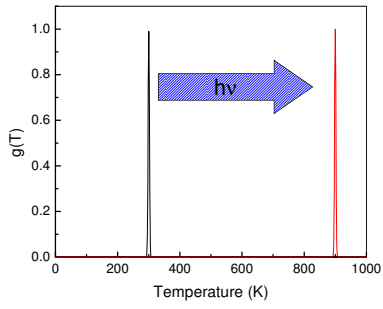
Students:

Maj-Britt S. Kirketerp Lisbeth M. Nielsen Camilla S. Jensen
Klaus Eriksen

FNU Lundbeckfonden Carlsbergfondet Villum Kann Rasmussen

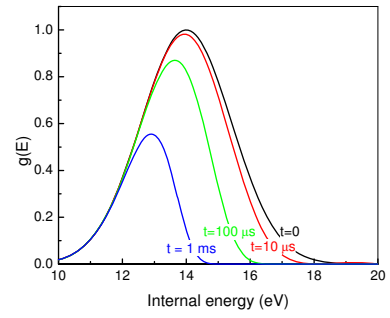
30

Heating by photon absorption

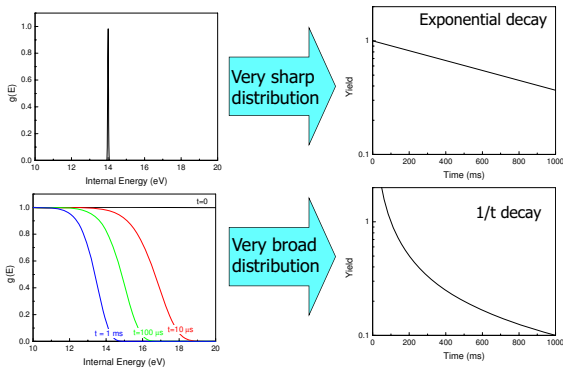


31

Energy distribution changes in time



32

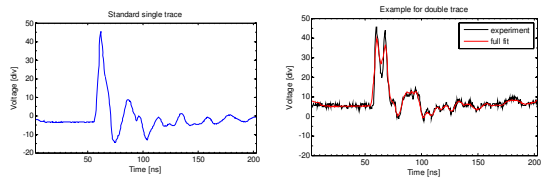


33

Table 1
Design parameters for ELISA

General parameters	
Injection energy	25 keV
Circumference	6.28 m
Revolution time	2.9 μs (p), 7.7 μs (C_{10})
Betatron tunes (Q_x, Q_y)	1.206, 1.439
Chromaticities (ξ_{x1}, ξ_{y1})	-1.7, -1.3
Momentum compaction (α_p)	0.50
160 spherical deflectors	
Electrode radii	235 and 265 mm
Nominal voltages	$\pm 4.0 \text{ kV}$
10 deflectors	
Plate distance	50 mm
Plate length	100 mm
Nominal voltages	$\pm 2.2 \text{ kV}$
Electrostatic quadrupoles	
Inscribed radius	26.2 mm
Electrode length	50 mm
Nominal voltages	$\pm 0.43 \text{ kV}$
Chopper and injector	
Rise/fall time	< 200 ns

34



35

DIAGNOSTICS FOR DESIREE

S. Das and A. Källberg[#], Manne Siegbahn Laboratory, Stockholm University, Frescativägen 26, S - 11418 Stockholm, Sweden

Abstract

The beam diagnostics system for the Double ElectroStatic Ion Ring ExpEriment (DESIREE) project under construction is briefly described. A system which can operate over a wide range of beam intensities and energies for the DESIREE has been built and tested using the CRYRING facility at MSL. Spatial resolution up to 2 mm is achieved.

INTRODUCTION

Single electrostatic ion storage rings have attracted considerable attention in recent years in atomic and molecular physics because of their several advantages over magnetic storage rings [1-6]. Motivated by the success of electrostatic ion storage rings and the possibility of performing merged-beams experiments with positive and negative ions, a Double ElectroStatic Ion Ring ExpEriment (DESIREE) has been under construction at Stockholm University and will soon be ready for experiments [7-9].

In this report we briefly describe the different elements to be used in the beam diagnostics system for DESIREE. A diagnostic system for radioactive beam experiment (REX) using the beam profile monitoring system (BPMS) [10,11] as part of DESIREE beam line has been built and tested for spatial resolution using the existing CRYRING facility at MSL [9]. A resolution of 2 mm has been achieved.

DESIREE

A schematic layout of the DESIREE is shown in Fig.1. It consists of two rings of same circumference of 9.2 m and a common straight section of length 1 m for the merged-beams experiments with ions of opposite charges. DESIREE will be operated at both room and cryogenic temperatures ($\sim 10\text{-}20\text{ K}$) under ultra high vacuum ($\sim 10^{-11}$ mbar) environment. In addition to the merged-beam experiments, DESIREE will be also used for single ring experiments.

The basic diagnostics components that will be used are Faraday cups (FC), electrostatic pickups (PU), Microchannel plates (MCP), and scrapers. FC will be used to measure the beam current before and after the injection of the beam in the storage rings, PU to measure the transverse beam position in the rings. Position sensitive MCP detectors will be used to detect the charged reaction products and the neutral particles that are occurred from the merged-beam experiments. Beam scrapers will be used in the straight merger section to attain the maximum beam size both horizontally and

vertically. It should be noted, however, that the properties of the detectors such as MCP change very rapidly with temperature and at cryogenic temperature very little data exist until now. Therefore, the development of the beam diagnostic system for the DESIREE project is a challenging one.

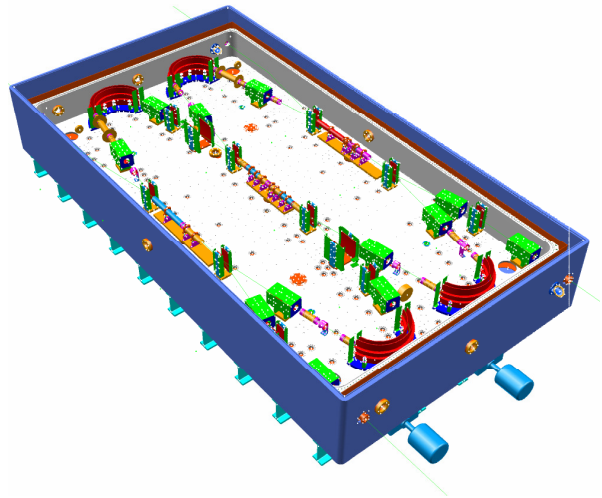


Figure 1: Schematic layout of DESIREE.

BEAM DIAGNOSTIC SYSTEM FOR REX

A diagnostic system based on the observation of low energy ($\sim 10\text{ eV}$) secondary electrons (SE) produced by a beam, striking a metallic foil has been built to monitor and to cover the wide range of beam intensities and energies [10,11].

The system consists of (i) a Faraday cup (FC) to measure the beam current, (ii) a collimator with circular apertures of different diameters to measure the spatial resolution of the system (Fig. 2), (iii) a beam profile monitoring system (BPMS), and (iv) a control unit (PC). The BPMS, in turn, consists of (a) an aluminum (Al) plate or foil, (b) a grid placed in front of the Al foil to accelerate the SE, (c) position sensitive MCP, (d) fluorescent screen (F.S), and (e) a CCD camera to capture the images (Fig. 3). The spatial resolution of the system depends on the voltage applied on the Al plate. The amplification of the MCP can be controlled by the applied voltage.

The collimator contains a set of circular holes of different diameters (Φ) and separations (d) between them as shown in Fig. 2. The collimator cuts out from the beam areas equal to the holes with separation d mm between the beams centers and creates well separated (distinguishable) narrow beams of approximately same intensity close to each other.

[#] kallberg@msl.se

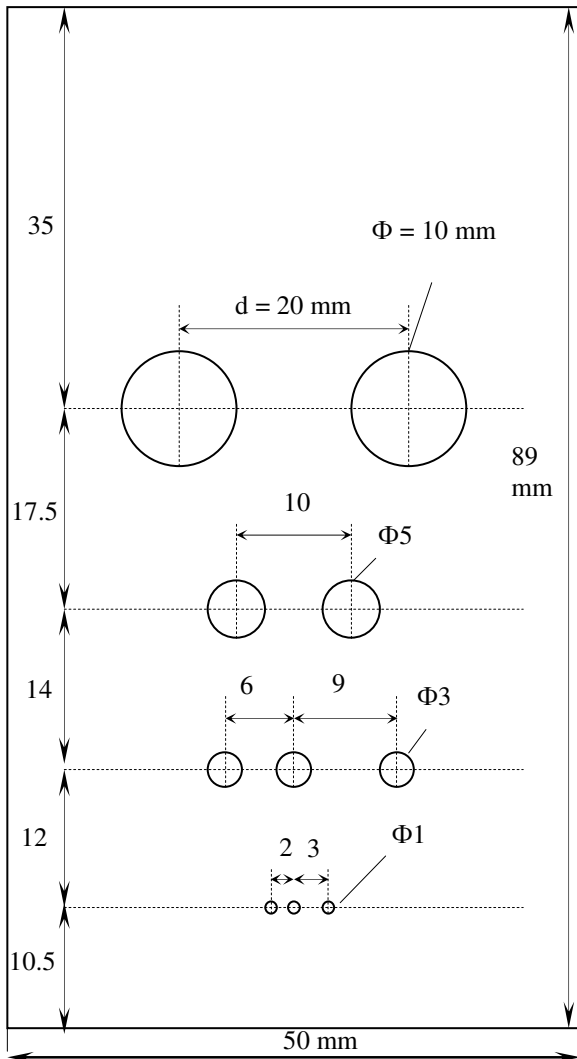


Figure 2: Collimator with circular holes of different diameters. Φ is the diameter of hole. d is the separation between the adjacent holes.

The three-dimensional (3-D) view of the BPMS is shown in Fig. 3. The schematic diagram and experimental setup of the beam diagnostic system are shown in Figs. 4 and 5, respectively. The collimator and the Al foil attached with the grid can be inserted and taken out of the beam path by a pneumatic feed-through. The 10 keV proton beam from the CRYRING source passes through the collimator, strikes the Al plate, and knocks off low energy (~ 10 eV) secondary electrons (SE). These SE are then accelerated by a homogeneous electric field applied between the Al plate and the grid that are kept at negative and ground potentials, respectively. The accelerated SE from the grid then travel the field free region to the position sensitive electron multiplier, micro channel plate (MCP). The amplified electrons from the MCP then hit the fluorescent screen (F.S) and produce flashes of light.

The F.S is kept at ground potential. The light is captured by the computer controlled CCD camera [12].

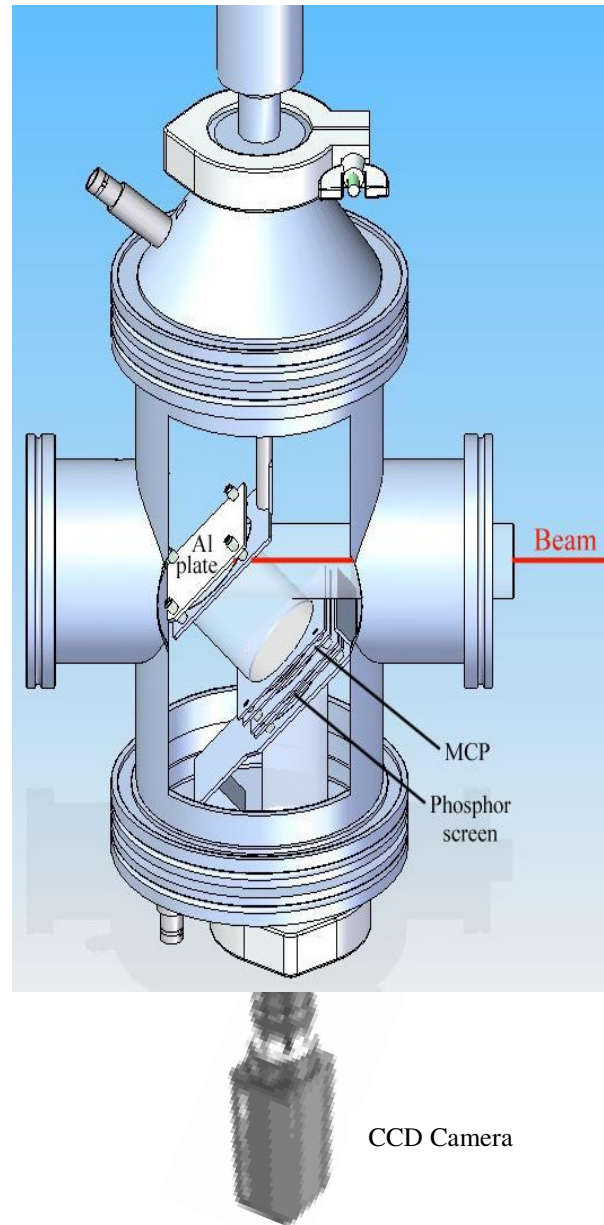


Figure 3: Three dimensional (3-D) view of the BPMS.

The CCD images of the collimator holes for fixed Al plate and MCP voltage recorded on the PC are shown in Fig. 6. It can be easily form the Fig. 6 that the collimator has created well separated beams. The figure shows that a spatial resolution of 2 mm can be achieved. The rest of the article is focused on the two holes of diameter 1 mm which are separated by 2 mm (see Fig. 2). The resolution of the system was tested for different Al plate and MCP voltages and the results are shown in Fig. 7.

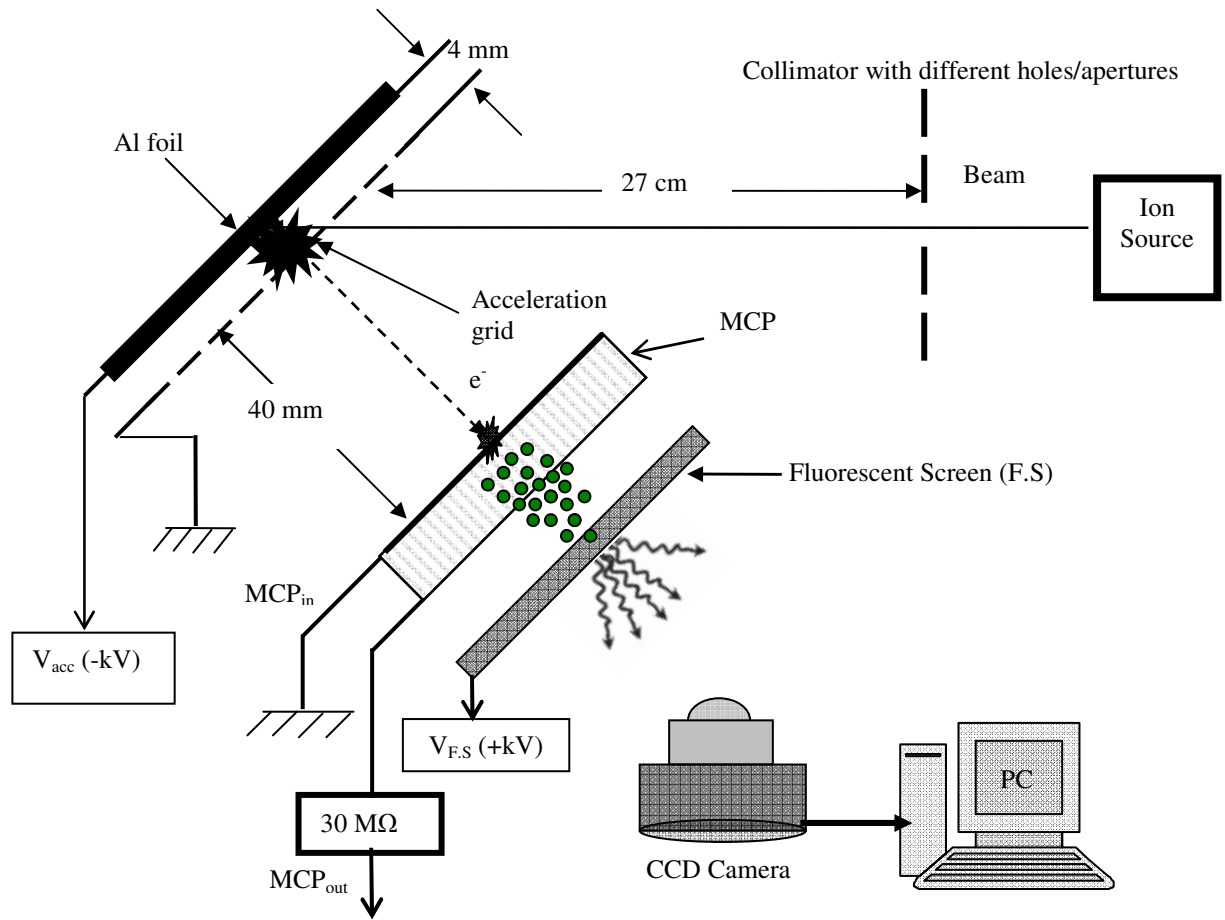


Figure 4: Schematic diagram of the beam diagnostic setup.

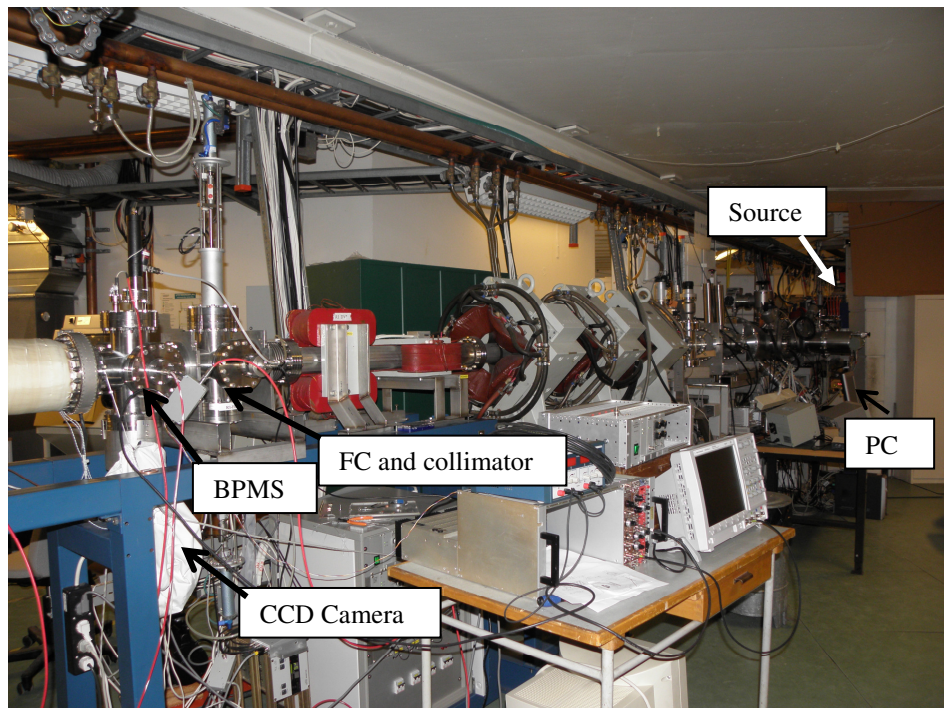


Figure 5: Experimental setup at the CRYRING facility at MSL, SU.

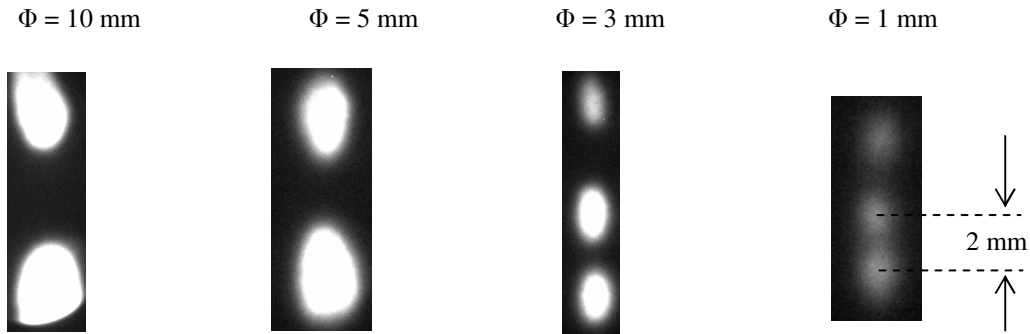


Figure 6: CCD images of the light produced in the fluorescent screen (F.S) for fixed Al plate ($V_{acc} = - 5$ kV) and MCP ($V_{MCP} = 1300$ V) voltage. The beam passed through the collimator and generated SE from the Al plate. Well separated beam spots are clearly seen on the screen showing a spatial resolution of better than 2 mm of the diagnostic system.

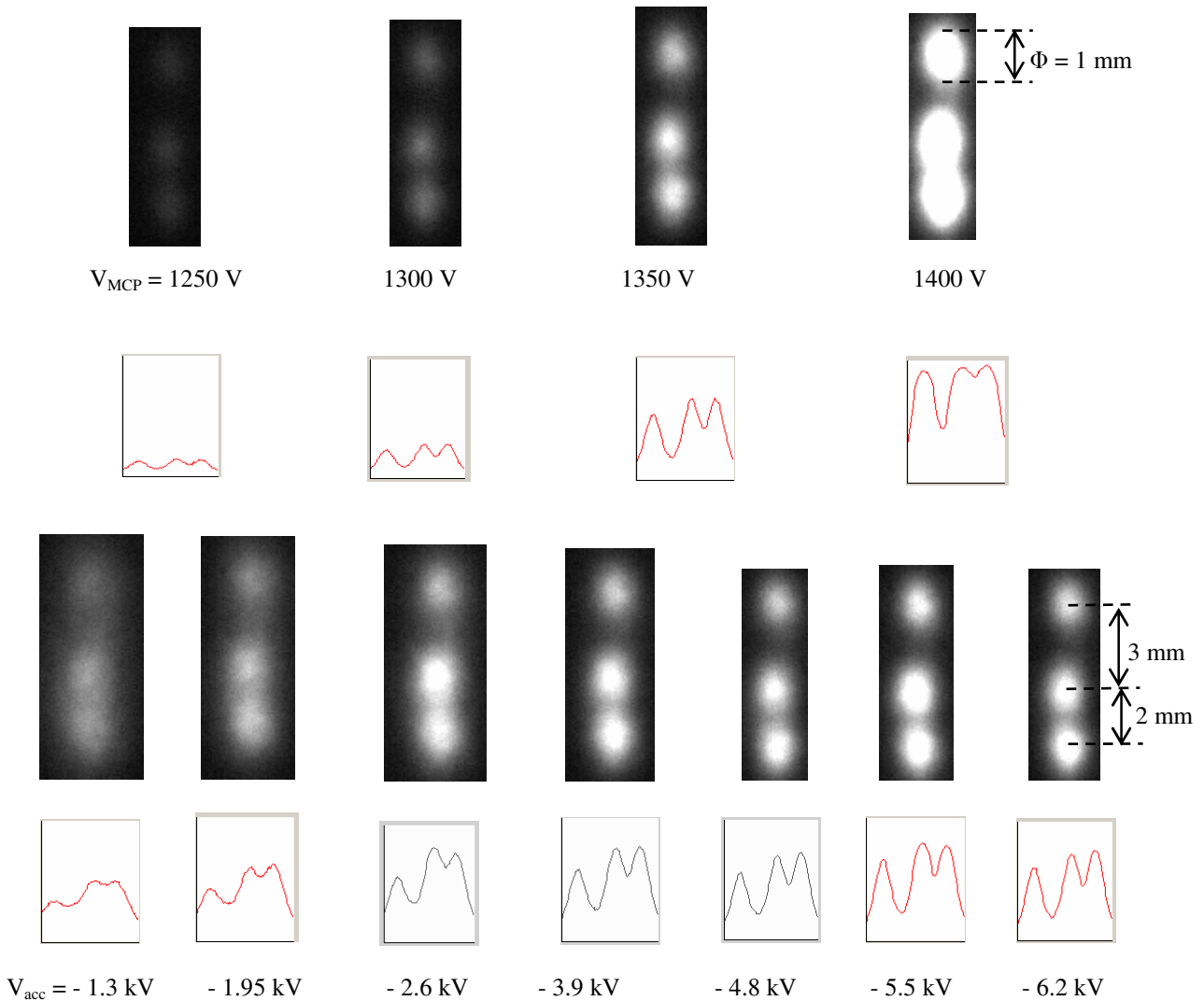


Figure 7: CCD images of the light produced in the F.S. The intensity distribution is shown as a function of V_{MCP} ($V_{acc} = - 5$ keV) (upper panel) and V_{acc} ($V_{MCP} = 1370$ V) (lower panel). The vertical beam profiles captured by the CCD camera are also shown.

Moreover, the change of resolution of the system as a function of Al plate voltage was also measured from the beam profiles recorded on the CCD camera (see lower panel of Fig. 7). For this, the length of the dip (Δ) between the two adjacent peaks was calculated as $\Delta = \left(\frac{a+b}{2} - c \right)$. Here, a , b , and c are the heights of two adjacent peaks, and the dip between them, respectively, as shown in Fig. 8. The ratio $\delta = \frac{\Delta}{\left[\frac{(a+b)}{2} \right]}$ was then plotted

as a function of Al plate voltage (Fig. 9). It can be seen from the Fig. 9 that the resolution of the system increases with increasing plate voltage.

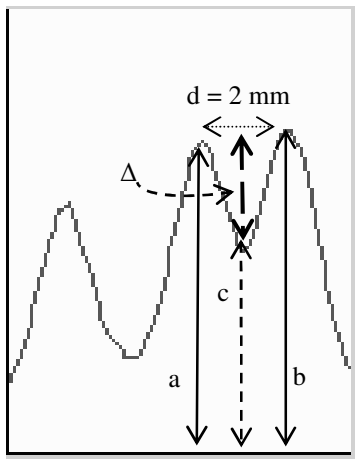


Figure 8: Vertical beam profile captured on the camera. Two apertures of diameter 1 mm, separated by 2 mm are considered. a , b , and c are the heights of the two adjacent peaks, and the dip between them, respectively. $(a+b)/2$ is average of the heights of two adjacent peaks.

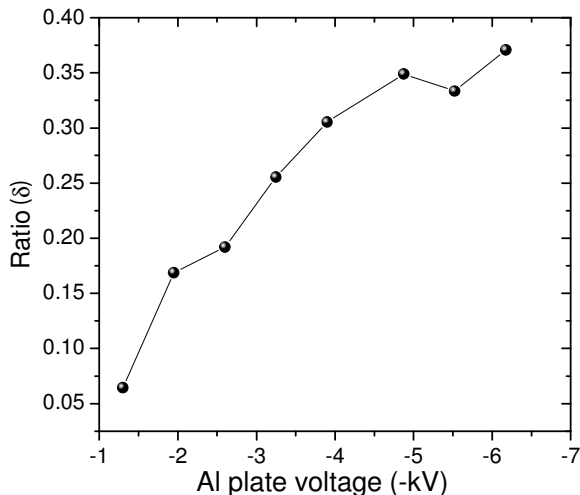


Figure 9: Plot of ratio as a function of Al plate voltage.

CONCLUSIONS

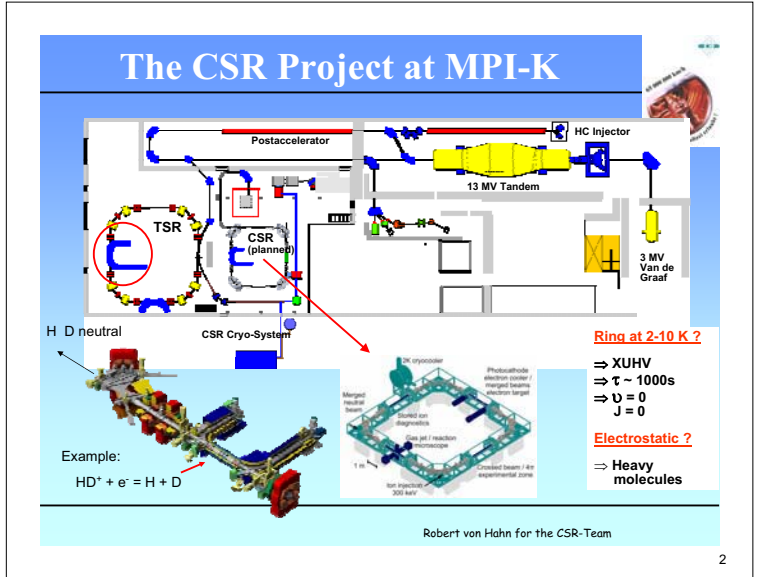
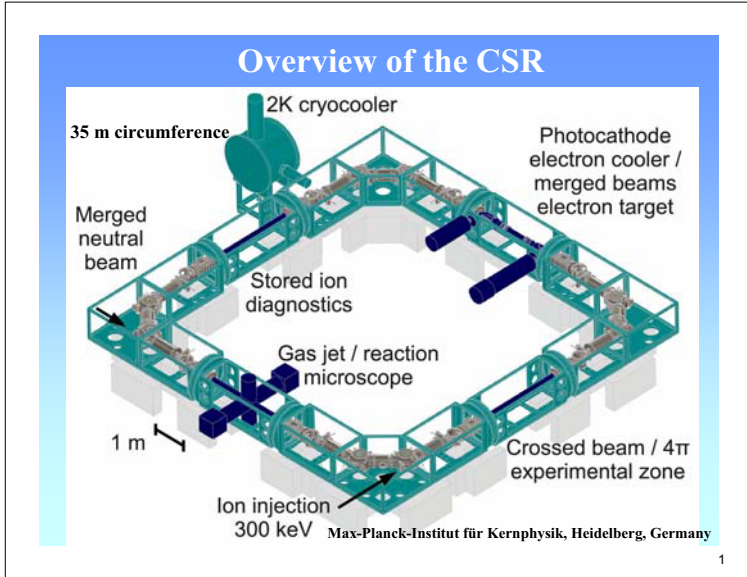
In summary, we have described briefly the diagnostics system for the DESIREE project. A system has been built using the CRYRING facility at the Manne Siegbahn Laboratory, Stockholm University as part of the DESIREE beam line diagnostics. A spatial resolution of better than 2 mm has been achieved. However, a more detailed and systematic investigation to improve the resolution of the system further is required.

ACKNOWLEDGEMENT

One of the authors (S. Das) acknowledges the financial support received from the Marie Curie Fellowship.

REFERENCES

- [1] S.P. Møller, Nucl. Inst. Methods. Phys. Res. Sec. A 394 (1997) 281.
- [2] T. Tanabe *et al.*, Nucl. Inst. Methods. Phys. Res. Sec. A 482 (2002) 595.
- [3] T. Tanabe *et al.*, Nucl. Inst. Methods. Phys. Res. Sec. A 496 (2003) 233.
- [4] T. Tanabe *et al.*, Nucl. Inst. Methods. Phys. Res. Sec. A 532 (2004) 105.
- [5] S.P. Møller *et al.*, Proc. EPAC 2000, Austria, p. 788.
- [6] C.P. Welsch *et al.*, Hyperfine Interactions 146/147 (2003) 253.
- [7] K. -G. Rensfelt *et al.*, Proc. EPAC 2004, Switzerland, p. 1425.
- [8] P. Löfgren *et al.*, Proc. EPAC 2006, Scotland, p. 252.
- [9] Manne Siegbahn Laboratory (www.msl.se), and Atomic Physics, Stockholm University http://www.atom.physto.se/Cederquist/desiree_web_hc.html.
- [10] K. Kruglov *et al.*, Nucl. Inst. Methods. Phys. Res. Sec. A 441 (2000) 595.
- [11] K. Kruglov *et al.*, Nucl. Inst. Methods. Phys. Res. Sec. A 701 (2002) 193c.
- [12] Matrix Vision (<http://www.matrix-vision.com>).



Requirements for the CSR

- Beam energy variable between 20 keV and 300 keV (*q),
- Very large mass range up to bio molecules

⇒ CSR should be electrostatic

- Long life time, molecules in ground state

⇒ Vacuum at low temperatures: $1 \cdot 10^{-13}$ mbar (RT equivalent)

⇒ CSR must be cryogenic (10 K),
For H₂ 2 K must be available at a determined number of positions

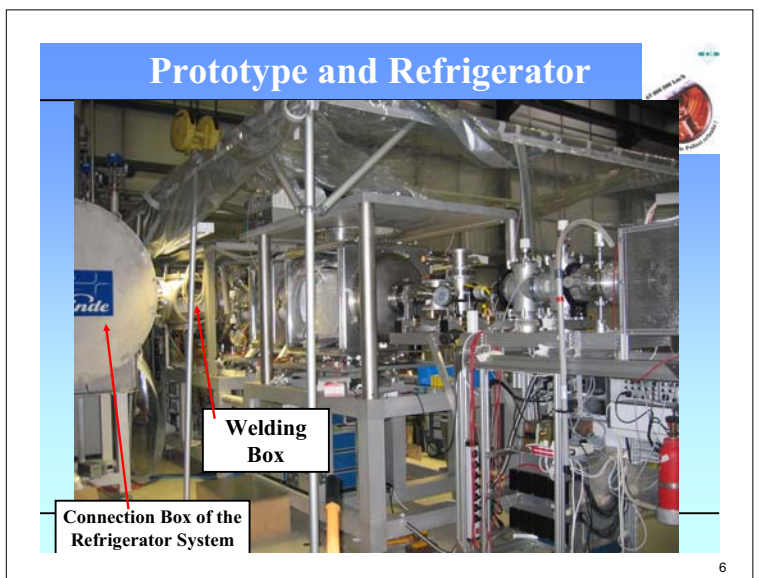
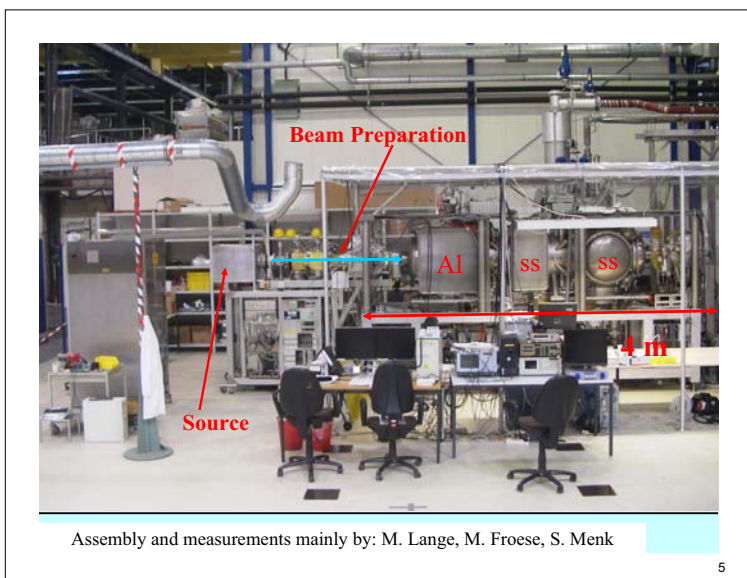
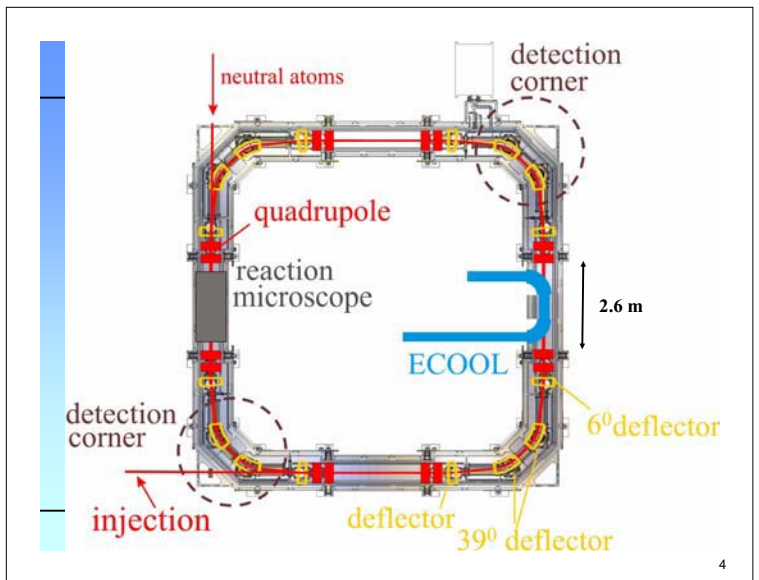
- Operation temperatures between 10 and 300 K

⇒ Usage of a Helium refrigerator delivering 2 K Helium

- Vacuum at room temperature: $1 \cdot 10^{-11}$ mbar

⇒ The ring must be baked up to 600 K

Robert von Hahn for the CSR-Team



Linear Electrostatic Ion Trap

Injected ion beam

Middle chamber

~1 m

Electrostatic ion trap

Gold plated electrodes

Pumping

~3 m

Robert von Hahn for the CSR-Team

Cooling techniques and thermal shielding

2K cooling units

Isolation vacuum

Super insulation

80 K shields

40 K shields

Helium pipe

2K liquid helium

Exp. vac.

2K pump pipe

2-10 cold chamber

Measured cryogenic temperatures at cool downs

2K cooling units

Temperature [K]

Position [mm]

Sebastian Menk: Diploma Thesis

Ion Trapping & Detection

Counting of neutral fragments on a chevron MCP

Detection

Cryogenic ion trap

Beam cleaner

Ion source

Produces N_2^+ ions with energies of 2-10 keV

Only ions

Batch length definition

Particles from source

$\frac{1}{\tau} = n \cdot \sigma \cdot \langle v \rangle \cdot p$

~ 4-5 μs

Static electrodes

N_2^+

$v = 200 \frac{mm}{\mu s}$

Switched electrodes

- Trapping of N_2^+ ions by switching the electrodes
- After ~400 ns electrode voltage at 95%
- Neutralisation by electron capture of the restgas (mainly H_2 at 2K)

Sebastian Menk: Diploma Thesis

Robert von Hahn for the CSR-Team

Storage Lifetime

2008: First storage of ions in CTF under cryogenic conditions

However: lifetime limited to 24 s – much shorter than expected

Improvements in 2009:

- Reduced ripple on trap voltages (fast HV switches)
- Cryogenic chamber baked for better vacuum at RT
- Improved differential pumping after ion source
- Improved shielding against infrared radiation at trap entrance+exit

Rate of neutral particles (s^{-1})

Time after injection (s)

• Measurement

— Double Exponential fit

— Background fit

$\tau_{short} = 62.7 s \pm 11.2 s$

$\tau_{long} = 343.2 s \pm 54.0 s$

Trap off

Feb+March 2009: 340 s storage lifetime!

With collision cross-sections from the literature, the new lifetime would translate to a residual gas density of 44000 cm^{-3} or $1.6 \cdot 10^{-12} \text{ mbar}$ (at Room Temperature).

Robert von Hahn for the CSR-Team

Trap Vacuum

CTF pressure: $8 \cdot 10^{-14} \text{ mbar}$

Cryogenic pumping of hydrogen at 1.8 K: Expect vacuum of few 10^{-13} mbar (RT equiv.)

Most likely particle loss from trap not dominated by residual gas collisions

- Model: 2 loss mechanisms:
 - residual gas collisions (proportional to pressure)
 - ion evaporation from trap acceptance volume (constant)
- Total rate from particle loss:

$$\frac{dN}{dt} = k N(t)$$

$$k = k_{ev} + k_{res} + k_{ev}$$
- Neutral particle rate:

$$R_o = \frac{1}{2} \alpha n N_o$$

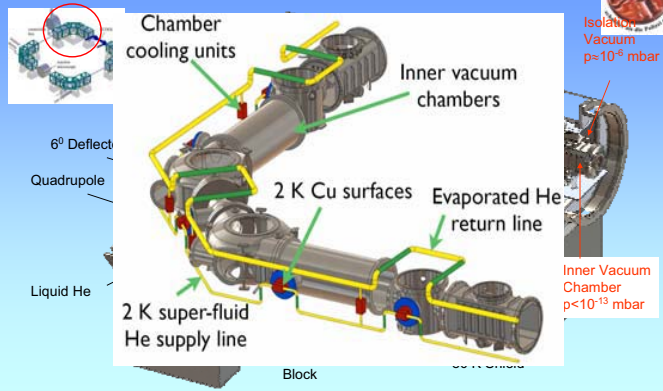
$n \text{ (cm}^{-3}\text{)}$

$R_o \text{ (s}^{-1}\text{)}$

Time after start of warm-up (h)

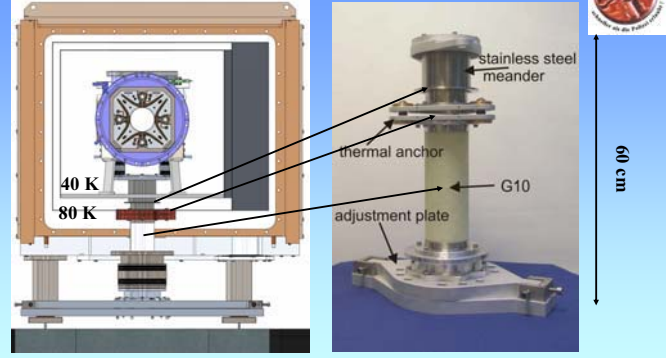
Robert von Hahn for the CSR-Team

CSR Mechanical Layout

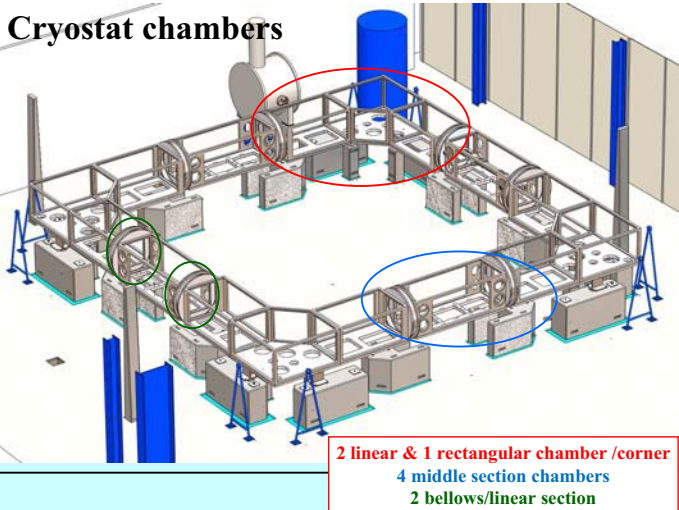


Robert von Hahn for the CSR-Team

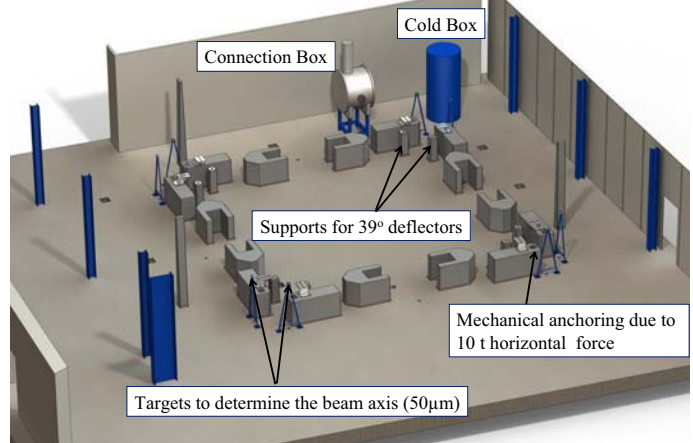
Support Concept



Cryostat chambers



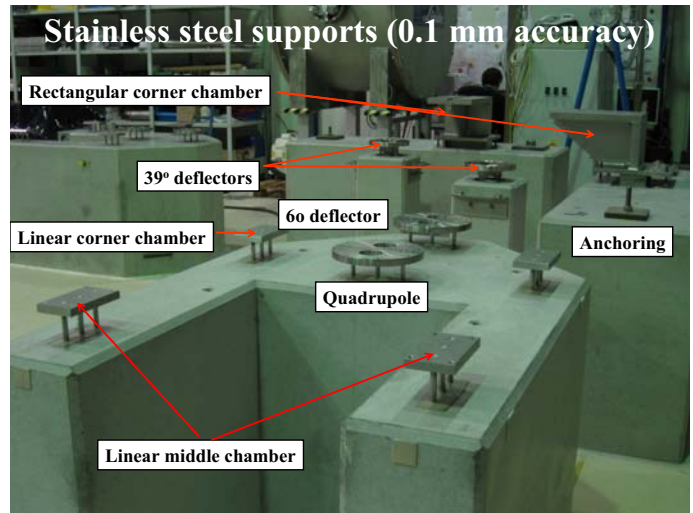
Schema of the support system



Support concrete blocks



Stainless steel supports (0.1 mm accuracy)

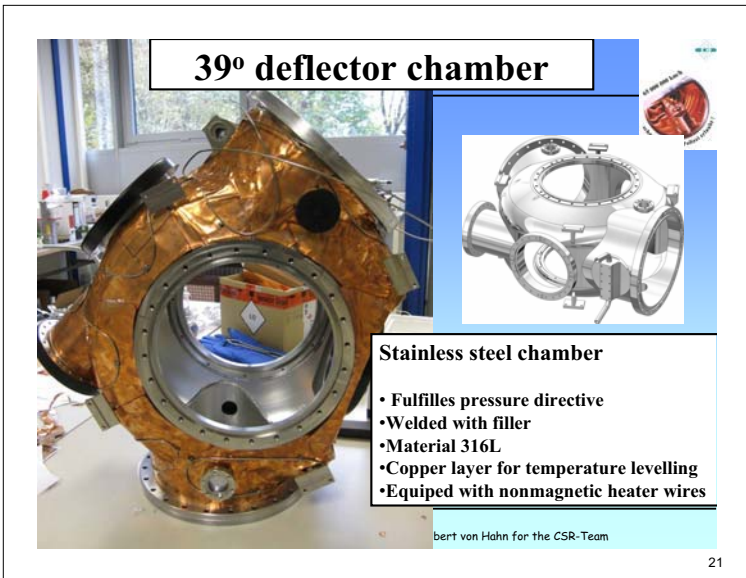




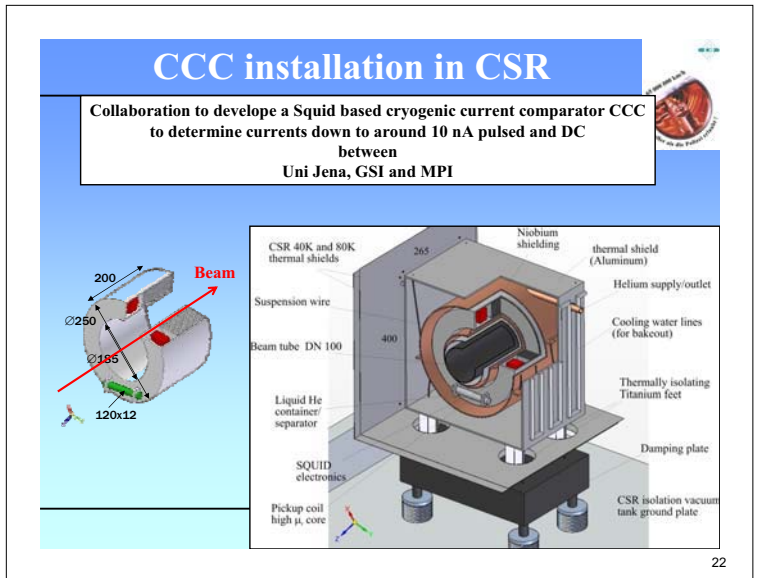
19



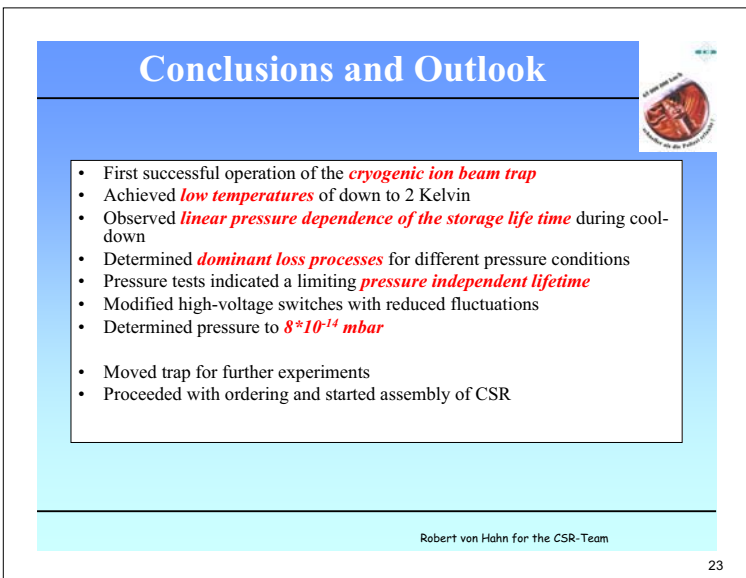
20



21



22



23



24

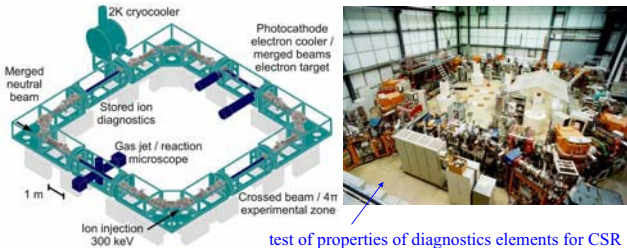
Diagnostics at CSR (and TSR)

Manfred Grieser

Max-Planck-Institut für Kernphysik

CSR storage ring under construction

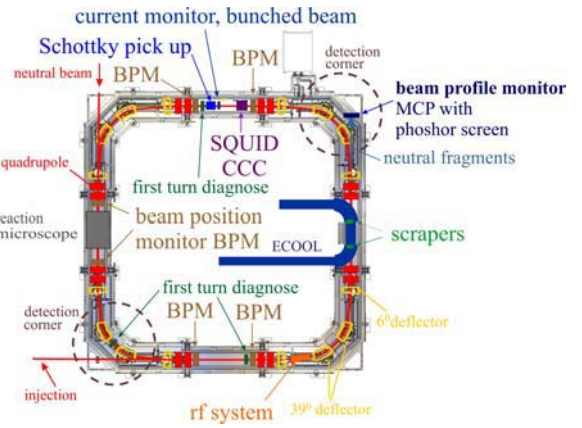
TSR storage ring



test of properties of diagnostics elements for CSR investigation of diagnostics procedure for the CSR

DITANET workshop November 24th and 25th

Diagnostic elements of the CSR



Measurement of the intensity of a bunched ion beam

Diagram of a drift tube with length L . Currents $I(t)$ and $I_a(t)$ are shown. A capacitor C and input resistance R are connected to the drift tube. The voltage $U(t)$ is measured across the capacitor.

current of the stored ion beam
 $I_a(t) = I(t - \Delta t)$
 after the drift tube
 flight time inside the drift tube

node theorem:
 $I(t) = I_a(t) + I_R(t) + I_C(t)$
 $\Leftrightarrow I(t) = I(t - \Delta t) + I_R(t) + I_C(t)$
 $I(t - \Delta t) = I(t) - \frac{\partial I}{\partial t} \Delta t = I(t) - \dot{I}(t) \frac{L}{v}$

With bunch length $l_b \gg L$:
 with $I_R(t) = \frac{U}{R}$ and $I_C(t) = C \cdot \dot{U}(t)$ differential equation for drift tube voltage $U(t)$
 $\frac{L}{v} \dot{I}(t) = C \cdot \dot{U}(t) + \frac{U(t)}{R}$

for $R \rightarrow \infty$ drift tube voltage: $U(t) = \frac{1}{C} \frac{L}{v} I(t) \Rightarrow U(t) \propto I(t)$

Measurement of the intensity of a bunched ion beam

relation pick up voltage $U(t)$ and stored ion current $I(t)$

for $R \rightarrow \infty$ $U(t) = \frac{1}{C} \frac{L}{v} I(t)$ ← ion velocity

ion velocities for singly charge ions at the CSR

very sensitive for a low velocity bunched ion beam !!

typically TSR velocity $\beta=0.1$

at the CSR the current sensitivity is improved by a factor >10 compared to the TSR

Measurement of the intensity of a bunched cooled ion beam

profile of an electron cooled bunched ion beam
 TSR measurement (no averaging)
 beam: $^{12}\text{C}^{6+}$
 $E=50 \text{ MeV}$
 $\beta=0.094$
 $I=19 \mu\text{A}$

determination of the beam current
 $\bar{I} = \frac{C \cdot v}{L \cdot v_a} \int_{-T/2}^{T/2} U(t) \cdot dt$

amplification factor $V_a = 15.14$
 attention: due to $\frac{U(t)}{R}$ no DC can be measured with a pick up

differential equation of the pick up voltage:
 $\frac{L}{v} \dot{I}(t) = C \cdot \dot{U}(t) + \frac{U(t)}{R}$

\Rightarrow we have to know where the region in the signal where $I(t)=0$

\Rightarrow base line has to shift where $I=0$!!!

Measurement of the intensity of a bunched ion beam

1. there are region with $I(t)=0$?
 2. where are the region with $I(t)=0$?
 for baseline ($I=0$) construction measurements and simulations for comparison were performed

longitudinal phase space of the injected beam at $U_0=0\text{V}$

bucket size at the final resonator voltage $U_0=100\text{V}$

rf bucket

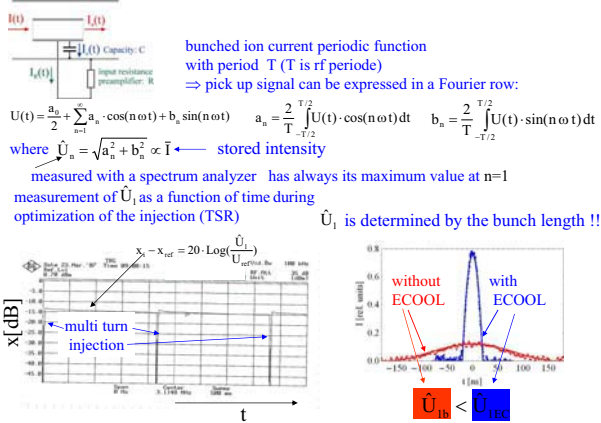
to get region in the signal with $I(t)=0$ the rf bucket size at the final resonator voltage after bunching has to fulfill:
 $A_b > A_{\text{beam}}$
 A_b - rf bucket area
 A_{beam} - longitudinal phase space area of the injected beam

beam: $^{12}\text{C}^{6+}$ 50 MeV

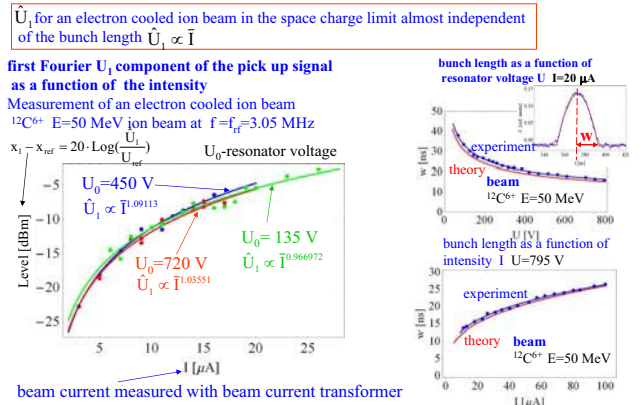
simulation measurement baseline

no averaging used in the measurements

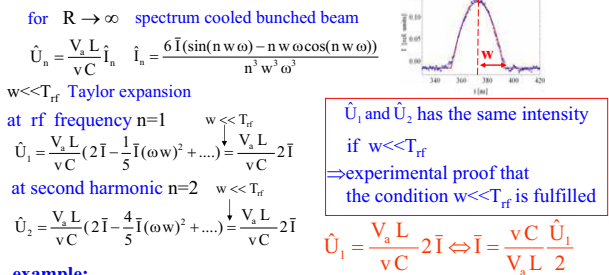
Spectrum of the pick-up signal



Measurement of the intensity of a stored bunched cooled ion beam

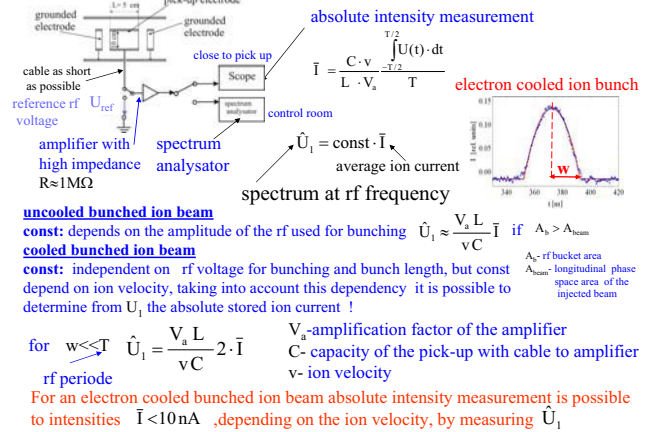


Spectrum of the pick up voltage for a electron cooled bunched ion beam

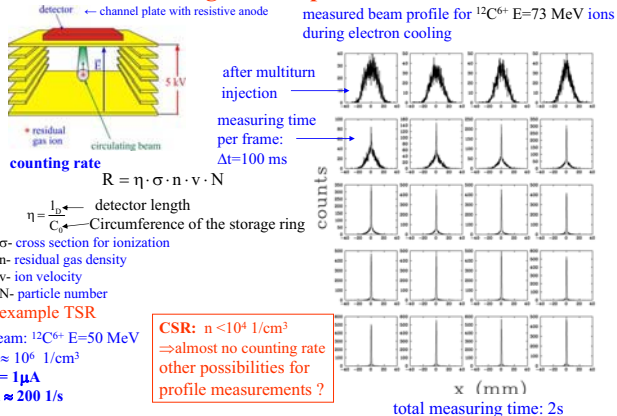


example:
 consider signal direct at the pick-up $V_a=1$, $\beta=0.01$, $L=5$ cm, $C=100$ pF
 $\bar{I}=10$ nA $\Rightarrow \hat{U}_1=3$ μV pick-up voltage without amplification
 easily to measure with a spectrum analyzer
 current sensitivity $\bar{I} < 10$ nA if the bunched ion beam is cooled

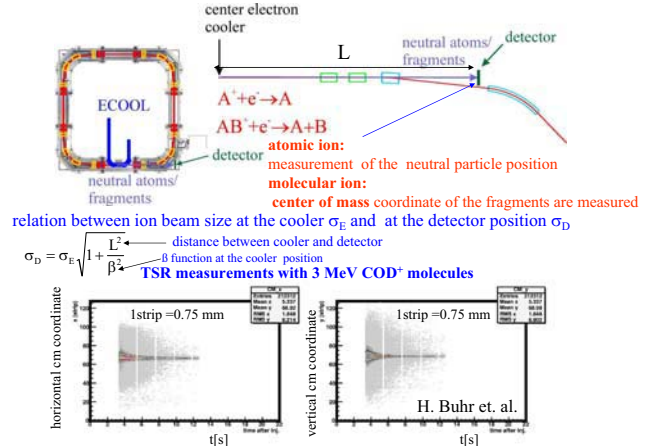
Current monitor for bunched ion beams at the CSR



Residual gas beam profile monitor

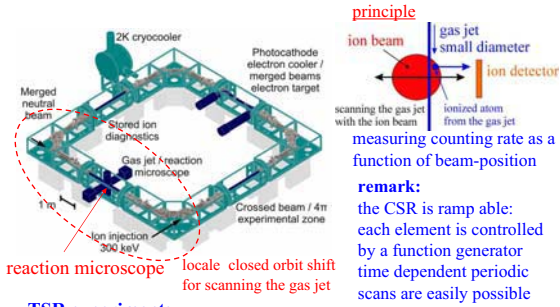


Beam profile measurements for singly charged ions and molecules



Beam-profile measurement using the reaction microscope

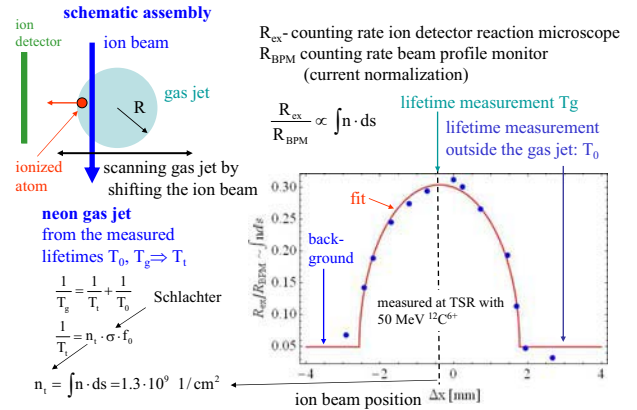
heavy ion are used in experiments using a reaction microscope



TSR experiment:

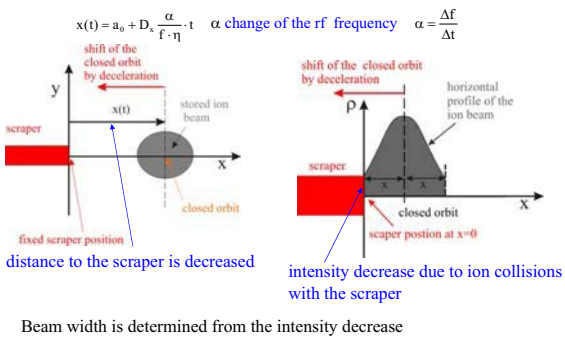
proof of principle, opposite way, scanning the gas-jet with an ion beam with small diameter to determine the profile of the gas-jet

Gas jet profile of the reaction microscope

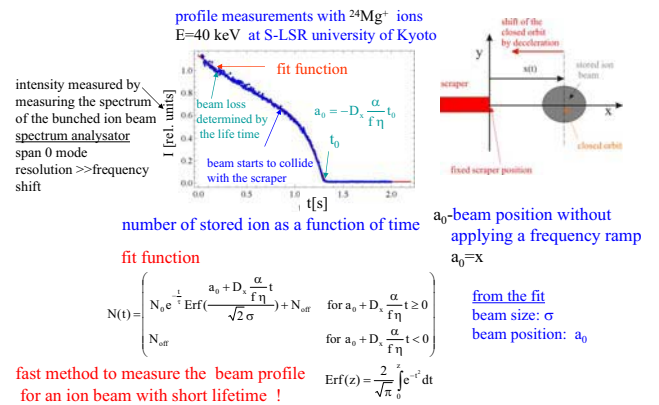


Measurement of the beam profile with a scraper

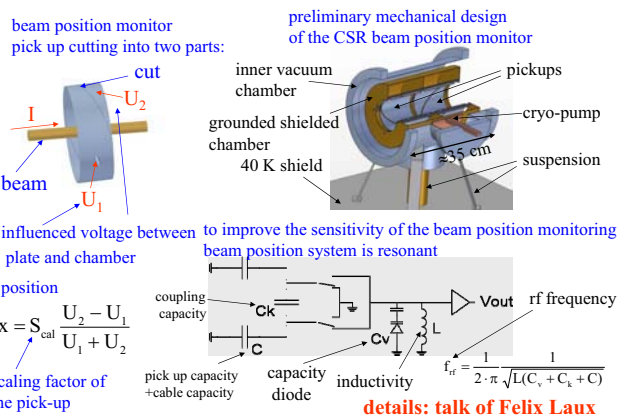
measurement are done by deceleration the stored ion beam to the scraper position



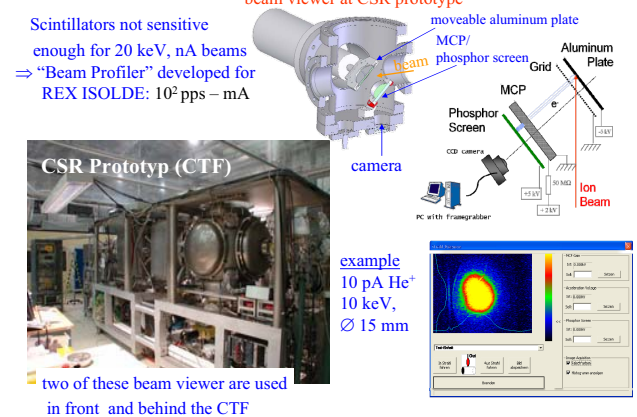
Measurement of the position and beam profile position



Beam position monitor of the CSR



First turn diagnose at the CSR



The Schottky pick up of the CSR

single ion interaction with the Schottky pick up

resistor describing the losses

capacity of pick up and cable to the coil

Inductivity

resonant at the observed Schottky band

Fourier row

current into LC circuit

$I_1(t) = Q \sum_n \delta(t - nT)$

$I_{1a}(t) = I_1(t - \Delta t) = Q \sum_n \delta(t - nT + \Delta t)$

$\Delta I_1(t) = I_1(t) - I_{1a}(t)$

$\Delta I_1(\omega_n) = \frac{2Q}{T} \sqrt{(1 - \cos(\omega_n \Delta t))^2 + \sin^2(\omega_n \Delta t)}$

$\Delta I_1(\omega_n)$ is maximum at $\omega_n \Delta t = \pi, 3\pi, \dots$

$\Delta I_1(\omega_n)$ is 0 at $\omega_n \Delta t = m \cdot \pi$

$\omega_n = 2\pi n f_0$

integer number

19

Spectrum of the Schottky signal coming from a single ion

$\Delta t = \frac{L}{v}$

$\Delta I_1(t) = Q \sum_n \delta(t - nT)$

\Rightarrow spectrum of ΔI_1 $\omega_n = n \omega_0$

$\Delta \hat{I}_1(\omega_n) = \frac{2Q}{T} \sqrt{(1 - \cos(\omega_n \Delta t))^2 + \sin^2(\omega_n \Delta t)} = \frac{2\sqrt{2}Q}{T} \sqrt{1 - \cos(\omega_n \Delta t)}$

$\Delta \hat{I}_1(\omega_n)$ is maximum at $\omega_n \Delta t = \pi, 3\pi, \dots$

$\Delta \hat{I}_1(\omega_n)$ is 0 at $\omega_n \Delta t = m \cdot \pi$

$\omega_n = 2\pi n f_0$

revolution frequency of the ion

integer number

resistor describing the losses

capacity of pick up and cable to the coil

Inductivity

resonant at f_n

$f_n = n f_0$

20

Spectrum of the Schottky signal coming from a single ion

resistor describing the losses

capacity of pick up and cable to the coil

Inductivity

resonant at f_n

ion charge

T revolution time

Q value of the LC circuit

signal on LC circuit from a single ion :

$\hat{U}_i(\omega_n) = \frac{Q_w}{\omega_n C} \frac{2\sqrt{2}Q}{T} \sqrt{1 - \cos(\omega_n \frac{L}{v})}$

\Rightarrow signal from a single ion proportion to the Q-value (Q_w) of the LC circuit !

details of the construction of a LC circuit with high Q value: talk of Felix Laux

$\hat{U}_i(\omega_n) = \frac{\sqrt{2}Q_w}{\pi n C} \sqrt{1 - \cos(\omega_n \frac{L}{v})}$

$n = \frac{f_n}{f_0}$

observation frequency

$f_n = n f_0$

revolution frequency

maxima in the signal: $\cos(n2\pi \frac{L}{C_0}) = -1$

$n = \frac{f_n}{f_0} = \frac{(1+2 \cdot m) \cdot C_0}{2 \cdot L}$

circumference of the storage ring

pick-up length

$m=0, 1, 2, 3, \dots$

harmonic number n where $\hat{U}_i(\omega_n)$ is maximum is determined by the pick-up length L

21

Maxima in the spectrum of a single ion

signal from a single ion

$\hat{U}_i(\omega_n) = \frac{\sqrt{2}Q_w}{\pi n C} \sqrt{1 - \cos(\omega_n \frac{L}{v})}$

$n = \frac{f_n}{f_0}$

observation frequency

$f_n = n f_0$

revolution frequency

maxima in the signal: $\cos(n2\pi \frac{L}{C_0}) = -1$

$n = \frac{f_n}{f_0} = \frac{(1+2 \cdot m) \cdot C_0}{2 \cdot L}$

circumference of the storage ring

pick-up length

$m=0, 1, 2, 3, \dots$

harmonic number n where $\hat{U}_i(\omega_n)$ is maximum is determined by the pick-up length L

resistor describing the losses

capacity of pick up and cable to the coil

Inductivity

resonant at f_n

22

Some thoughts about the pick-up length L

consider pick-up with capacity C

one single ion will produce a voltage during one passage in our simple model

$I_c(t) = \begin{cases} Q\delta(t - t_0) & t \leq t_0 \\ -Q\delta(t - (t_0 + \Delta t)) & t > t_0 \end{cases}$

$U(t) = \frac{1}{C} \int_{-\infty}^{t_0+\Delta t} I_c(t') dt'$

induced charge distribution $\Lambda(s)$

σ_{rms} -RMS value of $\Lambda(s)$

$\sigma_{rms} = \frac{a}{\gamma\sqrt{2}}$

radius of the tube

γ -relativistic γ

CSR: $\gamma=1$

If $L \gg \sigma_{rms}$ induced charge on the outside of the cylinder

$Q = \int_{-L/2}^{L/2} \Lambda(s) ds \Rightarrow U=Q/C$

voltage rise time: $t_{rise} \approx \frac{\sigma_{rms}}{v}$

ion velocity

Electrical field lines from a point charge

CSR: $a=5\text{ cm}$ $L \geq 6 \cdot \sigma_{rms} \approx 20\text{ cm}$ better $L \approx 35\text{ cm} \Leftrightarrow L/C_0=0.01$

ion

ion with charge Q

tube

23

Schottky signal from a single ion at different n

pick up signal of a single ion as a function of $n = \frac{f_n}{f_0}$

for $C=100\text{ pF}$

L -pick up length

C_0 -CSR circumference

$L/C_0=0.01 \Leftrightarrow L=35\text{ cm}$

$L/C_0=0.005 \Leftrightarrow L=17.5\text{ cm}$

$\frac{\hat{U}(n)}{Q_w} = \frac{\sqrt{2}}{\pi n C} \sqrt{1 - \cos(n2\pi \frac{L}{C_0})}$

γ -relativistic γ

CSR: $\gamma=1$

observation frequency

revolution frequency

f_0 single charge ions

$E=300\text{ keV}$

20 keV

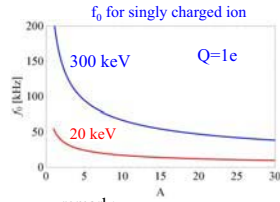
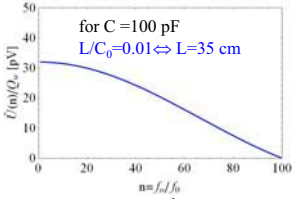
The resonance frequency of the LC circuit $f_{res} = f_n$ should be variable in a certain range to avoid zero signals in the voltage spectrum

24

Schottky signal from a single 300 keV proton

protons with 300 keV are the fastest \Rightarrow low n for observation can be chosen

$$\frac{\dot{U}(n)}{Q_w} = \frac{\sqrt{2}}{\pi} \frac{1}{n} \frac{Q}{C} \sqrt{1 - \cos(n2\pi \frac{L}{C_0})}$$



remark:
In the frequency range: 0.2-4 MHz
pick up is a pure capacity,
as assumed in the calculation,
because: $L \ll \lambda$.

for $n=1$ to $n=20$ $\dot{U}(n)/Q_w \approx 30$ pV
 \Rightarrow protons $E=300$ keV $f_0 \approx 200$ kHz
 observation frequency $f_n = 0.2-4$ MHz
 In that frequency range a LC circuit can be build with $Q_w \approx 1000$ if the LC circuit is cooled down to a temperature $T \approx 4$ K
 $\Rightarrow \dot{U} \approx 30$ nV

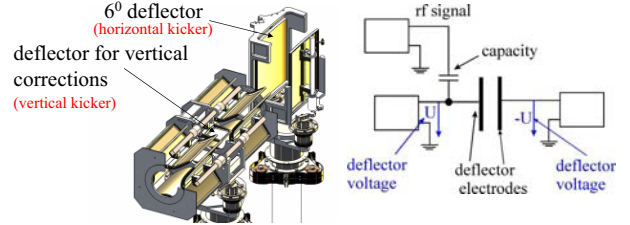
Tune measurements at the CSR

at low energies there is a large incoherent tune shift

$$\Delta Q = -\frac{q^2}{A} \frac{r_p N}{2\pi B \beta^2 \gamma^3 \epsilon}$$

N - number of ions
 β - velocity in units of c
 ϵ - emittance

distance to "danger" resonances has to be as large as possible
 important to know horizontal and vertical tune
 coherent tune is determined by BTF measurements, where the horizontal kicker is one of the 6^0 deflector and as a vertical kicker a vertical correction deflector is used. A beam position pick up of the CSR is used for detection the horizontal and vertical oscillations of the beam at $f = f_0(n \pm q)$ q - non integer part of the tune



Acknowledgements to Collaborators



MPI-K Heidelberg

- R. Bastert
- H. Buhr
- K. Blaum
- D. Fischer
- K.U. Kühnel
- C. Krantz
- F. Laux
- R. Repnow
- T. Siebert
- R. von Hahn
- A. Wolf



Kyoto university

- A. Noda
- H. Souda

FLAIR: A FACILITY FOR LOW-ENERGY ANTIPROTON AND ION RESEARCH

Carsten P. Welsch*

Cockcroft Institute and University of Liverpool, UK
for the FLAIR collaboration

Abstract

To exploit the unique possibilities that will become available at the Facility for Antiproton and Ion Research (FAIR), a collaboration of about 50 institutes from 15 countries was formed to efficiently enable an innovative research program towards low-energy antimatter-physics. In the Facility for Low-energy Antiproton and Ion Research (FLAIR) antiprotons and heavy ions are slowed down from 30 MeV to energies as low as 20 keV by a magnetic low-energy storage ring (LSR) and an electrostatic ultra-low energy storage ring (USR).

In this contribution, the facility and the research program covered are described with an emphasis on the accelerator chain and the expected particle numbers.

INTRODUCTION

Currently, the Antiproton Decelerator (AD) at CERN [1] is the only place in the world where physics with low-

energy antiprotons is done.

This facility has been in operation since 2000, and although the experiments at the AD have produced some widely published and recognized results, such as the first formation of anti hydrogen at rest, they are limited by the relatively low intensity of antiprotons from the AD, approximately 10^5 particles per second, and by the availability of pulsed extraction only. In addition, the particles are delivered from the AD at a kinetic energy of 5 MeV, which is significantly higher than the 100 keV or less which is best suited for these experiments.

At AD, the reduction in kinetic energy from 5 MeV to a few keV is made by degrading in a foil, which causes a rather large increase of the beam divergence and momentum spread, and there is also a high loss of antiprotons in the degrader foil. These effects limit the capture efficiency to about 10^{-4} .

An improvement was achieved by the installation of the RFQ-D used by the ASACUSA collaboration [2] that today provides beams at 100 keV energy. However, the

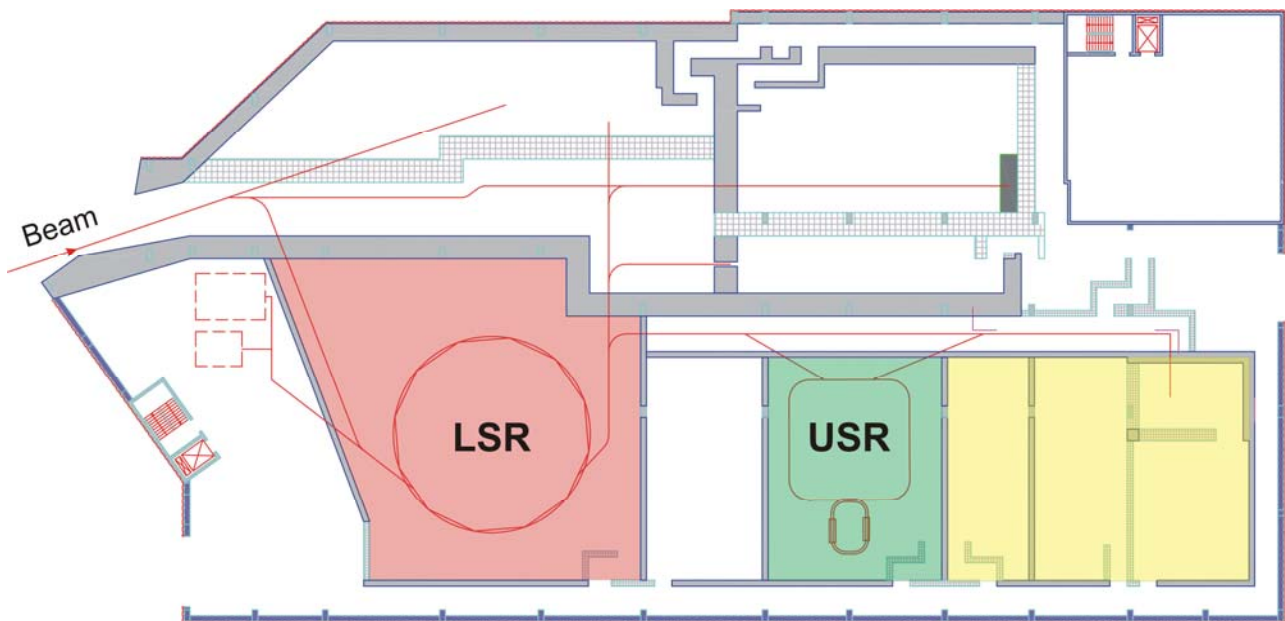


Figure 1: Layout of the FLAIR building. The low energy region can be divided into areas with beam energies between 30 MeV \rightarrow 300 keV (—), 300 keV \rightarrow 20 keV (—) and 20 keV \rightarrow rest (—).

*Work supported by the EU under contract PITN-GA-2008-215080, the Helmholtz Association of National Research Centers (HGF) under contract number VH-NG-328, and the GSI Helmholtz Centre for Heavy Ion Research GmbH.

rather large emittance $\varepsilon = 100$ mm mrad and energy spread $\Delta E/E = 10\%$ of the output antiproton beam require a large stopping volume and a high-power pulsed laser to induce transition for high precision spectroscopy. The laser bandwidth today limits the precision of the experiments.

A next generation facility clearly needs to overcome the present limitations and must also pave the way for experiments not possible at the AD by providing slow extracted, quasi-DC beams for nuclear physics type experiments and ultra-short bunches of only a few nanoseconds duration for internal collision experiments.

CONCEPT OF FLAIR

The future FAIR [3] facility on the site of the current GSI laboratory will be an international facility mainly for nuclear and hadron physics, but also for atomic physics, plasma research, biophysics and materials research. This will include physics with antiprotons, and the production rate of antiprotons will be at least 10 times higher than what is achieved at the AD today. This is due to the installation of three cooling and decelerating rings, similar to what CERN had at the time of proton-antiproton collisions at the SPS. In the case of FAIR, the antiprotons will be delivered from these rings at 30 MeV kinetic energy. The important new feature at FAIR is that the deceleration from 30 MeV is made at a dedicated facility, FLAIR (Facility for Low-energy Antiproton and Ion Physics), consisting of another two cooling and deceleration rings. In addition to antiprotons, also exotic unstable and highly charged ions will become available at FLAIR.

FLAIR will thus offer the unique possibility for low-energy antiproton and ion research and thus benefit from maximum synergies between the fields. Details about the proposed research program can be found in the submitted letter of intent [4].

The layout of the facility is shown in Fig. 1. The building is designed as a complex which includes the experimental areas requested by the experiments presented in the technical proposals submitted by the FLAIR and SPARC [5] collaborations, the hall for the low-energy storage ring (LSR) and the additional areas needed for off-line mounting and testing of setups, control and data acquisition rooms, laser labs, power supplies storage rooms, a small workshop and social rooms.

The accelerator structure to decelerate antiprotons and highly charged ions consists of the above mentioned LSR, an electrostatic ultra-low energy storage ring (USR), and finally a universal trap facility (HITRAP) [6]. These components of the facility can provide stored as well as fast and slow extracted cooled beams at energies between 30 MeV and 300 keV (LSR), between 300 keV and 20 keV (USR), and cooled particles at rest or at ultra-low eV energies (HITRAP).

Since one main focus of the FLAIR collaboration is the exploitation of physics with low-energy antiprotons, the

deceleration cycle within the facility and maximum particle numbers will be given here in this paper for this particular case.

The particles are injected from the NESR and are slowed down in a first step from 30 MeV to 300 keV in the LSR. Electron cooling will then be applied before transferring the antiprotons to the USR. Here, they are decelerated again to energies as low as 20 keV and can then be used either for in-ring experiments or be transferred via fast or slow extraction to external setups.

Since all the main parameters of the CRYRING facility at the Manne Siegbahn Laboratory are a perfect match with the requirements of the LSR and it was decided to discontinue its funding, a very attractive idea is to move the whole storage ring together with its integrated cooler and a low-energy injector to FLAIR. This would not only provide the LSR as one of the central installations of FLAIR, but would also allow off-line commissioning of the whole FLAIR facility and its experiments without the need of antiprotons or ions from the NESR. Furthermore, training of operators, as well as continuous development of the facility and experiments with ions of other species than those provided from the NESR would become feasible. Details about the storage ring as well as first dedicated experiments towards the machine performance in the FLAIR context can be found elsewhere at this conference [7].

The USR is a new development and will be the first energy-variable electrostatic cooler synchrotron installed within a large accelerator facility. It will not only decelerate the antiprotons and exotic ions to lowest energies of 20 keV/q, which will allow e.g. direct injection into traps, but will also enable in-ring experiments with at least six orders of magnitude higher event rates than in single pass setups and also pave the way for nuclear physics type experiments with slow extracted, quasi DC beams. Details about the USR lattice, its optical elements and the envisaged experiments are given in [8].

PARTICLE RATES

In the LSR, the space-charge limit for a coasting beam of protons at 300 keV is $N = 5 \times 10^8$, assuming a maximum tune shift $\Delta Q = -0.1$ and an emittance of $\varepsilon = 1 \pi$ mm mrad, see Fig. 2. However, the electron cooling at 300 keV is probably not strong enough to reach this emittance, but it is estimated that at least 1×10^8 antiprotons can be delivered within 1π mm mrad once every NESR cycle of perhaps 20 s, losses during extraction not counted. Since the space-charge limit is proportional to energy (non-relativistically) while equilibrium emittances in our case shrink with energy, one can expect that the number of antiprotons per unit time and emittance increases at least linearly with energy.

Some improvement could be obtained if the NESR beam is bunched at the 4th harmonic before extraction, and the four bunches are transferred to the LSR and

decelerated in four consecutive machine cycles. Each cycle taking about 5 s, LSR could then be able to deliver four batches of 1×10^8 antiprotons, minus extraction losses, within approximately 1π mm mrad emittance every 20 s.

For highly charged ions, the space-charge limit scales with A/Z^2 . The rates for intra beam scattering and electron cooling also change, such that one can expect that the equilibrium emittance, at the space-charge limit, does not depend strongly on the ion species for a given particle velocity. Again, the emittance shrinks with increasing energy. From this scaling, we can find, for example, that the limit of 1×10^8 antiprotons at 300 keV corresponds to $4 \times 10^7 U^{92+}$ at 4 MeV/u.

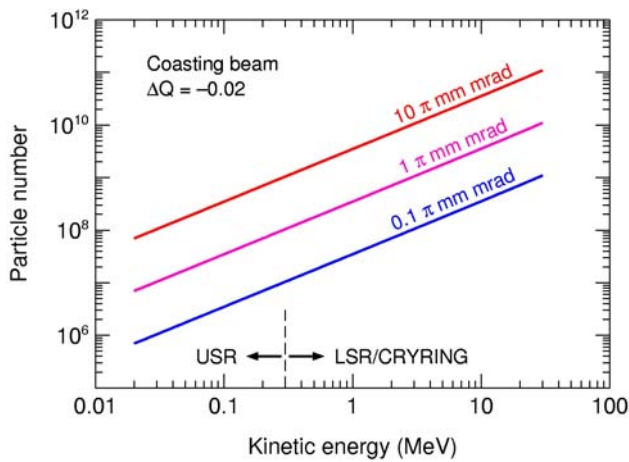


Fig 2: Antiproton space-charge limit for a coasting beam with an assumed Laslett tune shift of -0.02.

The resulting antiproton rates per unit time, averaged over the duration of a deceleration cycle starting from injection are listed in the following Fig 3.

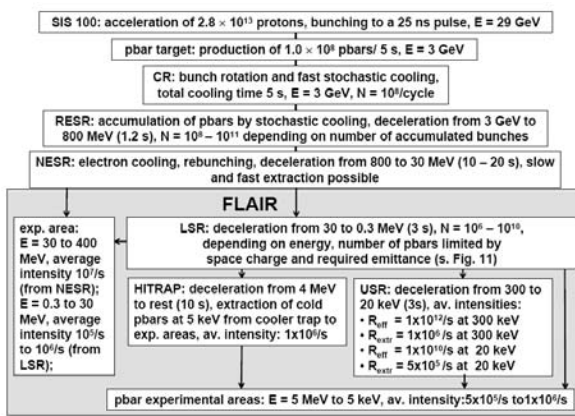


Fig. 3: Estimated antiproton intensities at FLAIR. R_{eff} is the effective antiproton rate in ring and R_{ext} the average rate of extracted antiprotons, assuming 90% losses throughout the overall deceleration cycle from the NESR.

This scheme gives about a factor 100 more antiprotons per unit time stopped in gas targets or trapped in ion traps as compared to the present AD at CERN where no dedicated accumulation and multi-stage deceleration rings are utilized. The availability of such beams, especially with the additional possibilities of performing in-ring experiments and measurements with slow extracted beams, will tremendously increase the number of experiments possible at this facility.

CONCLUSION

FLAIR is part of the FAIR joint core program and will be a world wide unique next-generation low-energy antiproton and ion facility. Cooled antiprotons down to 20 keV both in storage rings and extracted ions at lowest energies from ion sources will revolutionize low energy antiproton physics. Continuously extracted beams at these energies will enable nuclear and particle physics type experiments currently not possible at the AD of CERN. Furthermore, the availability of short-lived exotic nuclei at the future facility at Darmstadt creates utmost synergies by using antiprotons as hadronic probes for nuclear structure.

REFERENCES

- [1] S. Baird et al., "The Antiproton Decelerator: AD", Proc. Part. Acc. Conf. (1997)
- [2] W. Pirkel, A. M. Lombardi, and Y. Bylinsky, "First Operating Experience with the CERN Decelerating RFQ for Antiprotons", Proc. Part. Acc. Conf., Chicago, USA (2001)
- [3] W.F. Henning, H.H. Gutbrod, K.D. Groß, and V. Metag (editors), An International Facility for Beams of Ions and Antiprotons (FAIR CDR), GSI Darmstadt (2001)
- [4] <http://www.oeaw.ac.at/smi/flair/LOI.htm>
- [5] http://www.gsi.de/fair/experiments/sparc/index_e.html
- [6] W. Quint et al., "HITRAP: A Facility for Experiments with Trapped Highly Charged Ions", Hyp. Int. 132, 457 (2001)
- [7] H. Danared, A. Källberg, and A. Simonsson, "CRYRING Machine Studies for FLAIR", Proc. Europ. Part. Acc. Conf., Edinburgh, UK (2006)
- [8] C.P. Welsch et al., "An ultra-low-energy storage ring at FLAIR", Nucl. Instr. and Meth. A **546** (2005) 405-417.

DIAGNOSTICS FOR USR; LOW CURRENT BPMS*

J. Harasimowicz[#], C. P. Welsch, Department of Physics, University of Liverpool, Liverpool L69 7ZE, UK and The Cockcroft Institute, Daresbury, Warrington WA4 4AD, UK.

Abstract

The following paper presents the beam instrumentation foreseen for the Ultra-low energy Storage Ring (USR). The main focus of this work is on the development of beam position monitors (BPMS); a Faraday cup and a beam profile monitor will also be discussed.

INTRODUCTION

A novel electrostatic Ultra-low energy Storage Ring (USR) at the future Facility for Low-energy Antiproton and Ion Research (FLAIR), will slow down antiprotons and possibly highly charged ions to 20 keV/q. This multipurpose machine puts challenging demands on the necessary beam instrumentation. Ultra-short bunches for in-ring collision experiments on the one hand and a quasi-DC beam structure for nuclear-physics-type experiments on the other, together with variable very low beam energies, ultra-low currents and few particles, require the development of new diagnostic devices because most of the standard techniques are not suitable.

DIAGNOSTIC CHALLENGES

Table 1 presents the basic parameters of antiprotons available at the USR. The machine will be able to store and decelerate $\sim 10^7$ particles from 300 keV down to 20 keV. With a ring circumference of approximately 40 m, the revolution time of a 300 keV beam will be 5–6 μ s. Due to a highly flexible lattice design [1], the beam width will vary from a few millimetres up to almost 2 cm at some positions in the ring. Also, both slow and fast beam extraction will require special attention from the diagnostics point of view.

For the standard operation of the USR, ~ 100 -ns-long bunches are desired. For this case, a harmonic mode $h = 10$, corresponding to an RF frequency of 1.78 MHz and RF buckets of about 560 ns, will be chosen. The RF field will typically be applied after the beam has reached a quasi-DC state and will lead to the generation of 10 bunches with $\sim 10^6$ particles each. After deceleration, the main RF frequency will be decreased to 0.46 MHz to follow the longer revolution time, 22 μ s, of 20 keV antiprotons. Such bunches of ultra-slow particles ($\beta = 0.006$ – 0.025), carrying a very low charge (300 fC), will require highly sensitive detection techniques.

The most challenging mode of operation will be the production of ultra-short (few ns) bunches for in-ring experiments. Initially, a 20 keV coasting beam is planned

to be adiabatically captured into 50 ns buckets formed by a 20 MHz cavity operating at a high harmonic mode. With $h = 436$ one gets only $\sim 5 \cdot 10^4$ particles (8 fC) per bunch.

Table 1: Parameters of the antiproton beams stored and decelerated in USR

Energy	300 keV \rightarrow 20 keV
Relativistic β	0.025 \rightarrow 0.006
Revolution frequency	178 kHz \rightarrow 46 kHz
Revolution time	5.6 μ s \rightarrow 21.8 μ s
Number of particles	$\sim 10^8 \rightarrow \sim 10^7$
Bunch length	1 ns – DC beam
Effective in-ring pbar rates	$\sim 10^{10}$ pps – 10^{12} pps
Average rates of extracted pbars	$\sim 10^6$ pps

BEAM POSITION MONITORS

Capacitive Pick-up Design

For the non-destructive beam position determination, up to 8 capacitive pick-ups (PUs) will be installed at the USR. Their basic design has been discussed in [2], but a minor change has now been introduced. In order to avoid beam instabilities due to beam-to-ground impedance jumps, the PU should have the same diameter as the beam pipe. To increase the signal amplitude, the pipe diameter has been reduced from 250 mm to 100 mm.

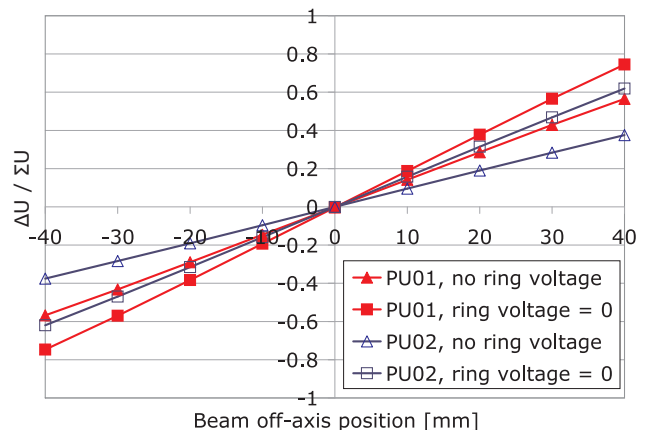


Figure 1: Response curves for two exemplary PU geometries with grounded separating rings (squares) and floating separating rings (triangles) introduced between the PU plates.

The coupling capacitance between opposite PU plates and adjacent PU units can be minimised by introducing separating rings at ground potential. With the proposed

*Work supported by the EU under contract PITN-GA-2008-215080, by the Helmholtz Association of National Research Centers (HGF) under contract number VH-NG-328, and GSI Helmholtz Centre for Heavy Ion Research.

[#]Janusz.Harasimowicz@quasar-group.org

diagonal-cut design a high linearity is achieved. The guard rings, separating adjacent plates, allow for a higher sensitivity to the beam displacement as shown in Figure 1.

Signal Estimations and Analysis

The peak voltage is expected to be as low as $\sim 100 \mu\text{V}$. If the coupling capacitance between two plates is ignored, one can assume a simple linear response $\Delta U/\Sigma U = x/r$, where ΔU is the differential signal between two opposite plates, ΣU is the sum signal and x is the beam displacement. In this case, the differential voltage for $x = 1 \text{ mm}$ will be as small as only a few μV . The expected weak signals require the use of high input resistance, high gain, low noise amplifiers together with a narrowband processing system. Fig. 2 presents the estimated differential signal which includes $30 \mu\text{V}_{\text{rms}}$ noise equivalent to thermal noise at $\text{BW} = 40 \text{ kHz}$. It is noticeable that the bunch structure is lost due to the low S/N ratio. However, the analysis of the frequency spectrum averaged over several dozens beam revolutions exhibits weak but clear peaks corresponding to the harmonics of the bunch repetition frequency. With high gain preamplifiers and a fast, high granularity ADC, the signal will be digitized and the further narrowband processing, including FFT analysis, will be performed allowing for closed-orbit measurements.

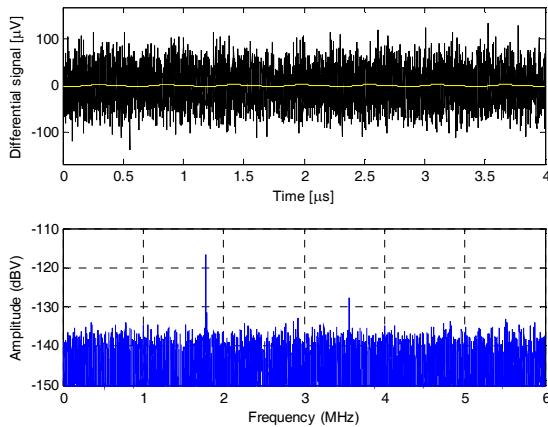


Figure 2: Top: differential signal (yellow) lost in noise (black). Bottom: its frequency spectrum for a 1 mm beam displacement averaged over $500 \mu\text{s}$.

Resonant Amplification

With a flexible signal processing system, a resonant amplification could be added to increase the overall position sensitivity. The initial idea was to introduce coils for each plate independently as presented in Fig. 3. The behaviour of such a PU has been studied in terms of the detectable voltage difference for $I_{\text{peak}} = 500 \text{ nA}$, $C = 100 \text{ pF}$, $R = 1 \text{ M}\Omega$, $\omega_0 = 2\pi f_{\text{RF}}$ and $L = 1/(\omega_0^2 C) = 80 \mu\text{H}$. With ohmic losses R_L in the inductance coil and no coupling capacitance C_c between the plates, a differential signal of more than $10 \mu\text{V}$ for 0.1 mm of

beam displacement is expected. A shift of the resonance frequency $\omega_d = (1 - R_L^2 C/L)^{0.5}$ occurs, but is as low as 3 kHz for $R_L = 50 \Omega$. However, when the coupling capacitance is considered, the resonant response is distorted, see Fig. 4. In this case, not only is the difference signal several times weaker, but also small changes in the symmetry of the setup easily affect the PU response. Several ideas on how to overcome this problem have been presented [3-4] and are presently under investigation.

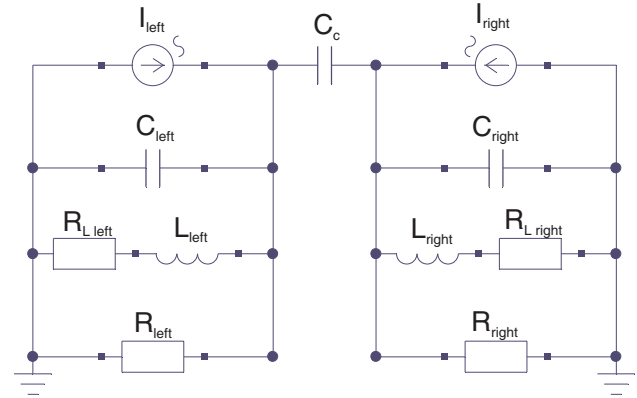


Figure 3: Equivalent circuit of the resonant capacitive PU with the image current I , plate-to-ground capacitances C , amplifier input resistors R and added inductance coils L . R_L and C_c represent coil ohmic losses and coupling capacitance respectively.

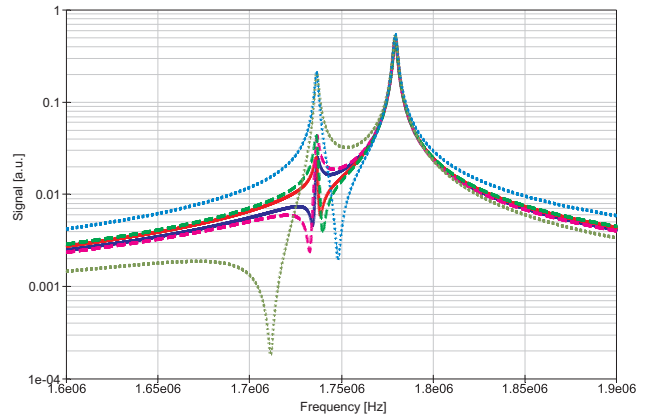


Figure 4: Resonant PU response spectra for different beam displacements (solid line: $\pm 1 \text{ mm}$, dashed line: $\pm 2 \text{ mm}$, dotted line: $\pm 10 \text{ mm}$) for two plates coupled with a parasitic capacitance.

FARADAY CUP

An electrostatic Faraday cup will be used as a simple destructive monitor for absolute beam current measurements. A limitation of this solution is, however, the interaction of antiprotons with the cup material. This can lead to the creation of not only secondary electrons but also MeV-scale charged pions and recoil ions. Such particles cannot be captured easily within the cup, and so the measured charge does not directly reflect the beam

current. It will, however, be very useful for the commissioning stage with protons or ions.

The mechanical design of the Faraday cup was optimized for the USR, i.e., the aperture size was set for beams of diameters up to 2 cm and the suppressing electrode length was adjusted to increase the electron collection efficiency. Fig. 5 shows the simulation of the electric field distribution inside the Faraday cup.

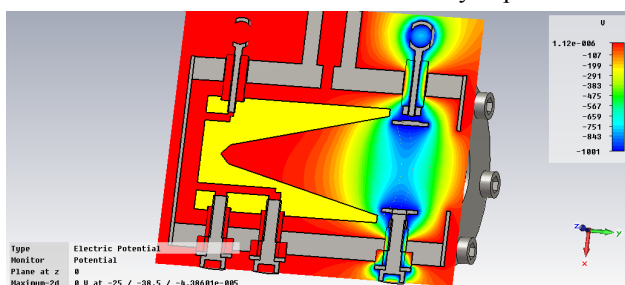


Figure 5: Simulation of the electric field distribution inside the Faraday cup.

For beam intensity measurements, a sensitive amplifier needs to be used because the expected average beam currents in the transfer lines could be as low as ~ 0.1 pA. For injection and fast extraction, the low currents can be measured by taking advantage of the bunched beam delivery and measuring the peak current with a fast current-to-voltage converter (transimpedance amplifier) working in the required bandwidth (50–200 kHz). For slow extraction, a sensitive solution should be applied for the weak DC currents. To overcome the difficulties with measurements for the different beam delivery schemes, a variable gain transimpedance amplifier DLPCA-200 from FEMTO was proposed. With a gain setting of 10^6 – 10^7 V/A, one will be able to follow the beam dynamically and get reasonably high signals. Using the highest gain of 10^{11} V/A and a limited bandwidth, it should be possible to measure intensities down to $\sim 10^6$ pps.

BEAM PROFILE MONITOR

A scintillator-based monitor will deliver information on the transversal beam profile. However, limited sensitivity and light yield decrease due to surface sputtering have been reported [5-6]; it is not clear if these results can be applied to the USR case for two reasons. First, the tests were mainly limited to plastic scintillators and other materials are still to be investigated under different irradiation conditions. And second, the thickness and other parameters of the screens were not optimized for the lowest possible beam currents. Therefore, further studies on scintillator-based monitors were undertaken using different types of screens.

The first experiments were realized at the Nuclear Physics Laboratory INFN-LNS in Catania, Italy with the invaluable help of Paolo Finocchiaro, Luigi Cosentino and Alfio Pappalardo. The tests were based on irradiation of the screens with a continuous beam of protons in the keV range with intensities down to a few fA. The scintillating materials used during the investigations

included CsI:Tl, YAG:Ce and a Tb-glass-based Scintillating Fibre Optic Plate (SFOP). In order to reduce the initial beam currents of a few pA to only a few fA, pepper-pot-like attenuators were used, which produced multi-peak images, see Fig. 6. This allowed resolution testing of the screens at the same time.

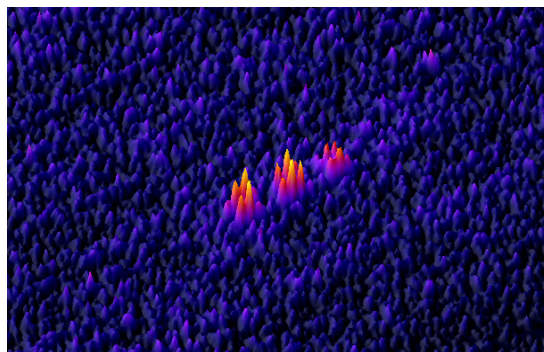


Figure 6: Intensity map of the 50 keV proton beam image taken with CsI:Tl.

The preliminary results for CsI:Tl and SFOP exhibited great sensitivity to low intensity, low energy beams such as those expected from FLAIR. For 200 keV protons, the beam was still visible at approx. 10 fA and only a few seconds of averaging. The achieved resolution was better than 0.5 mm. The YAG screen, despite its better radiation hardness, responded only in a very limited range.

REFERENCES

- [1] A. I. Papash and C. P. Welsch, "An Update of the USR Lattice: Towards a True Multi-User Experimental Facility", PAC'09, Vancouver, Canada, (2009).
- [2] J. Harasimowicz and C. P. Welsch, "Optimisation Studies of a Resonant Capacitive Pick-Up for Beam Position Monitoring of Low Intensity, Low Velocity Antiproton Beams at FLAIR", DIPAC'09, Basel, Switzerland, p. 300-302 (2009).
- [3] P. J. Chou et al., "Transverse Schottky Detectors for the Fermilab Main Ring", Fermilab Report, October 1994.
- [4] F. Laux et al., "Position Pickups for the Cryogenic Storage Ring CSR", these proceedings.
- [5] T. Sieber et al., "A Beam Diagnostics System for the Heidelberg Cryogenic Storage Ring CSR", EPAC'06 Proc., Edinburgh, Scotland, p. 1067-1069 (2006).
- [6] M. Vogel et al., "Scintillation Light Produced by Low-energy Beams of Highly-charged Ions", Nucl. Instrum. Meth. B 263(2), 518-522 (2007).

Design and Performance of a Ionization Beam Profile Monitor Based on a Gas-jet Curtain for Applications on Low Energy Accelerator Systems*.

M. Putignano[†], C. P. Welsch, Cockcroft Institute and The University of Liverpool, UK.

Abstract

Growing interest in the development of low energy projectiles, in particular heavy ions and antiprotons, calls for new beam instrumentation to be developed to match the strict requirements on ultra-high vacuum and low beam perturbation. When it comes to transverse profile monitoring, a convenient solution for simultaneous determination of both transverse profiles is found in a neutral supersonic gas-jet target shaped into a thin curtain and the two-dimensional imaging of the gas ions created by impacting projectiles. The resolution and vacuum efficiency of this monitor is directly linked to the characteristics of the gas-jet curtain.

In this contribution we describe the overall principle of operation of the monitor, including details of its expected performance and the design of a nozzle-skimmer system to be used for the creation of the jet curtain in the first prototype of such monitor. We also include a discussion on the geometry, shape of the extraction field and the experimental chamber that will house the experiment. Using numerical fluid dynamics simulations, we present the effects resulting directly from changes in the geometry of the nozzle-skimmer system on the characteristics of the jet curtain.

INTRODUCTION

Low-energy physics and storage rings are recently attracting growing interest in the scientific community, as remarkable characteristics of quantum systems are most conveniently studied at low projectile energies in the keV range [1,2].

Development of low-energy storage rings must be accompanied by developments in beam diagnostic technologies. In particular preservation of the beam lifetime causes perturbing profile monitoring (e.g. interceptive foils) to be ruled out [3]. Furthermore, existing non-perturbing techniques such as residual gas monitors can require about 100 ms [4] to make meaningful measurements, due to the low residual gas pressure, at the expected operating pressure of around 10^{-11} mbar.

A possible solution around these limitations is to use a neutral supersonic gas-jet target shaped into a thin curtain together with bi-dimensional imaging of the gas ions created by impact with the projectile beam. Such a monitor, as compared to those based on residual gas, allows injection of additional gas, in order to increase the ionization rate. The required vacuum level elsewhere in

the storage ring is maintained due to the high directionality of the supersonic jet [5]. Furthermore, the method allows simultaneous determination of both transversal profiles and beam imaging. Crucial to such a monitor is the control of the gas-jet in terms of achieved density and directionality.

In this paper, we describe in detail the working principle of the monitor. We then derive the fundamental equation governing its sensitivity and precision. Results of numerical simulations, which show that the geometry of the nozzle-skimmer system has a dramatic impact on the final result, and hence plays a central role in the optimization process, are presented. We then describe the nozzle skimmer system, the chamber that has been designed to house the experimental set-up, the extraction field for the curtain monitor, and finally draw some conclusions.

OPERATION PRINCIPLE

The proposed beam profile monitor relies on a neutral gas-jet, shaped into a thin curtain that intersects the target beam. In its simplest configuration, shown in Fig.1, the velocity vector of the atoms in the gas curtain is perpendicular to the propagation axis of the projectile beam, and the gas curtain plane forms with the same axis an angle of 45 degrees. When the projectile beam crosses the gas-jet, ionisation interactions occur and gas ions are created in the region of the curtain. These ions are accelerated by a 1 kV/m extraction field towards a Position Sensitive Detector (PSD) comprised of an amplification stage of Micro Channel Plates (MCP), a phosphor screen and a CCD camera. The magnitude of the extraction field is large enough to project the ions onto the PSD making the contributions of initial velocity spread negligible.

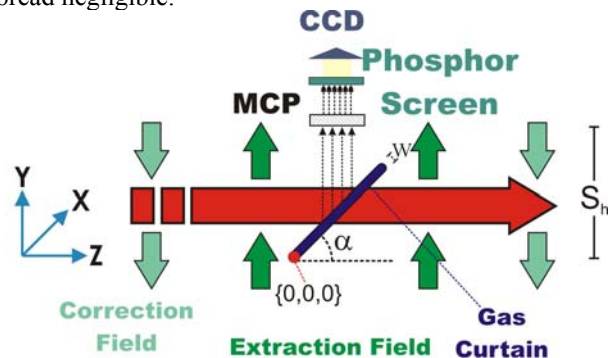


Figure 1: Sketch of the gas curtain ionization profile monitor working principle. The gas curtain, shown in purple, is crossed by the projectiles (red arrow), and the produced ions extracted by suitable electric fields (green arrows).

* Work supported by the EU under contract PITN-GA-2008-215080, by the Helmholtz Association of National Research Centers (HGF) under contract number VH-NG-328 and GSI Helmholtzzentrum für Schwerionenforschung GmbH.

[†]corresponding author: massimiliano.putignano@quasar-group.org

To counterbalance the effects of the extraction field on the main beam, two additional correction fields are added, as shown in Fig.1. Even at the lowest beam energies, this results in a net displacement of the beam from its main orbit of only 1mm at the interaction point, and both the displacement and the transverse momentum introduced by the extraction field are fully counterbalanced.

After the gas-jet crosses the beam in the interaction chamber, it flows into the dumping chamber, where an appropriate vacuum system captures the jet preventing it from affecting the vacuum in the rest of the ring.

The gas-jet consists of a high-density curtain-shaped region where densities in the range of 10^{10} to 10^{13} particles/cm³ can be obtained by varying the stagnation pressure of the gas-jet reservoir. Preliminary measurements show that the jet does not appreciably affect the vacuum in a 10^{-11} mbar chamber; this is due to its high directionality. If a 1 cm wide gas curtain (including also the lower pressure region around the main curtain) is made with Argon atoms, for whose ionization by slow antiproton impact cross section is in the order of 10^{-20} m² [6], then a probability of 10^{-6} to 10^{-3} interactions per particle per turn is predicted. Even in the worst case, allowing a hundred collisions before a particle falls out of acceptance, beam lifetimes of 1s are still possible in machines such as the USR (approx. 20 μ s revolution time).

For beams of 10^7 particles, these probabilities would in turn lead to a reaction rate in the order of 10^5 to 10^8 events per second, compatible with ms to μ s imaging and consequent single 1 μ s bunch measurement.

This profile measurement method allows the actual bi-dimensional imaging of the transverse beam density distribution, hence providing the measured function $\rho(x,y)$. From $\rho(x,y)$, both transverse profiles $\rho_{tot}(x)$ and $\rho_{tot}(y)$ can be computed by direct integration of the measured densities:

$$\rho_{tot}(x) = \int_{-\infty}^{\infty} \rho(x,y) dy ;$$

$$\rho_{tot}(y) = \int_{-\infty}^{\infty} \rho(x,y) dx$$

This, together with the method's compatibility with an ultra high vacuum environment, gives it advantages over the ionisation residual gas monitors, which provide only a measure of a single, already integrated transverse profile (either $\rho_{tot}(x)$ or $\rho_{tot}(y)$); hence two residual gas monitors are needed to measure both profiles, and the combined function $\rho(x,y)$ is not measurable.

SENSITIVITY AND PRECISION

To compute the sensitivity and resolution intrinsic to the monitor itself (i.e. without taking into account the extraction fields and the detection system) we analyze the monitor in its simplest configuration, referring again to Fig.1. A particle travelling along in the +x direction, and

starting at the point $\{x,y,0\}$ can ionize a gas atom anywhere in the segment

$$\left\{ \left(x; y; \frac{y}{\tan(\alpha)} \right); \left(x; y; \frac{y}{\tan(\alpha)} + \frac{w}{\sin(\alpha)} \right) \right\}$$

which would in turn result in a projection on the position sensitive detector in the segment

$$\left\{ \left(x; S_h; \frac{y}{\tan(\alpha)} \right); \left(x; S_h; \frac{y}{\tan(\alpha)} + \frac{w}{\sin(\alpha)} \right) \right\} .$$

An effective width of the curtain can then be defined as the distance travelled by a projectile through the gas in a straight line, i.e. $w/\sin(\alpha)$.

Using a subscript s to refer to the the coordinates of the image on the sensor and with the subscript i to the initial coordinates of the ionizing particle, the sensitivities of the profile monitor for each direction become:

$$S_x = \frac{dx_s}{dx_i} = I = M_x ;$$

$$S_y = \frac{dz_s}{dy_i} = \tan(\alpha)^{-1} = M_y ;$$

which also represent the magnification M_x and M_y of the beam profile's image on the position sensitive detector.

The precision can alternatively be calculated considering the influence of the uncertainty due to the curtain width on the position of ionization. This influences only the vertical (y axis) profile, introducing a flat error distribution with a full width of $w/\sin(\alpha)$. This in turn results in an intrinsic final resolution in the y direction poorer than in the x direction; this has also been reported in the work of Hashimoto [7], where much effort has been devoted to decreasing the curtain width.

It should be noted that a more correct indication of the precision would take into account the magnification of the beam profile image on the detector. We can introduce the modified error distribution full width W_{Err} scaled with the value of magnification:

$$W_{Err,y} = \frac{(w / \sin(\alpha))}{S_y} = \frac{w}{\cos(\alpha)}$$

Whilst it is in principle possible to minimize W_{Err} by decreasing the value of α , hence effectively improving the resolution, the equation above shows, however, that it is possible to gain only a factor $2\sqrt{2}$ as compared to the 45 degree case. We have chosen the value of α make the magnification equal in the x and y direction, leading to a non-deformed image, and thus avoiding the need of image post-processing. As the x-axis magnification is equal to unity and independent from the value of α , the y-axis magnification is also chosen to be unity, corresponding to $\alpha=45$ degrees.

It is now clear how the extent of the vertical resolution degradation depends only on the width of the curtain, which becomes a factor of primary concern in the design

of the nozzle-skimmer system used for the creation of the gas-jet.

NUMERICAL SIMULATIONS

The most common technique for the creation of a supersonic curtain-shaped gas jet involves the creation of an axis-symmetric jet of great intensity and the subsequent reshaping via collimators, after supersonic speed is attained [7]. Nevertheless, this approach results in several difficulties, amongst which the need of a large setup, to enable the gas jet to expand to the desired dimension; the use of large focusing magnetic fields to be coupled to the magnetic moment of the gas molecules, generally O₂; and the use of large quantities of gas, since most gas is collimated out, which results in large stagnation pressure needed at the source. We performed preliminary simulations, showing that it is possible to achieve a curtain-shaped jet by means of a suitable nozzle-skimmer system, at the gas source, if a rectangular slit nozzle and a skimmer shaped as a hollow trapezoidal prism is used in a suitable geometry, instead of the circular nozzle used in common applications.

To show the importance of the geometry of the nozzle-skimmer system for the curtain characteristics, we ran several sets of simulations, varying 5 geometric parameters, while monitoring 3 relevant observables, as described below.

The variables are: the skimmer aperture angles in the direction parallel (α), and perpendicular (β) to the curtain expansion, the width of the skimmer slit (SW), the depth of the skimmer structure (SD) and the nozzle-skimmer distance (Dist). We observed the Mach Number downstream of the skimmer (M), which gives an indication of the efficiency of the expansion and hence of the directionality of the jet, as well as the geometrical dimensions of the gas curtain: width and depth (W and D respectively), which directly affect the resolution of the monitor [5].

When analysing this system we are confronted with 5 variables, resulting in an exceedingly complex set of results, whose mathematical description needs a detailed treatment. Therefore, in this paper, we will express our results in the form of qualitative behavioural trends of each observable as a function of each variable, obtained by varying that variable alone while leaving the others constant.

For this analysis, a trend is said to be found when the form of the functional relationship between the observable and the variable under investigation is preserved in the simulations regardless of the actual values of the other variables. We are then able to draw a table, shown in Fig.2, which summarises the simulated behaviour of each observable (column entry) when the respective variable is increased (row entry).

We identify linear relationships (straight arrows), parabolic relationships (curved arrows), and more complex relationships (circles), where the form of the functional relationship depends on the value of some secondary variables (indicated inside the circle), and

hence, according to our previous definition, a trend is not found. This last is qualitatively different behaviour compared to the first two cases, where the shape of the trend does not depend on the remaining variables; in the last case the details of the trend, such as the gradient for the linear relationships, will depend on the values of the remaining variables.

In the table the bold orange lines represent the very clear trends, defined as those trends where the average over all points of the best fit Pearson value lies above 90%, while the slim, black lines represents less evident trends, where the average best fit Pearson value lies between 75% and 90%.

	Mach N.	D	W
α			
β			
SW			
SD			
Dist			

Figure 2: Table of simulated trends.

The table gives an indication of how sensitive the gas jet parameters are to the geometry of the nozzle-skimmer system, hence providing strong evidence in favour of the need of a detailed study for the goal of proper optimization. Furthermore, it also gives an insight as to which variables have a stronger impact on the performance of the jet in terms of directionality (namely α , β and Dist) and curtain width to depth ratio (α and SW).

CHAMBER DESIGN

In order to test the optimization of the jet curtain, it is necessary for the apparatus to fulfil two crucial requirements. First, it should include a nozzle-skimmer system whose geometry can be readily modified and secondly it should include a monitoring system able to deliver the density map of the jet curtain. The density of the curtain is indeed the crucial parameter for the operation of the profile monitor, as the reaction rate, and hence the sensitivity, will scale with it. In this section we present these two sub-systems.

Nozzle-Skimmer System

The holding system for the skimmer, shown in Fig.3, has been designed to grant maximum flexibility. It can accommodate up to two skimmers, which can be aligned in both angle (with a 5 degrees range) and in the longitudinal dimension (within 20 mm). The longitudinal adjustment is obtained by welding the smallest plate (violet) on the end flange of an inner chamber ending with an adjustable bellow, which sits inside the main chamber, welded in turn to the larger plate (green). Such

'nested' chamber design also allows the two skimmers to be placed very close to each other whilst still allowing differential pumping between them.

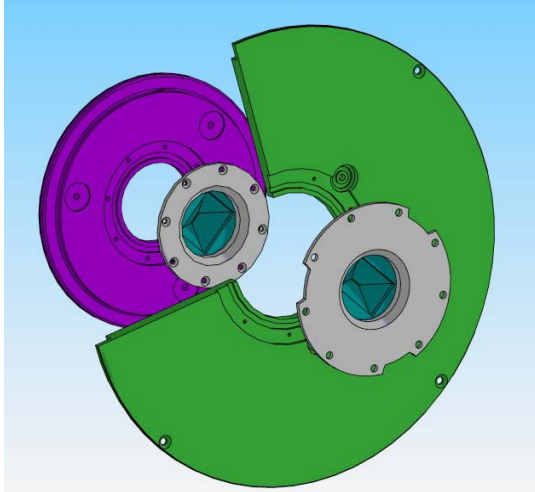


Figure 3: Skimmers holding system, exploded view.

The skimmer system is furthermore designed to allow the removal of both skimmer holders to enable the skimmers to be changed for different shaped ones without demounting the whole chamber, hence also preserving its alignment.

In order to preserve quasi-laminar flow downstream of the expansion fan, and hence allow the establishment of a stable supersonic jet, the skimmers need to be manufactured with walls thinner than 100 μm . Due to the large pressure difference across their walls caused by differential pumping, care must be taken to ensure they do not collapse towards the low pressure region. Therefore, we chose not to design a variable geometry mechanism, but rather had several skimmers of different geometries manufactured, which give over 18 configurations, 3 different values each for α and β , and 2 different values for SW.

Curtain Monitoring

In order to probe the curtain and map its density, our apparatus will rely on electron impact ionization of the gas atoms. The gas ions produced will then be extracted by a 1 kV/m electric field and guided to an MCP stack for amplification, before hitting a phosphor screen, whose emitted photons will be detected by a CCD camera. The current across the second MCP will be measured and will be proportional to the number of collected ions, while the CCD camera will record the spatial distribution of the collected ions, i.e. the depth of the curtain in the point of interaction with the electron beam. Therefore, coupling this information with the measured spot size of the electron beam and the known electron impact ionization cross sections, the density of the curtain can be calculated.

Due to the relatively large area of gas-jet under investigation (4x4 cm), a $\pm 12.5\text{mm}$ XY manipulator will

be attached to the electron gun, so as to increase the spatial range provided by electrical deflection of the electron beam. The experimental chamber designed for this monitor is shown in Fig.4.

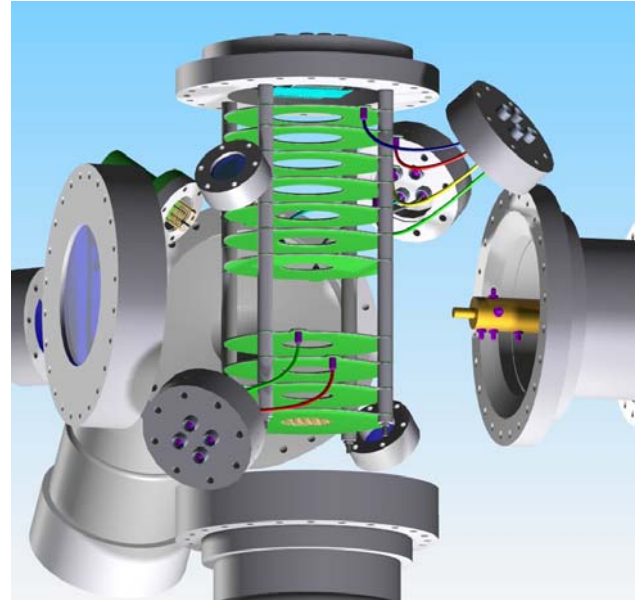


Figure 4: Experimental chamber and extraction system for the density mapping of the supersonic-jet curtain.

The spatial resolution of this mapping scheme depends mainly on the spot size of the scanning electron beam, which can be kept below 2 mm diameter. On the other hand, the accuracy depends on the quality of the extraction field and on the current stability of the electron beam. The electron gun is tested to yield a beam that is stable to within less than 1% of the nominal current when guided with a current feedback loop. The extraction field has been designed after having carried out extensive simulations with the SIMION 8.0 code. The simulations were intended to optimize the field in the central region of interest in the experiments, around the extraction electrodes axis; it is indeed in this region of interest that interaction between accelerated projectiles and the gas jet will take place in the final application for beam profile monitoring. Following the simulations, the voltages and geometry of the extracting field electrodes have been adjusted to yield the field shown in Fig. 5. This field is homogeneous within a 2.5% in the central region of interest of diameter 40 mm, where the curtain density measurements will lie.

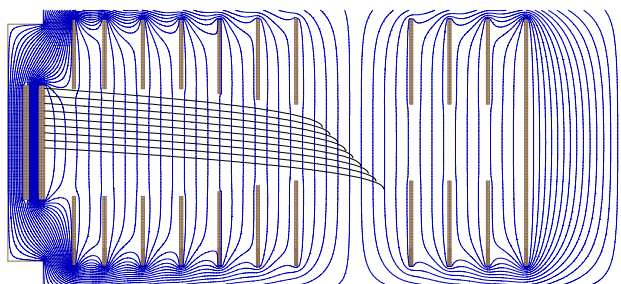


Figure 5: SIMION 8.0 simulated extraction field and tracking of the ions created on the curtain.

CONCLUSIONS

By means of numerical fluid dynamics simulations, it has been possible to highlight the importance of a nozzle-skimmer system geometry for the quality of a curtain-shaped gas-jet for use in a fast, nearly non-perturbing ionization beam profile monitor, suitable for operation at very low energy machines. It was also possible to pinpoint the most relevant observables and predict their behavioural trends when the geometric variables are changed. Finally, an experimental setup was designed to validate the numerical studies and characterize the supersonic gas-jet curtain.

REFERENCES

- [1] C.P.Welsch *et al*, “FLAIR – A facility for low-energy antiproton and ion research”, *Hyperf. Inter.*, 172, 71 (2006).
- [2] L.H. Andersen *et al*, “Physics with electrostatic rings and traps”, *J. Phys. B: At. Mol. Opt. Phys.*, 37, p. R57-R88 (2004).
- [3] J. Harasimowicz *et al*, “Beam instrumentation for the future ultra-low energy electrostatic storage ring at FLAIR”, LEAP08 proceedings, (2008).
- [4] T. Honma *et al*, “Design and performance of a non-destructive beam-profile monitor utilizing charge-division method at HIMAC”, *Nucl. Instr. and Meth. A*, 490 (3), p. 435-443 (2002).
- [5] M. Putignano *et al*, “A Fast, Low Perturbation Ionization Beam Profile Monitor Based on a Gas-jet Curtain for the Ultra Low Energy Storage Ring.”, LEAP08, Vienna, September 2008, accepted.
- [6] H. Knudsen *et al*, “Ionization of atoms and molecules by antiproton impact”, *Hyperfine Interactions*, 109, 133 (1997).
- [7] Y. Hashimoto *et al*, “Oxygen gas-sheet beam profile monitor for the synchrotron and storage ring”, *Nucl. Instr. Meth. Phys. Res. A*, 527 (3), 289-300 (2004).

Position Pickups for the Cryogenic Storage Ring CSR

F. Laux, F. Fellenberger, M. Grieser, M. Lange, R. von Hahn, T. Sieber, A. Wolf, K. Blaum
Max-Planck-Institut für Kernphysik, Heidelberg, Germany

Abstract

A cryogenic electrostatic storage ring (CSR) is under construction at the Max-Planck-Institut für Kernphysik in Heidelberg (MPI-K), which will be a unique facility for low velocity and in many cases also phase-space cooled ion beams. Amongst other experiments the cooling and storage of molecular ions in their rotational ground state is planned. To meet this demand the ring must provide a vacuum in the XHV range (10^{-13} mbar room temperature equivalent), which will be achieved by cooling the ion beam vacuum chambers to 2 - 10 K. This also provides a very low level of blackbody radiation. The projected beam current will be in the range of 1 nA - 1 μ A. The resulting low signal strengths together with the cold environment put strong demands on the amplifier electronics of the position pickups. In order to improve the precision and to push the limits of position measurement towards the nA intensity regime, we plan to make use of a resonant amplifying system, using an LC-circuit with a quality factor of ~ 1000 . A resonant amplification setup was tested in the MPI-K's Test Storage Ring (TSR). We report on signal-to-noise ratio improvements and on issues that have to be paid attention to, if resonant amplification is requested.

INTRODUCTION

The CSR will be a fully electrostatic storage ring used to store atomic, molecular and cluster ion beams [1]. The beam optics consist of quadrupoles, 6° deflectors to separate the ion beam from neutral reaction products and 39° deflectors. It will be possible to merge the ion beam with neutral particles and laser beams. The experimental straight sections contain an electron cooler and a reaction microscope for reaction dynamic investigations. One linear section is uniquely reserved for diagnostics which will contain a beam viewer for the first turn diagnose, a Schottky pickup, a current monitor for bunched ion beams, a sensitive SQUID based cryogenic current comparator and two beam position monitors (see Fig. 1) [2].

For the cold supply a commercially available Linde 4.5 K helium liquefier is combined with an additional connection box assuring the adaption to the CSR's helium pipe system. To reduce blackbody radiation, a maximum temperature of 10 K of the inner vacuum chamber is required. Efficient pumping of hydrogen as the main rest gas component is necessary to reach a vacuum in the XHV range which will be achieved by cooling parts of the vacuum chamber down to 2 K. For commissioning of the ring the ability of room temperature operation is required and part of the cryogenics concept is the possibility of baking

out the system to at least 300°C . The cryogenic concept leading to the ability to reach vacua in the desired range was successfully tested with the Cryogenic Trap Facility (CTF) [3].

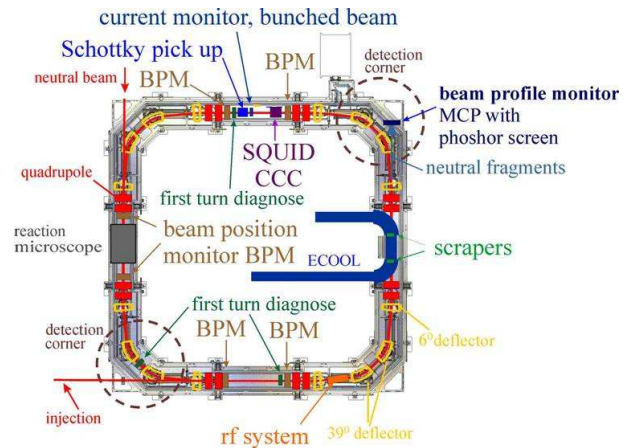


Figure 1: Overview over the CSR beam diagnostics system.

The extremely low temperatures, the large operational temperature range and the low pressures together with expected low signals are extremely challenging factors for the design of the storage ring components, particularly for the diagnostics equipment.

POSITION PICKUPS

In total six beam position monitors, each consisting of two pickups, are foreseen. One beam position monitor will be placed at each end of the diagnostics section as well as on both sides of the reaction microscope and of the third experimental section. The diagonal slit type linear pickups with a circular aperture will be used. The overall beam position monitor length will be ~ 35 cm and the aperture will be 10 cm.

Amplification Principle

Table 1 summarizes some of the relevant beam parameters. The lower current limit derives from a minimum design current to operate the ring in connection with exotic large molecules or rare short lived nuclides with a low current source and in experiments with high reaction cross sections in which it will be necessary to lower the reaction rate to prevent from detector saturation. It is requested to be able to measure the position of the center of charge of the beam to a precision of $\Delta x = 0.5$ mm. It requires a special support of the electrodes, in order to prevent the pickup from moving during cool down.

Table 1: Beam parameters

Mass range	1-200 amu
Energy range (1 ⁺ ions)	20 - 300 keV
Frequency range	5 kHz - 200 kHz
Intensity range	1 nA - 1 μ A

For amplification of pickup signals in the kHz to MHz regime, originating from bunched beams with long bunch lengths, usually high impedance amplifiers with an input DC-resistance of 1 M Ω are used. This 'conventional' - non-resonant - method is planned to be used in the CSR as well. Additionally it is planned to extend the system with the possibility of resonant amplification by means of an inductance supplementing the circuit in parallel with the combined capacity of the pickup electrodes, the signal feedthroughs and other parasitic capacities. At resonance the pickup signal is increased by the quality factor of the circuit, which is limited by losses due to the resistance of the inductance. The large range of planned frequencies is set by the extended mass range of the stored ions. A resonant system which would cover the first harmonic frequency range would have to have an extremely large and variable capacity or inductance range, which is not feasible. Therefore a system with a frequency range from 200 kHz to 400 kHz is planned, so that e.g. a beam coasting at 5 kHz had to be bunched to its 40th harmonic. From the viewpoint of the coupling to the resonance circuit a narrow span of signal frequencies would allow optimal impedance matching to minimize noise transfer. In principle it is possible to bunch the beam to even higher harmonics to also move the signal frequency further away from the 1/f-noise regime. Additionally the manufacturing of the inductance for which we intend to use coils made from high purity copper became much simpler and the side effects of a high inductance coil such as self-capacity and wire resistance lowering the quality factor were of minor importance. There is, however, an upper limit for the harmonics with which the beam can be bunched, if the beam displacement is calculated from the pickup signal based on a calibration function obtained using a wire with an applied RF-frequency as a beam replacement. The EM wave generated by the wire has no component in the longitudinal direction and thus represents a TEM wave in the pickup and therefore a field of a beam with $\beta = 1$, with β being the ratio of the particle velocity and the speed of light. As described by R. E. Shafer [4], for beams with $\beta \approx 1$ the difference of the signals at the electrodes divided by the sum ($\Delta U / \sum U$), which is usually evaluated, if the beam displacement is determined, is frequency independent. There is, however, a dependence of the calibration curve on the frequency for low- β beams. Estimations using equations provided in [4] indicate that up to a harmonic number h=40 no low- β effects are expected. This number, together with the low frequency limit of a coasting beam, leads to the lower limit of the frequency range which must be covered by the reso-

nant amplifying system. However, calculations of the low- β effects based on the finite elements method, are planned which include the special geometry of our pickup system, the result of which may shift the desired frequency range.

Signal-to-noise ratio calculations

The impedance of a non-resonant circuit with a high input resistance (1 M Ω) amplifier is determined by the impedance of the capacity ($Z \approx \frac{1}{\omega C}$). For the absolute value of the signal current I_s for bunches long compared to the length of the pickup electrode, the following equation holds [5]:

$$I_s = \omega I_b L/v. \quad (1)$$

Here I_b is the beam current, L the length of the pickup electrode ($L=8$ cm), v the velocity of the ions and ω the modulation frequency of the beam. If a capacity of 70 pF is assumed for the total system, a 1 nA beam coasting at $f_0 = 200$ kHz would cause a summed signal of both pickup electrodes of $\sum U = 150$ nV. Taking a reasonable scaling factor of $k = 60$ mm ($x = k \cdot \frac{\Delta U}{\sum U}$) the signal difference of both electrodes at $x = 0.5$ mm is just $\Delta U = 1.25$ nV, which points out the challenge of measuring the position of low current beams.

Three contributions to the total noise are considered to calculate the signal-to-noise ratio (S/N). The thermal noise $U_n = \sqrt{4 k T Z}$ with the Boltzmann constant k , the temperature T and the absolute value of the impedance of the amplification circuit Z . The voltage noise of the amplifier E_n , which is noise that is present independently of the source resistance. And the current noise I_n that becomes important for high source impedances as achieved in resonant circuits and contributes by $I_n \cdot Z$ to the total noise voltage. The signal is given by $I_s \cdot Z$ and thus the signal to noise ratio is given by:

$$S/N = \sqrt{\frac{I_s^2 Z^2}{(4 k T Z + I_n^2 Z^2 + E_n^2) \Delta f}}. \quad (2)$$

Δf denotes the resolution bandwidth of the signal recording system and for the following calculations it is chosen to be $\Delta f = 100$ Hz. The temperature is chosen to be $T = 4$ K. To use reasonable noise values E_n and I_n the data presented in [6] of an amplifier capable of withstanding temperatures as low as 4 K are taken. The values are $E_n = 4.7$ nV/ $\sqrt{\text{Hz}}$ and $I_n = 8$ fA/ $\sqrt{\text{Hz}}$ at $f = 682$ kHz. The S/N calculations are carried out for $f = 400$ kHz and since for the voltage noise a 1/f characteristic was found for frequencies <2 MHz the voltage noise for the calculations was corrected to $E_n = 8$ nV/ $\sqrt{\text{Hz}}$. A total capacity of $C=70$ pF is estimated for the CSR pickup amplifier system and thus an inductance of $L=2.2$ mH is required. In [6] the loss resistances (R_L) of different coils wound with copper and superconducting cables with $L=2.2$ mH are measured. To carry out the S/N calculations with presumably achievable quality factors, from the measured

values of R_L of three different coils, the quality factors for the exemplary CSR resonant system are calculated to be $Q=220$ with copper cable, $Q=1100$ with superconducting cable and $Q=3300$ with superconducting cable and modification of the coil shielding. The impedance in the non-resonant case at $f=400$ kHz is $Z_{non-resonant} = 5.6$ k Ω and the impedance at resonance and thus the signal is increased by Q . Hence, for $Q=3300$ the impedance is $Z_{resonant} = 18.5$ M Ω . The noise contributions to the total noise are for the non-resonant case: $U_n = 11$ nV, $E_n = 80$ nV and $I_n Z = 0.4$ nV. For the resonant case ($Q=3300$): $U_n = 640$ nV, $E_n = 80$ nV and $I_n Z = 1,47$ μ V. Due to the higher impedance in the resonant case a low value of the current noise is of special interest. In the non-resonant case it is the voltage noise that contributes most to the total noise. Note at this point that in principle a better S/N ratio would be achieved if the high impedance of the resonant circuit would be transformed to the noise resistance of the amplifier $R_n = E_n/I_n$, which is in this case $R_n = 1$ M Ω . This, however, is not foreseen for the CSR resonant amplification system since the impedance transformation had to be changed for every measurement frequency and its moderate benefits do not compensate for the effort of realizing such a feature.

As an example, for a $I_b = 1$ nA beam, coasting at $f_0 = 200$ kHz with the HF set to $f_{HF} = 400$ kHz and a quality factor of $Q=1100$ the signal-to-noise ratio is $S/N_{resonant} = 142$ and with non-resonant amplification it is $S/N_{non-resonant} = 1$. The minimum S/N ratio needed for a precision of Δx can be calculated by $S/N_{minimum} = \frac{2k}{\Delta x}$. If an ideal scaling factor of $k = 50$ mm is assumed, for a precision of $\Delta x = 0.5$ mm a ratio of $S/N_{minimum} = 200$ is required. The minimum beam current for a beam coasting at $f_0 = 200$ kHz with the HF set to $f_{HF} = 400$ kHz is therefore for resonant amplification $I_{resonant} = 1.4$ nA and for non-resonant amplification $I_{non-resonant} = 0.2$ μ A.

Effects of coupling

For the position measurement a simultaneous measurement of the signals from both pickup electrodes is preferable. Due to the large opposing areas of the pickup electrodes, there is always a considerably large coupling capacity present. If resonant amplification of both electrodes is used, the presence of a capacity between the electrodes causes a coupling of the resonant circuits, resulting in a double resonance and a drastically reduced displacement sensitivity (Fig. 2).

To overcome this situation it is investigated to use a measurement system as depicted in Fig. 3, with which the position is measured stepwise. With relays, one electrode is short cut to ground. By this the coupling capacity simply adds up to the capacity of the active electrode which is itself connected to the resonant amplifying system. In a second step the relays are switched to the other electrode. Another benefit from this measurement is clearly that the two signals are amplified by exactly the same amplifier and

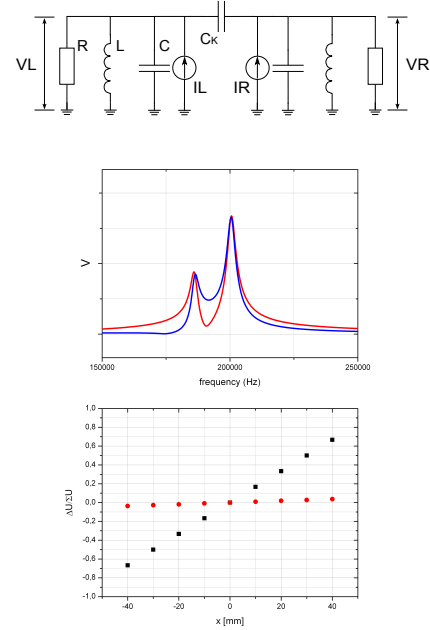


Figure 2: The effect of the coupling capacity on the resonant pickups. Top: Equivalent circuit with the capacity of the pickup electrode (+cables etc.) and the coupling capacity C_k . The difference of the signal currents IL and IR is for a diagonally slit pickup linearly dependent on the beam displacement. For beam position measurements the left and right voltages VL and VR are processed. Middle: Frequency response with the resonant circuits tuned to 200 kHz and $C = 4$ pF. The curves (red: VR , blue: VL) are calculated for a beam position of $x = 30$ mm. Bottom: Calibration curves. Black: Calibration curve for non-resonant amplification, i.e. without the inductances. The slope is decreased due to coupling with respect to the ideal case where $(VR - VL)/(VR + VL) = 1$ at $x = 50$ mm. Red: Calibration curve with resonant amplification. Its slope is decreased by a factor of 20 with respect to non-resonant amplification.

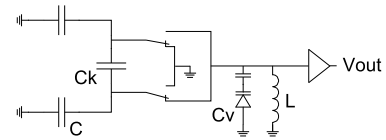


Figure 3: An amplification scheme using two relays and one tuning diode C_v .

essentially the same resonant circuit and thus less systematic errors may be expected that affect the measurement accuracy.

However, since the signal is proportional to the inverse of the loss resistance, $U_{signal} \propto \frac{1}{R_L}$, it is important that the losses due to the switches are the same. If a comparability of the signals of 10^{-3} is demanded, for a resonant circuit with $R_L = 20$ Ω ($Q=275$) this requires that the resistances

of the two relays must not differ by more than 0.02Ω . If the system is realized differently such that one changer is switching from one electrode to the other and each electrode can be short cut to ground with an own switch, it is the two electrical lines in the changer which must not differ by a certain resistance in dependence on the quality factor.

For non-bunched, uncooled beams lifetimes in the order of 10^3 s are expected. If, however, the non-cooled beam is bunched, the lifetime strongly depends on the RF-noise, which will possibly decrease the lifetimes to the order of minutes. If the stepwise measurement method is used, the measured signals have to be corrected for the decreasing intensity. However, the measurement time required for $\Delta f = 100$ Hz including the time for signal acquisition, switching and rise time, which has to be considered due to high Q values, is estimated to be < 150 ms. Therefore the systematic error, that would be present in the result if a lifetime of minutes is not take into account is very low.

Test Measurement at the TSR

At the MPI-K's Test Storage Ring (TSR) the increase of S/N with the resonant method was demonstrated. For this a 50 MeV C^{6+} beam was used which had a revolution frequency of $f_0 = 509.3$ kHz. For the measurement it was decided to use a frequency of $f = 3.056$ MHz. However, when we set the RF-system to $f = 3.056$ MHz, so that six bunches are circulating in the ring, we noticed a strong crosstalk to the pickup. Therefore we decided to bunch the beam to three bunches, i.e. $f_{HF}=1.528$ MHz. For an non-cooled, bunched beam the ion current can be described by $I(t) \approx 2 \bar{I} \cos^2(\pi f_{HF} t)$, where \bar{I} is the average current, and therefore the frequency spectrum has no higher harmonics. A cooled beam with short bunches was therefore used which has a strong second harmonic, which frequency is at $f = 3.056$ MHz. The advantages of this method are that there is no crosstalk from the RF-system present at the measurement frequency. However, in the CSR, position measurements with non-cooled beams are required and therefore one has to reduce crosstalk from the CSR RF system as much as possible.

The switching between the electrodes was carried out with changers as depicted in Fig. 3. An amplifier was developed which has three stages. The first stage consists of a FET cascode with a DC input impedance of $1 M\Omega$. At its input a capacity changing diode is used to tune the resonant circuit. The second stage is an operational amplifier that provides a fixed gain and the last stage features a variable gain amplifier. The results of the noise measurement of the amplifier are for the voltage noise $E_n \sim 3$ nV/ \sqrt{Hz} and for the current noise $I_n \sim 150$ nV/ \sqrt{Hz} . A coil from isolated copper wire was wound with a body made from Teflon. The inductance of the coil is $L = 19.9 \mu H$. The quality factor of the system was determined to be $Q=116$. With the variable gain stage of the amplifier the signal was adjusted to the SIS3301 Flash ADC range, which has a resolution of 14 bits and a sampling rate of $f_{samp} = 80$

MHz. The memory of the SIS3301 is capable of storing 128k samples, which results in a resolution of $\Delta f = 625$ Hz.

With the wire-method the scaling factor was measured to be $k = 130$ mm. Hence, for a precision of $\Delta x < 0.5$ mm a signal-to-noise ratio of $S/N > 520$ is required. For a 50 MeV C^{6+} beam and a measurement frequency of $f = 3.056$ MHz one can calculate a minimum current of $I_b = 0.1 \mu A$ for a resonant system with the decisive parameters given above. For non-resonant amplification with the same amplifier the minimum current is $I_b = 1.7 \mu A$ if a precision of $\Delta x < 0.5$ mm is required. The theoretical signal-to-noise improvement is thus 18 dB. From a number of $N = 20$ position measurements in a series during which the beam was not moved the standard deviation of a single measurement was deduced to be $s_{measured} = 0.12$ mm. During the measurement the beam current was measured with a Beam Profile Monitor and found to be $I_b = 0.5 \mu A$. The calculated standard deviation is $s_{calculated} = 0.07$ mm. The measured and calculated values are considered to be in good agreement. The calculated standard deviation of a non-resonant amplification measurement of the position is 18 dB larger, i.e. $s_{calculated} = 1.2$ mm.

CONCLUSION

Calculations show that with resonant amplification it will be possible to measure the position of even nA beams to a high precision in a reasonable time, if the crosstalk of the RF system to the pickup amplifier system can be reduced significantly. The problem of coupled resonant circuits can be overcome by measuring the signal of the electrodes stepwise. Due to this in addition a lower influence of systematic errors may be expected. The drawbacks of this method are the increase of measurement time by roughly a factor of two and the fact that for low lifetimes the consecutively measured signals have in principle to be corrected for the decreasing beam intensity.

REFERENCES

- [1] M. Froese et al., "Cryogenic ion beam storage", PAC 09 Proceedings, Vancouver, May 2009.
- [2] T. Sieber et al., "Beam diagnostics development for the Cryogenic Storage Ring CSR", WEPB23, DIPAC 07 Proceedings, Venice, May 2007.
- [3] M. Lange et al., "A Cryogenic Electrostatic Trap for Long-Time Storage of keV Ion Beams", submitted to Review of Sci. Instrum.
- [4] R. E. Shafer, "Beam position monitor sensitivity for low- β beams", Proc. Beam Instr. Workshop BIW, Santa Fe, p. 303.
- [5] P. Forck, "Lecture Notes on Beam Instrumentation Diagnostics", Proc. of Joint University Accelerator School, Darmstadt, 2009
- [6] H. Kracke, "Entwicklung der kryogenen Nachweis-Elektronik zur Bestimmung der axialen Frequenz des Protons in einer Penning-Falle", Diploma Thesis, University of Mainz, 2007.

A PEPPER POT EMITTANCE DEVICE FOR 8 KEV/U LIGHT ION BEAMS – GENERAL LAYOUT AND INVESTIGATIONS ON THE SCREEN MATERIAL

M. Ripert, A. Peters, T. Winkelmann, HIT, Heidelberg, Germany.

Abstract

The ion cancer therapy facility HIT in Heidelberg is producing ions (H, He, C and O) from two ECR sources at an energy of 8 keV/u with different beam currents from about 80 μ A up to 2 mA. Typical sizes for the beam in the LEBT range from are 5 – 30 mm. By using on-line emittance measurements it is possible to improve the beam quality by retuning the ion source conditions. For that, a pepper-pot measurement device is under design. In order to quantify the fast ion flux intercepted by a diagnostic ion probe, it is necessary to determine the absolute luminosity of its screen for low-energy ions. Here, Qualitative results of ion luminescence measurements are presented for candidate materials.

However, this method is really slow because the second slit has to be scanned through the range for every position of the first slit.)

With the multi-wire collector method, collector wires collect the beam particles that pass through the slit. The disadvantage of this method is that it requires an amplifier for every wire in the collector.

The Allison-type emittance scanner is faster than the multi-wire collector method but slower than the pepper – pot method.

PEPPER POT DEVICE

Location

The Pepper-Pot Scintillator Screen system should fit within the existing beam line components (vacuum boxes already used with beam diagnostics equipment like Faraday cups, profile grids and slits). The N1DK1 vacuum boxes will be equipped with a fast iris shutter, a pepper-pot mask and a scintillator screen. The N1DK2 vacuum boxes will contain a 45 degrees tilted mirror inside and a CCD camera outside. (Figure 1)

The pepper-pot principle

The pepper-pot mask, which is perpendicular to the beam and contains a regular array of identical holes, splits the beam into beamlets. The scintillator is used to create a photographic image of the beamlets with pixel intensity corresponding to the charge concentration of beam particles striking the scintillator. A CCD camera with a mirror placed at 45 degrees will record multi-shots.

Why using a pepper-pot device?

We want to measure both x-y components of the beam emittance simultaneously in one shot and to obtain data in real time. Four methods can be used and utilize a slit to select a portion of the beam for analysis. These methods are described in the following paragraphs.

The two-slit scanner method uses a second slit which can be scanned through the direction parallel to the first.

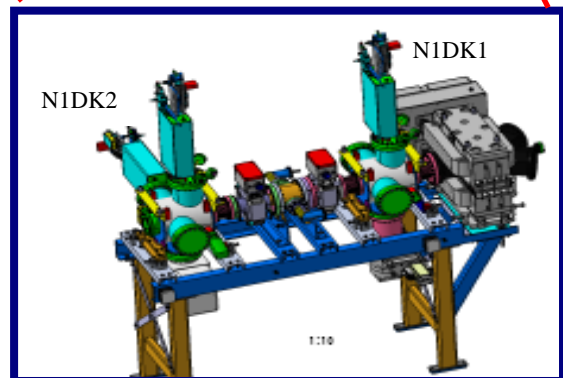
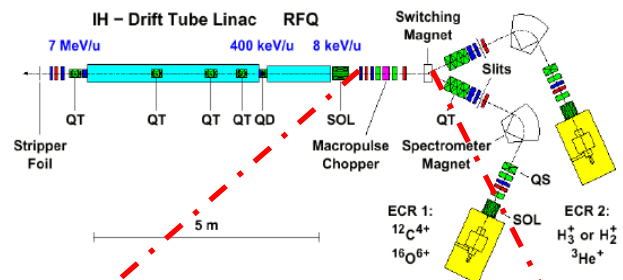


Figure 1: The Low Energy Beam Transport at HIT and the position of the Pepper-Pot Scintillator Screen device within the LEBT.

Who uses a pepper-pot device?

GS1 [1], BNL [2] and RAL [3-4] are recently developing or updating a pepper pot device. Sometimes, the use of a multi channel plate in combination with a scintillating surface has to be considered.

SCINTILLATOR

The pepper pot mask and the measurement screen will be aligned perpendicularly to the beam. The beam images will be thus produced by a transparent scintillator and will be captured by a suitable CCD camera.

Properties

The materials, selected because of their availability, radiation hardness, fast response, prior use in beam diagnostics, or spectral matching to detectors (CCDs) are:

- Inorganic Doped Crystal : YAG:Ce, and also YAP:Ce
- Inorganic Undoped Crystal : Sapphire, YAG
- Quartz and Borosilicate glass : Herasil 3 & 102, Infrasil 301 & 302, Suprasil 1 & 300 , D 263 T

One of the most important properties of fused quartz is its extremely low coefficient of expansion: 5.5×10^{-7} mm $^{\circ}\text{C}$. Its coefficient is 1/34 that of copper and only 1/7 of borosilicate glass. This makes the material particularly useful for applications which require minimum sensitivity to thermal changes.

Experiment at the Max Planck Institute - Heidelberg

These tests were made on the first week of November 2009. During these runs, the scintillator plate was placed in the beam path at a 45 degree angle and CCD camera was recording 15 frames per second. Three scintillators could be placed on a holder and be tested with the same conditions in one machine run.

The Ion Beam parameters used in this experiment are the following:

- Energy : 8 KeV/u
- Beam Current : 10 μ A
- Particles per pulse : 9.4×10^{11} – 3×10^{13}
- Variable Pulse Length : 15 ms – 500 ms
- Frequency : 1 Hz

Each material is irradiated with 3 macro pulses of 15 ms, 20 ms,until 500 ms (or less if the light output intensity became constant) with a frequency of 1 Hz. At the end of the test a total irradiation time of 1.5 sec to 2 sec have been applied to each material.

The measurements made with H ions having energies of ≈ 8 keV / u. Qualitative results are summarized and used to estimate light output, degradation, low time delay which are then compared with known published values.

The ion beam is first passing through a collimation entrance slits. Once the beam is tuned into the Faraday cup and a beam current measurement is acquired, the chopper is released and the beam travels down to the screen material situated in front of the Faraday Cup.

Three samples to be irradiated reside on a sample holder driven by a manual actuator. The target is heated to below the melting point by the beam energy.

The resultant ions were then accelerated towards the probe before passing through a collimation entrance slits. In this way flux up to 3×10^{13} pps for protons was achieved.

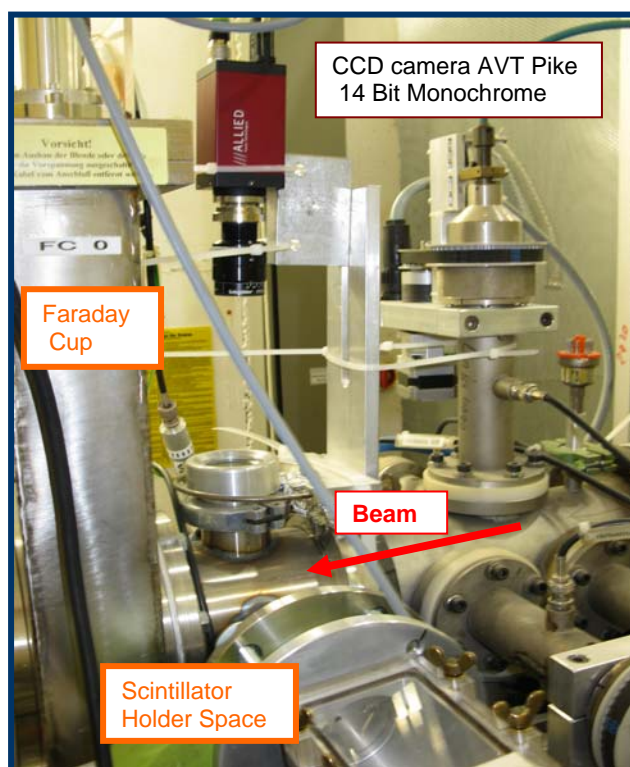


Figure 2: Ion Beam-Material Irradiation Test Setup at the Max- Planck Institute in Heidelberg.

Summary of the first results between Inorganic doped/undoped and Quartz/Glass

The Inorganic doped scintillators have a greater light output than the inorganic undoped scintillator and the quartz material. However, the undoped scintillators show constant light output intensity with respect to the beam pulse whereas quartz and inorganic doped scintillators shows an increase in the light output intensity with the increase of the beam pulse.

As a qualitative result, slighter damage with quartz material has been revealed. Only quantitative analysis will give us more details.

Influence of doping – comparison between YAG:Ce and YAG undoped

As envisaged, the light output of the doped scintillator is superior and increases with the beam pulses. That's not the case with undoped scintillators.

[3] Simon JOLLY, Presentation DIPAC '07

[4] D.Faircloth et al, The Front End Test Stand High Performance H- Ion Source at RAL, PAC 2009

Degradation Effect: damage visible with a 10 nA current

The video of the degradation of YAG:Ce shows a small beam current of 10 pA which have been used to reveal the blackening of the materials. However, a standard microscope doesn't show any damage (burning bubbles, changes in colour ...)

The damage of the undoped YAG (Figure 3) shows that after 1.3 seconds of total irradiation time the undoped material cannot be used anymore. Only a small part of the material scintillates, a big part (corresponding to the irradiated beam width of the previous day) doesn't scintillate at all. This material should be analyzed with care since undoped YAG should be stronger through radiation than YAG:Ce.

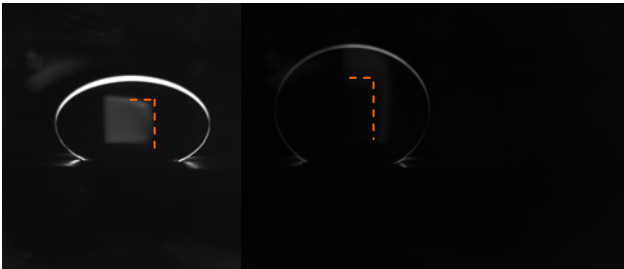


Figure 3: Degradation Effects of undoped YAG after an irradiation time of 1.3 seconds.

CONCLUSION

Inorganic Doped and quartz material are qualitatively good candidates. Of concern is the damage at the surface giving rise to stresses that could result in atomic mixing in the collision cascade. A model is needed in this area to better understand the beam target interaction and its effects on the target.

In order to find solutions such as the choice of the target, quantitative investigations on all materials should be performed.

REFERENCES

[1] T.Hoffmann, W.Barth, P.Forck, A.Peters, P.Strehl ,
Emittance Measurements of High Current Heavy Ion
Beams Using a Single Shot Pepper pot System

[2] Markus Strohmeier, Development of a pepper-pot
device to determine the emittance of an ion beam
generated by an ECR ion source, Poster PAC 2009

Various beams for RBS at IFIN-HH

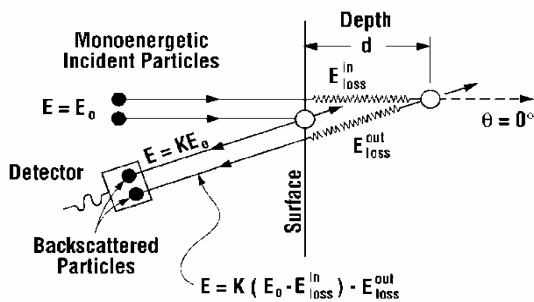
H. Schubert, D. Dudu, I.Vata

Horia Hulubei National Institute of Physics and Nuclear Engineering - IFIN HH; Str. Atomistilor no.407, P.O.BOX MG-6, Bucharest - Magurele, ROMANIA

At IFIN-HH, we are using our Cyclotron for Ion beam analysis, mainly RBS. Rutherford Back Scattering (RBS) is a widely used method for material analysis of thin films and surfaces. We give a brief overview about some results obtained with RBS, before we describe a new method for micro beam creation tested in our laboratory. Focusing the beam with a glass capillary seems to be a possible way, to enlarge our RBS applications to surface mapping and probably even channeling applications. More studies of the focusing effect itself are planned, involving more sophisticated beam analysis methods.

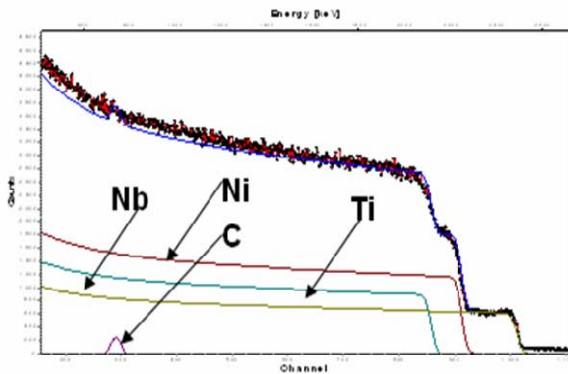
Introduction

Ions of a high kinetic energy (typically 1-3MeV) are directed at the sample. The incident ions are elastically scattered from the atoms in the sample. The number of scattered ions and their energy is measured. The energy loss of a given (in general low mass; He⁺) back scattered particle measured at a fixed angle is a function of initial energy, mass (kinematic factor) and depth of the target nucleus.



Picture 1: Principle of RBS

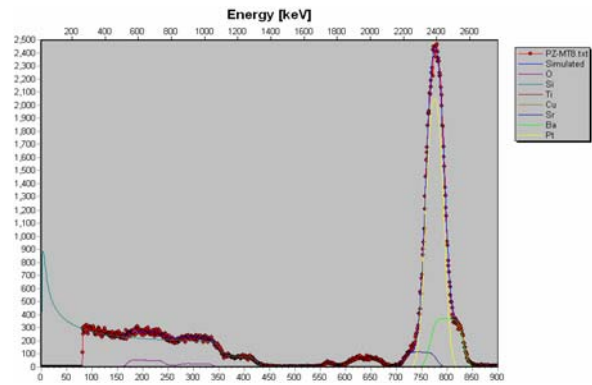
The measured energy spectrum is the sum of all contributions of the constitutive elements inside the probe. This data provides information on the composition of the sample, the distribution of those components and the thickness of the sample.



Picture 2: Example for Elemental composition

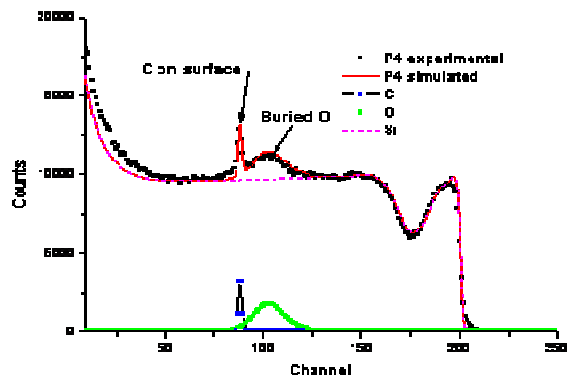
Application Samples

In praxis, the analyzed samples are consisting of different layers and the resulting spectra are more complex. A typical multi-layer sample is shown in picture 3:

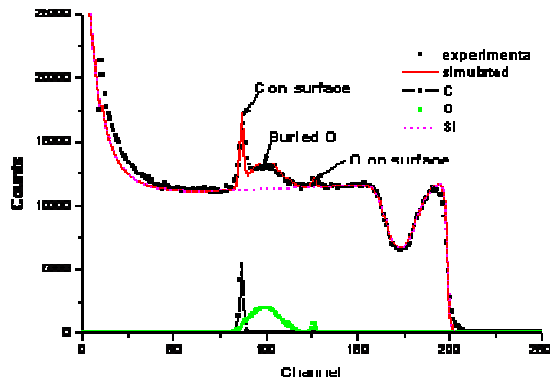


Picture 3: Sample with composed layers

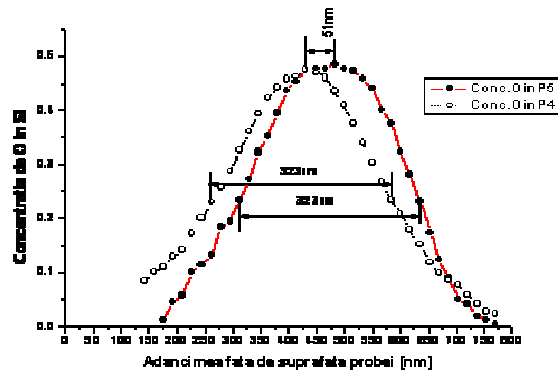
From measurements of depth profiles of probes before and after thermal treatments, diffusion processes can be analyzed. See pictures below:



Picture 4: measured and calculated spectrum of a probe with a buried Oxygen layer in Silicon (P4)



Picture 5: measured and calculated spectrum of the same probe after heat treatment (P5)



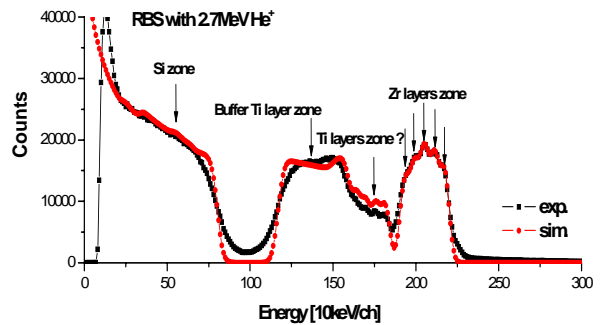
Picture 6: Position and concentration (shape) of the buried oxygen layer in Si before (P4) and after (P5) thermal annealing at 1000°C

The interesting result of this analysis is, that the layer is more or less keeping its shape (~320nm), but is shifted by ~50nm backwards (away from the surface). Similar analyses e.g. for intermediate layers have been performed for different “customers” in the last years. So even a cyclotron is not a dedicated machine for RBS, we can support other institutes and local industry with our analyses in order to improve their products or production processes.

Ambiguity problem / use of different ions

Due to the limited beam quality (energy spread ~1%) of the cyclotron, limited detector resolutions and the complexity of probes, some of the spectrums obtained are not precise enough to be clearly analyzed (fitted) without ambiguity. To resolve this ambiguity problem we can measure with different angles of the incident beam towards the probes’ surface in order to better separate different layers or elements from each other.

But sometimes, we end up with spectrums like this:



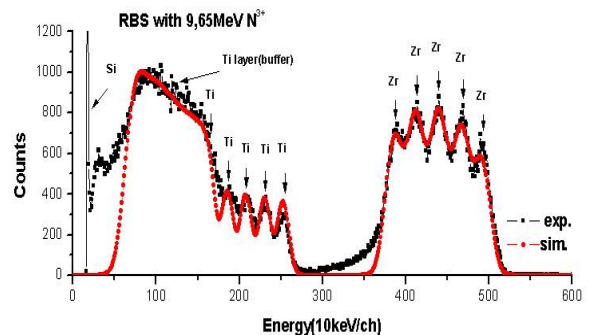
Picture 7: Nano-structured layers measured with He⁺

To analyze such samples a change of incident angle simply is not good enough to achieve acceptable results. Therefore, we were retuning the cyclotron for the use of different ion beams like e.g. Nitrogen:

No.	Ion	Energy (MeV)	Cross section[mm ²]	Beam intensity[nA]
1	⁴ He ⁺	2,7-5	0,25-25	3-100
2	² H ⁺	1,35-2,5		
3	¹⁴ N ⁺²	3		
4	¹⁴ N ⁺³	10		
5	H ₂ ⁺	1,35-2,5		

Table 1: Different beams from the cyclotron

Depending on the elemental composition, we can significantly improve our resolution by using various dedicated ion beams (varying mass (element) and angle of the incident ions). For layers with heavier atoms (obs.: RBS only occurs, if the incident ion has less mass than the target atom), the use of a Nitrogen beam can resolve the probes much better.

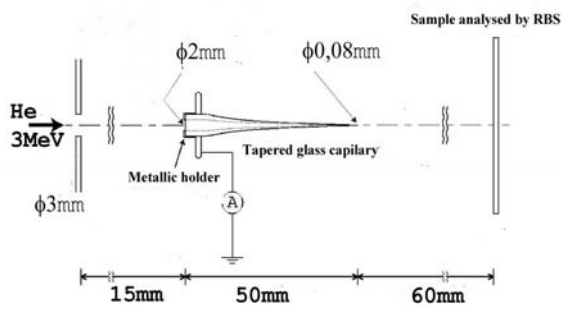


Picture 8: Experimental and simulated spectra of a nano-structured probe of 5 pairs of ZrN/TiN layers having 15 nm/layer deposited on Si with a Ti buffer layer of 300nm

Micro beam

In order to extend the field of application for RBS (and other IBAs), we have been looking for possibilities to achieve micro beams with our cyclotron. Because of the relatively poor beam quality from this cyclotron, standard procedures are not applicable. But we found another way.

By introducing a conical glass capillary into the beam line, we could achieve micro beams with reasonable intensities and acceptable quality (Energy spread, divergence). The principle is shown in Picture 9:



Picture 9: Beam handling with a glass capillary

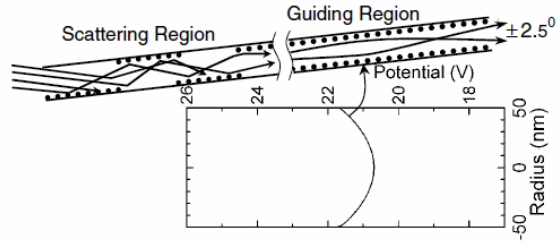
In comparison to a simple collimator (e.g. iris) the (perfect aligned) glass capillary is not only cutting out a part of the beam, but also shows a kind of focusing effect which leads to relative higher intensity of the remaining beam. First results are shown in table 2:

	I_{IN} [nA]	J_{IN} [nA/mm ²]	I_{OUT} [nA]	J_{OUT} [nA/mm ²]	Gain [J_{OUT}/J_{IN}]
Collimator 3mm	60	8.48	60	8.48	1
Capillary 2/0.15mm	26.66	8.48	6	339.5	40
Capillary 2/0.08mm	26.66	8.48	3	596.8	70.38

Table 2: Beam parameters and gain factor for different capillaries (* Beam intensities at the input of capillaries are reduced proportional to the cross sections ratio (4/9))

The gain factors of 40 and > 70 indicate clearly, that some kind of focusing occurs inside the capillary. This focusing effect is still topic of (basic) research and probably not yet totally understood. Some possible explanations are given in [1, 2, 3]. Without going into details, it seems there are two possible ways for the beam to pass through the capillary. First is low angle scattering at the surface or near surface atoms of the capillary, which also leads to energy losses of the

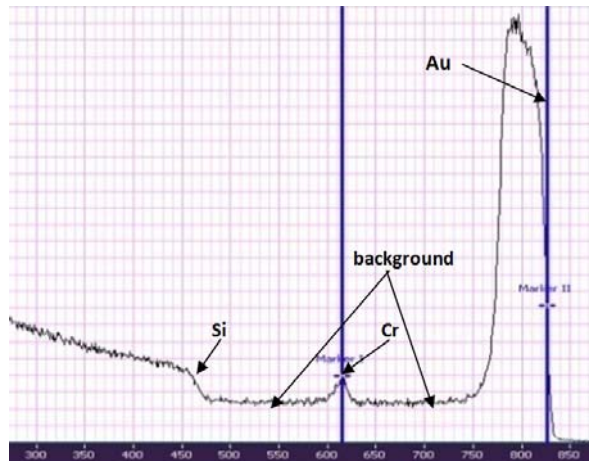
transmitted ions. Second parts of the beam seem to be guided through the capillary without (significant) energy change. How exactly this works is still topic of research.



Picture 10: beam in glass capillary [N. Stolterfoht, et al., Phys. Rev. Lett., 88,133201 (2002)]

First results

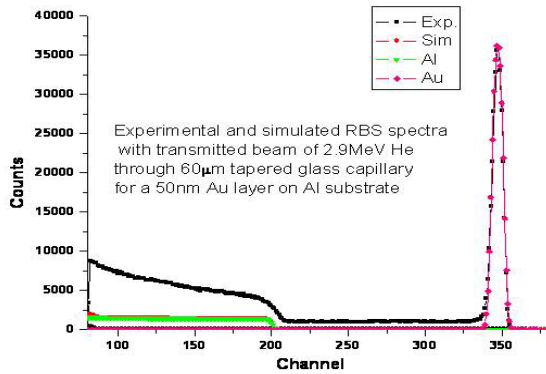
In order to analyze the beam after the capillary, we used one of our standard probes. Picture 11 shows a RBS spectrum for a layered sample of Au_{100nm}-Cr_{16nm}-Si_{thick} obtained with 3MeV He ions transmitted through a conical capillary ($\Phi_{out}=0.08mm$). The RBS spectrum shows two components of transmitted beam:
 -an "undisturbed" beam (initial energy and energy dispersion are more or less conserved)
 -a fraction of the initial beam having a large energy dispersion



Picture 11: Energy spectrum of transmitted beam

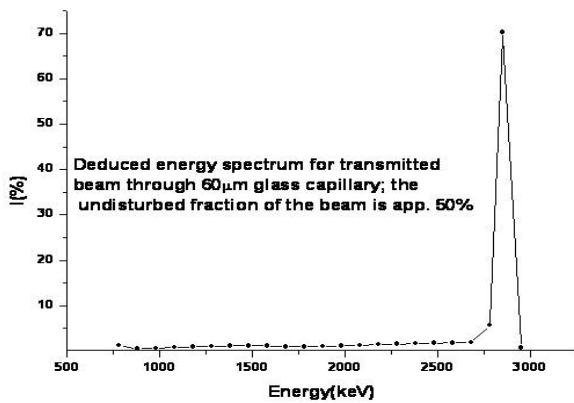
For more precise analysis of the transmitted beam, we were analyzing the reflected He ions from a 2.9MeV beam after passing through a 60 μm tapered glass capillary, using a 50 nm Gold layer on an Aluminum substrate (see picture 12). It is to mention, that the

cyclotron was running during this experiment for 24 h, with a stability of +/- 2 KeV!



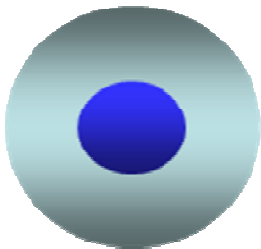
Picture 12: RBS Spectrum

From this spectrum we can deduce an energy spectrum (picture 13) of the transmitted beam, which shows that ~ 50% of the ions in the beam seem to be transmitted without energy loss.

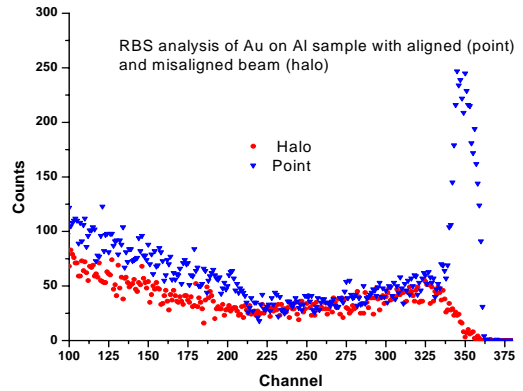


Picture 13: Deduced energy spectrum

Visual examination (phosphor screen) suggests, that the other 50% of the beam, which suffer energy loss also have a bigger divergence as the "undisturbed" beam and form a halo around the "undisturbed" center beam.

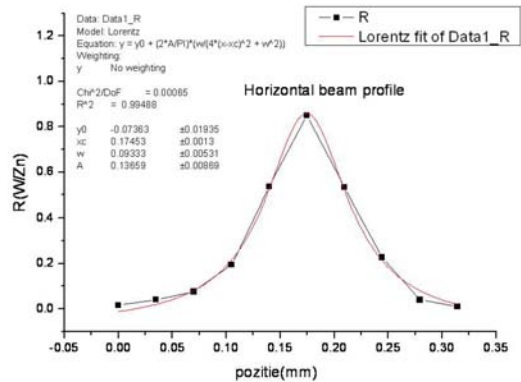


To crosscheck this, we measured two additional spectrums, one with proper alignment of the tube and one with identical setup, but slightly misaligned capillary.



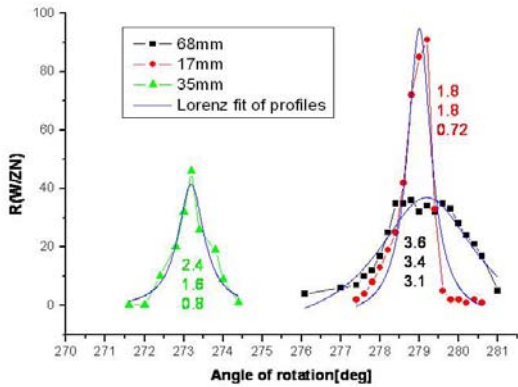
Picture 14: RBS Spectra with an aligned and misaligned capillary

Again with the aligned capillary ~ 50% of the ions in the beam seem to be transmitted without energy loss. To measure the beam profile we used a thin Wolfram wire of 20 µm, mounted on a rotating disk behind the capillary. From the measured RBS spectra we could deduct a beam profile with a width of 80 µm.

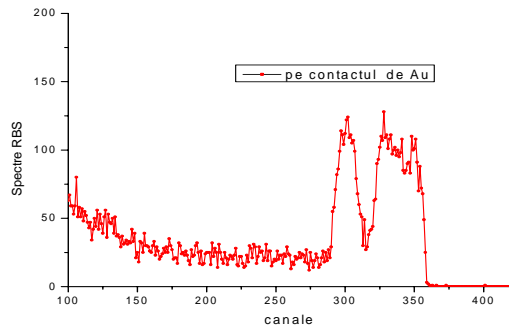
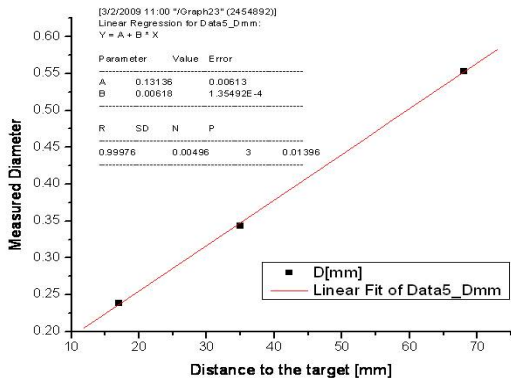
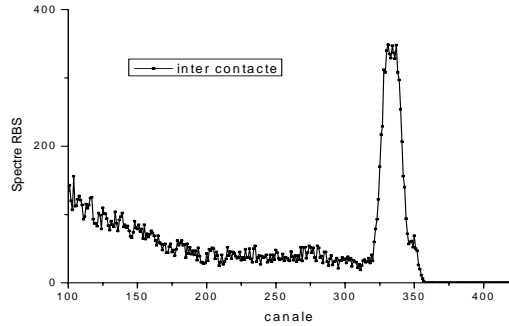


Picture 15: beam profile

By repeating this measurement with different distances (17, 35 and 68 mm) of the wire to the exit of the capillary, we could deduce a divergence of the "undisturbed" center beam of ~ 6 mrad. Visual observation by means of phosphor screens on 60 and 360 mm distance lead to the same result (5,5 -6 mrad).

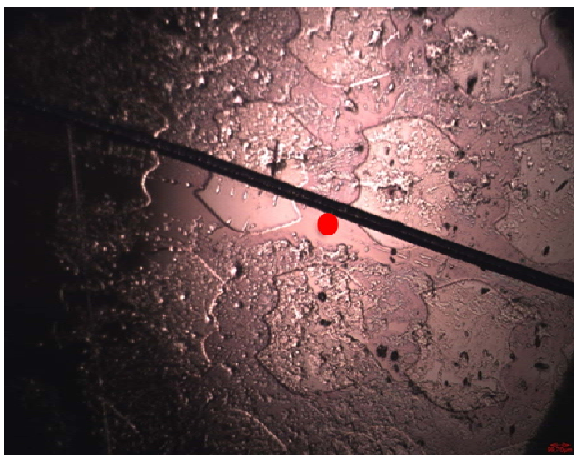


The resulting spectra show that we clearly can resolve the geometric different regions on this chip:



Picture 16 & 17: Measured Divergence of a 200µm capillary

To test the possibility of mapping surfaced with this kind of micro beam, we measured the spectra of a micro-structured semiconductor.



Picture 18: Semiconductor surface (black: wire with 60 µm, red: beam spot of 50 µm)

Conclusion:

Even a cyclotron is not dedicated for RBS, we can achieve interesting results and the capillaries most probably open the door for micro beam applications.

Further steps:

- Standardization of (simple) RBS for our customers (EN17025)
- More detailed studies on capillary focusing and new applications with micro beams
- New analyzing chamber with better adjustment possibilities (arrived in the meantime)
- Channeling experiments
- A new, dedicated accelerator (tandem) is planned

Acknowledgement:

The experiments could not be performed and analyzed without the help of Ion Rusen, Stefan Nitisor, Ofelia Muresan, the operator crew of the cyclotron and some inciting discussions with Eugen Ivanov.

References:

1. low energy ions of Ne^{7+} are guided through capillary tubes even for small angles of misalignment with the beam axis (N. Stolterfoht et al., Phys. Rev. Lett. 88, 133201/2002)
2. the transmitted beam of 8keV Ar^{8+} through a tapered glass capillary need some tens of seconds to reach its maximum of intensity (T. Ikeda et al., Phys. Rev. Lett. 89, 163502/2006)
3. Experiments with beams of MeV ions transmitted through tapered capillaries revealed a focusing effect most probable based on total reflection at small angles (T. Nebiki, et al., J. Vac. Sci. Technol. A 21, 1671 /2003).

Workshop on „Low Current, Low Energy Beam Diagnostics“
Hirschberg-Großsachsen, November 24-25, 2009

The SQUID based Cryogenic Current Comparator – an useful tool for beam diagnostics

Dr. sc. nat. Wolfgang Vodel
Friedrich-Schiller-Universität Jena
Low Temperature Laboratory



Outline

- Motivation
- Brief introduction to SQUID measurement technique
- Cryogenic Current Comparator (CCC) principle
- The CCC at GSI Darmstadt
- The CCC for DESY
- Experimental results
- Conclusions and Outlook

Motivation

In high energy physics there is a need for:

- Measurements of high energy ion beams in the range of 1 μ A...1 nA without back action (e.g. GSI Darmstadt)
- Measurements of so-called dark currents of superconducting acceleration cavities in the range below 50 nA (e.g. DESY Hamburg)
- Measurements of charged particles in the CSR (e.g. MPI Heidelberg)

Solution: SQUID-based Cryogenic Current Comparator

Brief introduction to SQUID measurement technique

Superconducting QUantum Interference Device

SQUID is an acronym for **S**uperconducting **Q**uantum **I**nterference **D**evice and is the most sensitive magnetic flux detector known today.

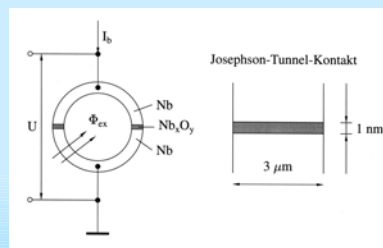
The working principle makes use of:

- **superconductivity**,
- the **flux quantization** in superconducting rings, and
- the **Josephson effect**.

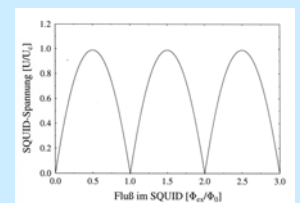
In principle, the SQUID consists of a superconducting ring with one or two weak links (Josephson tunnel junctions). We differ between:

- **dc SQUID** with two Josephson junctions and
- **rf SQUID** with one Josephson junction only.

DC-SQUIDS

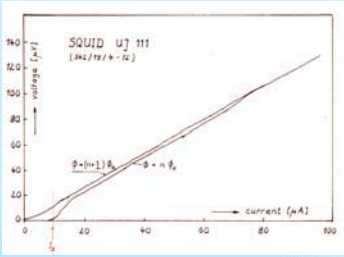


Simplified scheme of a dc-SQUID and a tunnel junction

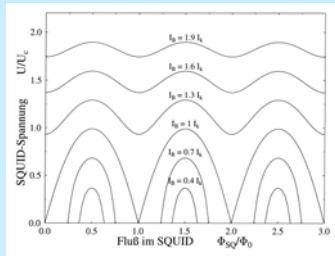


Output voltage of the SQUID vs. external magnetic flux

SQUID-Characteristics

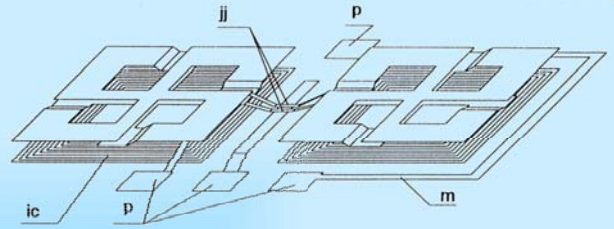


Voltage-Current-Characteristic of the SQUID UJ 111



Output voltage of the SQUID vs. external flux for different bias currents

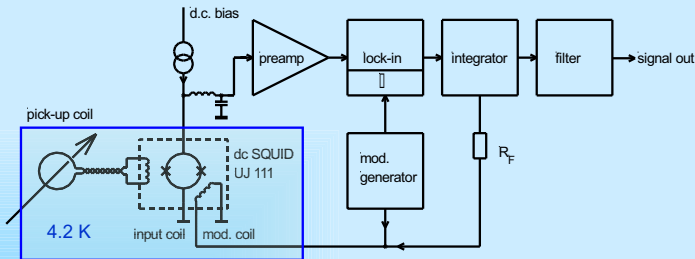
DC-SQUID lay-out



Simplified structure of the DC-SQUID UJ 111 (FSU Jena).

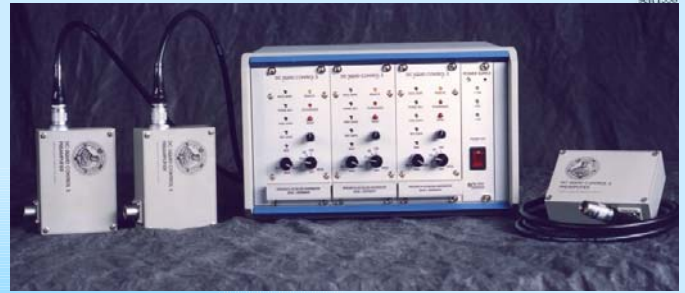
jj: Josephson junctions, p: Nb contact pads, m: modulation coil, ic: input coil

Block diagram of the dc SQUID system 5



Simplified electrical scheme of the dc SQUID electronics of Jena University with the thin film dc SQUID UJ 111

The dc SQUID system 5 of Jena University



Photograph of the complete 3 channel dc SQUID system 5 electronics with the connected low noise preamplifiers.

The dc SQUID system 5 of Jena University



1 channel of the dc SQUID system 5 (left) and the unclosed low noise preamplifier (right).

Main principle of the Cryogenic Current Comparator



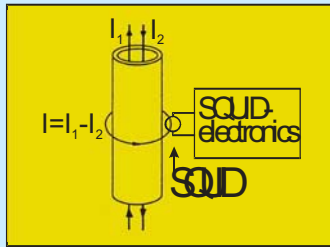


The CCC, first developed in 1972 by Harvey†, consists of:

- a superconducting pickup coil
- a high efficient superconducting shield
- a high performance SQUID measurement system

For absolute current measurements:

$$I = I_1 - I_2 = i_{\text{meas}} - 0$$



† Harvey, Rev. Sci. Instrum., Vol. 43, p. 1626, 1972



Outstanding advantages of the CCC:

- Non destructive method
- High resolution ($< 1 \text{ nA}/\sqrt{\text{Hz}}$)
- Measurement of the absolute value of the current
- Exact absolute calibration using an additional wire loop
- Independency of charged particle trajectories
- Independency of charged particle energies

Resolution limits



The theoretical resolution of the CCC is limited, above all, by the thermal noise of the ferromagnetic core material:

- Thermal noise generates a noise current $\sqrt{\langle I^2 \rangle}$
- In connection with the inductance L this noise current gives rise of the magnetic flux noise Φ_{thermal}
- For $\text{SNR} > 1$ the beam signal must meet the condition:

$$\Phi_{\text{beam}} = \int_A \vec{B} \cdot d\vec{f} \geq \Phi_{\text{thermal}} = L \cdot \sqrt{\langle I^2 \rangle}$$

Resolution limits

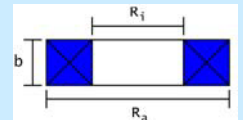


Minimum detectable current I_s :

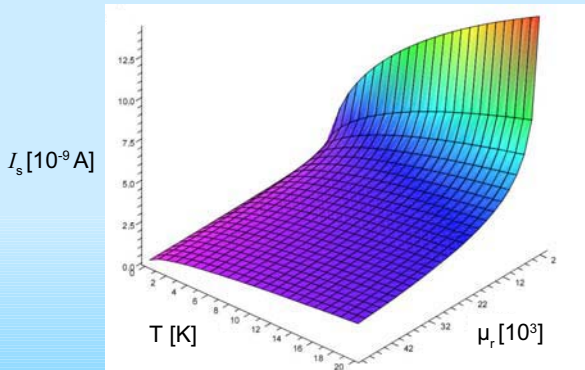
$$I_s = \frac{2\pi \sqrt{k_B T L}}{\mu_0 \mu_r f(R_a, R_i, b)} \Rightarrow I_s \propto \frac{1}{\sqrt{\mu_r}}$$

where T denotes the temperature, μ_r the relative permeability of core material, n the number of windings ($n=1$), and L the inductance of pick-up coil according to:

$$L = n^2 \cdot \frac{\mu_0 \mu_r b}{2\pi} \ln \frac{R_a}{R_i}$$



Resolution limits



Minimum detectable current I_s as a function of temperature and relative permeability μ_r , calculated for the currently used single turn toroidal pick-up coil.

Magnetic material



Vacuumschmelze Hanau

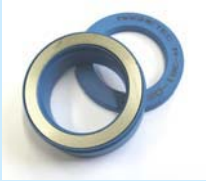
- **Vitrovac**
 - tape material
VC 6025, $\mu_r \sim 5.000$,
VC 6155, $\mu_r \sim 2.000$
 - toroidal tape wound cores
VC 6025 F, VC 6030 F,
VC 6150 F, VC 6200 F
with different μ_r from 1.200
to 200.000 at 300 K

- **Vitroperm**
 - toroidal tape wound cores
VP 250 F, VP 500 F
with different μ_r from 6.000
to 130.000 at 300 K

Magnetec Langensfeld

- **Nanoperm**
toroidal tape wound cores in plastic cases in different dimensions with μ_r from 25.000 to 100.000 at 300 K

Nanperm- magnetic cores



Nanperm-toroidal tape wound cores



Nanperm-toroidal tape wound cores M074 (50 windings)

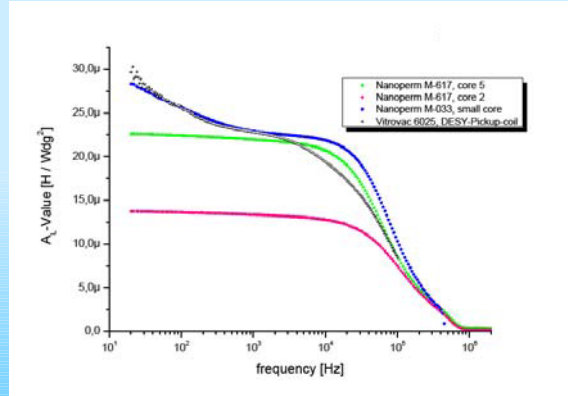


Nanperm-toroidal tape wound cores M060 (50 windings)

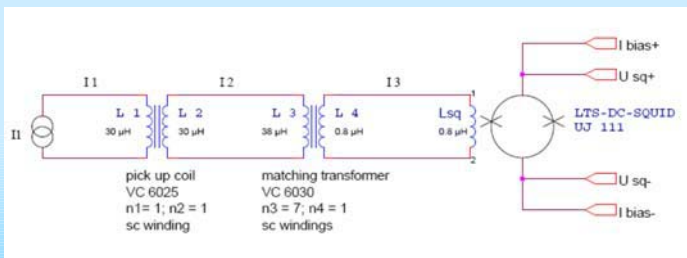


Nanperm-toroidal tape wound cores M033 (50 windings)

A_L -values of magnetic materials at low temperatures



Electrical Scheme of the input circuit



Current gain



Short circuit current gain of a transformer:

$$\frac{I_2}{I_1} = \frac{n_1}{n_2}$$

Current gain of a stressed transformer with an inductive load:

$$\frac{I_2}{I_1} = \frac{n_1}{n_2} \cdot \frac{1}{1 + L_1/L_2}$$

Total current gain of the system (pick up coil – matching transformer – SQUID input coil:

$$\frac{I_3}{I_1} = \frac{n_3}{n_4} \cdot \frac{1}{1 + L_{SQ}/L_4} \cdot \frac{n_1}{n_2} \cdot \frac{1}{1 + \frac{L_3 \cdot L_{SQ}}{(L_4 + L_{SQ}) \cdot L_2}}$$

Applications of the CCC



- Measurement of high energy ion currents of accelerators
Current resolution: $\leq 250 \text{ pA}/\sqrt{\text{Hz}}$
(GSI Darmstadt)
- Measurement of so-called dark currents of RF accelerator cavities
Current resolution: $\leq 40 \text{ pA}/\sqrt{\text{Hz}}$
(DESY Hamburg)

Supercond. Sci. Technol. 20, pp. 393-397 (2007)

The CCC at GSI Darmstadt



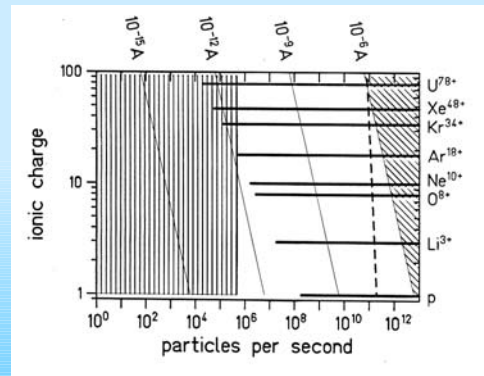
The CCC at GSI Darmstadt



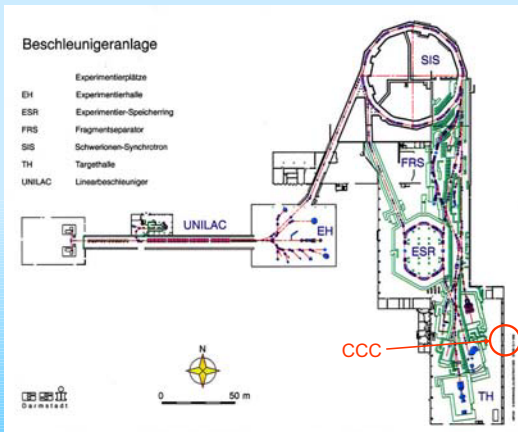
GSI (Darmstadt) and the Friedrich Schiller University Jena made an impressive demonstration of the capabilities of a CCC to measure extracted high energy ion-beams (Ar, Ne) with a resolution of:

0.25 nA/√Hz.

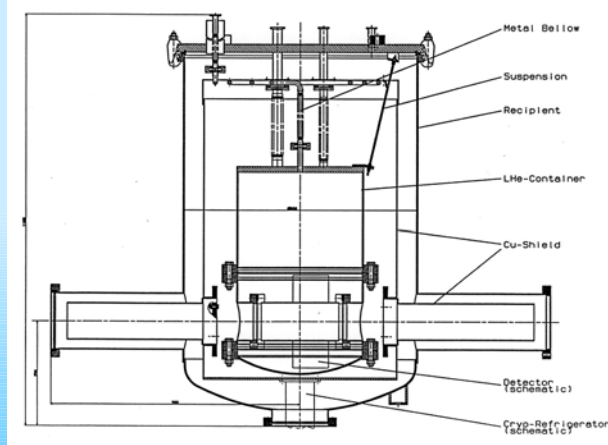
Motivation for the CCC at GSI Darmstadt



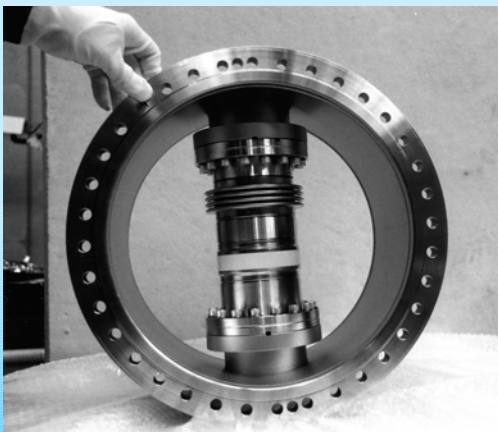
The SIS at GSI Darmstadt



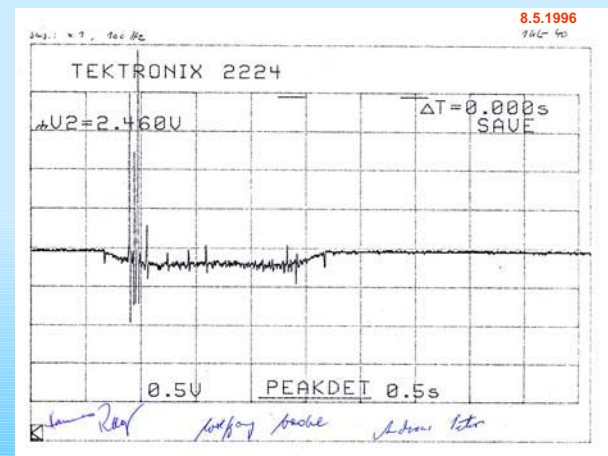
Cross section of the CCC



Technical details of the CCC



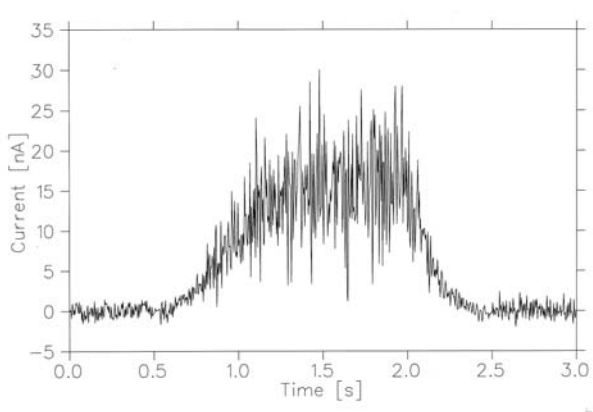
First beam measurement (²⁰Ne¹⁰⁺)



High resolution beam measurement



seit 1558



The CCC at DESY Hamburg



seit 1558

Motivation



seit 1558

The performance of superconducting cavities of accelerators is characterized by the Q-value vs. gradient dependency, measured in a cavity test stand (e. g. "CHECHIA" at DESY or "HoBiCaT" at BESSY).

But unfortunately there is:

"The existence of so-called **dark currents** (vs. gradient) which may have an influence on the accelerator operation".

The CCC for X-FEL



seit 1558



In collaboration with Jena University, GSI and DESY a CCC for the measurement of dark currents of the X-FEL accelerator cavities is under construction.

Dark currents:



seit 1558

- Unwanted particle source
- Limit the accelerator performance by
 - Additional thermal load (T = 1.8 K)
 - Propagating dark current
- An avalanche instability due to the propagating dark current arise if (statistically):

number of emitted electrons/cavity period > 1
- This limits the dark current of a 9-cell cavity to

$i_{\text{dark}} < 50 \text{ nA}$

Dark currents:



seit 1558

- Are caused by field emission of electrons in high gradient fields
- The forces of the applied external field are higher than the bounding forces inside the crystal structure.

Potential emitters are:

- Imperfections of the cavity shape, e. g. corners, spikes and other discontinuities where occur high field gradients
- Imperfections of the crystal matter, e. g. grain boundaries
- Inclusion of "foreign" contaminants (In, Fe, Cr, Si, Cu,... microparticles)

Dark current simulations



seit 1558



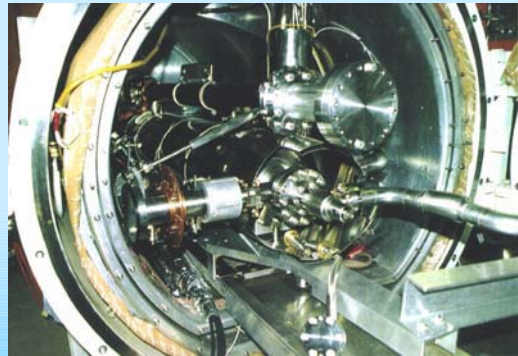
Reference

C. Stolzenburg, "Untersuchungen zur Entstehung von Dunkelströmen in supraleitenden Beschleunigungsstrukturen", (in German); Ph. D. Thesis, University of Hamburg 1996.

CECHIA test facility



seit 1558

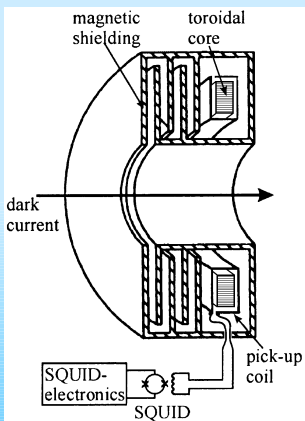


The proof measurements will be performed in the so-called „CHECHIA“ test stand at DESY.

Pickup coil with meander-shaped shield



seit 1558

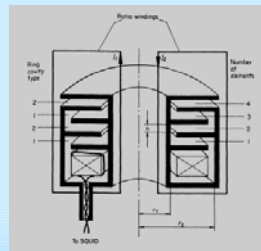


The single turn, superconducting pickup coil is arranged on a toroidal core (VITROVAC, Vakuumschmelze Hanau).

Superconducting shielding



seit 1558



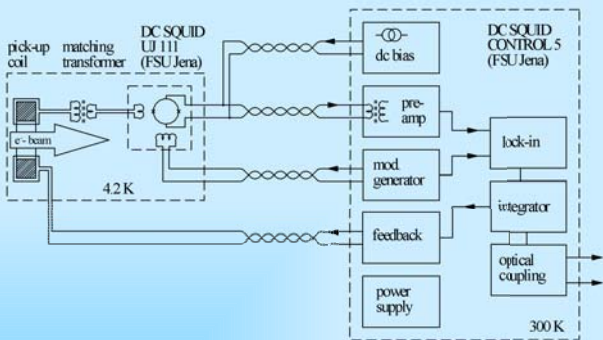
The resolution of the CCC is reduced if the toroidal pickup coil operates in the presence of external magnetic background fields. As this is in practice unavoidable, an effective shielding has to be applied.

- A circular, meander-shaped shielding structure is able to pass the azimuthal magnetic field of the dark current, while strongly attenuating non-azimuthal field components.
- A superconducting shielding material (niobium, lead) leads to an ideal diamagnetic conductor (Meissner-Ochsenfeld effect), providing an expulsion of external magnetic fields.

Electrical scheme of the CCC



seit 1558



A DC-coupled field compensation feedback loop is part of the SQUID electronics. The SQUID input coil and the pickup coil form a superconducting loop, so that the CCC is also able to detect DC-currents.

Pick-up coil



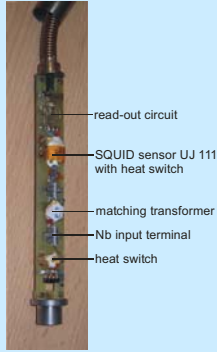
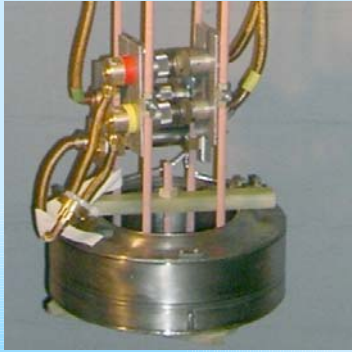
seit 1558



Toroidal core (VITROVAC 6025-F) housed in a VESPEL insulator.

Completed niobium toroidal pick-up coil with included VITROVAC core.

Experimental equipment



The completed niobium pick-up coil of the CCC with all special cabling for the SQUID prepared for low temperature tests in a wide-neck Helium cryostat.

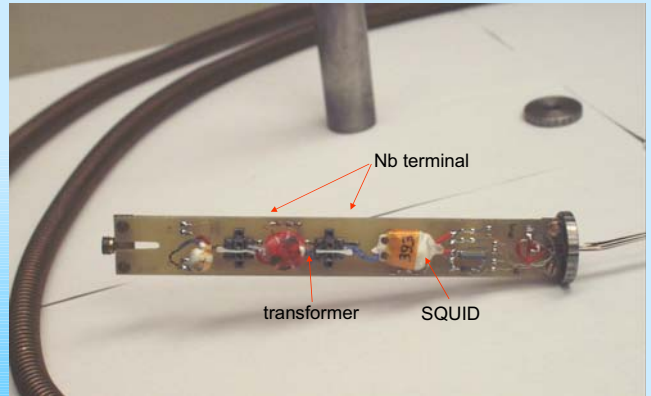
Low temperature probe with LTS SQUID, matching transformer and read-out circuit.

November 25, 2009

W. Vodel, FSU Jena

43/54

Measuring head with LTS DC-SQUID UJ 111 (FSU Jena)

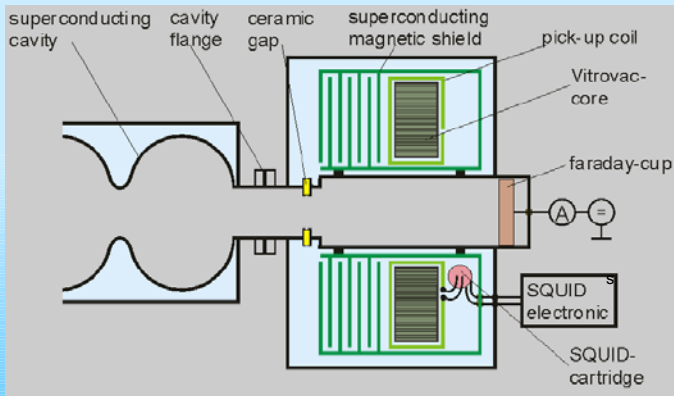


November 25, 2009

W. Vodel, FSU Jena

44/54

Schematic view of the CCC

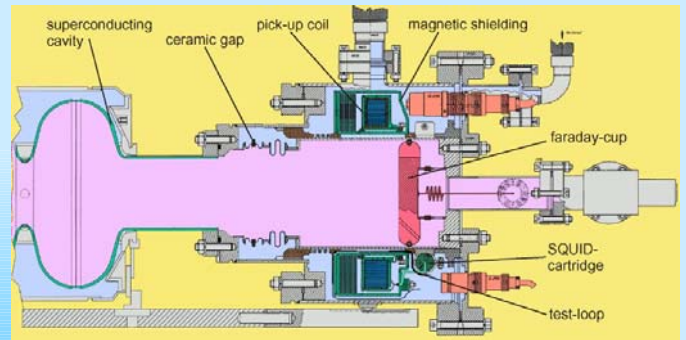


November 25, 2009

W. Vodel, FSU Jena

45/54

Cross section of the dark current measurement equipment



blue: Liquid Helium
green: Superconductive materials
pink: Ultra high vacuum
yellow: Insulating high vacuum of CHECHIA

November 25, 2009

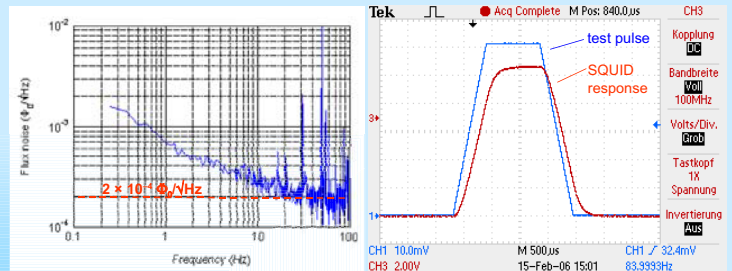
W. Vodel, FSU Jena

46/54

Experimental Results



Noise measurements and SQUID response (with connected pick-up coil)



Spectral flux noise density of the SQUID system with connected pick-up coil.

blue: test signal (1 ms current pulse)
red: SQUID system response

November 25, 2009

W. Vodel, FSU Jena

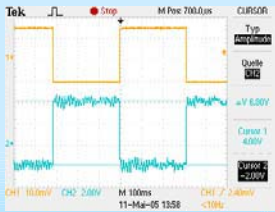
47/54

November 25, 2009

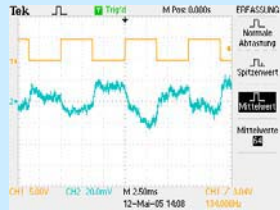
W. Vodel, FSU Jena

48/54

CCC tests with simulated dark current (in the noisy environment at DESY)

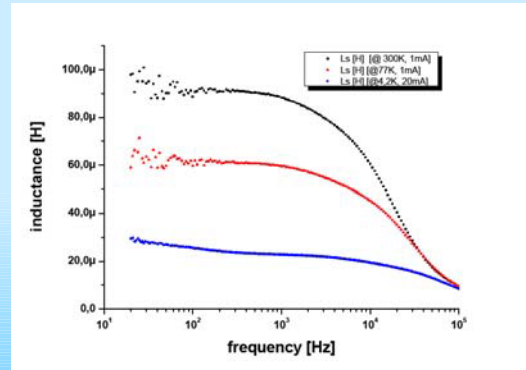


126.5 nA current pulse through the calibration coil (upper curve) and SQUID response (lower curve).



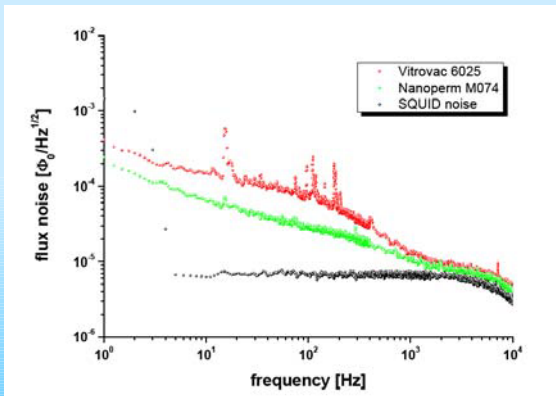
1.3 nA current pulse through the calibration coil (upper curve) and SQUID response (lower curve).

Inductance of pick-up coil



Inductance of the recent pick-up coil of the DESY-CCC in dependence of the frequency at different temperatures.

Spectral flux noise density of the CCC using different core materials



Measured performance of the DESY-CCC



- System bandwidth: dc...70 kHz
- System sensitivity: 167 nA / Φ_0
- Flux noise (in the white noise region): $8 \times 10^{-5} \Phi_0 / \sqrt{\text{Hz}}$
- Corresponding current noise: 13 pA / $\sqrt{\text{Hz}}$

But:
The current resolution of the final system will be decreased due to the additional noise contribution of

- disturbing magnetic background fields and
- mechanical vibrations of environment.

Conclusions and Outlook



- Tests of the pick-up coil with connected SQUID system were successfully done in a wide-neck LHe cryostat.
- The superconducting meander-shaped flux transducer is used to attenuate the magnetic background noise.
- Measurement bandwidth: **dc...70 kHz**
- CCC current sensitivity: **< 200 nA/ Φ_0**
- Noise limited current resolution (at LT Lab) : **40 pA/ $\sqrt{\text{Hz}}$**
- Noise limited current resolution (at DESY) : **500 pA/ $\sqrt{\text{Hz}}$**
- Magnetic flux drift of the CCC: **< 2 x 10⁻⁵ Φ_0 /s**
- Currently the DESY-CCC is ready for installation in the HoBiCaT test stand at BESSY.

SQUID-based CCC:



- No back actions
- Highest sensitivity – no alternatives
- Easily calibrated (by electrical current)
- Measurement of absolute current values
- Negligible low drift

Acknowledgment

Co-workers

- R. Neubert
- R. Geithner
- A. Steppe
- S. Hechler

Collaboration

- A. Peters, GSI Darmstadt/HIT Heidelberg
- M. Schwickert, H. Reeg GSI Darmstadt
- K. Knaack, K. Wittenburg DESY Hamburg
- T. Siebert, R. von Hahn MPI Kernphysik, Heidelberg



November 25, 2009

W. Vodel, FSU Jena

References

- [1] G. R. Werner, et. al., "Investigation of Voltage Breakdown cause by Microparticles"; Proc. of the Part. Acc. Conf., PAC2001, New York, pp.1071-73
- [2] C. Stolzenburg, "Untersuchungen zur Entstehung von Dunkelströmen in supraleitenden Beschleunigungsstrukturen", (in German); Ph. D. Thesis, University of Hamburg 1996.
- [3] R. Brinkmann, "Dark Current Issues"; Tesla Collaboration Meeting – CEA SACLAY, 4/2002.
- [4] A. Peters, et. al., "A Cryogenic Current Comparator for the Absolute Measurement of nA Beams"; Proc. of the 8th BIW, Stanford, 1998, AIP Conf. Proc. 451, pp.163-180
- [5] K. Grohmann, et. al.; CRYOGENICS, July 1976, pp.423-429
- [6] K. Grohmann, et. al.; CRYOGENICS, October 1976, pp.601-605
- [7] K. Grohmann and D. Hechtfischer ; CRYOGENICS, October 1977, pp.579-581
- [8] K. Knaack, et. al., "Cryogenic Current Comparator for Absolute Measurements of the Dark Current of Superconducting Cavities of TESLA"; Proc. of the DIPAC 2003, Mainz 2003

November 25, 2009

W. Vodel, FSU Jena

A CRYOGENIC CURRENT COMPARATOR FOR FAIR*

M. Schwickert, H. Reeg, GSI, Darmstadt, Germany
R. Geithner, W. Vodel, P. Seidel[#], Friedrich-Schiller-Universität Jena, Germany

Abstract

At present the Facility for Antiproton and Ion Research FAIR is designed and planned for realization at GSI [1]. The FAIR accelerators will deliver beams of unprecedented intensity for nuclear experiments and for the production of rare isotope beams or antiprotons. The availability of high intensity, high energy beams of ions and rare isotopes will be world-unique. Apart from high intensity beams produced by fast extraction from the synchrotrons, also slowly extracted beams have to be transported to the experiments. This operational mode demands for devices which allow for online measurements of beam currents in the nA-regime. To monitor slowly extracted beams a sensitive cryogenic current comparator (CCC) is currently developed in collaboration with FSU Jena and MPI-K Heidelberg. This contribution presents the actual state of the CCC developments for the FAIR beamlines and reports on recent improvements of the device.

GSI AND THE FAIR PROJECT

In November 2007 the FAIR project celebrated its kick-off event, with representatives of the international partners signing a communiqué on the imminent start of the FAIR project. Meanwhile the layout of the future facility and all of the technical subsystems has been further refined and GSI entered into the final planning phase [1]. Fig. 1 presents an overview of the future facility. The existing GSI machines (UNILAC, SIS18) will act as an injector (blue beamlines in Fig. 1, left part) for the new FAIR accelerators (red lines). As part of the FAIR project a proton Linac is planned for the production of high-current proton beams as needed for effective production of antiprotons. It is foreseen that in its final stage FAIR comprises two heavy ion synchrotrons (SIS100 and SIS300), the antiproton production target, the Super-Fragment Separator (Super-FRS) and four storage rings (CR, RESR, NESR and HESR). The FAIR accelerator complex is designed as a flexible, multi-purpose facility with the following goals:

- acceleration of all ion species from proton to uranium
- production of high-current primary beams
- generation of radioactive beams for fixed target or storage ring experiments
- production, accumulation and storage ring experiments with antiprotons

From the experimentalist's view 14 large experiments have been approved for installation at FAIR. The FAIR research programme is organized in four scientific pillars: APPA (Atomic, Plasma Physics and Applications), CBM (Compressed Baryonic Matter), NuSTAR (Nuclear

Structure, Astrophysics and Reactions) and PANDA (AntiProton ANnihilation in DArmstadt).

As a consequence of a severe cost overrun of the estimated realization costs it was decided in fall 2009 to reorganize the planned facility into modules and to start FAIR in a reduced "Modularized Start Version". The six modules are colour-coded in Fig. 1: Module 0: heavy ion synchrotron SIS100 (green), Module 1: experimental hall for CBM (ochre), Module 2: Super-FRS (yellow), Module 3: p-Linac, antiproton Target, CR, HESR (orange), Module 4: NESR (light blue) and Module 5: RESR (red). The FAIR start version presently consists of modules 0 to 3, whereas modules 4 and 5 are foreseen to follow in the future. It is important to note that all international partners, as well as the scientific steering committee, endorsed the new modularized attempt and great care had been taken to retain the physics case for all scientific communities involved.

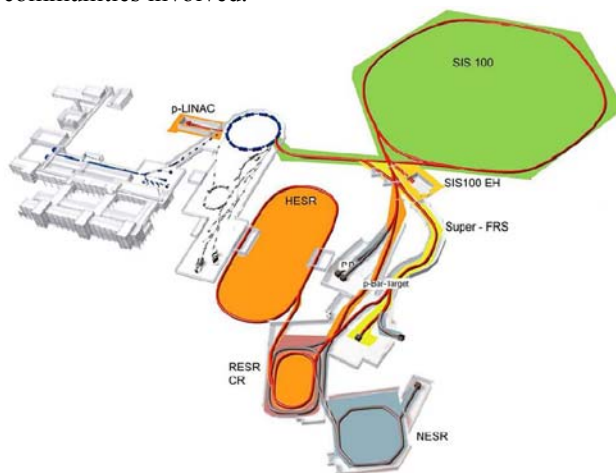


Figure 1: Present layout of GSI and the upcoming FAIR facility. The modules of the "Modularized Start Version" are colour-coded, see text.

BEAM CURRENT MEASUREMENT

This contribution focuses on beam current measurement in the extraction beamline of the fast ramped superconducting synchrotron SIS100 and in the high energy beam transport (HEBT) section of FAIR.

The unique beam parameters of the FAIR machines require carefully designed diagnostic equipment. E.g. the extreme UHV condition down to 5×10^{-12} mbar in the SIS100 is a strict requirement for all vacuum installations inside, or in close vicinity to SIS100. The fast-ramped heavy-ion synchrotron SIS100 will be the working horse of the whole facility, allowing to store and accelerate high currents (up to the space charge limit) of primary beams in low charge states. For the HEBT sections the main goal

is to achieve a high resolution and low detection limit for all diagnostic devices, because both, slow and fast extracted beams have to be monitored, casually changing in a pulse-to-pulse manner. In order to prevent destruction of devices by high-intensity ion beams and to allow for online measurements non-intercepting beam diagnostic devices, like e.g. beam current transformers for current measurements, are preferred as standard devices.

Especially the production of rare isotope beams requires slowly extracted primary beams from the SIS100 synchrotron. To monitor slowly extracted beams with maximum values in the order of 10^{12} particles/s, corresponding to $4.5 \mu\text{A}$ for U^{28+} , instrumentation with maximum sensitivity is ultimately required. The only non-intercepting current measurement device capable of measurements down to the nA-range is the SQUID-based CCC. Altogether six installations of the CCC are foreseen in the HEBT section, for direct measurement of the beam current and, secondly, to monitor transmission between machines or between accelerator and experiments.

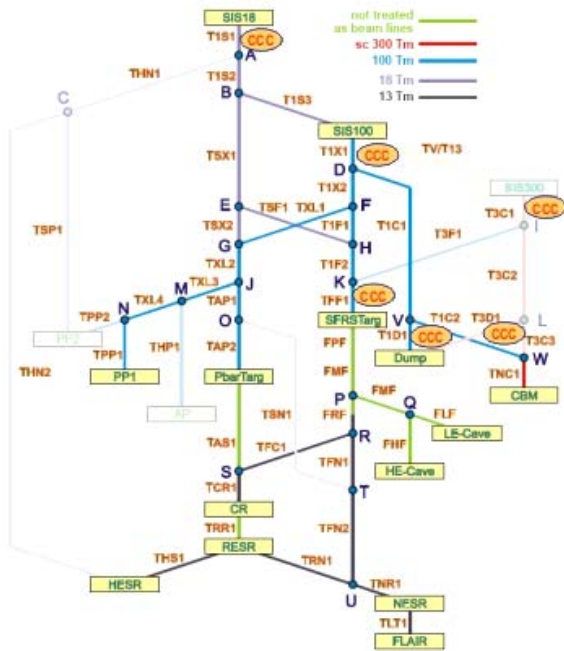


Figure 2: Schematic view of the high-energy beam transport section of FAIR [1], interconnecting the accelerators and experiments (yellow rectangular). Yellow ellipses indicate the installation locations of the CCCs. The total length is 2.6 km

A schematic view of the HEBT beamlines is depicted in Fig. 2. CCCs are foreseen at the following positions: 1. in beamline T1S1 connecting the synchrotrons SIS18 and SIS100, 2. in SIS100 extraction section T1X1, 3. in T1D1 before the SIS100 beam dump (to verify complete beam extinction), 4. in beamline TFF1, i.e. the entrance of the Super-Fragment Separator. The two installations in beamlines T3C1 and T3D1 belong to FAIR modules 4 and 5, and thus will be realized at a later stage.

CRYOGENIC CURRENT COMPARATOR

A SQUID-based cryogenic current comparator is a sensitive device for the measurement of the azimuthal magnetic field of a flux of charged particles.

Measurement Principle

The basic physical effect deployed by a CCC is that for an ideal superconductor the magnetic flux is expelled from the bulk material by shielding currents on the materials surface (Meissner-Ochsenfeld-effect). A schematic view of a CCC sensor is presented in Fig. 3. As depicted, the ion beam longitudinally penetrates a superconducting cylinder and induces screening currents in the surface of the niobium cylinder, which contains a toroidal pick-up coil with ferromagnetic core [2]. The pick-up coil detects the magnetic field of the induced screening currents and the current signal is transferred via a superconducting loop to an LTS SQUID. The SQUID electronics is connected to a Josephson-junction and generates an output voltage proportional to the number of magnetic flux quanta applied.

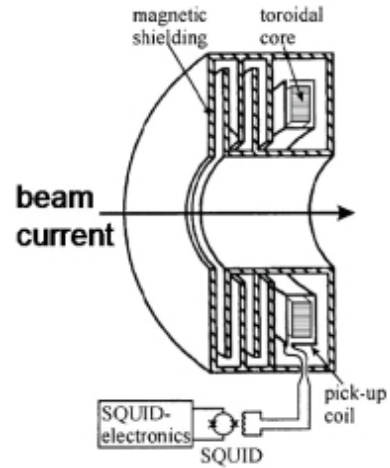


Figure 3: CCC sensor principle

In order to suppress disturbing external magnetic fields a meander-shaped superconducting niobium shield covers the pick-up coil and effectively suppresses non-azimuthal components of magnetic stray fields from outside the CCC. This is of course important if the device is installed in an accelerator environment, e.g. near fast ramped magnets of the beam transport system. In 1994 a CCC prototype was built at GSI in collaboration with FSU Jena. The prototype achieved a current resolution of $\leq 250 \text{ pA}/\sqrt{\text{Hz}}$ and was successfully tested for the measurement of high-energy ion beams in the nA-range [3]. A more recent development of a CCC for the measurement of dark currents in superconducting cavities in the frame of the CHECCHIA test stand achieved a higher resolution of $40 \text{ pA}/\sqrt{\text{Hz}}$ [4].

Apart from an optimized magnetic shielding the overall system noise defines the resolution of CCC. Therefore a detailed study of the various noise contributions of the CCC system was carried out at FSU Jena. As a result it

turned out that the choice of the ferromagnetic core material is of major importance for a good resolution. The noise performance could be improved by using core materials with highest possible relative permeability μ_r , since the signal to noise figure is proportional to the square root of μ_r (I_N : noise current, I_S : signal current, cf. [5]):

$$B, L \propto \mu_r \Rightarrow \frac{I_s}{I_n} \propto \sqrt{\mu_r}.$$

Sensor Improvements

In search of a maximum relative permeability, various materials have been studied with respect to their μ_r as a function of temperature and frequency. The frequency behaviour is of course important to achieve a high analog bandwidth of the device and thus to allow for sampling rates in the kHz range.

The studies of different core materials revealed especially nanocrystalline alloys like Vitroperm [6] and Nanoperm [7] as good candidates for the CCC core. Fig. 4 epitomises the relative permeability of ferromagnetic core materials as a function of temperature. For these measurements the temperature has been defined by an automated dip-stick setup that sets the sample temperature by positioning the test item in the gas phase above the liquid helium inside a cryostat.

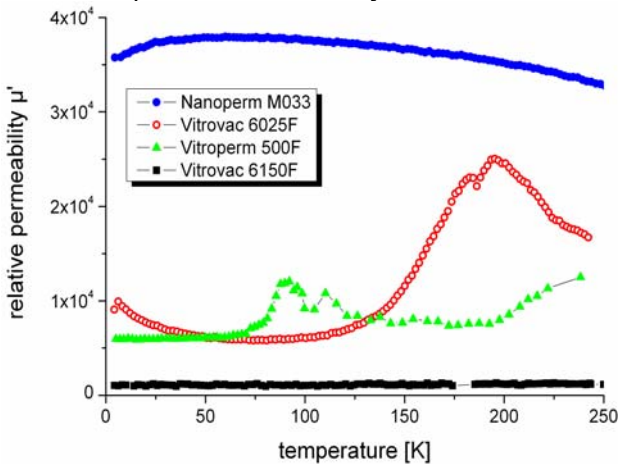


Fig. 4: Relative permeability μ_r at 100 Hz for various ferromagnetic core materials as a function of temperature

The plots in Fig. 4 clearly indicate that over the whole temperature range (4 K to 250 K) the relative permeability of the ferromagnetic alloy Nanoperm M033 exceeds the Vitrovac and Vitroterm samples by a factor of ~ 4 , resulting in a factor of 2 for the signal-to-noise ratio. Thus Nanoperm presently is the preferred core material for the FAIR CCC. More details on the materials analysis regarding μ_r can be found in [5] and [8].

Next Steps

As a next step Nanoperm cores of adequate diameter will be purchased for further system tests in the cryostat. Secondly an improved magnetic shielding with a greater number of meanders will be manufactured. Both

components are designed to fit to the mechanical layout of the CCC for the cryogenic storage ring.

CCC FOR CRYOGENIC STORAGE RING

Presently the Cryogenic Storage Ring is developed and realized at MPI-K Heidelberg. The CSR will be an electrostatic storage ring with a circumference of 35 m dedicated for molecular and atomic physics experiments [9]. Special features of CSR are the operation at L-He temperature, extreme vacuum conditions in the 10^{-13} mbar regime and beam intensities between 1 nA and 1 μ A. The cryogenic environment of the CSR facilitates the installation of a SQUID-based CCC for the measurement of lowest beam intensities [10]. To minimize noise and zero drift of the SQUID all components of the CCC have to be cooled down to L-He temperature, with a stability of 50 mK. Currently, as part of the collaboration between FSU Jena, MPI-K and GSI, the mechanical layout of the superconducting shielding of a CCC for CSR is finalized and detailed design work for the CCC chamber has started.

OUTLOOK

At the moment the beamline instrumentation and thus all installation locations for the CCC inside the HEBT beamlines of FAIR are being determined and user demands for the required CCC performance are collected. These requirements will be included in the design of the CCC prototype. It is planned to manufacture a prototype coil structure and to implement it in a cryogenic system. The installation of a CCC prototype inside the CSR will be an ideal test bench for the development of the FAIR CCC.

REFERENCES

- [1] FAIR Baseline Technical Report, <http://www.gsi.de/fair/reports/btr.html>
- [2] A. Peters et al., EPAC2004, London, UK, p. 290.
- [3] A. Peters et al., Proc. of Beam Instrumentation Workshop 1998, Stanford, USA.
- [4] W. Vodel et al., Superconductor Science and Technology, Vol. 20, 2007, Washington, USA, p. S393.
- [5] W. Vodel et al. Proc. PAC 2009, Vancouver, CA, TH5RFP046.
- [6] <http://www.vacuumschmelze.de>
- [7] <http://www.magnetec.de>
- [8] W. Vodel, Proceedings of the DITANET-Workshop on "Low Current, Low Energy Beam Diagnostics", 23.-25.11.2009, Hirschberg, Germany.
- [9] R. v. Hahn, Proceedings of the DITANET-Workshop on "Low Current, Low Energy Beam Diagnostics", 23.-25.11.2009, Hirschberg, Germany.
- [10] T. Sieber et al., DIPAC2009, Basel, CH, WEOA02, p. 418.